Institut für Erd- und Umweltwissenschaften
Mathematisch-Naturwissenschaftliche Fakultät
Universität Potsdam

East African Climate Variability on Different Time Scales

The Suguta Valley in the African-Asian Monsoon Domain

Annett Junginger

**Kumultative Dissertation zur Erlangung des akademischen Grades
„doctor rerum naturalium (Dr. rer. nat.) in der Wissenschaftsdisziplin „Geologie“**

Potsdam, im November 2011

Selbständigkeitserklärung
Hiermit versichere ich, die vorliegende Arbeit selbstandig und nur unter Verwendung der angegebenen Quellen und Hilfsmittel angefertigt zu haben.

Declaration of independent work
Hierwith I declar that I have written this paper on my own, distinguished citations, and used no other than the named sources and aids.

Potsdam, im November 2011

Online veröffentlicht auf dem
Publikationsserver der Universität Potsdam:
URL http://opus.kobv.de/ubp/volltexte/2011/5683/
URN urn:nbn:de:kobv:517-opus-56834
http://nbn-resolving.de/urn:nbn:de:kobv:517-opus-56834

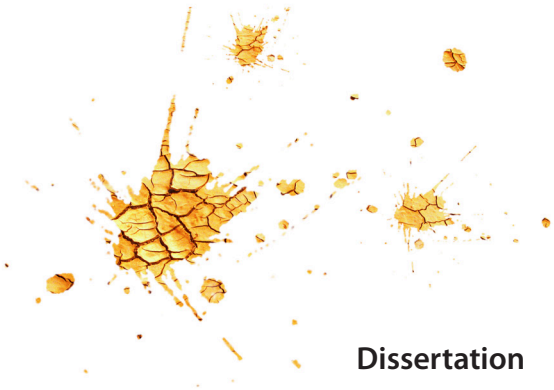

Dissertation

East African Climate Variability on Different Time Scales

The Suguta Valley in the African-Asian Monsoon Domain

Annett Junginger

Table of Contents

Abstract

Societal and economic needs of East Africa rely entirely on the availability of water, which is governed by the regular onset and retreat of the rainy seasons. Fluctuations in the amounts of rainfall, as it is a permanent feature in East Africa for at least the past 15,000 years, has tremendous impact causing widespread famine, disease outbreaks and human migrations. Efforts towards high resolution forecasting of seasonal precipitation and hydrological systems are therefore needed, which requires high frequency short to long-term analyses of available climate data that I am going to present in this doctoral thesis.

Long-term studies | The nature and causes of intensity variations of the African and Indian summer monsoons during the African Humid Period (AHP, 14,800 - 5,500 years BP, BP = before present), especially their exact influence on regional climate relative to each other, is currently intensely debated. As an example, no consensus exists concerning the abrupt vs. gradual onset and termination of this event, as well as the character and style of the internal climate variability during the AHP. The **main part** of this doctoral thesis presents a well ^{14}C-dated, reservoir-corrected, lake-level record from the remote Suguta Valley in the northern Kenya Rift for the AHP. The reconsruction of water level changes is based on the combined analysis of dated shoreline elevations, sediment compositions and hydrological modelling. The results uncovered that during the AHP only 26% of additional rainfall caused the presently desiccated valley to be filled by a 300 m deep and 2,200 km^2 large palaeo-lake that was, due to its extreme catchment size of 13,000 km^2 and amplifier-lake characteristic, highly sensitive to relatively moderate climate changes. This record from the Suguta Valley, located between the West-African and Indian Monsoon systems, explains very deep lakes in the East African Rift during the AHP as an indirect consequence of a strengthened Indian Summer Monsoon (ISM) during the precessional forced insolation maximum over the northern hemisphere. Besides the general enhanced atmospheric moisture availability, a possible deepening of the Tibetan Low due to higher insolation was responsible for a larger atmospheric pressure gradient between East Africa and India that caused the longitudinal shift of the Congo Air Boundary (CAB) eastwards over the East African Plateau. During the generally wet AHP, minor humidity changes causing abrupt lake level fluctuations of up to 100 m in less than 100 years are explained by small-scale solar irradiation changes that have caused a reversal of the process used to explain the AHP. Instead, the termination of the AHP occurred nonlinearly. The change towards an equatorial insolation maximum ca. 6.5 ka ago in the course of the earth's precession cycle caused a prolonged intense West-African monsoon whereas the ISM weakened and thus the pressure gradient necessary to pull the CAB over the East African Plateau. This change has led to a 1000-year earlier termination of the East African Plateau lakes as the result of missing CAB related rainfall, in contrast to the Ethiopian Rift lakes including Lake Turkana and West Africa. The study also explains, that topographic barriers play an important role in defining the response of large lakes to climate change during the AHP in the context of monsoon instabilities due to solar radiation fluctuations and associated displacements of circulation systems.

200 years | The **second part** of the thesis is on testing these relationships between climate forcing and lake hydrology for shorter timescales during different climatic preconditions. The results of a 200 year-old sediment core study from Lake Naivasha in the Central Kenya Rift, one of the very few present freshwater lakes in East Africa, revealed and confirmed, that the appliance of proxy records for palaeo-climate reconstruction for the last 100 years within a time of increasing industrialisation and therefore human impact to the proxy-record containing sites are broadly limited. Since the middle of the 20th century, intense anthropogenic activity around Lake Naivasha has led to cultural eutrophication, which has overprinted the influence of natural climate variation to the lake usually inferred from proxy records such as diatoms, transfer-functions, geochemical and sedimentological analysis as used in this study. The results clarify the need for proxy records from remote unsettled areas to contribute with pristine data sets to current debates about anthropologic induced global warming since the past 100 years.

14 years | In order to avoid human influenced data sets and validate spatial and temporal heterogeneities of proxy-records from East Africa, the **third part** of the thesis therefore concentrated on the most recent past

14 years (1996-2010) detecting climate variability by using remotely sensed rainfall data. The advancement in the spatial coverage and temporal resolutions of rainfall data allow a better understanding of influencing climate mechanisms and help to better interpret proxy-records from East Africa in order to reconstruct past climate conditions. The study focuses on the dynamics of intraseasonal rainfall distribution within catchments of eleven lake basins in the East African Rift, namely Ziway, Awassa, Abaya, Turkana, Suguta, Baringo, Nakuru, Naivasha, Natron, Manyara and Tana often used for palaeo-climate studies. We discovered that rainfall in adjacent basins exhibits various amplitudes in intraseasonal variability, showing biennial to triennial precipitation patterns and even do not necessarily correlate often showing opposite trends. The variability among the watersheds is driven by the complex interaction of topography, in particular the shape, length and elevation of the catchment and its relative location to the East African Rift System and predominant influence of one of the main convergence zones ITCZ or CAB. The location and intensities of these convergence zones are dependent on low developments over India, sea surface temperature variations in the Atlantic, Pacific or Indian Ocean, Quasibiennial Oscillation phases and the 11-year solar cycle. Among all seasons we observed that July to September is the season of highest complex rainfall variability, especially for the East African Plateau basins most likely due to the irregular penetration and sensitivity of the CAB. These findings confirm conclusion from the main part of this doctoral thesis that large lakes in the early to mid-Holocene AHP in equatorial East Africa were directly related to a rather regular contribution of CAB related rainfalls to the studied area, but due to high topography sensitive to changes in solar irradiation and earth's precession.

Zusammenfassung

Die sozialen und ökonomischen Bedürfnisse Ostafrikas sind in erster Linie abhängig von der Verfügbarkeit von Wasser, welche durch das regelmäßige Einsetzen der Regenzeiten bestimmt wird. Jegliche Veränderungen der Wasserverfügbarkeit innerhalb der Regenzeiten verursacht Hungersnöte, Ausbruch von Krankheiten oder auch Bevölkerungswanderungen. Variationen in der Wasserverfügbarkeit ist mindestens seit 15000 Jahren ein beständiges Merkmal in Ostafrika, deren Ursachen jedoch noch nicht vollständig verstanden sind. Klärung dieser Ursachen erfordert die Auswertung von hoch-auflösenden Kurz- als auch Langzeitanalysen, welche ich in dieser Arbeit präsentieren werde.

Langzeitanalysen | Die Ursachen von Intensitätsvariationen des West-Afrikanischen und Indischen Sommer Monsuns während der letzten Afrikanischen Feuchtphase (AHP, 14800 - 5500 Jahre BP - vor heute), besonders ihr genauer Einfluss auf das regionale Klima relativ zu einander, ist momentan intensiv diskutiert. Es existiert zum Beispiel keine Einigkeit darüber ob das Ende dieser Phase abrupt oder graduell erfolgte. Ebenso wenig ist über den Charakter und die Art der internen Klimaschwankungen während der AHP bekannt. In der **Hauptstudie** dieser Doktorarbeit präsentiere ich einen hoch-auflösenden Radiokarbon-datierten, Reservoir-alter korrigierten, Seespiegeldatensatz aus dem abgeschiedenen, unbewohnten Suguta Tal im nördlichen Grabenbruch in Kenia. Die Rekonstruktion fluktuierender Wasserspiegel benutzte eine neue Methode, die datierte Strandlinienhöhen, Seesedimentkompositionen und Hydromodellierungen kombinierte. Das momentan extrem trockene Tal brauchte nur 26% zusätzlichen Niderschlag während der AHP um mit einem 300 m tiefen Paläo-See von einer Größe von 2200 km^2 befüllt zu werden. Wegen seinem großem Einzugsgebiet von 13000 km^2 und seiner speziellen Morphologie zählt dieses Tal zu jenen, die hochsensibel auf relativ moderate Klimaveränderungen reagieren. Die Erkenntnisse in Form einer Seespiegelrekonstruktion aus dem Suguta Tal, welches sich zwischen dem West-Afrikanischen und Indischen Monsun System befindet, erklärt die Bildung von großen, tiefen Seen während der AHP als indirekte Konsequenz der Verstärkung des Indischen Sommer Monsuns während eines Einstrahlungsmaximums auf der Nordhalkugel. Neben einer generellen Erhöhung atmosphärischer Feuchte war die Verstärkung des Tibetischen 'Tiefs' wegen dieser erhöhten Einstrahlung vermutlich verantwortlich für einen höheren atmosphärischen Druckgradienten zwischen Indien und Ost-Afrika, welcher die Verschiebung der feuchten Kongo Luftmassengrenze (CAB) ostwärts über das Ostafrikanische und Äthiopische Plateau verursachte. Während der sehr feuchten AHP haben geringere Feuchtigkeitsveränderungen zu starken Seespiegelschwankungen des Suguta Sees von bis zu 100 m in weniger als einem Jahrhundert verursacht. Diese Schwankungen können über geringe Veränderungen in der solaren Ausstrahlung erklärt werden, welche zu einer kurzzeitigen Umkehrung des Prozesses führten, welcher als Ursache für hohe Seespiegel während der AHP erklärt wurde. Im Gegensatz dazu erfolgte das Ende der AHP nicht linear. Ein Wechsel des Präzessionsminimums zum Äquator vor etwa 6500 Jahre BP verursachte die Verlängerung des Westafrikanischen Monsuns, jedoch die Schwächung des Indischen Sommer Monsuns und damit Druckgradienten, welcher verhinderte, dass die CAB nicht mehr über das Ostafrikanische Plateau gezogen werden konnte und somit das Ende der Feuchtphase dort mehr als 1000 Jahre früher einsetzte als in den nördlich gelegeneren Seen des Äthiopischen Plateau, dem Turkana See und Seen aus West-Africa. Die Studie hat gezeigt, dass topographische Barrieren eine große Rolle spielten bei der Reaktion von großen Seen in Ostafrika während der AHP im Zusammenhang mit Monsun-Instabilitäten infolge von solaren Ausstrahlungsfluktuationen und damit verursachten Verlagerung von Zirkulationssystemen.

200 Jahre | Der **zweite Teil** dieser Arbeit beschäftigt sich mit der Prüfung der neuen Erkenntnisse über die Beziehungen zwischen Klima-antreibenden Prozessen und See-Hydrologie für kürzere Zeitskalen unter anderen klimatischen Vorbedingungen. Die Ergebnisse einer Sedimentkern-Studie an 200-Jahre alten Seesedimenten des Naivasha See aus dem zentralen Kenia Rift, einem der wenigen Frischwasserseen in Ostafrika, bestätigte schon zuvor erhobene Zweifel, dass die Anwendung von Proxy-Datensätzen für die Rekonstruktion des Paläo-Klimas für die letzten 100 Jahre, einer Zeit geprägt von steigender Industrialisierung und deshalb erhöhtem menschlichen Einfluss auf die Proxy-Daten enthaltenden Seen, stark limitiert sind. Seit

Mitte des 20. Jahrhundert hat der zunehmende Einfluss des Menschen um den Naivasha See zu kultureller Eutrophierung geführt, welche den Einfluss der natürlichen Klimavariabilität auf den See überprägte. Die natürliche Klimavariabilität sollte mittels Proxy-Datensätzen von Diatomeen, Transferfunktionen, geochemischen und sedimentologischen Analysen in dieser Studie aufgedeckt werden. Die Ergebnisse verdeutlichen die Notwendigkeit von Proxy-Daten aus unbesiedelten Gebieten, wenn man ‚reine' Daten zur momentanen Debatte über den anthropogen gesteuerten Klimawandel der letzten 100 Jahre beitragen will.

14 Jahre | Um menschlichen Einfluss auf Klima-Datensätze zu vermeiden und zeitliche sowie räumliche Unregelmäßigkeiten in Proxy-Daten von Ostafrika besser zu verstehen, konzentrierte sich der **dritte Teil** dieser Arbeit auf die Auswertung von ausschließlich fernerkundlich erworbenen täglichen Niederschlagsreihen der letzten 14 Jahre (1996-2010). Der Fortschritt dieser Art von Daten liegt in der räumlichen und zeitlichen Auflösung, welche ein besseres Verständnis über die klimatischen Einflussmechanismen erlaubt. Dies wiederum hilft dabei Proxydaten, welche für die Rekonstruktion von vergangenen Klimabedingungen benutzt werden, besser zu interpretieren. Die Studie beschäftigt sich mit der Dynamik saisonaler Niederschlagsverteilung innerhalb der Einzugsgebiete von elf Seebecken im Ostafrikanischen Riftsystem, welche oft für Paläo-Klimastudien benutzt werden. Bei diesen Seebecken handelt es sich um Ziway, Awassa, Abaya, Turkana, Suguta, Baringo, Nakuru, Naivasha, Natron, Manyara und Tana. Die Studie ergab, dass Niederschläge in angrenzenden Becken tatsächlich höchst unterschiedlich sein können: sie zeigen variierende Amplituden in der saisonalen Variabilität, zwei- bis dreijährige Niederschlagsmuster, oder aber sogar gegensätzliche Trends. Die Variabilität unter den einzelnen Seebecken ist stark beeinflusst durch die komplexe Wechselwirkung von Topographie, im besonderen die Form, Länge und Höhe des Einzugsgebietes und seine relative Lage zum Ostafrikanischen Rift System sowie dem Einfluss der Hauptkonvergenzzonen ITCZ oder CAB. Die Lage und Intensität dieser Konvergenzzonen ist von vielen Faktoren abhängig, wie z.B. der Entwicklung eines Tiefs über Indien, Meeresoberflächentemperatur Veränderungen im Atlantischen, Pazifischen oder Indischem Ozean, Phasen der Quasibiennial Oscillation und dem 11-Jahres Sonnenzyklus. Im direkten Vergleich aller untersuchten Monate stellte sich heraus, dass JAS die Jahreszeit mit höchster und komplexester Niederschlagsvariabilität ist, besonders für die Becken des Ostafrikanischen Plateau, was durch den unregelmäßigen Einfluss der CAB verursacht wird. Diese Beobachtung bestätigt Schlussfolgerungen aus dem Hauptteil dieser Doktorarbeit, bei die Entwicklung tiefer Seen im äquatorialen Ostafrika während der AHP durch den regelmäßigen Einfluss der CAB vorgeschlagen wurde. Wegen hoher Topographie jedoch war auch dieser Einfluss leicht beeinflussbar, wie z.B. durch solare Ausstrahlungsveränderungen oder Veränderungen der Erdparameter.

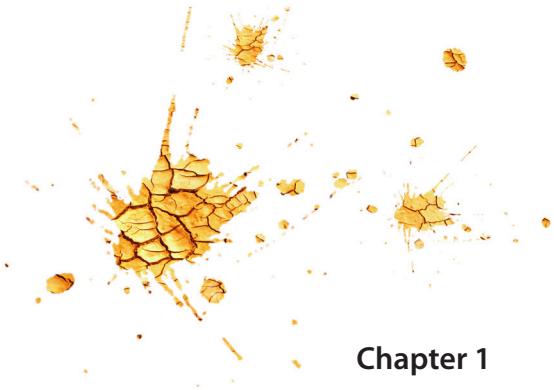

Chapter 1

Introduction into this doctoral thesis

Annett Junginger

1.1 General Introduction

Today, more than 290 Million people live in East Africa (Fig 1.1): life, vegetation and economies rely heavily on the availability of water, which is controlled by the regular onset and retreat of the rainy seasons. Fluctuations in the amounts of rainfall towards both directions wet or dry, or a delayed or failure of seasonal rainfall has tremendous impact to the people resulting in widespread famine and/or disease outbreaks up to human migrations (Linthicum et al., 1999; WHO, 2000; Anyamba et al., 2002). Fluctuations in rainfall are a permanent feature in East Africa for at least the past 15,000 years. During the African Humid Period (AHP, 14.8 - 5.5 ka BP, 1 ka = 1000 years before present; e.g., Gasse, 2000) was East Africa covered by large and very deep lakes in the presently almost desiccated area (Fig. 1.2, Fig. 2.2) suggesting a much wetter climate. This wetter climate, however, was also interrupted by several pronounced droughts, and finally terminated some time between 6.6 and 5.0 ka ago (e.g., Gillespie et al., 1973; Johnson and Halfman, 1991; Shanahan et al., 2006; Gasse, 2000; Barker et al., 2004) not without several short-term excursions between then and today towards more humid conditions (e.g., Verschuren et al., 2009; Tierney et al., 2011). Within the last decades East Africa has experienced an intensifying dipole rainfall pattern characterized by anomalous strong precipitation causing floods in the northern and declining amounts over the southern sector (Schreck and Semazzi, 2004).

The large variations in the climatic pattern on different time-scales within this geologically short time period, where only minor tectonic deformation occurred, which could not account for influencing atmospheric circulation systems, has aroused great scientific interest. Numerous research programmes lead to the identification of main forcing mechanisms of East African climate variability, summarized in the following: Present day rainfall in East Africa is generally associated with the latitudinal migration of the Intertropical Convergence Zone (ITCZ) be-

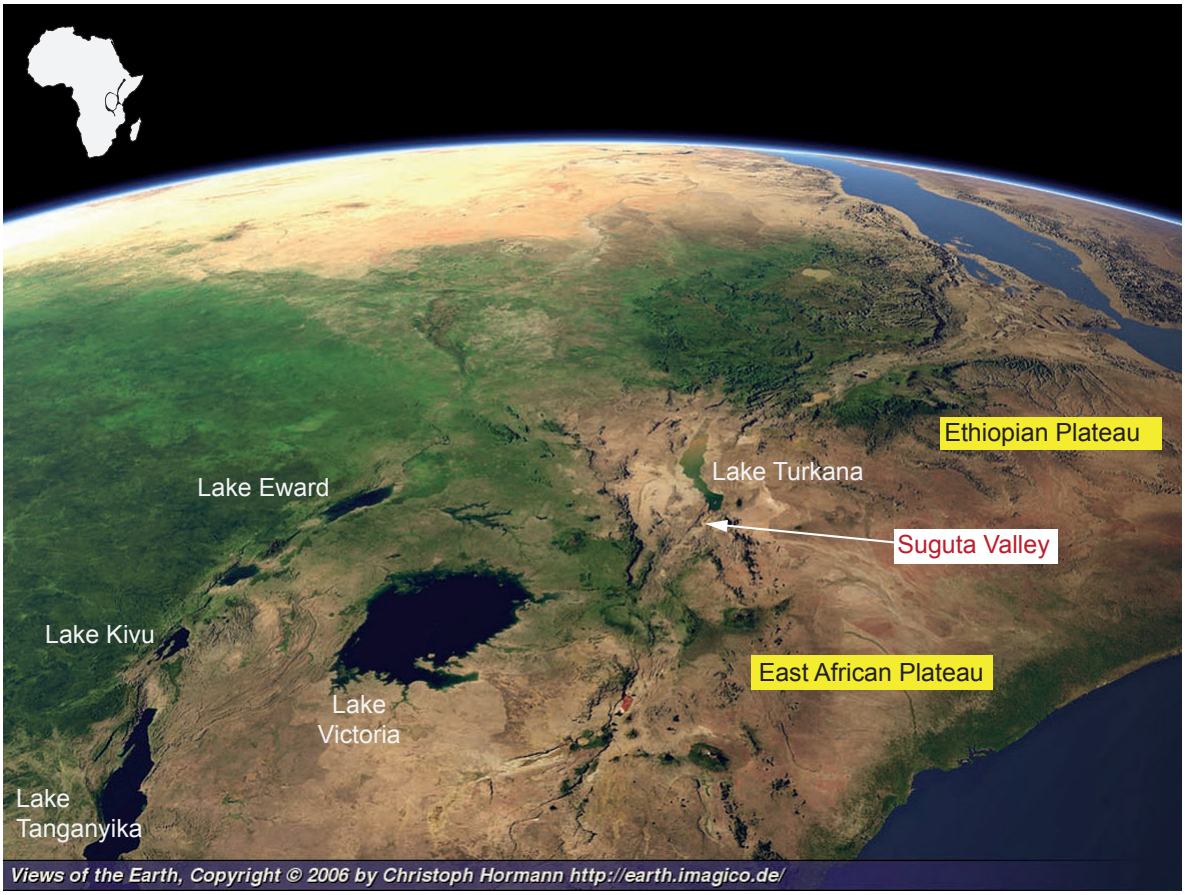

Figure 1.1 Overview Map of the East African Rift System with major lakes and plateaus.

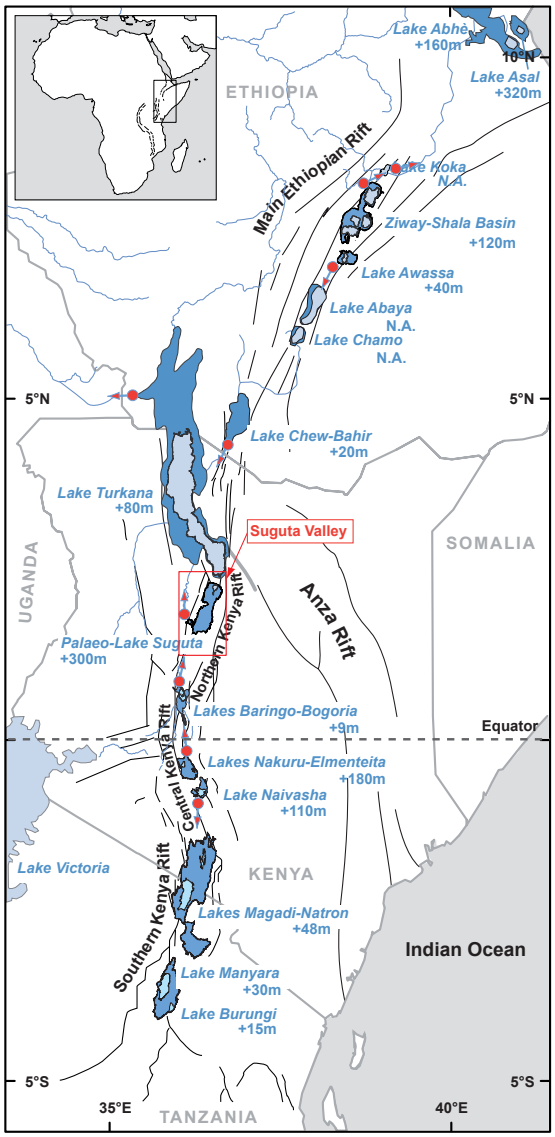

Figure 1.2 Map of equatorial and northern Africa showing the location of the Suguta Valley and important rift valley lakes showing present (light blue) and Early Holocene (dark blue) lake dimension and their related lake depths during the African Humid Period (AHP). Red arrows indicate overflow direction during AHP lake highstands. References: Lake Asal – Gasse and Fontes (1989); Lake Abhé – Gasse (1977); Ziway-Shala – Gillespie et al. (1983); Lake Awassa – Telford et al. (1999); Lake Chew-Bahir – Grove et al. (1975); Lake Turkana – Owen et al. (1982); Palaeo-lake Suguta – Garcin et al. (2009); Lakes Baringo-Bogoria – Tiercelin et al. (1987); Lakes Nakuru-Elmenteita – Richardson & Dussinger (1986); Lake Naivasha – Bergner et al. (2003); Lakes Magadi-Natron – Hillaire-Marcel et al. (1987); Lakes Manyara-Burungi – Casanova (1992) (modified after Garcin et al., 2009).

tween ca. 10° north and south of the equator and associated seasonal eastward shift of the Congo Air Boundary (CAB) over parts of East Africa (Fig. 1.3; Nicholson, 1996; Camberlin, 1997). At present day, significant precipitation anomalies are usually linked with sea-surface temperature (SST) anomalies in the Indian and Pacific Ocean associated with the Indian Ocean Dipole (IOD; Saji et al., 1999; Clark et al., 2003) and the El Niño Southern Oscillation (ENSO; Camberlin et al., 2001; Camberlin and Philippon, 2002) phenomenon. Additionally to these well-known phenomenons was also observed that SST variations in the Atlantic Ocean (Diro et al., 2010a), the quasibiennial circulation (QBO; Indeje and Semazzi, 2000), the Indian summer monsoon strength (ISM; Camberlin, 1997) and regular fluctuations in solar flux (Neff et al., 2001; Wang Y.I. et al., 2005; Kodera et al., 2007; Meehl et al., 2009) also contribute to East African precipitation variations. The current knowledge about climate influencing factors on centennial and millennial time scales is that small perturbations in solar radiation resulted in rainfall fluctuations in central and West-Africa (Stager et al., 2002; Weldeab et al., 2007; Mulitza et al., 2008) and important monsoonal moisture transport to areas of the ISM domain (Neff et al., 2001; Fleitmann et al., 2003; Wang Y.J. et al., 2005). On time scales of ten thousand years, orbital variations account for variations in the thermal contrast between ocean and land masses causing the strengthening of the monsoon systems of India and West-Africa and are explained to have caused the development of large and huge lakes in East Africa (e.g., Kutzbach, J.E., 1985; Street-Perrott, 1985; Barker et al., 2004).

Despite the main forcing mechanisms of climate variability are well identified, their exact influence on regional climate, in particular relative to each other, is intensely debated. As an example, the influence of glacial-interglacial shifts on periodically-increased African aridity relative to low-latitude solar heating (deMenocal, 1995; Trauth et al., 2005), the abrupt vs. gradual onset and termination of the AHP as a linear or nonlinear (threshold-type) response to insolation changes (e.g., deMenocal et al., 2000; Kuper and Kröpelin, 2006), the influence of reduced solar radiation on Little Ice Age climate in East Africa (Verschuren et al., 2000; Thompson et al., 2002), the development and relationship of El Niño Southern Oscillation (ENSO) and IOD (Kodera et al., 2007; Williams and Funk, 2011) and hence future implications for East African climate either turning into a drier or wetter region (Intergovernmental Panel on Climate Change, 2007; Williams and Funk, 2011) are subject of current discussions and topic of many publications. The sources of these scientific controversies are diverse. Crucial to any discussion of contrasting

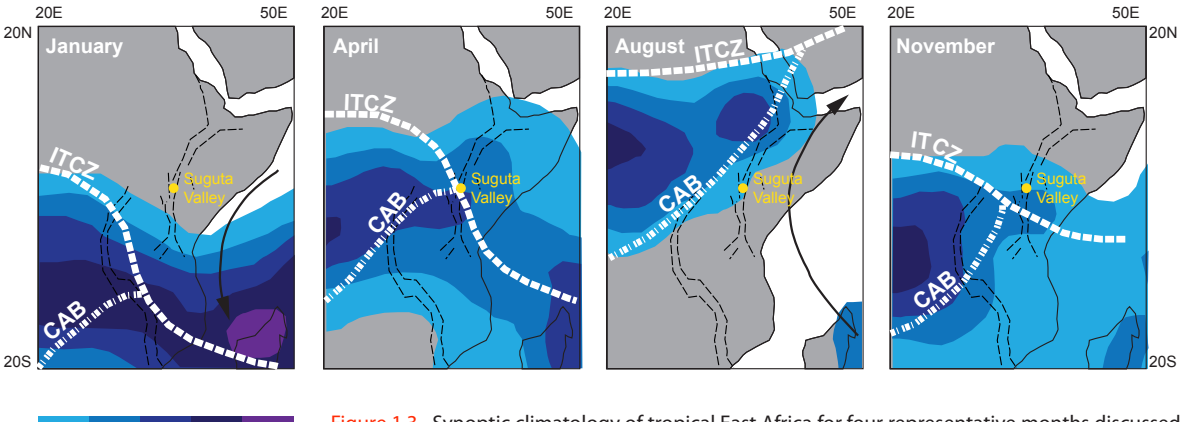

Figure 1.3 Synoptic climatology of tropical East Africa for four representative months discussed in this study. The blue shaded area (contours at 50 mm intervals) explains the seasonal migration of the Intertropical Convergence Zone (ITCZ) and associated rain belts across the studied region. The distribution is based on gauge data over land, and satellite estimates over sea. Dotted white lines show the mean position of the Congo Air Boundary (CAB) and ITCZ. Black dashed line outlines the East African Rift System and yellow numbered dots the studied lake basins. 1-Ziway, 2-Awassa, 3-Abaya, 4-Turkana, 5-Suguta, 6-Baringo, 7-Nakuru, 8-Naivasha, 9-Manyara, 10-Natron, 11-Tana. Rainfall distribution was provided by: http://iridl.ldeo.columbia.edu/maproom/.Regional/.Africa/.Climatologies/Precip_Loop.html (March 2011) and refer to monthly mean data from 1961-1990.

views of climate change is the correct assessment and unambiguous interpretation of available data sets, either in terms of palaeo-climate data contained in marine vs. terrestrial archives and/or as instrumentally recorded data sets in historical times to present times.

In cases of palaeo-climate data sets clear differences exist. Whereas marine palaeo-climate records cover typically very long time periods, integrating a large area of influence but therefore often mask smaller environmental changes, terrestrial records provide a more pristine view of environmental changes. Complications arise in the availability of such necessary terrestrial palaeo-climate data sets in the tropics, as e.g. East Africa. Beside the problem that terrestrial tropics generally lack numerous possibilities for proxy records in contrast to the data-rich middle and high latitudes, the remoteness of regions attractive for climate reconstructions, especially in East Africa, complicate programmes to study past climate change in sufficient spatial coverage to solve some of the controversies described above. One of the few possibilities to study past climate changes in East Africa are provided by lake basins within the East African Rift System (EARS). The eastern branch offers unique conditions for high-resolution studies of African-Asian monsoon variability, since these basins are known to host the so-called amplifier lakes (Street-Perrott, 1985), that react very sensitively to even moderate climate changes due to the combination of a certain morphological basin constitution with steep graben walls and a highly contrasting tropical climate in a catchment of high topography (Olaka et al., 2010; Trauth et al., 2010). The interpretation of proxy records in lake sediments from these basins (and in general), however, is often largely affected by fluctuating sedimentation rates combined with large dating errors in short and discontinuous records often hamper the correlation of environmental changes through time and space (Trauth et al., 2009). Furthermore, geological processes such as faulting or changes in drainage networks often mask climate-related hydrological changes. Dating uncertainties such as distortions in the radiocarbon age of samples derived from a carbon reservoir not in equilibrium with the atmosphere (the so-called reservoir effect) and differing interpretations of climate proxies from lake sediments may also introduce further complications in correlating different archives of past climate change. The detection and consideration of those influencing factors within each record is of major importantance when wishing to contribute to the tackling of existing conundrums.

In **Chapter 2** I present the results of a comprehensive study on early Holocene mega-lake deposits from the remote Suguta Valley in the northern Kenya Rift (Fig. 1.1, Fig. 1.2, Fig. 1.4). The presently desiccated valley was covered by a 300 m deep and 2,200 km^2 large palaeo-lake that was, due to its extreme catch-

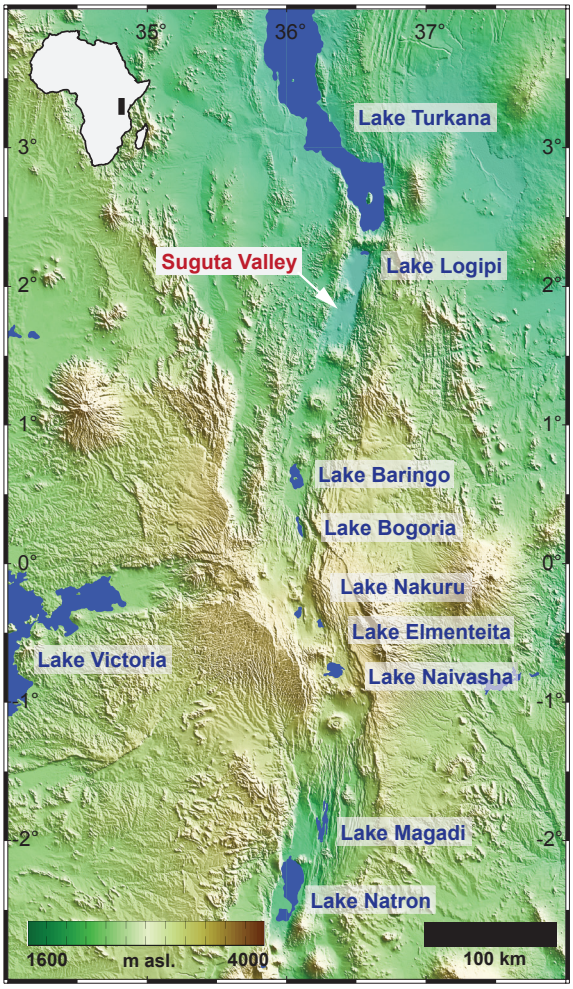

Figure 1.4 Digital Elevation Map of the Kenya Rift System showing the three graben segments, Rift lakes and locationo of the Suguta Valley. (Map was created by C. Strohmeyer).

ment size of 13,000 km^2 and amplifier-lake characteristic, highly sensitive to relatively moderate climate changes, providing a high signal-to-noise ratio of the lacustrine record and shoreline dataset extracted from the palaeo-environmental inventory of the valley. The material for this study was taken and processed by myself during the field campaigns in 2007, 2008 and 2010. Here, I present the methods and results for the first high-resolution ^{14}C-dated, reservoir-corrected, multiproxy lake-level record for East Africa. This record, spanning the time interval from 14.8-5 ka, from a valley located between the West African and Indian monsoon systems, allows me to shed light on current debates about the gradual vs. abrupt onset and termination of the AHP and solve the question about the asynchronicity of high lake levels in equatorial to northern Africa. The results of the study will help to understand in detail the fundamental role of the CAB in rapid lake level fluctuations in the eastern branch of the EARS and how it is related to ISM variabilities. The new investigated method of a combination of shoreline data, lacustrine sediment investigations and the appliance of a hydro-balance model allowed me to define the magnitude of lake-level variations within an amplifier lake system, which might be a good method to be applied elsewhere for lake level studies. The exact estimation of the magnitude of lake-level variations and their natural causes will help to contribute to the current studies about its influence on human expansions, technological innovations and food production. The outcome of this study identifies new linkages between different sectors within the African-Asian monsoon system, and their exact influence on equatorial East Africa's climate, in particular relative to each other. The chapter 2 has been submitted as a manuscript to the journal *Nature* (Junginger and Trauth, subm.).

On historical to present time scales, the application of lake sediments as palaeo-climate archives becomes increasingly problematic due to increasing anthropogenic impact. Lakes are generally sensitive recorders of climate change through the fossil flora and fauna and sedimentary characteristics preserved in their deposits. Increasing human activities in the catchment and lake area, however, alter flora, fauna and sedimentary characteristics concealing environmental changes that were due to natural processes (Hausmann et al., 2002; Lotter and Birks, 1997). Lake sediments as archives for climate change from historical times are consequently often criticized as failing to accurately reflect previous environmental changes (Fritz, 2008).

Chapter 3 presents a collaborative work with two other members of the Graduate School GRK 1364, Kathleen R. Stoof-Leichsenring (Biology, Molecular Genetics) and Lydia A. Olaka (Hydrology, Geomorphology). Kathleen Stoof-Leichsenring and myself have contributed equally to this manuscript accepted by the *Journal of Palaeolimnology* and available online (Stoof-Leichsenring and Junginger et al., in press). This work is about the past 200 years history of Lake Naivasha, one of the very few freshwater lakes in East Africa (Fig. 1.4), during a time where human occupation and therefore influence on lake chemistry progressively increased. The material used for this study was taken from the first

three authors during a field campaign in 2007. The main interest and outcome of this study was a better understanding of the response of diatoms, geochemistry and sedimentary processes in the course of a warmer climate and increasing anthropogenic activities in the catchment. The study discusses hydro-chemical changes, in particular the change in conductivity and phosphorous concentration of the lake water inferred from diatom assemblages (Stoof-Leichsenring) during a changing pattern of sedimentation and geochemistry (organic, inorganic carbon and nitrogen content; Junginger) with regard to a changing climate and the increasing human influences (Junginger, Olaka, Stoof-Leichsenring). The results show that proxy records revealed from lake sediments within times of a changing environment due to human activity can show unexpected developments. It becomes clear that the accurate reconstruction of tropical palaeo-climate of the historical past just on the transition to the era of instrumentally recorded data is therefore only possible, when using lake sediments from remote, anthropogenic unaffected areas.

For the most recent time period, proxy records from lake sediments can be replaced by direct instrumentally measurements of climate parameter. Using direct instrumentally measurements allow the best way to understand the individual influencing factors to a lake basins. However, instrumentally data from East Africa are rare due to the sparse distribution of weather stations. Available data from these stations provide relatively accurate estimates at the geographically position of recording. However, the interpolation of these data in rain-fields over a wide area in tropical regions, where most rainfall has a convective origin with high spatial variability at the daily level exhibit a great deal of uncertainty (Meisner and Arkin, 1987; Dai, 2001). Advancements in spatial and temporal resolutions of remote sensing systems recording today's climate offers possibilities to overcome these uncertainties of interpolation.

Chapter 4 presents a collaborative work with Lydia A. Olaka (Hydrology, Geomorphology), also member of the Graduate School GRK 1364. This on-going study reveals a new concept to obtain seasonal rainfall data from remote areas, which are not equipped with rainfall stations. Here we use rainfall estimates from remotely sensed data to investigate the intraseasonal precipitation variability in the catchments of eleven lake basins from the EARS, namely Ziway, Awassa, Abaya, Turkana, Suguta, Baringo, Nakuru, Naivasha, Natron, Manyara and Tana, for the time period 1996-2010. We intend to provide for the first time insights into the complex interaction of local and regional climatic processes along the topographically complex eastern branch of the EARS (Fig. 1.1) as well as the identification of the governing atmospheric circulation processes leading to intraseasonal rainfall distribution in the investigated lake basins of East Africa. The results of this study shall provide the base for on-going or future studies on these lake basins to better understand governing processes to their lakes and thus proxy-records when reconstructing past climate conditions. This in turn helps to better validate climate models and thus improve reliability for the future predictions (Stute et al., 2001; Donders et al., 2008), important for the inhabitants of East Africa relying entirely on the availability of water for their livelihoods. The manuscript will be submitted to the journal *Climate Dynamics*, when completed.

Figure 1.6 Picture of the seasonal Lake Logipi taken in May 2010 (Photo by A. Junginger). Here an unusual large lake has evolved during the rainy season between March-May.

1.2 The Suguta Valley - a general overview

1.2.1 Geographical setting of the Suguta Valley

The Suguta Valley is part of the East African Rift System (EARS) that extends from the Afar Triangle in the north, over 4,000 km down to Mozambique in the south, cutting throuth the Ethiopian and East African Plateau (Baker & Wohlenberg, 1971; Baker, 1986) (Fig. 1.1). The EARS splits apart at 3°N around the Nyanza Kraton (Achauer & Masson, 2000) into the western branch, which is characterized by large and deep lakes such as Lake Edward or Lake Tanganyika, and the eastern branch that hosts only shallow, mostly alkaline lakes, such as Lake Logipi in the Suguta Valley. The Suguta Valley is located in the Northern Kenya Rift, which is part of the eastern branch on the East African Plateau. The Kenya Rift (KR) presents one of the most spectacular topographic expressions of active continental extension with a length of about 500 km, a width of 60 - 80 km, and an average cross-sectional relief of more than 1,000 m (Fig. 1.4). It consists of the Turkana and Kenya rift zones (Bosworth and Strecker, 1997; Bosworth et al., 2003) and broadly follows the boundary between the Proterozoic Mozambique Belt and the Archaean Tanzania Craton (Smith and Mosley, 1993; Hetzel and Strecker, 1994). Due to striking, the KR can be subdivided into the two NNE trending northern and southern branches, which have mean rift floor elevations of around 300 m asl., and the NNW trending central KR, which is characterized by mean elevations of the rift floor of around 1800 m asl. All three segments have halfgraben geometries due to earlier faulting and pronounced subsidence along their western boundary faults (Chapman et al., 1978; Crossley, 1979; Roessner and Strecker, 1997).

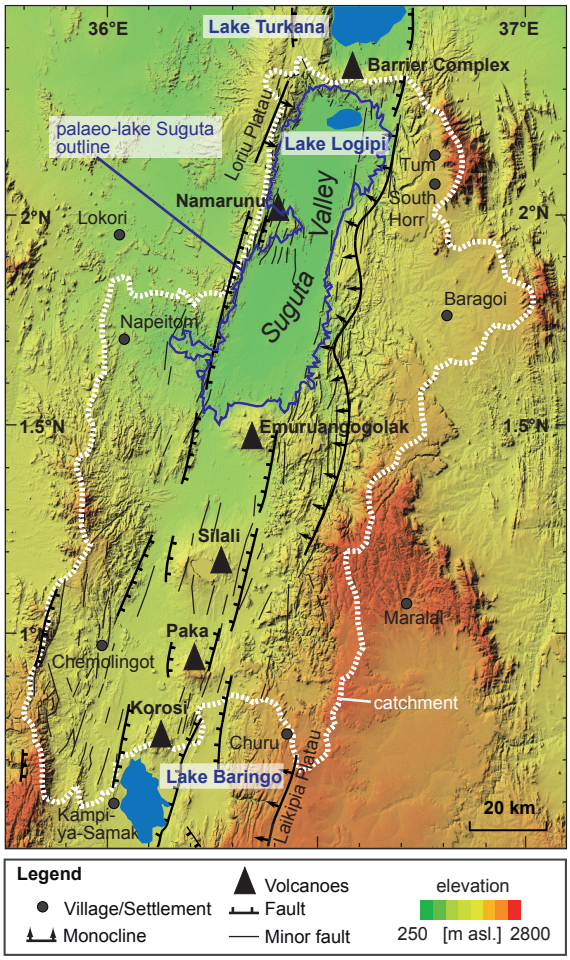

Figure 1.5 Digital Elevation Map of the catchment of the Suguta Valley. (Map was created with the program RIVERTOOLS).

The Suguta Valley is part of the NNE trending northern Kenya Rift, where Quaternary volcanism, faulting, and coeval sedimentation processes are ubiquitous (Garcin et al., 2009). The Suguta Valley has a N-S extension of 100 km (1.5°N - 2.4°N) and a varying E-W width between 10 – 25 km (36.1°E - 36.7°E). The catchment area of 13,000 km^2 is about 200 km long (0.6°N - 2.4°N) and has a width of 50 km (35.8°E - 37.0°E) (Fig. 1.5). It is bounded to the south by the Korosi Volcano Complex, which separates the catchment of the Suguta Valley and Lake Baringo, and to its north by the Barrier Volcanic complex that separates Lake Turkana and Lake Logipi (Fig. 1.6). The western boundary of the asymmetric graben structure is delimited by a major border fault system (750 m asl.), and to the east by a series of smaller fault-bounded escarpments, which are part of a westward dipping monocline, that reaches elevations of 1100 m asl. (Baker, 1963; Dodson, 1963; Makinouchi et al., 1984; Dunkley et al., 1993). The valley floor has a marked northward gradient starting from 1000 m asl. in the area of Lake Baringo to 275 m asl. at Lake Logipi, which constitutes the lowest sector of the Kenya Rift and Eat African Plateau (Fig. 2.2 see page 42). Lake Logipi is an alkaline lake, 0.5 – 5 m deep and primarily fed by the only perennial 175 km long Suguta River (Fig. 1.7), ephemeral streams from flanks during rainy seasons, and a possible seepage from Lake Turkana, as well as hot springs along the volcano-tectonic axis (Casanova et al., 1988; Castanier et al., 1993). The lake is highly seasonal and dries up very quickly every year (Fig. 1.6, Fig. 2.6 see page 49).

1.2.2 Geological development of the Suguta Valley

The development of the Suguta Valley is closely related to the geological origination of the Kenya Rift, which is described in detail for example by Baker & Wohlenberg (1971) and Chorowicz (2005). Although a depression has already existed since the Miocene (Matsuda et al., 1984; Williamson and Savage, 1986; Saneyoshi et al., 2006), the main onset of the relief development of the Suguta Valley started between 3 and 1.8 Ma ago (Truckle, 1976; Dunkley et al., 1993) (Fig. 1.8). Antithetic faulting and basin-ward tilting with coeval land slipping at the rift margins took place, accompanied with the generation of an active volcano-tectonic axis (Dunkley et al., 1993). The large trachyte shield volcano Emuruangogolak in the South of the Suguta Valley started to be volcanically active between 1.3 and 0.5 Ma ago (Weaver, 1977; Dunkley et al., 1993). The generation of the northern Barrier volcano complex (Champion, 1935), and thus the initiation of the hydrological isolation of the Suguta Valley from the Turkana basin, began also 1.3 Ma ago. However, the Suguta Valley became finally hydrologically isolated when the Kakorinya volcano was constructed on the Barrier between 0.2-0.1 Ma ago (Dunkley et al., 1993) (Fig. 1.10). In the center of the main depression, the renewal of the Pliocene Namarunu volcano occurred 0.8 Ma ago (Dunkley et al., 1993). A geological map is provided in chapter 2 Figure 2.11 see page 56.

During the tectonic and topographic development of the Suguta Valley, several fluvio-lacustrine episodes highly valuable for palaeo-climatic stud-

ies were recorded in the valley. The oldest lacustrine sediments found in the Suguta Valley are of Miocene age and occur as highly consolidated coloured sediments in the southeastern part of the valley (Fig. 1.10) and are described by Pickford (1984). Evidences for younger lake episodes, when the valley was more developed, occur largely as finely laminated diatomites often covered by basaltic lava flows (Fig. 1.11). These lake episodes have an age of around 0.8 Ma (Dunkley et al., 1993). Investigations on these sediments are in progress and subject of a post-doctoral project. Indications for humid periods at 400 ka, 130 ka, 80 ka, 60 ka and 35 ka ago come from a study about enhenced hydrothermal activity on volcano flanks in the catchment of the Suguta Valley (Sturcio et al., 1993).

The most recent humid period, recorded in the Suguta Valley, started 15 ka ago and lasted until 5 ka (Garcin et al., 2009; Junginger and Trauth, subm.). Evidence from this period are best preserved, since geological modifications of the valley have been minor over the past 15,000 years. This lake episode is documented by shorelines and unconsolidated sediments (Fig. 1.12, Fig. 2.6 see page 49) proposing a palaeo-lake of ~300 m depth that has covered the 100 km long and ~25 km wide basin (Fig. 1.5; Garcin et al., 2009; Junginger and Trauth, subm.) surpassing first estimations from prior investigations on this lake episode by Truckle (1976), Sturcio et al. (1993) and Casanova (1988).

There are also indications from shorelines, that the Medieval Warm Period was humid in Northern Kenya (Junginger and Trauth, subm.). The modern Suguta Valley is essentially dry, except for the northernmost sector of the valley, which is covered by the shallow Lake Logipi. Due to climatic variability this lake may grow considerably in extent as proposed by the occurrence of lacustrine sediments and shorelines. How fast this lake can grow will be discussed in chapter 2.

1.2.3 Present climate in the Suguta Valley

East Africa in general is considered to be one of the meteorological most complex parts of Africa due to the interaction of highly variable topography, large inland water bodies and maritime influence with several convergence zones, producing rapid changes of the climate pattern over short distances (Nicholson, 1996). The general climate in equatorial East Africa, however, is controlled by the yearly latitudinal migration of the ITCZ between the equator and 10° north and south, following the maximum insolation with a time lag of 4-6 weeks (Nicholson, 1996; Fig. 1.3). This migration produces a bimodal precipitation cycle along the equator with „long rains“ in March-May and „short rains“ in October-November. Precipitation is associated with the ITCZ which has its origin in large-scale moist advection from the Indian Ocean (Levin et al., 2009). Additionally precipitation receive the western parts of equatorial East Africa when the northern most position of the ITCZ allows the southwestern humid Congo air stream associated with the West-African monsoon to reach parts of East Africa (Fig. 1.3; Nicholson, 1996, Camberlin, 1997). Moisture associated with the humid Congo air stream has its origin in the Atlantic and is recycled over the Congo basin (Nicholson, 1996). This unstable flow from the Atlantic converges with drier air masses from the Indian Ocean along a north-south-trending zone known as the Congo Air Boundary (CAB). The timing and strength of the ITCZ and CAB control the seasonal

Figure 1.7 Picture of the Suguta River in the central Suguta Valley (Photo by A. Junginger).

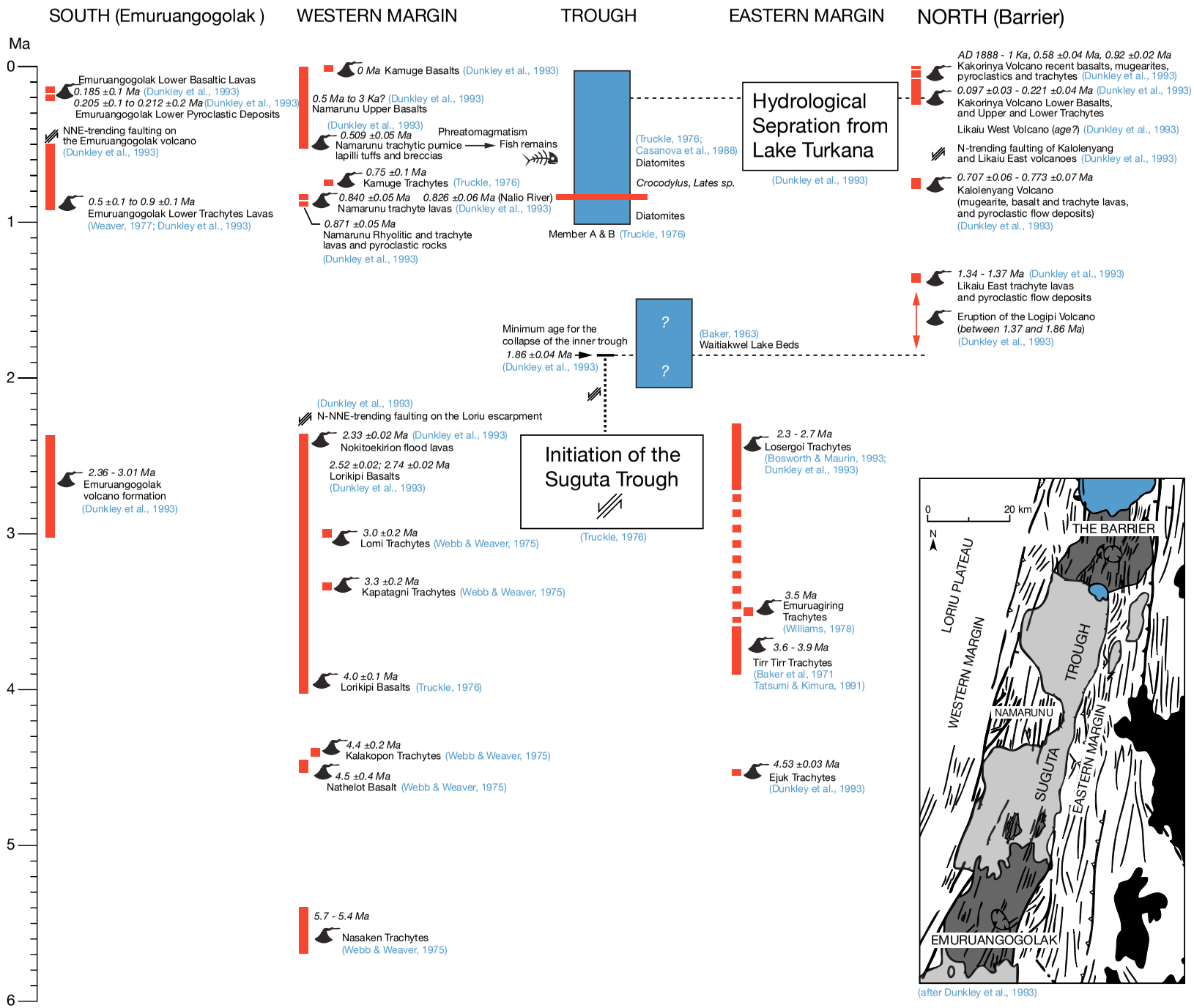

(after Dunkley et al., 1993)

Figure 1.8 Geological development of the Suguta Valley between 6-1 Ma. Grey bar indicates extra Figure for the geological and hydrological development over the past 200 ka displayed in Figure 1.8. (Figure was first created by Y. Garcin and later modified).

distribution of rainfall in East Africa. In contrast, the months during the Indian summer and winter monsoons, are generally dry in equatorial East Africa (Nicholson, 1996). Present precipitation anomalies are regarded to be highest in East Africa during November/December and linked to Indian Ocean SSTs anomalies attributed to IOD/ENSO with intensified rains during high SSTs in the western Indian Ocean and vice versa (Nicholson, 1996; Saji et al., 1999).

The Suguta Valley marks the most arid environment in Kenya (Ojany and Ogenoo, 1973). Dunes and a sparse vegetation coverage of xerophytic plants in the center of the valley underscore the arid character of Suguta. A sparse grass cover (*Gramineae, Cyperaceae*) and Palm trees (*Hyphaene*) support the wide flood plain of the valley floor. With rising altitude the vegetation changes to more developed deciduous trees dominated by Acacia, Commiphora, Hyphaene palms, Salvadora and small euphorbias (Hemming, 1972; Vincens, 1982). Limited available data on climate conditions propose for the centre of the Suguta Valley mean yearly rainfall amounts of less than 500 mm yr^{-1} and mean temperatures of 30°C (Appendix 01 see page 138). Temperatures can reach occasionally more than 50°C in the northern part of the Suguta Valley (Dunkley et al., 1993), which explains very high evaporation rates of ca. 4000 mm yr^{-1} (Morgan, 1971). A general decrease in precipitation and increase in temperatures occurs from the higher elevated parts in the south around Lake Baringo to the flat areas in the north (Fig. 1.13). The seasonal distribution of precipitation and temperature as displayed in Figure 1.13 demonstrates the generally bimodal cycle with rainfall peaks in April-May, as well as in October-November for the Suguta Valley, whereas the higher elevated catchments show generally higher precipitation throughout the year with indications for a bimodal pattern. The southwestern part of the catchment appears temporarily to be influenced by the humid Congo airstream during August.

1.2.4 Climate variability in East Africa

Environmental instabilities in East Africa are known to be caused directly by the interaction between tectonic movements forming the EARS and associated plateaus, orbitally driven changes in insolation and variations in total solar irradiance (Kutzbach and Street Perrott, 1985; Nicholson, 1996; Verschuren et al., 2000; Trauth et al., 2003; Barker et al., 2004; Sepulchre et al., 2006). Indirectly, the uplift of the Tibetan plateau and the associated generation of the African-Asian monsoon system, orbitally driven glacial-interglacial cycles and sea surface temperature variations driven by ocean-atmosphere phenomenon such as the Indian Ocean Dipole (IOD) and the El Niño/Southern Oscillation (ENSO) are remote influences on environmental changes of East Africa (e.g., Kutzbach and Street-Perrott,1985; Saji et al., 1999; Schreck and Semazzi, 2004).

Figure 1.10 Picture of colourful Miocene sediments from the Suguta Valley often creating palaeo-valleys providing accomodation spaces for Holocene lake sediments (grey material) (Photo A. Junginger).

On orbital time scales, the East African climate responds to variations in insolation resulting from Earth's orbital precession every 23-19 kyrs (Rossignol-Strick, 1983; Kutzbach and Street-Perrott, 1985; Clemens & Prell, 1991). Insolation controls the strength of the monsoon circulation through the differential heat capacity of land and oceans and fuels the large-scale convective overturning in the tropics (Kutzbach and Street-Perrott, 1985). Between 15 and 5 ka BP, enlarged lakes in many East African lake basins such as Lake Asal (+320 m) (Gasse and Fontes, 1989); Lake Abhé (+160 m) (Gasse et al., 1977), Lake Ziway (+112 m) (Gillespie et al., 1983), Lake Turkana (+80 m) (e.g., Owen et al., 1982; Johnson & Halfman, 1991; Brown & Fuller, 2008), Lake Suguta (+295 m) (Garcin et al., 2009), Lakes Elmenteita-Nakuru (+180 m) (Washbourn-Kamau, 1970; Richardson & Dussinger, 1986) or Lake Naivasha (+110 m) (Bergn-

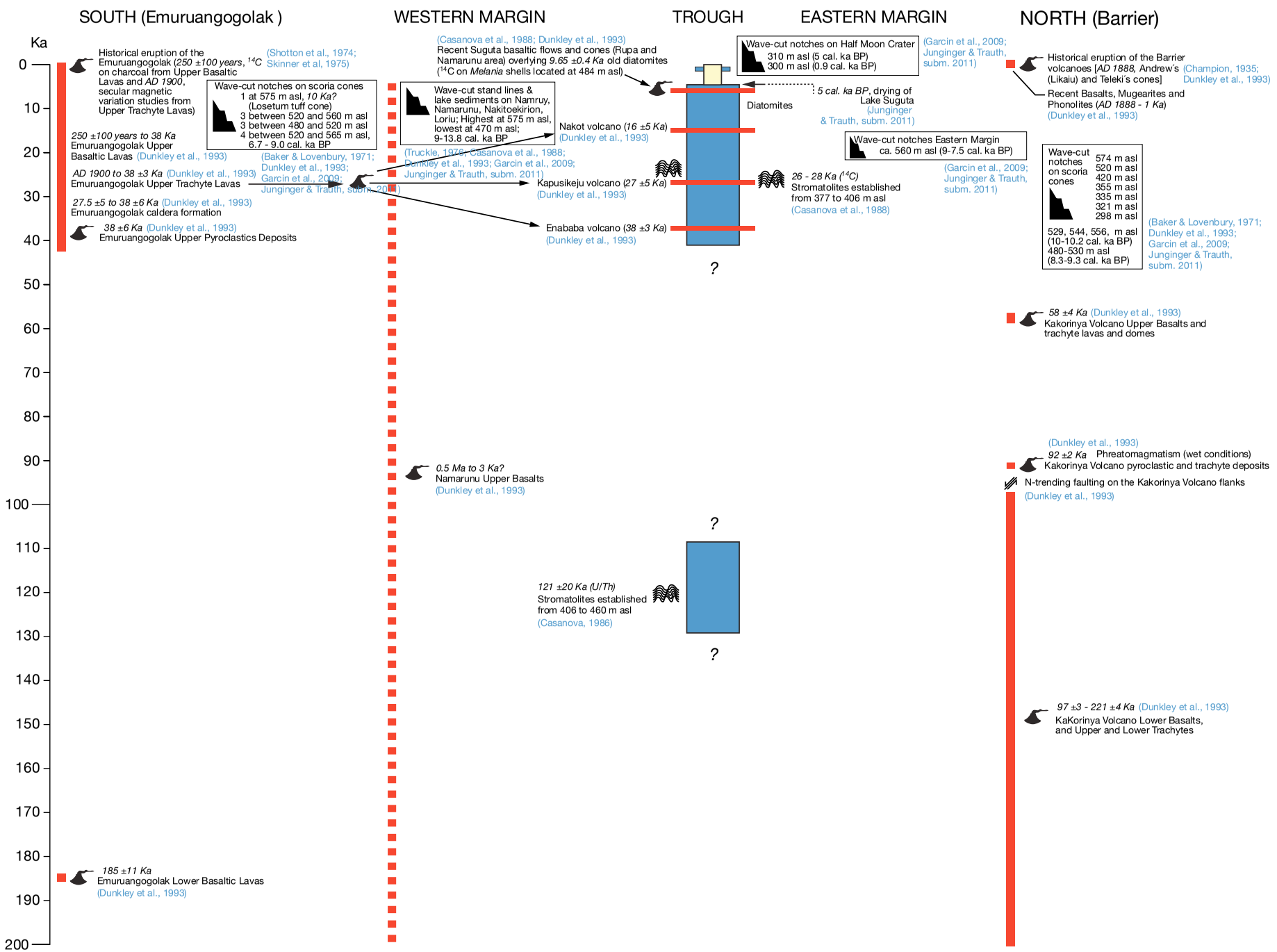

Figure 1.9 Geological and hydrological development of the Suguta Valley for the last 200 ka. (Figure was first created by Y. Garcin and later completed with new results from this thesis).

Figure 1.11 Picture of Mid-Pleistocene lacustrine sediments covered by basaltic lava flows. Lacustrine sediments mainly consist of laminated diatomites (insert). (Photo A. Junginger).

er et al., 2003) have been reported, whereas most basins today host relatively shallow and highly alkaline lakes (e.g., Gasse, 2000; Barker et al., 2004) (Fig. 1.2). This period of enhanced humidity is known as the African Humid Period (AHP) (e.g., Gasse, 2000; Barker et al., 2004). A maximum Northern Hemisphere June-July insolation, that has caused the strengthening of the Indian summer monsoonal (ISM) circulation, has been proposed as a potential mechanism to explain this phenomenon. However, in chapter 2 of this doctoral thesis I will present a hypothesis, how the a stronger ISM can have produced large lakes in the East African Rift, since nowadays the months during the ISM are dry in equatorial East Africa.

Beside the precessional forced enhanced insolation, other mechanisms seem to have influenced the tropical African climate as indicated by climate-proxy data from Africa that do not closely follow the gradual increase in summer insolation during the late Pleistocene-early Holocene and its subsequent gradual decrease during the mid-Holocene (Kutzbach and Street-Perrott, 1985). The abruptness of the onset and termination of the AHP and associated environmental shifts therefore is a matter of debate (e.g., deMenocal et al., 2000; Kröpelin et al., 2008; Brovkin and Claussen, 2008; deMenocal, 2008; Cole et al., 2009; Chase et al., 2010).

Also intensely debated is the relative importance of extra tropical high-latitude glacial shifts and reduced thermohaline circulation during Heinrich and Younger Dryas (YD) events during that time interval (Trauth et al., 2003; Brown et al., 2007; Tierney et al., 2008; Garcin et al., 2009; Stager et al., 2011). An abrupt brief return into full-glacial conditions in the Northern Atlantic region such as during the YD between 12.8 – 11.6 ka BP influenced the hydrological budget in tropical East Africa (e.g., Gasse, 2000; Barker et al., 2004). Several African lakes have re-

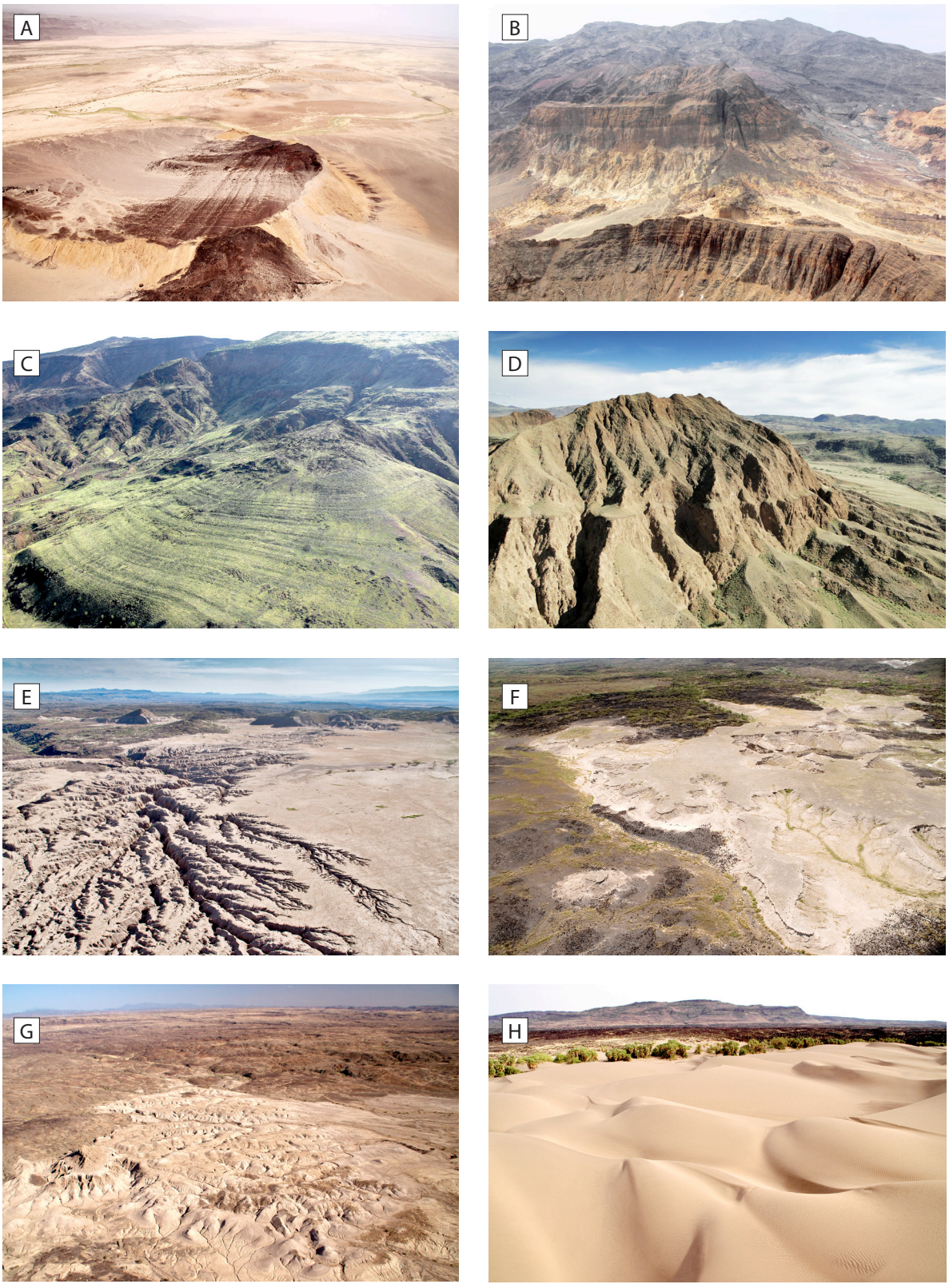

Figure 1.12 Well-developed wave cut notches (A-D) in an absolutely desiccated present Suguta Valley (E) and extensive outcrops of lacustrine sediments (F-G), partly even associated with former shorelines, indicate the existence of a palaeo-lake Suguta surpassing all other lakes during the African Humid Period. (Photos by A. Junginger (A, E-H); M. Trauth (D); D. Melnick (B,C))

corded a pronounced lake level drop or even dried out during this time (Gillespie et al, 1983; Street-Perrott and Perrott, 1990; Talbot and Johannessen, 1992; Williamson et al., 1993; Gasse, 2000; Shanahan et al., 2006).

Additionally, abrupt dry intervals interrupted the AHP, in particular at ca. 8.5 ka BP as well as at 4-3.5 ka BP (Telford and Lamb, 1999; Lamb et al., 2000; Chalié and Gasse, 2002). The nature and causes of such events are fragmentary and underscore the need of well-dated high-resolution records, especially in the current debate of a prominent role of the tropics in global climate change (Henderson and Slowey, 2000, Trauth et al., 2003).

Fluctuations within decades as proposed by Vershuren et al. (2000) for the last millennium, correlate with long-term changes in solar radiation suggesting that decadal-scale rainfall variations are largely controlled by solar forcing. Other records of East African climate changes during the last millennium illustrate spatial complexity of environmental changes on relatively short time scales. How solar variation affect large lakes in equatorial East Africa during a precession minimum and associated insolation maximum is going to presented in chapter 2.

1.2.5 The Suguta Valley and its importance for palaeo-climatic studies

The geographical-climatological location of the remote, unhabited Suguta Valley provides unique conditions to contribute to unresolved relationships between topography, climate variability and human expansion in East Africa over the past 15,000 years. The Suguta Valley is located at the northern base of the East African Plateau (Fig. 2.1 see page 41), with a catchment of ca. 13,000 km^2 draining a climatologically relatively homogeneous domain, characterized by a pure tropical equatorial region, in contrast to the nearby equatorial Lake Turkana that receives a mixed summer monsoonal, tropical equatorial climate signal due to its 130,000 km^2 large catchment expanding over ca. 900 km in North-South direction towards the Ethiopian Plateau. It has been proposed that the Suguta Valley belongs to a so called Amplifier Lake Basin, that are known to provide valuable

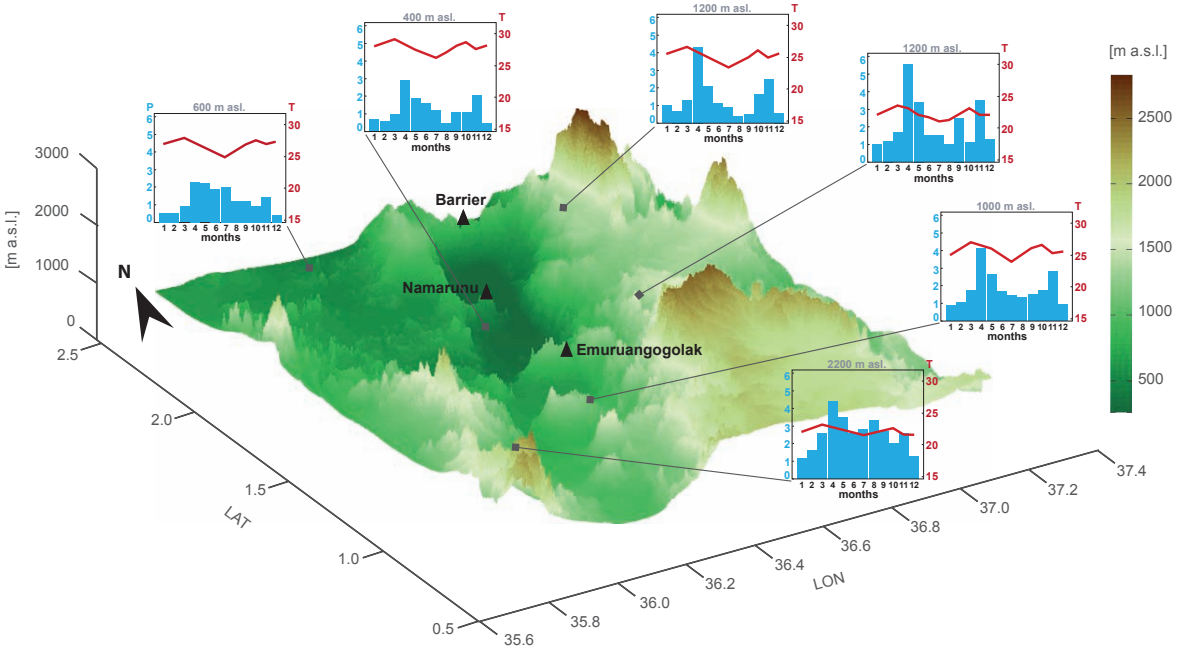

Figure 1.13 3D Map of the Suguta Valley with the seasonal distribution of precipiation and temperature demonstrating a generally bimodal cycle with rainfall peaks in April-May, as well as in October-November. Higher elevated catchments show generally higher precipitation throughout the year with indications for a bimodal pattern. The southwestern part of the catchment appears temporarily to be influenced by the humid Congo airstream during August. (http://iridl.ldeo.columbia.edu/maproom/.Regional/.Africa/.Climatologies/Precip_Loop.html) (February 2011).

accommodation areas for lake sediments especially useful for the detection of minor climate variability since they react very sensitively to even moderate climate changes (Olaka et al., 2010, Trauth et al., 2010). The characteristics for Amplifier Lake Basins are a climate distribution with high precipitation in the higher elevated parts of the catchment and high evaporation along the basin floor in combination with a pronounced u-shaped basin morphology with steep graben walls (Fig. 1.13). The amplifier lake characteristics of the Suguta Valley and its geographical-climatological location between the West-African and Indian monsoon systems make the valley an ideal place for detecting even moderate changes in the intensity of the two monsoon systems at least over the past 15,000 years. This is particularly true since the amplitude of lake-level variations considered within this work (10^1-10^2 m, see chapter 2) are generally one order of magnitude larger than typical displacements of sediments and shorelines by faulting in the tectonically active valley (Garcin et al., 2009, less than 10^2 m). The amplification effect of the graben morphology with steep walls and flat bottoms, in combination with extreme climate contrasts within the catchment ranging from humid mountainous regions (<1,500 mm mean-annual precipitation, Appendix 01 see page 138) to the arid valley (~4,000 mm evaporation) guarantee high signal-to-noise ratios of the extracted climate information as compared with the climate time-series extracted from crater lakes with small catchments (<10 km^2, Olaka et al., 2010).

1.3 References

Achauer, U. & Masson, F. Seismic tomography of continental rifts revisited: from relative to absolute heterogeneities. *Tectonophysics* 358, 17-37 (2000).

Anayamba, A., Tucker, J.C., and Mahoney, R. From El Nino to La Nina: Vegetation Response Patterns over East Africa and Southern Africa during the 1997-2000 Period. *J. Climate* 15, 3096-3103 (2002).

Baker, B.H. Geology of the Baragoi area. Geological Survey of Kenya, *Report* 53, Nairobi, 74 pp (1963).

Baker, M.J. & Lovenbury, H.T. The South Turkana Expedition: Scientific Papers VII: The 1969 Season Survey. *Geogr. J.* 137, 349-360 (1971).

Baker, B.H. & Wohlenberg, J. Structure and evolution of the Kenya Rift Valley. *Nature* 229, 538-542 (1971).

Baker, B.H. Tectonics and volcanism of the southern Kenya Rift Valley and its influence on rift sedimentation. In: FROSTICK, L.E. et al. (Eds), *Sedimentation in African Rifts*. *Geological Society of America – Special Publication* 25, 45-57 (1986).

Barker, P.A. et al. In: *Past Climate Variability through Europe and Africa* (eds Battarbee, R.W., Gasse, F., Stickley, C.E.) 117-138 (Kluwer Academic Publishers, 2004).

Bergner, A.G.N., Trauth, M.H. & Bookhagen, B. Paleoprecipitation estimates for the Lake Naivasha Basin (Kenya) during the last 175 k.y. using a lake-balance model. *Global Planet. Change* 36, 117-136 (2003).

Bosworth, W., Burke, K., Strecker, M. Effects of stress fields on magma chamber stability and the formation of collapse calderas. *Tectonics* 22/4, 1042, doi:10.1029/2002TC001369 (2003).
Bosworth & Maurin, 1993

Bosworth, W. & Strecker, M.R. Stress field changes in the Afro-Arabian rift system during the Miocene to recent period. *Tectonophysics* 278, 47-62 (1997).

Brovkin, V. & Claussen, M. Comment on "Climate-Driven Ecosystem Succession in the Sahara: The Past 6000 Years". *Science* 322, 1326b-c (2008).

Brown, E.T., Johnson, T.C., Scholz, C.A., Cohen, A. S. King, J. W. Abrupt change in tropical African climate linked to the bipolar seesaw over the past 55,000 years. *Geophys. Res. Lett.* 34, L20702 (2007).

Brown, F.H. & Fuller, C.R. Stratigraphy and tephra of the Kibish Formation, southwestern Ethiopia. *J. Hum. Evol.* 55, 366-403 (2008).

Camberlin, P. & Philippon, N. The east African March-May rainy season: associated atmospheric dynamics and predictability over the 1968-97 period. *J. Clim.* 15, 1002-1019 (2002).

Camberlin, P., Janicot, S., and Poccard, I. Seasonality and atmospheric dynamics of the teleconnections between African rainfall and tropical sea-surface temperature: Atlantic vs. ENSO. *Int. J. Climatol.* 21, 973-1005 (2001).

Camberlin et al., 1997, Rainfall anomalies in the source region of the Nile and their connection with the Indian summer monsoon, *J. Climate* 10, 1380-1392 (1997).

Casanova, J. & Hillaire-Marcel, C. Chronology and Paleohydrology of Late Quaternary High Lake Levels in the Manyara Basin (Tanzania) from Isotopic Data (^{18}O, ^{13}C, ^{14}C, Th/U) on Fossil Stromatolites. *Quaternary Research* 38, 205-226 (1992).

Casanova, J., Hillaire-Marcel, C., Page, N., Taieb, M., Vincens, A. Palaeohydrology and Late Quaternary stratigraphy of lacustrine deposits in the Suguta Rift (Kenya). *C. R. Acad. Sci. Paris Sér.* II 307, 1251–1258, (1988).

Castanier, S., Bernet-Rollande, M.-C., Maurin, A., Perthuisot, J.-P. Effects of microbial activity on the hydrochemistry and sedimentology of Lake Logipi, Kenya. *Hydrobiologia* 267, 99–112 (1993).

Chalié, F. & Gasse, F. Late Glacial-Holocene diatom record of water chemistry and lake level change from the tropical East African Rift Lake Abiyata (Ethiopia). *Palaeogeogr. Palaeoclimatol. Palaeoecol.* 187, 259-283 (2002).

Champion, A.M. Teleki's volcano and the lava fields at the southern end of Lake Rudolf. *Geogr. J.* 85, 323–

336 (1935).

Chapman, G.R., Lippard, S.J., Martyn J.E. The stratigraphy and structure of the Kamasia Range, Kenya Rift Valley, *Journal of the Geological Society, London* 135, 265-281 (1978).

Chorowicz, J. The East African rift system. *J. Afr. Earth Sci.* 43, 379-410 (2005).

Clark, C.O., Webster, P.J., and Cole, J.E. Interdecadal Variability of the Relationship between the Indian Ocean Zonal Mode and East African Coastal Rainfall Anomalies. *Journal of Climate* 16, 548-554 (2003).

Clemens, S.C. & Prell, W.L. Late Quaternary forcing of Indian Ocean summer-monsoon winds: a comparison of Fourier model and circulation model results. *J. Geophys. Res.* 96 (12), 22683-22700 (1991).

Cole, J.M., Goldstein, S.L., deMenocal, P.B., Hemming, S.R., Grousset, F.E. Contrasting compositions of Saharan dust in the eastern Atlantic Ocean during the last deglaciation and African Humid Period. *Erth. Planet. Sci. Let.* 278, 257–266 (2009).

Crossley, R. The Cenozoic stratigraphy and structure of the western part of the rift valley, southern Kenya. *Journal of the Geological Society, London* 136, 393-405 (1979).

Dai, A. Global precipitation and thunderstorm frequencies. Part II: Diurnal variations. *J. Clim.* 14, 1112–1128 (2001).

deMenocal, P.B. Africa on the edge. *Nature Geoscience* 1, 650-651 (2008).

deMenocal, P., Ortiz, J., Guilderson, T., Adkins, J., Sarnthein, M., Baker, L., Yarusinsky, M. Abrupt onset and termination of the African Humid Period: rapid climate responses to gradual insolation forcing. *Quat. Sci. Rev.* 19, 347-361 (2000).

deMenocal, P.B.Plio-Pleistocene African climate. *Science* 270, 53-59 (1995).

Diro, G.T., Grimes, D.I.F., and Black, E. Teleconnections between Ethiopian summer rainfall and sea surface temperature: part I – observation and modeling. *Clim. Dyn.* DOI 10.1007/s00382-010-0837-8 (2010a).

Dodson, R.G. Geology of the South Horr area. Geological Survey of Kenya, *Report* 60 (1963).

Donders, T.H., Wagner-Cremer, F., and Visscher, H. Integration of proxy data and model scenarios for the mid-Holocene onset of modern ENSO variability. *Quat. Sci. Rev.* 27, 571-579 (2008).

Dunkley, P.N., Smith, M., Allen, D.J. & Darling, W.G. The Geothermal Activity and Geology of the Northern Sector of the Kenya Rift Valley. British Geological Survey Research, *Report* SC/93/1, 185pp., NERC, Nottingham (1993).

Fleitmann, D. et al. Holocene Forcing of the Indian Monsoon Recorded in a Stalagmite from Southern Oman. *Science* 300, 1737-1739 (2003).

Fritz S.C. Deciphering climatic history from lake sediments. *J. Paleolimnol.* 39, 5-16 (2008).

Garcin, Y. et al. Late Pleistocene-Holocene rise and collapse of Lake Suguta, northern Kenya Rift. *Quat. Sci. Rev.* 28, 911-025 (2009).

Gasse, F. Evolution of lake Abhé (Ethiopia and TFAI) from 70,000 b.p. *Nature* 265, 42-45 (1977).

Gasse, F. & Fontes, J.-C. Palaeoenvironments and Palaeohydrology of a tropical closed lake (Lake Asal, Djibuti) since 10,000 yr B.P. *Palaeogeogr. Palaeoclimatol. Palaeoecol.* 69, 76-102 (1989).

Gasse, F. Hydrological changes in the African tropics since the Last Glacial Maximum. *Quat. Sci. Rev.* 19, 189-211 (2000).

Gillespie, R., Street-Perrott, F.A. & Switsur, R. Postglacial arid episodes in Ethiopia have implications for climate prediction. *Nature* 306, 680-683 (1983).

Grove, A.T., Street, F.A. & Goudie, A.S. Former Lake Levels and Climatic Change in the Rift Valley of Southern Ethiopia. *The Geographical Journal* 141/2, 177-194 (1975).

Hausmann. S. et al. Interactions of climate and land use documented in the varved sediments of Seebergsee in the Swiss Alps. *Holocene* 12, 279-289

(2002).

Chase, B.M., Meadows, M.E., Carr, A.S. & Reimer, P.J. Evidence for progressive Holocene aridification in southern Africa recorded in Namibian hyrax middens: Implications for African Monsoon dynamics and the "African Humid Period". *Quaternary Research* 74, 36–45 (2010).

Hemming, C.F. The South Turkana Expedition: Scientific Papers VIII: The ecology of South Turkana: a reconnaissance classification. *Geogr. J.* 138, 15–40 (1972).

Henderson, G.M. & Slowey, N.C. Evidence from U-Th dating against Northern Hemisphere forcing of the penultimate deglaciation. *Nature* 404, 61-66 (2000).

Hetzel, R. & Strecker, M.R. Late Mozambique Belt structures in western Kenya and their influence on the evolution of the Cenozoic Kenya Rift. *J. Struct. Geol.* 16/2, 189-201 (1994).

Hillaire-Marcel, C. & Casanova, J. Isotopic hydrology and paleohydrology of the Magadi (Kenya)-Natron (Tanzania) basin during the Late Quaternary. *Palaeogeogr. Palaeoclimatol. Palaeoecol.* 58 , 155-181 (1987).

Indeje M., Semazzi, F. H. M. & Ogallo, L. J. ENSO signals in East African rainfall seasons. International *Journal of Climatology* 20, 19-46 (2000).

Intergovernmental Panel on Climate Change. The IPCC 4th Assessment Report, Climate Change 2007: *Synthesis Report* (2007).

Johnson, T.C., Halfman, J.D. & Showers, W.J. Paleoclimate of the past 4000 years at Lake Turkana, Kenya, based on the isotopic composition of authigenic calcite. *Palaeogeogr. Palaeoclimatol. Palaeoecol.* 85, 189-198 (1991).

* Junginger, A. & Trauth, M.H. Solar Variations and Holocene East African Climate. subm. to *Nature*, (2011).

Kodera, K., Coughlin, K., and Arakawa, O. Possible modulation of the connection between the Pacific and Indian Ocean variability by the solar cycle. *Geophys. Res. Lett.* 34, L03710, doi:10.1029/2006GL027827 (2007).

Kröpelin, S., et al. Climate-Driven Ecosystem Succession in the Sahara: The Past 6000 Years. *Science*, 320, 765-768 (2008).

Kuper, R. & Kröpelin, S. Climate-controlled Holocene occupation in the Sahara: motor of Africa's evolution. *Science* 313, 803-807 (2006).
Kutzbach, J.E., Street-Perrott, F.A. Milankovitch forcing of fluctuations in the level of tropical lakes from 18 to 0 kyr BP. *Nature*, 317, 130-134 (1985).

Lamb, A.L., Leng, M.J., Lamb, H.F., Umer, M. A 9,000-year oxygen and carbon isotope record of hy-drological change in a small Ethiopian crater lake. *The Holocene* 10, 167-177 (2000).

Levin, N.E., Zipser, E.J., Cerling, T.E. Isotopic composition of water from Ethiopia and Kenya: Insights into moisture sources for eastern Africa. *J. Geophys. Res.* 114, D23306, doi:10.1029/2009JD012166 (2009).

Linthicum, K.J., Anyamba, A., Tucker, C.J., Kelly, P.W., Myers, M.F., and Peters, C.J. Climate and satellite indicators to forecast rift valley fever epidemics in Kenya. *Science* 23, 1656-1659 (1999).

Lotter, A.F. & Birks, H.J.B. The separation of the influence of nutrients and climate on the varve time-series of Baldeggersee, Switzerland. *Aquat. Sci.* 59, 362-375 (1997).

Makinouchi, T., Koyaguchi, T., Matsuda, T., Mitsushio, H., Ishida, S. Geology of the Nachola area and the Samburu Hills, west of Baragoi, Northern Kenya.. *Afr. Stud. Monogr.* 2 (Suppl. Issue), 15–44 (1984).

Matsuda, T., Torii, M., Koyaguchi, T., Makinouchi, T., Mitsushio, H., Ishida, S. Fission-track, K-Ar age determinations and palaeomagnetic measurements of Miocene volcanic rocks in the western area of Baragoi, Northern Kenya: ages of hominoids. *Afr. Stud. Monogr.* 2 (Suppl. Issue), 57–56 (1984).

Meehl, G.A., Arblaster, J.M., Matthes, K., Sassi, F. and van Loon, H. Amplifying the pacific climate system response to a small 11-year solar cycle forcing, *Science* 325, 1114–1118 (2009).

Meisner, B. and Arkin, P. Spatial and annual variations in the diurnal cycle of large-scale tropical convective cloudiness and precipitation. *Mon. Wea. Rev.* 115, 2009 –2032 (1987).

Morgan, W.T.W. The South Turkana Expedition: Scientific Papers IV: Land Units of the Lokori Area. *Geogr. J.* 137, 14–28 (1971).

Mulitza, S. et al. Sahel megadroughts triggered by glacial slowdowns of Atlantic meridional overturning. *Paleoceanography* 23, PA4206, doi:10.1029/2008PA001637 (2008).

Neff, U. et al. Strong coherence between solar variability and the monsoon in Oman between 9 and 6 kyr ago. *Nature* 411, 290-293 (2001).

New, M., Lister, D., Hulme, M. & Makin, I. A high-resolution data set of surface climate over global land areas. *Clim. Res.* 21, 1-25 (2002).

Nicholson, S.E. A review of climate dynamics and climate variability in eastern Africa. In: *The Limnology, climatology and paleoclimatology of the East African lakes* (eds Johnson, T.C. & Odada, E.O.) Gordon & Breach, Amsterdam, 25-56, (1996).

Ojany, F.F., Ogenoo, R.B. Kenya: A Study in Physical and Human Geography. *Longman, Nairobi*, 228 pp. (1973).

Olaka, L.A., Odada, E.O., Trauth, M.H. & Olago, D.O. The sensitivity of East African rift lakes to climate fluctuations. *J. Paleolimnol.* 44, 629-644 (2010).

Owen, R.B., Barthelme, J.W., Renaut, R.W., Vincens, A. Paleolimnology and archaeology of Holocene deposits north-east of Lake Turkana, Kenya. *Nature* 298, 523-529 (1982).

Pickford, M. Fossil mullusca from the Samburu Hills, Northern Kenya. *Afr. Stud. Monogr. 2* (Suppl. Issue), 141-145 (1984).

Richardson, J.L. & Dussinger, R.A. Paleolimnology of mid-elevation lakes in the Kenya Rift Valley. *Hydrobiologia* 143, 167-174 (1986).

Roessner, S. & Strecker, M.R. Late Cenozoic tectonics and denudation in the Central Kenya Rift: quantification of long-term denudation rates. *Tectonophysics* 278, 83-94 (1997).

Rossignol-Strick, M. African monsoons, an immediate climate response to orbital insolation. *Nature* 304, 46-49 (1983).

Saji, N.H., Goswami, B.N., Vinayachandran, P.N. & Yamagata, T. A dipole mode in the Indian Ocean. *Nature* 401, 360-363 (1999).

Saneyoshi, M., Nakayama, K., Sakai, T., Sawada, Y., Ishida, H. Half graben filling processes in the early phase of continental rifting: The Miocene Namurungule Formation of the Kenya Rift. *Sediment. Geo.* 186, 111–131 (2006).

Schreck, C.J. & Semazzi, F.H.M. Variability of the recent climate of eastern Africa. *Int. J. Climatol.* 24, 681-701 (2004).

Sepulchre, P., Ramstein, G., Fluteau, F., Schuster, M., Tiercelin, J.J., and Brunet, M. Tectonic uplift and eastern Africa aridification: *Science* 313, 1419–1423 (2006).

Shanahan, T.M. et al. Paleoclimatic variations in West Africa from a record of late Pleistocene and Holocene lake level stands of Lake Bosumtwi, Ghana. *Palaeogeogr. Palaeoclimatol. Palaeoecol.* 242, 287-302 (2006).

Shotton, F.W., Williams, R.E.G. & Johnson, A.S. Birmingham University Radiocarbon Dates VIII. *Radiocarbon* 16, 285-303 (1974).

Skinner, N.J., Iles, W. & Brock, A. The Recent Secular Variation of Declination and Inclination in Kenya. *Erth. Planet. Sci. Lett*. 25, 338-346 (1975).

Smith, M. & Mosley, P. Correction to "Crustal heterogeneity and basement influence on the development of the Kenya Rift, East Africa", *Tectonics* 12(3), 791–793, doi:10.1029/93TC01133 (1993).

Stager, J.C., Ryves, D.B., Chase, B.M. & Pausata, F.S.R. Catastrophic Drought in the Afro-Asian Monsoon Region During Heinrich Event 1. *Sciencexpress* (2011).

Stager, J.C., Mayewski, P.A. & Meeker, L.D. Cooling

cycles, Heinrich event 1, and the deiccation of Lake Victoria. Palaeogeogr. *Palaeoclimatol. Palaeoecol.* 183, 169-178 (2002).

* Stoof-Leichsenring, K.R., Junginger, A., Olaka, L.A., Tiedemann, R., Trauth, M.H. Environmental variability in Lake Naivasha, Kenya, over the last two centuries. *J. Paleolimnol.*, in press (2011).

Street-Perrott, F.A. & Perrott, R.A. Abrupt climate fluctuations in the tropics: the influence of Atlantic Ocean circulation. *Nature* 343, 607- 612 (1990).

Street-Perrott, F.A. & Harrison, S.P. In: Hecht A.D. (eds), Paleoclimate Analysis and Modeling. *Wiley, New York*, 291-340 (1985).

Sturcio, N.C., Dunkley, P.N. & Smith, M. Climate-driven variations in geothermal activity in the northern Kenya rift valley. *Nature* 362, 233-234 (1993).
Talbot, M.R. & Johannessen, T. A high resolution palaeoclimatic record for the last 27,500 years in tropical West Africa from the carbon and nitrogen isotopic composition of lacustrine organic matter. *Erth. Planet. Sci. Let.* 110, 23-37 (1992).

Tatsumi, Y. & Kimura, N. Secular variation of basalt chemistry in the Kenya Rift: Evidence for the pulsing of asthenospheric upwelling. *Erth. Planet. Sci. Let.* 104, 99-113 (1991).

Telford, R.J. & Lamb, H.F. Groundwater-mediated response to Holocene climatic change recorded by the diatom stratigraphy of an Ethiopian crater lake. *Quat. Res.* 52, 63-75 (1999).

Thompson, L.G. et al. Kilimanjaro Ice Core Records: Evidence of Holocene Climate Change in Tropical Africa. *Science* 298, 589-593 (2002).

Tiercelin, J.-J. & Vincens, A. Le Demi-Graben de Baringo-Bogoria, Rift Gregory, Kenya, 30,000 Ans d'Histoire Hydrologique et Sédimentaire. *Bull. Centres de Rech. Expl. Prod. Elf-Aquitaine, Pau, France* 11, 249–540 (1987).

Tierney et al., Late Quaternary behaviour of the East African monsoon and the importance of the Congo Air Boundary. *Quat. Sci. Rev.* 30, 798-807 (2011).

Tierney, J.E., Russell, J.M., Huang, Y., Sinninghe Damsté, J.S., Hopmans, E.C., Cohen, A.S. Northern Hemisphere Controls on Tropical Southeast African Climate During the Past 60,000 Years. *Science* 322, 252-255 (2008).

Trauth et al. Human evolution in a variable environment: The amplifier lakes of Eastern Africa. *Quat. Sci. Rev.* 29, 2981-2988 (2010).

Trauth, M.H., Larrasoaña, J.C. & Mudelsee, M. Trends, rhythms and events in Plio-Pleistocene African climate, *Quat. Sci. Rev.* 28, 399-411 (2009).

Trauth, M.H., Maslin, M.A., Deino, A. & Strecker, M.R., Late Cenozoic moisture history of east Africa. *Science* 309, 2051-2053 (2005).

Trauth, M.H., Deino, A., Bergner, A.G.N., Strecker, M.R. East African climate change and orbital forcing during the last 175 kyr BP. *Erth. Planet. Sci. Let.* 206, 297-313 (2003).

Truckle, P.H. Geology and Late Cainozoic lake-sediments of the Suguta Trough, Kenya. *Nature* 263, 380–383 (1976).

Verschuren, D. et al. Half-recessional dynamics of monsoon rainfall near the East African Equator. *Nature* 462, 637-641 (2009).

Vincens, A. Palynologie, environnements actuels et plio-pléistocénes à l'Est du lac Turkana (Kenya). *Ph.D. thesis, Univ. Aix-Marseille II, Marseille*, *France*, 244 pp (1982).

Wang, Y.J et al. The Holocene Asian Monsoon: Links to Solar Changes and North Atlantic Climate. *Science* 308, 854-857 (2005).

Washbourn-Kamau, C.K. Late Quaternary Chronology of the Nakuru-Elmenteita Basin, Kenya. *Nature* 226, 253-254 (1970).

Weaver, S. The quaternary caldera volcano emuruangogolak, kenya rift, and the petrology of a bimodal ferrobasalt-pantelleritic trachyte association. *Bull. Volcanol.* 40, 209-230 (1977).

Web, P & Weaver, S. Trachyte shield volcanoes: a new volcanic form from South Turkana, Kenya. *Bulletin of Volcanology* 39, 294-312 (1975).

Weldeab, S., Lea, D.W., Schneider, R.R. & Andersen, N. Centennial scale climate instabilities in a wet early Holocene West African monsoon. *Geophys. Res. Lett*. 34, L24702, doi:10.1029/2007GL031898 (2007).

Williams, A.P. & Funk, C. A westward extension of the warm pool leads to a westward extension of the Walker circulation, drying eastern Africa. *Clim. Dyn.* 0930-7575, doi: 10.1007/s00382-010-0984-y, 1-19 (2011).

Williams, L.A.J. Character of Quaternary volcanism in the Gregory Rift Valley. in Geological background to fossil man (ed Bishop. W.W.), *Edingburgh, Scottish Academic Press*, 55-69 (1978).

Williamson, P.G., Savage, R.J.G. Early rift sedimentation in the Turkana basin, northern Kenya. In: Frostick, L.E. (Ed.), *Sedimentation in the African Rifts. Geol. Soc. London, Spec. Publ*. 25, 267–283 (1986).

Williamson, D., Taieb, M., Damnati, B., Icole, M., Thouveny, N. Equatorial extension of the younger Dryas event: rock magnetic evidence from Lake Magadi (Kenya). *Global Planet. Change* 7, 235–242 (1993).

(* Manuscripts part of the Doctoral Thesis)

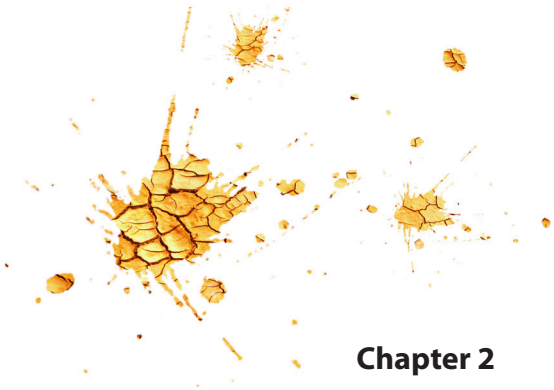

Chapter 2

Solar Variations and Holocene East African Climate

Annett Junginger, Martin H. Trauth
submitted to *Nature*

2.1 Solar Variations and Holocene East African Climate

Annett Junginger[a,b,*], Martin H. Trauth[a]

[a]Institute for Earth- and Environmental Sciences, University of Potsdam, Potsdam, Germany
[b]DFG Graduate School "Shaping the Earth's Surface in a Variable Environment",
University of Potsdam, Germany
*corresponding author at Institute for Earth- and Environmental Sciences, University of Potsdam, Karl-Liebknecht-Str. 24, 14476 Potsdam, Germany. Tel. +49-331-977-5857, Fax +49-331-977-5700, E-mail annett.junginger@geo.uni-potsdam.de

Abstract

The nature and causes of intensity variations of the West-African (WAM) and Indian Summer monsoons (ISM) during the African Humid Period (AHP, 14.8-5.5 ka), especially their exact influence on regional climate relative to each other, is currently intensely debated. Here, we present a high-resolution multiproxy lake-level record spanning the AHP from the remote Suguta Valley in the northern Kenya Rift, located between the WAM and ISM domains. Our record explains the synchronous onset of large lakes in the East African Rift System (EARS) with the longitudinal shift of the Congo Air Boundary (CAB) over the East African and Ethiopian Plateaus, as the direct consequence of an enhanced atmospheric pressure gradient between East-Africa and India due to a precessional-forced northern hemisphere insolation maximum also known to have strengthened the ISM. Abrupt internal lake level fluctuations during the generally wet AHP are explained by small-scale solar irradiation changes that caused besides the lowering of atmospheric moisture a reduction of this pressure gradient preventing the CAB to reach the study area. Instead, the termination of the AHP occurred, despite a gradual weakening of the ISM, in a non-linear manner due to a change towards an equatorial insolation maximum ca. 6.5 ka ago extending the AHP over Ethiopia and West-Africa.

2.1.1 Introduction

Today, more than one billion people in Africa and Asia rely on monsoonal rainfalls for their living. Great scientific interest therefore exists in understanding and simulating the dynamics and variability of monsoons on different time scales. At present day, variability in the intensity of monsoonal precipitation is associated with sea-surface temperature (SST) anomalies of the Indian Ocean attributed to the Indian Ocean Dipole (IOD) and El Niño/Southern Oscillation (ENSO) dynamics with changes on annual to decadal timescales[5]. During the early to mid-Holocene, when orbital variations caused the strengthening of the west-African (WAM) and Indian summer monsoon (ISM) resulting in significant lake-level rises in Africa[6,13] and enhanced humidity much further inland Asia[2], IOD/ENSO dynamics, however, have been suppressed during that time due to lowered equatorial ocean temperatures as the result of the enhanced circulation[7]. Nevertheless, important fluctuations in the strength of monsoonal rainfall occurred also, as observed in records from both monsoon domains, which have been attributed to small perturbations in solar radiation[4,8-11]. Despite the main forcing of monsoon intensity variations are well identified, their exact influence on regional climate, in particular relative to each other, is controversially debated, often evoked through the correct assessment and unambiguous interpretation of palaeo-climatic data contained in marine vs. terrestrial archives and geographical location of discussed study sites.

2.1.2 Setting

The remote Suguta Valley (2°N, 36.5°E) in the Northern Kenya Rift, located between the WAM and ISM domain (Fig. 2.1, 2.2), provides unique conditions to contribute to unresolved relationships between the two monsoon systems. In contrast to the pres-

ently essentially dry Suguta Valley, only covered by the shallow, highly alkaline, seasonal Lake Logipi in the north of the basin, during the AHP the valley was covered by a 2,200 km^2 large and almost 300 m deep lake[12] (Fig. 2.2, 2.5 see page 48). The sheer dimension of this palaeo-lake, its 13,000 km^2 large catchment, as well as widespread lacustrine deposits and well-developed palaeo-shoreline features (Fig. 2.6 see page 49) make the valley an ideal place for palaeo-climate reconstructions.

2.1.3 Present day climate

At present day, the intra-annual distribution of rainfall is mostly controlled by the seasonal migration of the Intertropical Convergence Zone (ITCZ) causing long rains in April/May and short rains in October/November, in contrast to the ISM season in July/August[14] (Fig. 2.2). During the boreal summer and winter Indian monsoonal season, relatively dry winds flow from the southeast and northeast, respectively, into the SSW-NNE oriented Suguta Valley (Fig. 2.1). Beyond this general scheme, the catchment can receive extra rain during August, when the ITCZ in its northernmost latitudinal position attracts convective rainfall associated with the Congo Air Boundary (CAB) northeastwards, approaching the peripheral parts of the East African Plateau. The CAB, in turn, receives its moisture from the Atlantic Ocean, which is recycled over the Congo basin before it reaches the western base of the plateau regions[14]. In addition to this, significant precipitation anomalies are linked with Indian and Pacific Ocean sea-surface temperature (SST) anomalies, attributed to the IOD and ENSO, respectively, causing more intense November/December rains during their warm phases[5,14].

2.1.4 Methods

The early Holocene climate history of equatorial East Africa is deduced from a lake-level record from the Suguta Valley, Northern Kenya Rift. Lacustrine sediments offering 25 to 40 m thick sequences are exposed in the north-eastern, central and southwestern sectors of the basin. Here, three sequences were sampled in detail every 25 to 50 cm for analyses of grainsize distributions, magnetic susceptibility, carbon and nitrogen content and snail shell abundances. The additional use of a shoreline data set[12] from the same region, which has been now reservoir-corrected allow the exact determination of the water level above a certain sediment composition, assumed parallel data sets beeing available. A water-balance model was then used to link observed lake-level variations revealed from the sediment-shoreline data sets with abrupt vs. gradual climate shifts. Age control is provided by 43 AMS ^{14}C ages mostly from charcoal, but also from carbonate shells of the gastropod *Melanoides tuberculata*. In order to determine the anticipated reservoir effect of palaeo-Lake Suguta, we systematically dated snail shells and charcoal fragments parallel. The detected reservoir age was used to correct all carbonate-derived ^{14}C ages (see supplementary materials for further information).

2.1.5 Results

Past climate variability during the AHP in the Suguta Valley is recorded in three, up to 40 m thick lacustrine sequences that were deposited between 11.35-8.55 ka (1ka=1,000 calibrated years before

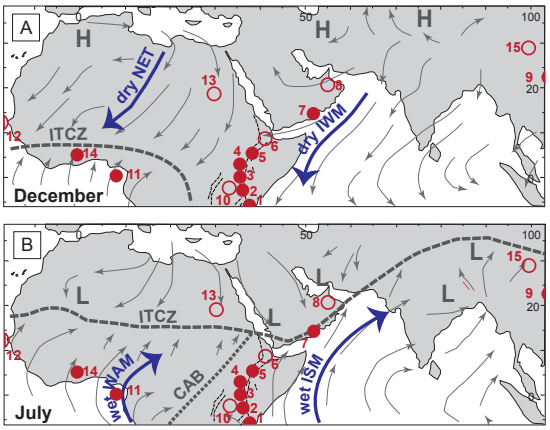

Figure 2.1 Seasonal (A) December and (B) July atmospheric pressure and surface wind fields, major convergence zones (ITCZ–Intertropical Convergence Zone; CAB–Congo Air Boundary, denoted as dotted lines), large-scale circulation systems (ISM–Indian Summer Monsoon, IWM–Indian Winter Monsoon; WAM–West African Monsoon. NET–Northeasterly Trade Winds) and locations of proxy records discussed in the text (transparent red circles) and shown in Figures 2 and 3 (filled red circles) (1–Kilimanjaro[22]; 2–Lake Nakuru-Elmenteita[24], 3–Suguta Valley, this study, 4–Lake Turkana[29,30], 5–Ziway-Shala basin[6], 6–Lake Asal[19]; 7–Qunf cave[3]; 8–Hoti cave[10]; 9–Dongge cave[4,26]; 10–Lake Victoria[8]; 11–Tropical East Atlantic MD03-2707[9,23]; 12–sub-tropical East Atlantic GeoB9508-5[16,25]; 13–East Sahara, Nubian lakes, Sudan[17], 14–Lake Bosumtwi[13], 15–Hongyuan peat bog[60] (Figure modified after Nicholson, 1996[14] and http://iridl.ldeo.columbia.edu/maproom).

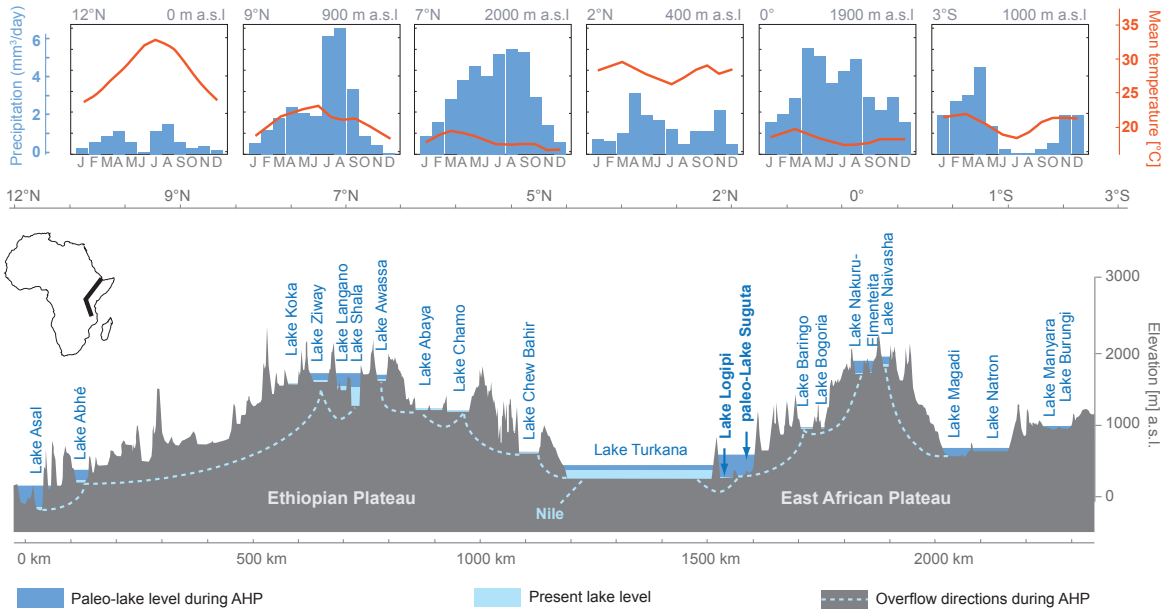

Figure 2.2 Cross-section (lower panel) of the eastern branch of the EARS showing present and early Holocene lake levels and modern monthly temperature and precipitation distribution along the rift floor (upper panel). Present climate patterns over the two plateau regions indicate that the Suguta Valley and the Turkana Basin, both located just north of the equator, are influenced by very similar climate regimes, but while the Turkana Basins mainly receives water from the Ethiopian Plateau via Omo River in the North, the Suguta Valley catchment expands to the South and is therefore influenced mainly by a equatorial climate. Data source: Modern climate data from http://iridl.ldeo.columbia.edu/maproom/; maximum palaeo-lake levels and overflow information from Lake Asal[66], Lake Abhe[67], Lakes Ziway-Shala-Langano[68], Lake Abaya and Chamo[N.N.], Lake Awassa and Lake Chew Bahir[69], Lake Turkana[29]; Lakes Baringo and Bogoria[70], Lakes Nakuru and Elmenteita[24], Lake Naivasha[44], Lakes Magadi and Natron[71], Lakes Manyara and Burungi[72].

present) (Fig. 2.10 see page 55). A multiproxy climate record from these sequences is complemented by a palaeo-shoreline data set[12] providing the evidence for a major lake episode in the Suguta Valley between 13.9-5.0 ka. Lake-balance modelling of the 300 m highstand suggests that only a relatively moderate (+26%) increase in precipitation caused the formation of palaeo-Lake Suguta during the AHP. Some evidence for a more recent, possibly less pronounced wet episode is indicated by a single shoreline deposit at 50 m above the valley floor dated at ca. 0.94 ka, which falls into the end of the medieval warm period (Fig. 2.3). (see supplementary information for a detailed description of the methods employed and the palaeo-limnological results)

2.1.6 Discussion & Conclusions

2.1.6.1 Onset of the AHP

The Suguta Valley palaeo-lake record provides important insights into the dry-wet transition at the beginning of the AHP. The onset of the episode of wetter conditions has been linked to the more intense heating of the northern hemisphere during boreal summer as a consequence of a precessional minimum[6]. The associated increase of land-sea thermal contrast resulted in the strengthening of the WAM and ISM with associated displacement of the ITCZ further north and inland Asia[2,3,15]. There are indications from southern to equatorial Africa for an early onset of enhanced precipitation starting at around 17 ka most likely associated with a warming trend in Antarctica[6], whereas evidences for pronounced African lake fillings north of 10°S started not before 15 ka[6], contemporaneous with pronounced precipitation increases inland Asia[2] at ~14.8 ka as a late response to insolation due to the cooling effect of the Arctic sea-ice expansion[1] reaching a first maximum of enhanced summer precipitation in Asia at ~13.9 ka (Fig. 2.3). The timing of the dry-wet transition at the beginning of the AHP in the Suguta Valley is in good agreement with these chronologies of monsoon intensity and high lake levels in Africa north of 10°S, as abundant fossil *M. tuberculata* and reworked

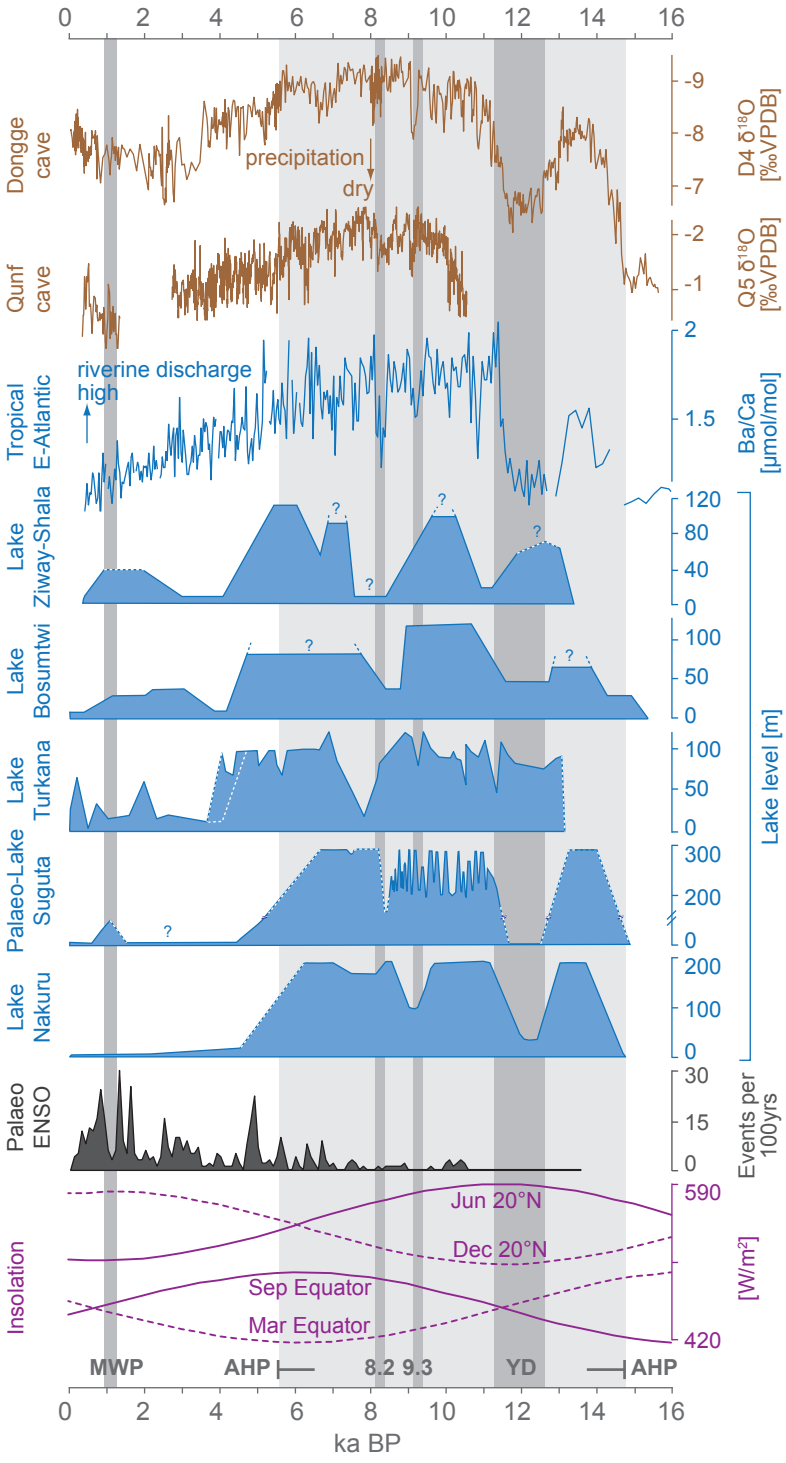

Figure 2.3 Comparison of onset and termination of East African lake levels[6,13,24, 29,30] with a riverine runoff record from West Africa[23], the oxygen-isotope records from Qunf[3] and Dongge[26] Caves, the palaeo-ENSO record from Laguna Pallcacocha[7], southern Ecuador, and insolation variations[27] . Records are sorted from South to North. Dotted lines indicate water level estimations not supported by data. (AHP–African Humid Period, YD–Younger Dryas, MWP–Medieval Warm Period). Orginal radiocarbon dates were converted into calendar years.

oyster shells within lacustrine deposits of the same age indicate the existence of a lake level maximum at around 13.9 ka. We do not yet know about the exact duration of this earlier highstand, but assumed a similar timing as adjacent basins[6], our hydrological modelling results suggest a minimum age of the onset of ~14.9 ka, assuming a gradual onset of this lake episode, and 14.2 ka, respectively, if the lake was established abruptly in the valley.

Whereas the intensification of the WAM and ISM circulation and the northward displacement of the ITCZ best explains the onset of the AHP [9,16-18], the meridional synchronicity of the dry-wet transition through the African continent, especially regions usually not affected by both monsoon systems such as the Kenya Rift, suggests a more complex mechanism. We hypothesize an eastward shift of the longitudnal position of the CAB resulting in enhanced/prolonged summer rainfalls across the East African and Ethiopian Plateaus. Our interpretation is corroborated by a study about present rainfall data in eastern Africa, where correlations between the deepening of atmospheric pressure low systems over India correlate with enhanced rainfalls in western Kenya[73]. Additionally, results of a provenance study of Early-Holocene $\delta^{18}O$ values from snail shells in the Afar region are indicating an Atlantic Ocean source of precipitation during a rapid lake-level rise during the AHP[19]. The most likely climatological scenario for the early-Holocene rainfall maximum on the Ethiopian Plateau and Afar region therefore was explained as the logical consequence of the mechanism used to explain humidity changes in the eastern Sahara during the AHP. The precessional-induced enhanced summer insolation over the northern hemisphere shifted and deepened the East Saharan atmospheric low and therefore strengthened the WAM attracting moist Atlantic Ocean-derived air masses in northeasterly direction towards the eastern Sahara and hence shifting the Sahelian belt northward[15]. The strengthened WAM, in turn, was associated with the contemporaneous weakening of the African easterly jet, that is responsible for humidity export outside Africa[20]. The consequence of this dramatic increase in moisture availability provides a possible explanation for the greening of the Sahara and filling of the present-day hyperarid Nubian basin[17]. Even more, the even deeper Tibetan low, responsible for a stronger ISM[21], could have attracted the same Atlantic-derived moisture even further eastward across Ethiopia and Kenya towards the more stable, drier Indian Ocean air masses resulting in dramatically increased precipitation[19]. The entire system as a whole therefore stabilizes itself, as prolonged summer rains in West Africa[16] and the CAB being trapped on the East African and Ethiopian Plateaus during times of a stronger ISM.

2.1.6.2 Internal variability of the AHP

The lake record from the Suguta Valley also provides sufficient detail to infer short-term (10^2-10^3 years) variations in the hydrology. The amplitudes of lake-level variations are generally larger (tens of meters, up to 300 meters) than typical displacements of faults in the tectonically active valley (less than 10 meters[12]). Beyond the orbitally-controlled humid episode between 14.9-5 ka causing high lake levels between 13.9 and at least 6.8 ka, the most dramatic hydrological event in our record is a significant lake retreat of 300 m before 11.6 ka, which correlates with the global Younger Dryas event (YD, 12.8-11.6 ka) in the high latitudes that caused major drought conditions in Africa north of 10°S[6] (Fig. 2.3). After this dry spell, the return to full humid conditions and a high palaeo-Lake Suguta occurred within less than 200 years, as suggested by the sedimentological changes within all three lacustrine sequences in combination with hydrological modelling, but slowed down between 11.2-11.0 ka before the lake reached its overflow level towards Lake Turkana via Kerio Valley again. Within dating error, this rapid termination of the YD in the Suguta Valley is coeval with corresponding signatures in records of tropical East Africa[22], the WAM[23], and ISM realm[26], corroborating the rapid reorganization of low-latitude atmospheric circulation after the global YD event. After the re-establishment of the lake after the YD, multiple lake-level fluctuations not causing a complete desiccation of the lake are documented between 11.35-8.55 ka. The AHP was punctuated by short-term drier intervals during 11.1, 10.7, 10.4-10.5, 10.25-10.05, 9.85, 9.5-9.25, 9.1, 9-8.8, and 8.7-8.4 ka, causing lake-level declines of 80-100 m occurring within 70-90 years, respectively, in addition to several minor events. Most of these events occur simultaneously with dust events interpreted as enhanced droughts in the Kilimanjaro ice record[22], small-scale lake-level drops in Central[8] and reduced river runoff in western Africa[25] as well as with weakened ISM intensity inferred from records in Oman[10],

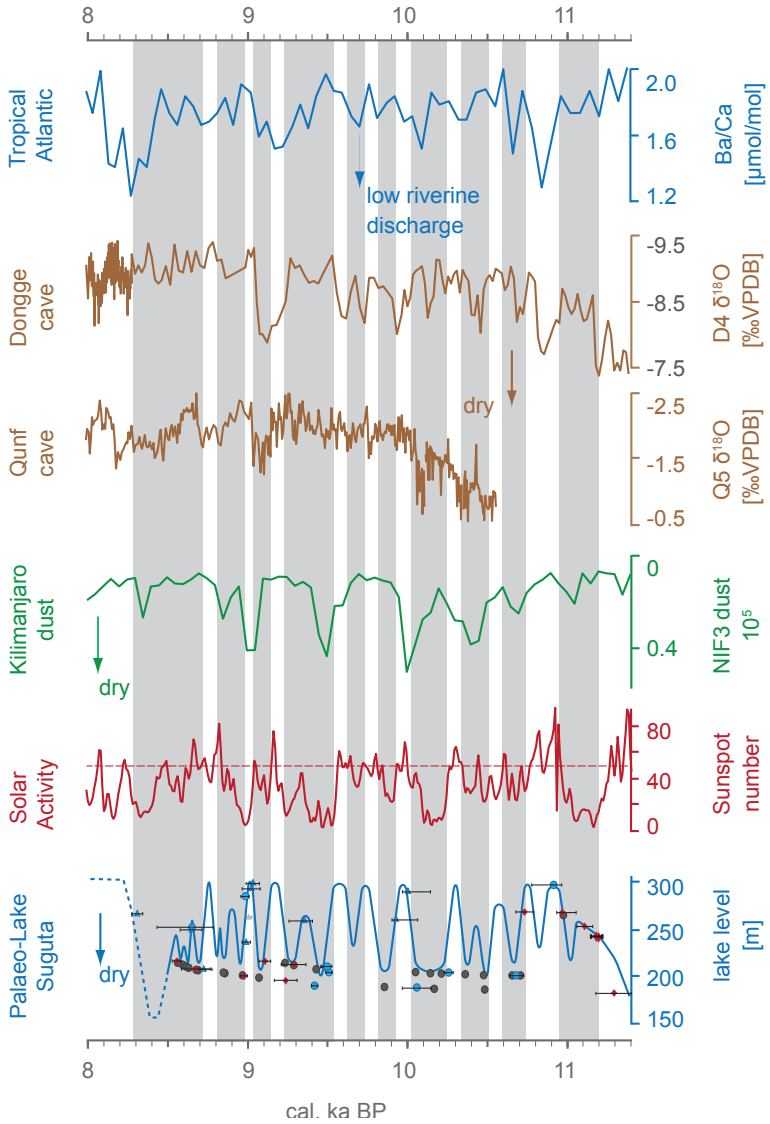

Figure 2.4 Correlation of short-term lake-level fluctuations of palaeo-Lake Suguta during the African Humid Period (AHP) compared to proxy records[3,22,23,26] of centennial-scale climate fluctuations caused by solar irradiation variations[27,28]. Grey bars mark dry intervals during reduced solar activity. In the Suguta record, AMS ^{14}C age control points shoreline deposits are marked by triangles, whereas blue circles refer to dated snail shells, diamonds depict data from charcoal, and grey circles marked layers with abundant snail shells not dated (see supplementary material for details on methods and shoreline reconstruction).

the Tibetan Plateau[24] and Southeast Asia[26] (Fig. 2.4).

The most likely mechanism to explain the short-term aridity shifts in the Suguta Valley and elsewhere in the African-Asian monsoonal realm is a weakening of the WAM and ISM that is caused by significant differences in sensible heating of the adjacent continents[4] weakening the pressure lows over the Sahara and Tibetan plateau. This in turn leads to a reduced land-sea pressure gradient with a weaker summer circulation and reduced cross-equatorial moisture transport through the ITCZ. The accompanied weakening of the pressure gradient would be not strong enough to shift the CAB eastward over the plateau regions of at least not as far as the Suguta Valley. This combined mechanism of reduced general precipitation and isolation from the CAB would explain why only abrupt precipitation changes are suggested by our hydromodel to cause the observed lake level declines of palaeo-Lake Suguta (see supplement).

Since the location of the CAB has been explained to be also dependent on the location of the ITCZ[14] provides a study about WAM weakening support,

where reduced moisture was attributed also to a combination of lowered precipitation and displacement of the ITCZ further south[25].
The weakening of the WAM was accompanied with the strengthening of the African easterly jet, amplifying the humidity export out of Africa[20]. The reason for the differences in surface heating are be attributed to variations in solar output, as indicated by a near-perfect correlation of the lake-level fluctuations in the Suguta Valley with solar radiation changes[28] (Fig. 2.4), and similar to the solar radiation changes reduced precipitation in West and Central Africa[8,9], Oman[10,11], and Southeast Asia[4], highlighting the sensitivity of the ISM to relatively small changes in solar output[10,21].

Differently from most other high-frequency events prior is the event between 8.7-8.3 ka, which shows a gradual decline of the lake level with abrupt short-term interruptions despite relative low variations in solar radiation[28]. This episode of a low-level gradual trend towards drier climate occurred also in other low-latitude records[3,9-11] predating the sharp cooling event at 8.2 ka observed in high-latitude climate records.
While the return to the maximum lake level after 8.3 ka is not well defined, the Suguta lake record suggests full humid conditions at around 7.4 ka and 6.8 ka, respectively, despite comparatively low solar radiation after 7.8 ka. The time period at around 7.8 ka was reported to mark the onset of a very slow weakening of the ISM[3,26]. However, high lake levels until at least 6.8 ka in the Suguta record suggest, that the ISM was still strong enough to keep the ITCZ at a northerly position to drag the CAB as far east as the East African and Ethiopian plateaus. Instead, the far-reaching decline of the African-Asian monsoon system was initiated at around 6-5.5 ka, reaching a first minimum around 5.2-4.5 ka (Fig. 2.3).

2.1.6.3 Termination of the AHP

The Suguta Valley lake record also contributes to the current discussion on the timing of the Mid-Holocene humid-arid transition in Africa. Whereas several proxy records and climate modelling results indicate an abrupt decline of the African-Asian monsoon between 4.5-5 ka[1,2], an equally-large body of evidence points towards a gradual aridity trend since the beginning of the mid-Holocene at around 7.8 ka[3,4,11,21]. In the Suguta Valley, the AHP seem to have terminated at around 6.8 ka as indicated by a distinct lake level retreat of 250 m within 1,600 years or slightly less. Hydrological modelling results link the lake-level decline to variations in climate clearly indicating a gradual decrease in precipitation rather than an abrupt change in humidity at the end of the AHP. On the other hand, palaeo-Lake Suguta almost vanished at 5.0 ka, when other African proxy records just started indicating a change in climate. We propose two different hypotheses to explain the unexpectedly early termination of the AHP in the Suguta Valley, as compared with the timing of this climate transition in other sectors of the African-Asian monsoon realm.

Hypothesis No. 1 explains the time difference simply by the unavailability of lake-level data for the interval between 6.8-5.0 ka. Assuming this hypothesis to be true, palaeo-Lake Suguta might have been high at least until 5.2 ka, consequently associated with a termination caused by an abrupt reduction in rainfall, or until >5.4 ka, assuming a more gradual termination of the AHP. In any case, the timing of the termination of the AHP fits well into the general pattern of climate change elsewhere in the Mid-Holocene (Fig. 2.3).

Hypothesis No. 2 suggests that the most dramatic change in climate has occurred at around 6.8 ka rather than at ~5.4 ka. This timing for the termination of the AHP correlates with the time when precessional-controlled insolation maximum changed from 20°N to the equator (Fig. 2.3), causing a the Tibetan Low beeing less strong causing a weakening of the ISM and also pressure gradient between India and Africa thus preventing the CAB from reaching the study area.
This interpretation is in line with the lake-level history of Lake Bosumtwi[13], Lake Ziway-Shala[6], Lake Turkana[29,30], Lake Nakuru[24] and palaeo-IOD/ENSO reconstructions[7], where a non-linear, two-step like termination of the AHP is indicated. The first step at ~6.8 ka might be attributed to a general weakening of the ISM system as the result of precessional-controlled northern hemisphere insolation minimum that allowed a slight intensification of IOD/ENSO-related SST anomalies.

A possible link between Indian Ocean SSTs and prolonged East African humidity can be attributed to a change in the orbital precession resulting in maxi-

mum equatorial September insolation at around 6 ka. This assumption is in agreement with modelling results of the WAM and ISM at 9.5 and 6 ka[18] indicating that the WAM sustained longer at high intensities than the ISM due to precessional-induced insolation changes. The intensification of the September ITCZ might have prolonged humid conditions in Africa although possibly not intense enough to maintain maximum lake levels in the Suguta Valley, contributing to our theory about the major influence of the CAB to produce high lake levels in East Africa under exceptional deep pressure low developments over India associated with intense heating. The lake-level record from Lake Turkana, about 20 km north of the Suguta Valley, seems to support the interpretation according to Hypothesis No. 2, as the lake stopped overflowing into the White Nile at around 6.7 ka, but remained at high levels until around 4 or 5 ka, respectively, depending on the proxy record used for its lake level reconstruction[29,30].

2.1.7 Summary

The Suguta Valley lake record supports evidences for solar variation induced African-Asian summer monsoon weakening and propose associated droughts in tropical East Africa. Our results highlight the importance of solar irradiation/monsoon intensity connection to East African climate even for relatively moderate fluctuations in solar output. Despite the new insights into the character of the termination of the AHP from the Suguta Valley lake-level record, our results clearly indicate the need for a high-resolution, well-dated record for this interesting episode of climate change in East Africa. At present, the available data and their interpretation of humid-arid transitions in the tropics should be handled with care, and taking the geographical, geological and climatologically situation of the study site into consideration while concluding about the relative importance of drivers of climate change in the tropics. The Suguta Valley lake record also contributes to the current discussion on the potential influence of humid-arid transitions on human expansions, technological innovations and food production.

2.2 Supplementary information 1 - Lacustrine sediment investigations

2.2.1 Methods

2.2.1.1 Materials

Lake sediments preserved in the Suguta Valley usually occur as lens-shaped sediment bodies along the rift margins. Three lacustrine sediment sequences, 25-40 m thick, are exposed in the southwestern, eastern and northeastern sectors of the valley (Fig. 2.5). These sequences were sampled for radiocarbon dating, and detailed sedimentological, geochemical and palaeontological analyses in a sampling resolution of 25-50 cm. The sediments consist of dark clays and fine silts intercalated with fine sand layers (Fig. 2.6). The correlation of the three sequences was corrected for the possibility of a 10-15 m downwarp of the western valley margin as a result of tectonic activity in the EARS[12].

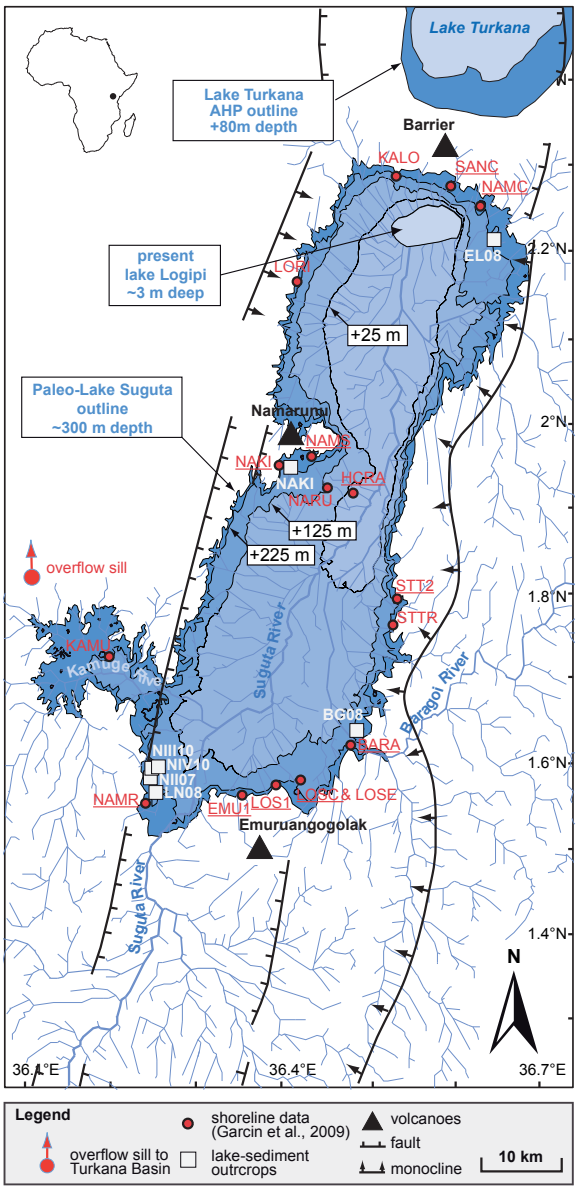

Figure 2.5 Map showing Suguta Valley with shoreline data[12] and sampling sites for lacustrine sequences. Different colours of blue outline the dimension of palaeo-Lake Suguta during the Early Holocene transgression. Underlined shoreline sites were radiocarbon dated.

2.2.1.2 Age control

For the early and late Holocene time period, the only way to achieve a consistent chronology is radiocarbon dating of biogenic material within the lake sediments. Radiocarbon dating of carbonate shells from mollusc living in a lake can bear the risk of showing ages that are unreaölistically old,, known as the so-called reservoir effect[31]. Aquatic organisms incorporate the isotopic composition (especially of ^{14}C) of their aquatic habitat[32], which is ideally in an isotopic equilibrium with the atmosphere. Mechanisms, that might alter this equilibrium and produce the reservoir effect, are diverse and ranging from the size of the lakes surface area and their exposition to the atmosphere, lake mixing, inflowing aged groundwater, runoff from a carbonaceous catchment area and/or humus as well as additional CO_2 produced by the decomposition of organic matter, volcanically active areas and so forth[32,33]. Regarding to our study site, we might expect such a reservoir effect, since the volcanically active rift valley is a zone of degassing ^{14}C-depleted CO_2. The dissoluted ^{14}C-depleted CO_2 in the lake water will then be incorporated by snails (and other aquatic organisms) causing ^{14}C-depleted carbonate shells to be precipitated, and hence anomalously high radiocarbon ages of the fossils[34]. The most suitable material for radiocarbon dating therefore is charcoal or other terrestrial plant residues not originated from the lake. In order to determine the anticipated reservoir effect of palaeo-Lake Suguta, we systematically dated carbonate snails shells from the gastropod Melanoides tuberculata and charcoal fragments, about 250 µm large or less, sampled from the same sediment layer. The established reservoir age was used to correct the age of all carbonate samples, including previously

Figure 2.6 Photographs of the Suguta Valley and lacustrine sediments analysed in this study. Photos A and B illustrate the extreme sensitivity of the Suguta Valley to precipitation today by means of a comparison of the water coverage of the basin in May 2008 (dry conditions) and May 2010 (wet conditions). Photos C to F show representative sediment sections sampled and analysed in this study. Photos G-J are showing different styles of sedimentation as recorded in the sections.

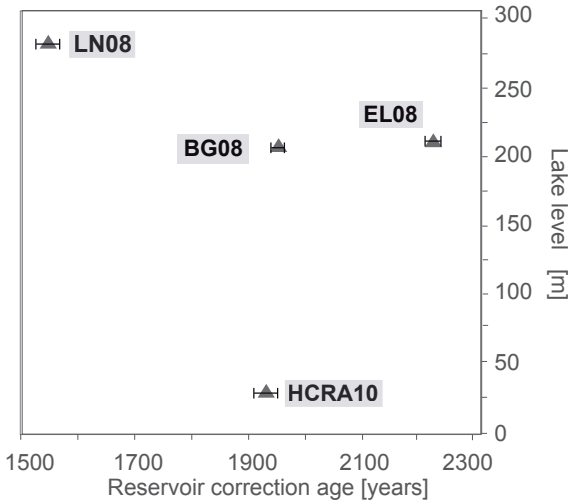

Figure 2.7 Overview of reservoir ages as determined from parallel dating of *Melanoides tuberculata* and charcoal particles without any evidence for a lake depth-reservoir age dependency.

published 17 AMS ^{14}C ages of shoreline deposits[12]. The dating sets of 26 new AMS ^{14}C data as well as the 17 AMS ^{14}C ages of shoreline deposits[12] were conducted at the Leibniz Labour at the university of Kiel in Germany. For the conversion into calendar ages, we used CALIB version 5.01[35] with the IntCal04 curve[36]. All radiocarbon ages are reported as calendar years or kilo years (ka) BP with 1σ error bounds. Mean total sediment rates were estimated based on sedimentation interpolations between the AMS ^{14}C age control points.

2.2.1.3 Grain-size and magnetic susceptibility

A variety of factors control distributions of ferromagnetic minerals, which complicates the interpretation of magnetic susceptibility (MS) as a palaeoenvironmental proxy. Influencing factors can be, as an example, changes in the source rocks due to topographic changes and hence erosion in the catchment, the expansion of the palaeo-lake and erosion of larger areas of the catchment, various pedogenic processes[37], and in situ dissolution and authigenesis of magnetic carriers[38]. In many examples, however, MS follows grain-size variations in the sediment profiles, and can consequently be used as a indicator for grain-size variations. Measurements of the volume specific magnetic susceptibility (κ) were performed with a AGICO Kappabridge MFK-1A instrumentation. Semi-quantitative estimates of grain-size variations were also recorded during sampling and profile description in the field.

2.2.1.4 Geochemical analyses

Total Carbon (TC) and Total Nitrogen (TN) were analysed concurrently by IR-spectroscopy and heat conductivity detection after burning weighed aliquots in an oxygen gas flow at 1,350°C, using a LECO CNH 2000 Elemental Analyzer (LECO Corp., St. Joseph, MI). Total organic carbon (TOC) was determined after release of CO_2 by reaction with hot 4% and 25% hydrochloric acid followed by using the LECO, CNH 2000 system again. Total inorganic carbon (TIC) was calculated from the TC-TOC difference. C/N ratios are calculated from TOC/TN ratios.

C/N analyses of bulk organic matter have become a useful indicator of sources of organic matter despite the fact that some diagenetic alteration of organic matter inevitably occurs in the early stages of deposition[39]. Organic sources are either related to allochtonous input with mainly terrestrial plant residues, such as grasses, shrubs, and trees on land and emergent macrophytes in lakes, supplied by surface runoff and wind[39] or to the autochthonous production with mainly bacteria, macrophytes, phytoplankton, and zooplankton. C/N ratios of 4-10 are usually described as indicative of fresh non-vascular aquatic plants, which are protein-rich and cellulose-poor, whereas vascular plants land plants, which are protein-poor and cellulose-rich, typically produce C/N ratios of 20 or more[39]. These fundamental differences in the organic matter composition is usually preserved during decent in the water column and burial in the sediment[39]. C/N ratios of diatom-bearing sediment vary between 5-8, and a mixture of aquatic and higher plant material are more variable in their C/N ratios of 10-20, whereas ratios above 20 indicate the predominance of higher plants[39].

2.2.1.5 Occurrence of of *Melanoides tuberculata*

Most of the shoreline ages are based on radiocarbon dating of carbonate shells of Melanoides tuberculata. At present day, this prosobranch species occurs abundantly in a wide range of fresh and brackish water habitats throughout Africa and Asia[40,41]. Its littoral habitat is mostly associated with aquatic and subaquatic plants in up to 2 m water depth, that provide the snails with protection from wave action, as well as food and egg laying sites[41]. There are reports about Melanoides tuberculata living within fine-grained sediment in larger water depths up to 10-15 m where they can form high population den-

sities[40]. Shoreline ages based on Melanoides tuberculata that were not found within fine sediments might be therefore attributed to a direct elevation of the associated shoreline with a maximum of 2 m water coverage. The direct association with a shoreline does not need to reflect a final lowstand since the life span of Melanoides tuberculata is short between one season and 5 years[41] and only reflects the elevation of the associated shoreline for this short time period. Shells in fine-grained sediment deposits might indicate water levels up to 10-15 m depth.

2.2.2. Results

2.2.2.1 Chronology

The series of measured and corrected AMS ^{14}C ages used in this study are summarized in Table 2.1. Radiocarbon ages of biogenic carbonates were systematically older than the associated charcoal samples. Parallel charcoal/carbonate snail shells dating reveals a reservoir ages of 1,680 (LN08), 1,940 (HCRA2), 1,970 (BG08), and 2,240 (EL08) years, respectively (Fig. 2.7). The reservoir ages are in good agreement within the error bars of the method, without an evidence for a systematic change within the sections. We therefore used a mean reservoir age of 1,900 years to correct all carbonate sample ages for the reservoir effect of palaeo-Lake Suguta. Using this age information, our multi-proxy lake record represents a high-resolution history of past climate change between 11.35-8.55 ka (Fig. 2.9). Together with the previously published palaeo-shoreline data set[12], this data set provides the evidences for a major humid period in the Suguta Valley between 13.9-5.0 ka, followed by a relatively dry climate and an intermittent short episode of wetter climate at around 900 years BP.

2.2.2.2 Description of investigated lake sediment sections

Section LN08 | This section is located in the southwestern part of the Suguta Valley in the Namruy area (Fig. 2.5). It contains one of the highest elevated early Holocene lacustrine units and consists of light-coloured fine to medium, unconsolidated silts, intercalated with fine sand layers (Fig 2.6, 2.8). It is located at elevations between 515–561 m asl., close to the maximum highstand shoreline (MHS). Even though LN08 contains 40 m of sediments it inhibits the shortest lacustrine record of ~500 years deposited between 11.2-10.7 ka. The age model suggests a constant depositional rate of 117 mm/yr for the period of available radiocarbon dates (Fig. 2.9). These high sedimentation rates within a section of fine to medium silt intercalated with very fine sand sized sediments can only be ascribed to the rapid erosion of young faults from a very large catchment and the close location to a former delta system from the main Suguta River carrying high amounts of water masses during a humid period (Fig. 2.5). Additionally, transversal entering of smaller rivers might have also contributed to the very high sedimentation rates at LN08. Due to the high sedimentation rate, the sequence is ideal to record short-term lake-level fluctuations due to its vicinity to the MHS.

The lower 15 m (11.2-11.1 ka) of LN08 show a depositional situation predominantly dominated by periodic flooding as indicated by alternating silt and sand layers with fining upward trends for each event. Desiccation cracks without major erosion unconformities support the interpretation of flood plain deposits (Fig. 2.6G). Charcoal occurs in high abundances whereas mollusc shells are rare in this section. After 11.1 ka, the sedimentation pattern changes towards fine to medium silts for the following ~50 years contained in 6 m of sediment before a major disruption of lacustrine sedimentation is indicated by a 5 m thick layer of coarse sands including the time interval between 11.05-10.8 ka. We cannot exclude erosion of parts of the sand layer, because finer sands in between indicate lacustrine sedimentation, but clear evidences are missing. The missing evidences in LN08 can only be interpreted as a pronounced lake level drop after 10.95 ka below the sediment surface, which might have caused pronounced erosion of the possible lacustrine units in between the major sand layer. The return to full humid conditions by subsequent flooding is indicated by cross bedding of fine sands starting at ~10.8 ka followed by fine silt deposition. We assume a similar sedimentation rate of 117 mm/yr after this event due to the very similar sediment type to the previous time. Lacustrine deposition ended at LN08 at ~10.7 ka indicated by the onset of coarse sand deposition, proposing another lake level lowering. Further lacustrine sedimentation after this drought event was most likely prevented due to the filling of the accommodation area of LN08 to the MHS. A freshwater oyster shell of Etheria Ellipitca from top

Table 2.1 AMS ^{14}C ages of material from lacustrine sequences and of shoreline deposits in the Suguta Valley

Kiel ID	Site	sample elevation [m asl.]		Latitude N	Longitude E	Material	^{14}C age [yr BP]	^{14}C age reservoir corr. [yr BP]	$\delta^{13}C$ [‰]	Calibrated ^{14}C age [cal. yr BP]	1-σ error bounds [cal. yr BP]	relative area 1-σ	2-σ error bounds [cal. yr BP]	relative area 2-σ
KIA33901*	SANC1	481		2°16'20.6"	36°34'41.1"	M	9840 ± 45	7940 ± 45	-5.15 ± 0.42	8740 ± 50	8694 / 8787	0.439	8637 / 8984	1
KIA33902*	SANC2	528		2°16'11.6"	36°34'27.4"	M	10205 ± 45	8305 ± 45	-1.69 ± 0.73	9345 ± 75	9272 / 9417	1	9195 / 9440	0.915
KIA33903*	SANC3	533		2°16'21.1"	36°34'41.6"	M	9365 ± 50	7465 ± 50	0.47 ± 1.3	8320 ± 30	8287 / 8348	0.513	8187 / 8376	1
KIA33908*	LOSC	532	+	1°34'41.7"	36°23'59.5"	M	10000 ± 45	8100 ± 45	-4.86 ± 0.21	9020 ± 20	8995 / 9039	0.575	8974 / 9139	0.903
KIA33909*	LOS1	519		1°34'31.8"	36°22'22.0"	M	9775 ± 45	7875 ± 45	-5.38 ± 0.42	8660 ± 70	8594 / 8726	0.949	8554 / 8791	0.881
KIA33911*	NAMC1	529		2°14'45.8"	36°36'51.7"	M	10795 ± 50	8895 ± 50	-8.54 ± 0.81	10000 ± 80	9920 / 10081	0.778	9885 / 10194	0.942
KIA33912*	NAMC2	544		2°14'52.7"	36°36'47.3"	M	10930 ± 50	9030 ± 50	-5.22 ± 0.55	10215 ± 25	10185 / 10236	1	10133 / 10267	0.929
KIA33913*	NAMC3	556		2°14'52.4"	36°36'49.4"	M	10760 ± 50	8860 ± 50	-8.96 ± 0.35	10070 ± 90	9983 / 10155	0.701	9760 / 10172	0.989
KIA 33914	NAKI1	466		1°56'48.2"	36°22'49.3"	M	10260 ± 45	8360 ± 45	1.30 ± 1.02	9430 ± 30	9397 / 9462	0.566	9272 / 9482	1
KIA33915	NAKI2	484		1°57'00.3"	36°22'51.9"	M	10415 ± 45	8515 ± 45	-2.13 ± 0.57	9510 ± 20	9492 / 9534	1	9465 / 9564	1
KIA33916*	NAKI3	507		1°56'59.5"	36°22'49.9"	M	9970 ± 45	8070 ± 45	-0.88 ± 0.97	9005 ± 25	8976 / 9033	0.648	8855 / 9124	0.855
KIA33917*	NAMS1	564		1°57'19.7"	36°24'56.1"	M	10025 ± 45	8125 ± 45	-11.11 ± 1.51	9050 ± 40	9008 / 9092	0.888	8992 / 9143	0.892
KIA33918*	NAMS2	564	+	1°57'19.7"	36°24'56.1"	M	10750 ± 50	8850 ± 50	-0.39 ± 0.41	10105 ± 45	10057 / 10150	0.378	9736 / 10168	1
KIA35809*	HCRA1	312		1°54'46.0"	36°27'54.5"	O	6345 ± 40	4445 ± 40	2.32 ± 0.3	5020 ± 50	4970 / 5066	0.536	4952 / 5088	0.451
KIA43247	HCRA10A	300	R	1°37'46.3"	36°27'55.3"	C	955 ± 60		-25.00 ± 0	840 ± 40	795 / 878	0.686	737 / 962	1
KIA43248	HCRA10B	300	R	1°37'46.3"	36°27'55.3"	M	2895 ± 25	955 ± 25	-5.61 ± 0.11	840 ± 15	827 / 864	0.516	795 / 886	0.698
KIA36872*	STT2	559		1°47'23.1"	36°30'55.3"	M	9980 ± 55	8080 ± 55	-5.82 ± 0.29	9035 ± 55	8977 / 9093	0.786	8767 / 9137	0.973
KIA33910*	NAMR1	532		1°32'14.3"	36°13'32.4"	M	13725 ± 60	11825 ± 60	-1.30 ± 1.02	13700 ± 70	13629 / 13769	1	13493 / 13813	1
KIA33907*	NAMR2	530	+	1°32'14.2"	36°13'32.3"	E	13900 ± 60	12000 ± 60	-8.43 ± 0.42	13860 ± 70	13786 / 13925	1	13739 / 14000	1
KIA37054	LN08-0.30	511		1°32'16.0"	36°13'30.6"	C	9780 ± 40		-22.37 ± 0.15	11210 ± 20	11194 / 11233	1	11162 / 11252	1
KIA37055	LN08-1.35	512		1°32'16.0"	36°13'30.6"	C	9740 ± 45		-12.29 ± 0.1	11195 ± 35	11157 / 11225	1	11091 / 11243	0.983
KIA37056	LN08-11.20	522		1°32'16.0"	36°13'30.6"	C	9635 ± 45		-24.08 ± 0.23	11120 ± 50	11070 / 11168	0.495	10781 / 11036	0.607
KIA37057	LN08-24.70A	536	R	1°32'16.0"	36°13'30.6"	M	11125 ± 55	9555 ± 55	-0.59 ± 0.5	11010 ± 60	10948 / 11073	0.528	10702 / 11109	0.991
KIA37058	LN08-24.70B	536	R	1°32'16.0"	36°13'30.6"	C	9555 ± 40		-25.77 ± 0.08	11010 ± 60	10952 / 11070	0.587	10915 / 11089	0.518
KIA37059	LN08-26.95	538		1°32'16.0"	36°13'30.6"	C	9510 ± 55		-12.51 ± 0.11	10745 ± 55	10692 / 10800	0.507	10650 / 10897	0.584
KIA37060	LN08-Top	561	+	1°32'16.0"	36°13'30.6"	E	11495 ± 60	9595 ± 60	-9.57 ± 0.16	10885 ± 95	10787 / 10975	0.713	10742 / 11166	1
KIA33919	NII07-T1	553		1°32'58.8"	36°13'20.1"	M	9945 ± 50	8045 ± 50	-8.93 ± 0.46	8995 ± 25	8970 / 9023	0.407	8720 / 9035	0.96
KIA43294	NIV10-5.87B	520		1°33'02.0"	36°13'35.0"	C	7820 ± 200		-16.37 ± 0.12	8610 ± 180	8425 / 8791	0.786	8278 9139	0.97
KIA36873*	EMU1	565		1°33'39.1"	36°20'03.2"	M	7850 ± 50	5950 ± 50	-3.37 ± 1.3	6765 ± 45	6720 / 6805	0.689	6664 / 6901	1
KIA37061	BG08-(-1.25)	456		1°37'46.3"	36°27'55.3"	C	9880 ± 120		-18.72 ± 0.34	11300 ± 110	11190 / 11412	0.711	11073 / 11824	0.976
KIA37062	BG08-4.50	462		1°37'46.3"	36°27'55.3"	M	10780 ± 55	8880 ± 55	-10.66 ± 0.36	10070 ± 90	9982 / 10155	0.754	9767 / 10188	1
KIA37063	BG08-12.75	470		1°37'46.3"	36°27'55.3"	C	8210 ± 45		-12.88 ± 0.23	9250 ± 70	9113 / 9260	0.908	9021 / 9302	1
KIA37064	BG08-17.50	475		1°37'46.3"	36°27'55.3"	C	8045 ± 40		-16.24 ± 0.82	8990 ± 20	8974 / 9021	0.51	8767 / 9031	0.993
KIA37065	BG08-24.25A	482	R	1°37'46.3"	36°27'55.3"	M	9870 ± 50	7900 ± 50	-10.82 ± 1.74	8690 ± 90	8601 / 8776	0.933	8593 / 8811	0.732
KIA37066	BG08-24.25B	482	R	1°37'46.3"	36°27'55.3"	C	7900 ± 45		-30.41 ± 0.51	8690 ± 90	8603 / 8774	0.985	8594 / 8798	0.754
KIA37067	BG08-31.75	490		1°37'46.3"	36°27'55.3"	C	7780 ± 40		-18.92 ± 0.33	8570 ± 30	8537 / 8599	0.881	8453 / 8629	1
KIA36866*	BARA-SL01	557		1°37'08.3"	36°27'39.2"	M	8510 ± 60	6610 ± 60	-7.93 ± 0.44	7490 ± 30	7459 / 7519	0.643	7426 / 7581	1
KIA33904	EL07-T1-4.30	475		2°13'09.4"	36°37'52.7"	M	11345 ± 50	9445 ± 50	-8.26 ± 0.67	10695 ± 45	10645 / 10737	0.714	10552 / 10793	0.928
KIA33905	EL07-T2-6.70	478		2°13'09.4"	36°37'52.7"	M	11045 ± 50	9145 ± 50	-12.24 ± 0.46	10270 ± 30	10235 / 10300	0.625	10223 / 10432	0.969
KIA33906	EL08-12.30	483		2°13'09.4"	36°37'52.7"	M	10415 ± 45	8515 ± 45	-10.75 ± 0.64	9510 ± 20	9492 / 9534	1	9465 / 9546	1
KIA37071	EL08-12.40	483		2°13'09.4"	36°37'52.7"	M	10360 ± 45	8460 ± 45	-5.71 ± 0.3	9495 ± 25	9465 / 9524	1	9420 / 9537	1
KIA37069	EL08-14.50A	486	R	2°13'09.4"	36°37'52.7"	M	10485 ± 45	8245 ± 45	-3.79 ± 0.13	9300 ± 80	9130 / 9291	1	9081 / 9329	0.87
KIA37070	EL08-14.50B	486	R	2°13'09.4"	36°37'52.7"	C; HA	8245 ± 45		-25.25 ± 0.25	9300 ± 80	9130 / 9291	1	9081 / 9329	0.87
KIA37068	EL08-18.00	489		2°13'09.4"	36°37'52.7"	Cb	8195 ± 55		-15.27 ± 0.36	9120 ± 35	9077 / 9149	0.408	9010 / 9304	0.995

(*) Garcin et al., 2009[12]; (R) parallel measurements for reservoir age estimation, (+) samples are regarded to be displaced; M - *Melanoides tuberculata*, E - *Etheria elliptica*, O - ostracods, C - charcoal, Cb - charcoal bulk, HA - humic acids. Reservoir correction age: 1900 years. Radiocarbon ages given before Year 1950. ^{14}C calibration method: Program CALIB 5.0.1[35], IntCal04 curve[36].

of the section revealed an older age and must have been reworked, since oysters normally live in high energetic environments and not in unconsolidated sands. We assume this freshwater oyster to have lived along the MHS probably at one of the river mouths entering the high palaeo-Lake Suguta from the south.

The results of geochemical investigations are displayed in Figure 2.10. The MS record of LN08 shows large variations in amplitude and frequency, with extremely low values in lithozones mainly consisting of diatom bearing silts and very high values predominantly in fine to coarse sands. TC consists mainly of TOC, although low compared to EL08 and BG08, with 0.12–0.87 wt% and even less TIC ranging between 0-0.67 wt%. TN is 0.01-6.09 wt% and therefore almost double the amount of EL08 and BG08. TN values are anticorrelated to grain-sizes; highest when grain-sizes are smallest. C/N ratios in the studied sequence range generally between 0.05-10 within the section but do reach values of more than 40 in the sands on top of LN08, which might be attributed to a grassland vegetation of the area. High values of C/N appear as abrupt peaks mostly in medium to coarse silts at the transition from higher to finer grain-sizes or vice versa.

Section BG08 | This section is the lowest (455–495 m asl.) elevated studied lacustrine sequence located in the southeast of the Suguta Valley (Fig. 2.5, 2.8). The transversal influenced section covers the longest time period of deposition between 11.3-8.55 ka (Fig. 2.9). The sediments generally consist of mostly unconsolidated dark clays, fine to coarse silts containing rare fragments of snail shells from *Melanoides tuberculata* (Fig. 2.6, 2.10). The base of the section consists of unconsolidated light grey clayey silts, indicating a higher lake level during deposition. Grain-sizes to the top of the section increase and culminate in a fluvial depositional pattern with conglomerates and coarse sands. This development is reflected in the age model, which shows comparatively low sedimentation rates of 4.4 mm/yr between 11.3-10 ka and progressive increasing rates towards the top of the section of 62.5 mm/yr between 10-8.55 ka (Fig. 2.9). Higher sedimentation rates in the younger parts of the section might be attributed to rapid shoreline fluctuations close to the sediment surface. Since we do not have any age data from the conglomerates on top of the section,

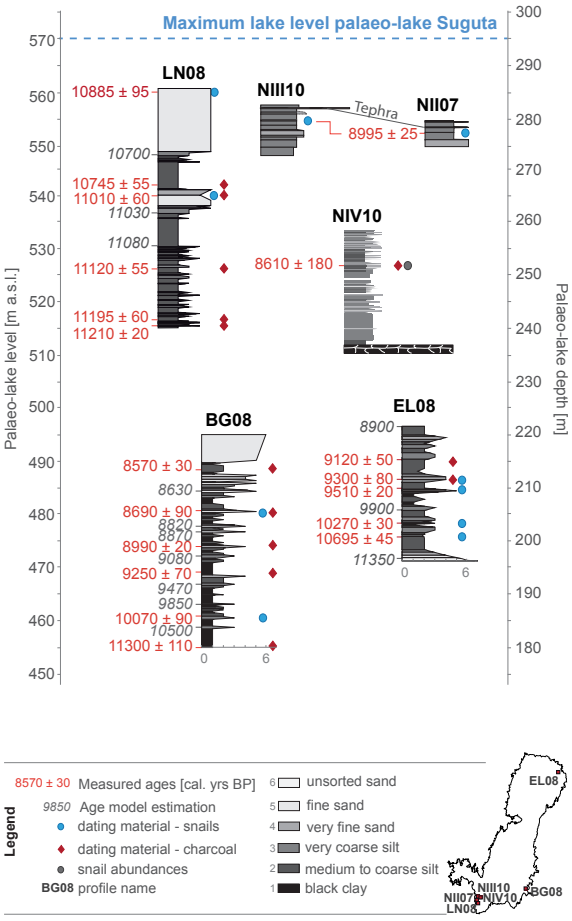

Figure 2.8 Location of all lacustrine sequences mentioned in the text regarding to their depositional elevation in the Suguta Valley. Dotted line shows maximum possible highstand at the overflow level of palaeo-Lake Suguta towards the Kerio Valley.

we cannot provide an age for the final filling of this accommodation area.

The results of geochemical investigations are displayed in Figure 2.10. The MS of BG08 generally shows very low values, compared to ones of sections EL08 and LN08. Higher values occur between the base of the section and at 10 m (11.3–9.3 ka), within fine to medium/coarse silts and dark clays with intermittent lower values. After 9.3 ka, the sedimentation pattern changes towards high frequencies of coarser and finer grain-sizes together with variations in MS values, although generally lower than in the previous time. The change might reflect a change in the catchment area of the entering Baragoi River, which consists of a variety of phonolithic, basaltic, and trachytic rocks as well as biotite gneisses and Miocene lacustrine sediments with different content of magnetic carriers (Fig. 2.11). TC is mainly

composed of TOC ranging from 0.14-3.16 wt% with a general trend towards higher values from bottom to top. The trend towards higher values stops at 8.8 ka and decreases slightly towards 8.5 ka. TIC content is low with 0-0.78 wt%. TN values range between 0-3.14 wt% with a general anticorrelation to MS and grain-sizes showing high TN values within reduced MS or grain-sizes. C/N ratios vary between 0.2-12.3 and do appear also as abrupt peaks in fine silt layers always directly before or after a period of enhanced grain-sizes with progressive increasing ratios towards the top of the section.

Section EL08 | This section crops out in a river valley east of Lake Logipi in the northeastern part of the Suguta Valley at elevations between 471-497 m asl. (Fig. 2.5, 2.8). The base of the section consists of component-supported conglomerates containing large boulders of gneisses and basalts deposited in a lubricated stacking, which indicates a fluviatile deposition rather than an alluvial fan (Fig. 2.6). The sediments of EL08 contain repeated layers of Melanoides tuberculata shells often within medium to coarse silts (Fig. 2.10). The transversal influenced section underwent lacustrine deposition between 11.3-8.75 ka, probably longer since no coarser material on top indicates an end of lacustrine deposition, which suggests major erosion of the top of the lacustrine unit. Sedimentation rates of EL08 are very similar to those from BG08, implying the age model to be well established (Fig. 2.9).
Due to larger sampling intervals, the general pattern of geochemical analyses is not as variable as the one of BG08, which has been deposited during the same time interval at a slightly lower elevation. However, MS shows a similar trend with large variations in amplitude and frequency, with extremely low values in lithozones mainly consisting of diatomites or diatom-bearing silts and very high values predominantly in fine to coarse sands following mostly the grain-sizes. This makes the MS also in this section a valuable tool to detect internal variations of mineral support, where very high values can be mainly ascribed to the magnetite and titanomagnetite bearing basalts in the catchment (Fig. 2.11). Mean values decrease from the beginning of lacustrine sedimentation until 9.5 ka and then rise again. TOC are also the major contributors to TC content with values ranging from 0.3-2.3 wt% showing high peaks between 9.5-9.9 ka. TIC are, similar to BG08, low with 0-0.87 wt%. TN values are generally lower compared to BG08 with 0.07-2.9 wt% generally anticorrelating with grain-zises and MS. High values occur similar to BG08 around 9.0-9.5 and 10.5-10.8 ka. C/N ratios in the studied sequence show large variations between 0.4-14.7. Broad peaks are due to higher sampling distances and might include more than one event. They occur also within mainly medium and coarse silts.

Sections NII07, NII10, and NIV10 | The sections are part of the upper Namruy sedimentation area 1.5 km northwest of LN08. NII07 and NIII10 describe the highest elevated preserved lacustrine units of the AHP (Fig. 2.5, 2.8). The top of the sections marks a wide former shoreline in the field associated with the MHS. The sediments consist mainly of silty diatomites. At ca. 554 m asl., a grey 20 cm thick silt layer is containing Melanoides tuberculata shells in high abundances. Two meters above this event layer, a

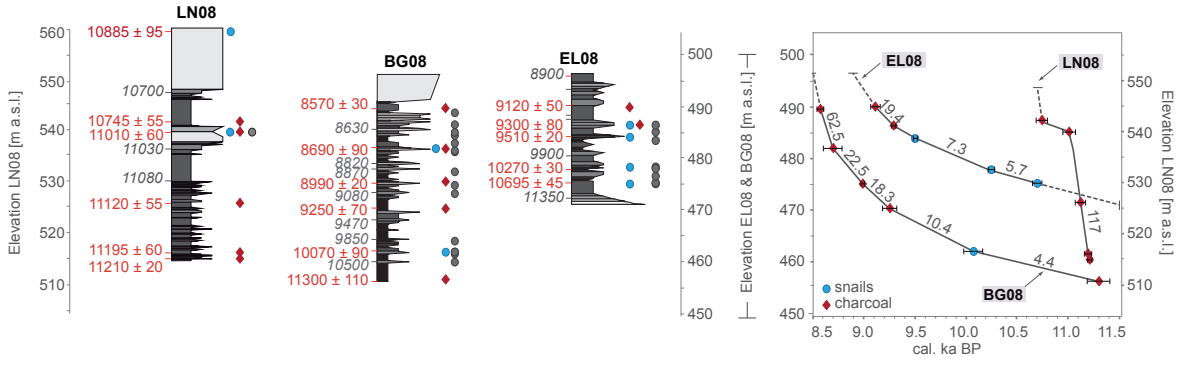

Figure 2.9 Age model for the three sediment sequences LN08, BG08 and EL08 sampled in greater detail within this study. Chronology is based on 26 AMS ^{14}C ages including three parallel measurements on snail shells and charcoal fragments to determine the reservoir age of palaeo-Lake Suguta (see Fig. 2.8). Note scale change for LN08 due to its higher elevation. For legend see Fig. 2.8.

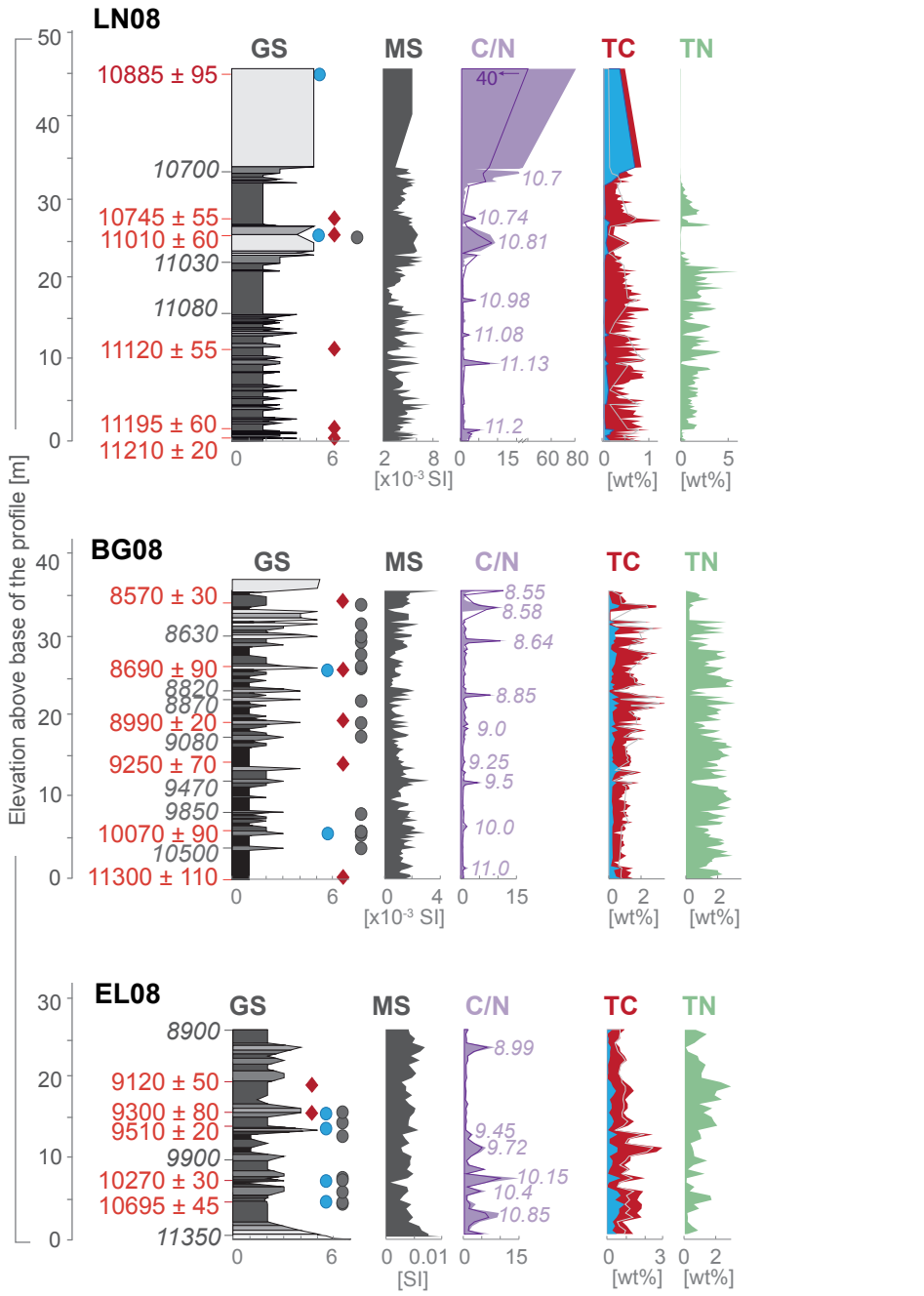

Legend

- **BG08** profile name
- **GS** grain size
- **MS** magnetic susceptibility
- **C/N** C/N ratio; purple TOC/TN ratio
- **TN** total nitrogen
- **TC** total carbon with TOC (grey) & TIC (blue)
- 8570 ± 30 Measured ages [cal. yrs BP]
- *9850* Age model estimation [cal. yrs BP]
- dating material - snails
- dating material - charcoal
- snail abundances
- *9.6* Age model estimation for C/N peaks [cal. kyr BP]
- 6 unsorted sand
- 5 fine sand
- 4 very fine sand
- 3 very coarse silt
- 2 medium to coarse silt
- 1 black clay

Figure 2.10 Results of sedimentological and geochemical investigations at BG08, EL08 and LN08 used for early to mid Holocene lake-level reconstructions. NII10, NII07 and NIV10 were only sampled for shoreline indicators, for example, snail shells.

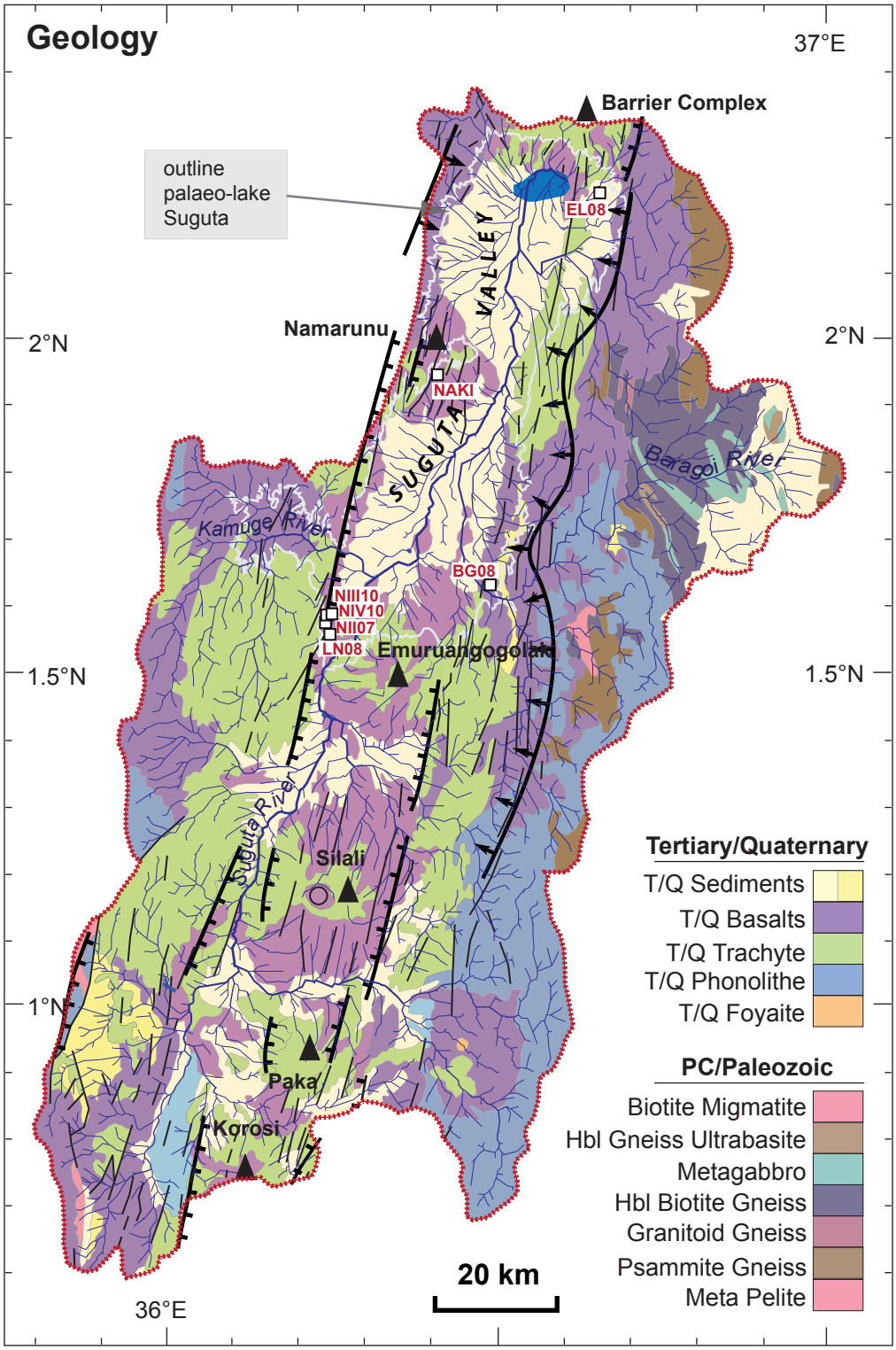

Figure 2.11 Geological map of the catchment area of palaeo-Lake Suguta and the location of the sampled lake-sediment sections (red squares) (see Fig. 2.5 page 48 for map legend).

silty layer with light, up to 1 cm large pumice lapilli suggests a short volcanic eruption some time after 9 ka. This hardly identified layer was not observed in other lacustrine deposits. Section NAMR[12] is also part of the lower Namruy area closely located to LN08 in the southwestern part of the Suguta Valley.

Sedimentation area NAKI is situated on the western escarpment within the Namarunu volcanic complex (Fig. 2.5). Three dated snail samples from various elevations between 460-510 m asl. are indicative for low lake levels at 9 ka and around 9.3 ka.

2.2.3 Interpretation of lake-sediment sections

2.2.3.1 Water level above sediments

In order to estimate the water column above a certain sediment composition to assure the correct application of geochemical parameters we used the previous published set of shorelines[12] based on the abundance of *Melanoides tuberculata* and abundances of those shells also in the lacustrine sediments as indicator for the vicinity to a shoreline. We compared them with geochemical investigations of deeper deposited sediments, especially C/N ratios. Snails sampled within lacustrine sediments occur in a wide range from coarse silts to well sorted sands implying a range of water depth from 15-2 m, respectively. Direct evidences for maximum water levels above certain sediment composition and rapid shoreline fluctuations is provided at 11.0, 10.9, 10.7, 10.25-10.05, 10-9.9, 9.5, 9.35, 9.25, 9.1, 9.0 and 8.7 ka (Fig. 2.14b) (See chapter 2.4 for the entire shoreline reconstruction).

2.2.3.2 Geochemical investigations

The results from geochemical investigations on three different lacustrine sequences from the Suguta Valley revealed occasionally large differences in intensities but similarities in individual trends, which suggests the age models being well established. Results are illustrated in Figure 2.10. Based on the background information listed in the methods section, we interpreted the geochemical data as follows.

The **MS** in all lacustrine sequences shows large variations in amplitude and frequency, with extremely low intensities in lithozones mainly consisting of diatomites or diatom bearing clays and silts and very high intensities predominantly in fine to coarse sands following grain-size distributions, which allows us to use the MS as a proxy for grain-sizes. Different intensities in MS among the three different sites are attributed to different source rocks of the individual catchment areas (Fig. 2.11).

TC, TOC, TIC and **TN** vary in all three profiles but show similarities in their individual trends. Different intensities in the individual lacustrine sites are the result of a complex interaction of water depth, distance from shore, catchment lithologies, grain-size, different origins of organic matter, initial production of biomass and subsequent degree of degradation[39]. TOC and TIC are in all three profile mainly positively correlated with TC, whereas TIC is very low and TOC almost as high as TC and therefore describes the majority of carbon content in the sediments. Since carbonaceous rocks in the catchment are not abundant, we relate the minority of TIC to the dissolution of carbonate snail shells within the sediments. TN is highly variable, but occurs mostly when grain-sizes are smallest, indicative for higher water levels.

The **C/N ratios** always appear as distinct peaks predominantly in silt layers at the transition between coarse to fine grain-sizes or vice versa. The restriction of C/N peaks to silt layers exclude a grain-size effect[39] as an explanation. We therefore interpret them as indicators for either flood events or rapid lake level lowering associated with abrupt onset or termination of precipitation, respectively. Fining or grading upward trends in grain-size records help to distinguish those two possible events. These abrupt events might cause in deeper parts of the basin a dramatic rise in temporal lake bio-productivity due to the release of nutrients to the lake and/or enhanced lake mixing. In shallower parts of the lake basin, the input of terrestrial plants to the lake from the flooded land surface might directly reflect these events in the peak height of C/N ratios. Apart from the top of LN08, that show C/N ratio of 40 and higher, all C/N ratios reach only values of 2-13. C/N ratios between 2-9 are used to explain mostly planktonic diatom contributions, whereas values between 10-15 are more indicative for a mixture of aquatic and terrestrial plants from the vicinity of shorelines[39]. Values up to 40 explain terrestrial plants as major

contributor to TOC and no water coverage.

In the direct comparison of the sequences of BG08 and EL08, which are both located at the eastern valley margin at similar elevations only 15 m elevation difference and deposited within the same time, show pronounced differences in C/N ratios between 11.3-9.5 ka. EL08 shows distinct peaks of 5-9 indicative for planktonic TOC content whereas C/N ratios at BG08 remain generally below 2.5. The differences seem to be attributed to a complex pattern of the depositional environment, sediment composition and degradation. One of these complex mechanisms could be attributed to the existence of dark clays in BG08 indicative for anoxic, calm and deep-water depositional conditions, whereas EL08 shows mainly light silts, indicative for a oxic depositional environment. The dark clays could have affected circulating waters to remain longer within the sediment and allowing prolonged microbial reworking whereas medium to coarse silts at EL08 did not retain water for longer times within the sediments. Additional to water retaining sediments is that TOC mostly consistent of algae are more affected by degradation through microbial reworking than terrestrial plants[39]. This is supported by the increasing values towards the top of the section, where a regressing shoreline allows the input of terrestrial material indicated by peaks of 10 and above at BG08, less affected by microbial reworking. However, peaks at EL08 between 11.3-9.5 ka of 5-9 indicate that the water level remained above the sediment surface which restricts peaks here to enhanced mixing of lake rather than input of terrestrial plant material.

A different explanation is needed for the time at ~11 ka where a broad peak of similar height of 8-9 indicative for the major abundance of diatoms at LN08 and EL08 occurs, despite major differences in grain-sizes and depositional elevation. LN08 is much higher elevated and therefore much closer to the MHS than EL08. Coarse sands and the interruption within the age model of LN08 have indicated a lake level lowering below the sediment surface during this time. An explanation could be attributed to a generally low TOC content of that layer with additional almost non-existent TN content. However, another possible lake retreat within that drought event might explain abundances of TOC from aquatic origin.

2.2.4 Conclusion

In summary, grain-sizes and C/N ratios provide the most promising proxies for lake level variations in the investigated sediments. However, organic content in the sediments of the Suguta Valley are due to their possibilities for degradation are usually better interpreted in combination with additional proxies, as e.g. snail abundances. The comparison of these proxies revealed direct evidences for rapid lake level fluctuations within the AHP which can now be tested by a hydrological modelling (chapter 2.3) that allows the reconstruction of non-shoreline supported episodes of lacustrine sedimentation, which will be discussed in chapter 2.4.

2.3 Supplementary information 2 - Lake-balance modelling

2.3.1 Methods

2.3.1.1 Description of the model

The hydrological modelling involved the reconstruction of a 3D basin geometry and the modelling of the modern and early Holocene hydrological budgets by using the MHS[12] information from the reconstructed palaeo-lake level record of the Suguta Valley. The lake-balance model was developed, modified and used by several studies in the past[42-45]. The steady-state hydrological budget for a closed-basin lake can be written as:

$$\Delta V_{lake} = P_{bas} - [E_w \alpha_w + E_1(1- \alpha_w)] - S_{bas} = 0$$

ΔV_{lake} expresses the volumetric change in the water body, P_{bas} the basin-averaged precipitation. E_w and E_1 containing the values of the basin-averaged evaporation over water and over land, α_w contains the lake-area ratio and S_{bas} is used to describe the basin-averaged seepage that is regarded to be zero in our model, due to a closed basin run.

For the appliance of the hydrologic modelling, we first modelled the present-day scenario by using modern climate parameters. The modern climate parameters, summarized in Table 2.2, were obtained from a high-resolution gridded data set of surface climate over global land areas[46]. The data set contains eight climate elements; precipitation, wet-day frequency, temperature, diurnal temperature range, relative humidity, sunshine duration, ground frost frequency and wind speed[46]. The difficulties determining E_1 is based on the complexity of related parameters and their spatial variability in the catchment[44]. Nevertheless, the formula clearly indicates that higher lake levels and larger lakes are always a consequence of increased precipitation and/or reduced evaporation and seepage, as long as no major tectonic movements affected the basin geometry during the studied time-period[44]. In order to eliminate differences in record length and temporal resolution, we computed annual means of all given parameters. Since modern Lake Logipi in the northern sector of the Suguta Valley is subject to dramatic fluctuations in water levels and desiccating completely every year, we used for modern conditions a modern lake area ratio of zero. The result was intensely tested for robustness and sensitivity to all parameters. In the second step, we modelled the maximum depth of palaeo-Lake Suguta by changing the climate parameters until the palaeo-lake level[12] was reached. In the third step, in order to relate observed lake level changes from variations in sedimentology and shoreline distribution to abrupt versus gradual precipitation changes, different assumptions starting from abrupt precipitation shut down to various steps of gradual precipitation decreases from 300 to 2,000 years have been added to the model.

2.3.1.2 Initialization of the model

Before applying the hydro-balance model for palaeo-lake level changes in the Suguta Valley, it is necessary to test the model for present environmental conditions. All parameters that are going to be explained in the following are summarized in Table 2.2. Due to the high relief and large vegetation changes, the catchment of the present Suguta Valley shows extreme gradients for single environmental parameters. In order to take this spatial heterogeneity into account, basin-averaged values for the Suguta Valley catchment were used. The climatic parameters of temperature, precipitation, wind speed, and relative humidity[46] were calculated by means of gridded values using data. Applying this method, the modern annual basin-average precipitation rate (P_{bas}) is 856.45 mm yr^{-1}, air temperature (T_a) varies between 297.45 K (24.3°C) over land and 302.15 K (29°C) over water, wind speed (ws) is 3.2 m s^{-1} and relative humidity (rh) reaches mean values of 57%. The solar radiation was set to 415 ± 3 Wm^{-2} [47], and cloud coverage (cc) of 45%[48]. Short- and long-wave cloud coefficients symbolizing the predominant character of clouds in the catchment and were described and obtained from Bookhagen et al. (2001)[43]. The mean values for air pressure of 849 hPa over land and 975 hPa over the area of modern Lake Logipi were calculated by applying the barometric elevation formula.

A second group of parameters describes all environmental influencing factors considering surface character as emissivity, soil moisture availability, albedo and surface roughness. These parameters were cal-

Table 2.2 Input and output parameters for the recent and early Holocene lake balance modelling

Parameter (variables)	Units	Input value	Calculated value modern	Calculated value palaeo	Reference
Catchment area	km^2	12986.14	-	-	Values taken from DEM
Minimum lake level (modern)	m a.s.l.	275	-	-	Values taken from DEM
Lake area ratio (modern)	(%)	-	0.01	-	-
Water body (modern)	km^3	-	0.02	-	-
Lake area (modern)	km^2	-	9.45	-	-
Maximum lake level (AHP)	m a.s.l.	570	-	-	Garcin et al. (2009)[12]
Lake area ratio (max)	%	-	-	0.17	-
Water body (max)	km^3	-	-	397.8	-
Lake area (max)	km^2	-	-	2181	-
Temperature on surface modern	-	-	-	-	-
land (t_s_ld)	K	-	310.20	-	-
lake (t_s_lk)	K	-	310.70	-	-
Temperature air modern conditions mean	-	-	-	-	-
land (t_a_ld);	K	297.45	-	-	New et al. (2002)[46]
lake (t_a_lk);	K	302.15	-	-	New et al. (2002)[46]
Evaporation modern	-	-	-	-	-
land (e_ld)	mm yr^{-1} m^{-2}	-	855.39	-	-
lake (e_lk)	mm yr^{-1} m^{-2}	-	2208.87	-	-
Precipitation modern	mm yr^{-1} m^{-2}	856.45	-	-	New et al. (2002)[46]
Precipitation palaeo (max. lake level)	mm/yr (%increase)	-	-	1078.75 (+26%)	-
Net short wave radiation down land/lake (r_sw)	-	CALC	-	-	-
Net long wave radiation up land/lake (r_lup)	-	CALC	-	-	-
Net long wave radiation down land/lake (r_ldw)	-	CALC	-		-
Surface emissivity	-	-	-	-	-
land (emis_ld)	-	0.92	-	-	Hastenrath et al. (1983)[48]
land (emis_lk)	-	0.96	-	-	Hastenrath et al. (1983)[48]
Sensible heat rate (h)	-	CALC	-	-	-
Latent heat of vaporization (l)	J kg^{-1}	2.4E6 (FIX)	-	-	-
Cloud-free shortwave radiation r_sw (r_swc)	W m^{-2}	415	-	-	Griffiths (1972)[47]
Albedo over	-	-	-	-	-
land (albedo_ld)	-	0.22	-	-	Hastenrath et al. (1983)[48]
lake (albedo_lk)	-	0.06	-	-	Hastenrath et al. (1983)[48]
Stefan Boltzmann constant (sigma)	kg s^{-3} K^{-4}	5.67E-8 (FIX)	-	-	-
Relative humidity (rh)	%/100	0.57	-	-	New et al. (2002)[46]
Moisture avail. function over	-	-	-	-	-
land (f_ld)	%/100	0.232	-	-	Bergner et al. (2003)[44]
water (f_lk)	%/100	1 (FIX)	-	-	-
Saturation vapour pressure (%es)	%	CALC	-	-	-
Cloud cover (cc)	%/100	0.45	-	-	Hastenrath et al. (1983)[48]
Short wave cloud parameters (a,b)	-	0.39, 0.38	-	-	Bookhagen et al. (2001)[43]
Long wave cloud parameters (a_2, b_2)	-	0.22, 2.00	-	-	Bookhagen et al. (2001)[43]
Wind speed 10 m above ground (ws)	m s^{-1}	3.2 ± 0.1	-	-	New et al. (2002)[46]
Surface drag coefficient	-	-	-	-	-
land (cds)	-	1.1E-3	-	-	Schmugge and Andre (1991)[51]
lake (cds)	-	7.3E-4	-	-	Schmugge and Andre (1991)[51], Bookhagen et al. (2001)[43]
Specific heat capacity of dry air (cp)	kJ kg^{-1} K^{-1}	1005.0 (FIX)	-	-	-
Air pressure	-	-	-	-	-
land (p)	Pa	8.49E4	-	-	Barometric elevation formula
lake (p)	Pa	9.75E4	-	-	Barometric elevation formula
Gas constant for dry air (r)	J K^{-1} kg	287.0 (FIX)	-	-	-

CALC = will be computed by the algorithm; FIX = is a constant value.

culated for land and water surfaces, separately. We used a basin-averaged surface albedo of 0.22 over land reflecting mixed vegetation coverage with 50% light and 50% dark areas, and an albedo of 0.06 for water surfaces[50]. The surface drag coefficient (cd) is an important empirical parameter for the estimation of evaporation that characterizes height and type of vegetation[49,50]. We used a cd-value of 0.0011 for land, that reflects arid regions, and 0.00073 for water[43,51] for the Suguta Valley catchment. Values for surface emissivity (emis) are 0.92 over land and 0.96 over water[48]. The determination of soil moisture is the parameter that is very difficult to determine, since there are no data available for the Suguta Valley so far. Nevertheless, we have chosen the value of 0.232 for land explaining large, swampy areas, braided streams, and Lake Logipi at least in the months after the rainy seasons. Gas constant for dry air (r), specific heat capacity of dry air (cp), moisture availability over water (f_lk), Stefan Boltzmann con-

stant (sigma) and latent heat of vaporization (l) are constant values.

Applying the input parameters for the present-day conditions, the model computes a theoretical small pond precisely at the modern level of Lake Logipi at 275 m asl. A mean evaporation rate over land of 855.39 mm yr^{-1} and 2208.87 mm yr^{-1} over open water was modelled for the modern Suguta Valley. In order to maintain the shallow lake level of Lake Logipi, mean annual precipitation has to reach 856.45 mm.

2.3.2 Results

2.3.2.1 Modelling precipitation for the lake highstand

To calculate the amount of precipitation increase required to fill the Suguta Valley by a ~300 m deep and 2,200 km^2 large lake[12] we used the same value for the catchment area assuming no major changes in the geometry occurred since that time. The main volcanic complexes as Namarunu, Emuruangogolak and Barrier (Fig. 2.5) were largely inactive during the Holocene lake level highstand[52] and only a few small volcanic centres in the southern inner graben (might) have erupted after or during this event without significantly changing the shape of the recent catchment. The offset of the western shorelines[12] is assumed to have occurred after the termination of the AHP, also without changing the catchment size, since those tectonic movement affected the inner graben and not the wider catchment. Since no climate parameters for the early Holocene Suguta Valley exist, we assumed the most effective mechanism of changing the lake hydrology by either higher lateral moisture transport increasing precipitation or reduced basin-averaged temperatures lowering evaporation. Applying these arguments for the modelling, all environmental parameters were kept at their modern values assuming that the entire change in the hydrologic budget is attributed to a change in rainfall as proposed by Bergner et al. (2003)[44]. The simulation for the maximum highstand of palaeo-Lake Suguta suggests a precipitation increase of minimum 26% (1078.75 mm yr^{-1}) and a lake area ratio enhanced by a factor of 17 (Tab. 2.2; Fig. 2.12).

2.3.2.2 Modelling abrupt and gradual changes

Past climate variability during the AHP in the Suguta Valley is recorded in three, up to 40 m thick lacustrine sequences that were deposited between 11.35-8.55 ka (Fig. 2.10, see chapter 2.2). A multiproxy climate record from these sequences is complemented by a palaeo-shoreline data set[12] providing the base for a high-resolution reconstruction of lake-level fluctuations for the time between 13.9-5.5 ka (Fig. 2.14). Direct evidence for lake level variations from the combined application of sedimentology and shoreline distribution show water levels changes of 30-90 m that occurred within 30-90 years, respectively. In order to test these lake level fluctuations for their abruptness, we compared the observed magnitude of lake level changes and their rapidity with the water-balance model where we calculated the rapidity of lake level changes to different assumptions (abrupt vs. gradual) of precipitation decreases. What we observe is, that all of the internal variations correlate with the modelled curve for abrupt reduction in precipitation (Fig. 2.13). In contrast to that, the termination of the AHP in the Suguta Valley is only documented by two shoreline radiocarbon ages, showing a lake retreat of 250 m within 1,600 years, which correlates with one of the modelled assumptions for a gradual decrease.

2.3.3 Interpretation of the modelling results

The Suguta Valley did not experience major volcano-tectonic movements since the early Holocene that might have changed the morphology and size of the catchment and major configuration of the drainage network. Minor tectonic displacements of shorelines have affected the western part of the valley[12] and were taken into consideration before applying the hydromodel. Today, the present Lake Logipi is a relict of the palaeo-Lake Suguta and has no surface outlet. Due to the remoteness of the valley, no reliable data are available for subsurface flow in or out of the basin. Being the deepest part in a chain of rift lakes (Fig. 2.2), faulted marginal parts of the valley might provide excellent pathways for groundwater and seepage from Lake Turkana. However, the known quantities of the present groundwater movements are of minor importance compared to the annual and inter-annual fluctuations in precipitation and evaporation. During the early Hol-

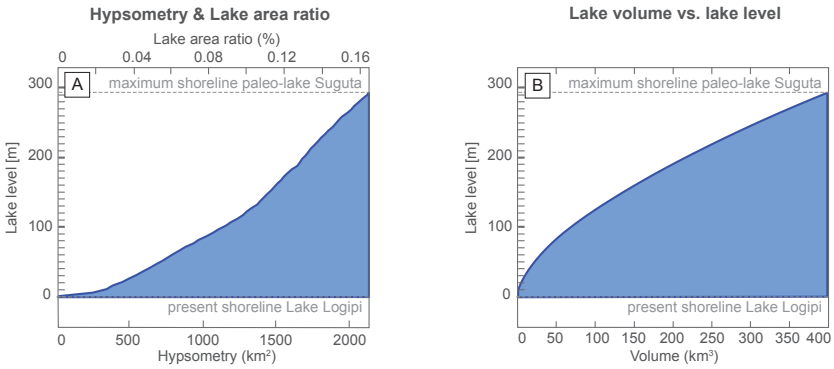

Figure 2.12 Hydrologic modelling results for rising lake levels in the Suguta Valley. (A) Hypsometry (= area of a lake at a certain level) and lake-area ratio (= fraction of basin surface covered by water at this level) of the Suguta basin. (B) Volume of the water body at a certain lake level. .

ocene, palaeo-Lake Suguta have had at least temporarily a surface outflow via Kerio Valley into lake Turkana, when it reached its maximum lake level of 295 m at an elevation of 570 m asl.[12]. The amount of groundwater discharge is still unknown, but seepage to Lake Turkana might have changed when the lake surface of palaeo-Lake Suguta reached higher elevations than the maximum lake level of Lake Turkana, probably the case above 460 m asl. These possibilities of extra water releases during the early Holocene would underestimate the precipitation-evaporation ratio in a closed-basin simulation. However, we regard these influences to be compensated by additional water entering the Suguta Valley from the overflowing lakes Baringo, Bogoria and Nakuru in the higher elevated southern parts of the Rift during synchronous highstands (Fig. 2.2).

Our hydro-balance model reveals, compared to today, an early Holocene precipitation increase of +26% for a dramatic lake level increase in the Suguta Valley. This value is of the same order of magnitude as precipitation estimations for early Holocene high lake levels in other East African lake basins. For example, a precipitation increase of 10-20% was modelled for Lake Turkana and Victoria basin[48], 23% for Lake Nakuru-Elmenteita[53] and ~30% for Lake Naivasha [44,48,53]. Similar values of precipitation increase explain the same climate pattern that caused high lake levels in this area during the AHP. Although the majority of parameters could be determined, a general weak point of lake-balance modelling is the estimation of soil moisture and land albedo, which are dependent on changes in the vegetation coverage. An example is provided by modelling the Lake Naivasha highstand, where a change towards more humid conditions would lead to vegetation changes in the catchment and subsequent higher transpiration resulting in ~7-15% higher precipitation[44,48]. Factors as changes in cloudiness and temperature attributed to vegetation changes would follow and therefore cannot be ignored when interpreting palaeo-environmental records derived from lake archives. Cloudiness and temperature exert a significant influence of rates of evaporation, therefore directly impacting the lake water balance[55]. The knowledge about past vegetation changes would therefore increase the knowledge about palaeo-precipitation changes via hydrologic modelling, but seems to remain difficult to determine, since pollen in tropical lacustrine sediments, especially when exposed to the surface for a long time, are often scarce and/or intensely oxidized.

2.3.4 Conclusions

Our modelling results regarding the magnitude of lake level changes in the Suguta Valley due to different precipitation changes provide valuable insights into the sensitivity of this natural system. The present-day character of the modern Lake Logipi represents a snapshot of its natural variability and the climate system. As demonstrated by our modelling, a relatively small change in humidity can rise the lake level from less than 10 m to more than 300 m, an area 240 times larger would be flooded by water. Palaeoclimatic reconstructions from other basins suggest, that high and large lakes are a common feature in East Africa, in particular during the early

Holocene climatic optimum[6] suggesting a similar mechanism behind.

2.4 Supplementary information 3 - Final lake-level reconstructions & interpretation

The application of shoreline data alone in order to reconstruct the impact of past climate variability in the Suguta Valley is difficult since they provide often only a snap shot of maximum shoreline elevations and are not temporally continuous. Lacustrine sediments provide a complete history of internal lake variations but using them alone does not provide insights into the magnitude of water level changes that causes the records internal variability. The calculation of possible precipitation changes in form of a hydro-balance model only provides hypothetical possibilities for lake level variations. Only the combination of all three methods allows us a detailed break down of the climatic variations during the AHP.

2.4.1 Method on completing lake level reconstruction

The exact determination of the magnitude of lake level changes to a certain time is possible when sediment and shoreline data are available. For episodes where one of them is missing, the magnitude of lake level changes was inferred by applying the hydro-balance model, as outlined in chapter 2.3 (Fig. 2.13). For the time interval of the investigated lacustrine sequences (chapter 2.2) we reconstructed the lake level as follows: According to time intervals, where both sediment and shoreline data were available, the internal variations occurred abruptly (see main text for possible reasons). Assuming abrupt precipitation changes for variations in the sedimentation pattern and taking abundances of Melanoides tuberculata as evidence for shallower water conditions, we inferred a lake level drop or rise if the hydro-modelling results for abrupt changes and the sedimentary pattern supports this interpretation. This approach enables us to report maximum lake level changes, as shown in Figure 2.14.

2.4.2 Results and interpretation

2.4.2.1 Onset of the AHP

The onset of the AHP is not directly documented, neither by shorelines nor by continuous lacustrine sequences throughout the valley, but abundant reworked 13.9 ka old oyster shells (NAMR2) within highly-elevated lacustrine deposits as well as shoreline deposits (NAMR1) dated at 13.7 ka indicate the existence of a lake level maximum at the beginning of the AHP. We do not yet know about the exact duration of this earlier highstand, but hydrological modelling results suggest a minimum age of the onset of around 14.9 ka, assuming a gradual onset of this lake episode, and 14.2 ka, respectively, if the lake was established abruptly in the valley. The estimation of 14.9 ka is contemporaneous with evidences for pronounced African lake fillings north of 10°S[6] and pronounced precipitation increases inland Asia[2] reported ~14.8 ka (Fig. 2.3).

2.4.2.2 Younger Dryas (YD)

The YD cold event between 12.8-11.6 ka has caused major desiccation all over Africa north of 10°S and terminated abruptly at 11.7 ka across southern equatorial Africa[6,56]. This rapid termination of the YD is documented, e.g., by the onset of the ice accumulation on Mt. Kilimanjaro with the tentative age of 11.65 ka[22] and rapid regression of Lake Nakuru[24] in East Africa and various studies from the WAM[13,23]

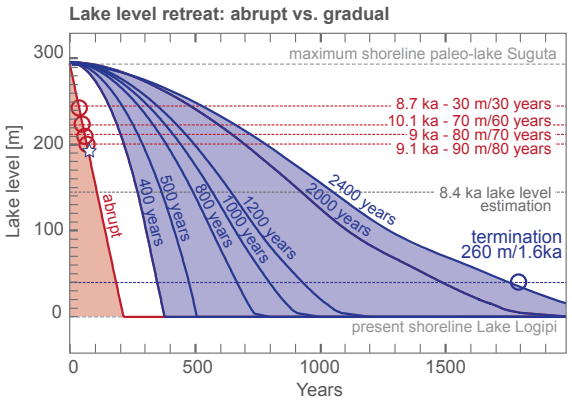

Figure 2.13 Modelling of abrupt (red) vs. linear (blue) precipitation changes and their related lake level curves. Dotted coloured lines indicate examples for lake level fluctuations as suggested by shoreline indicators. The evaporation model uses a Penman approach as described in Bookhagen et al. (2001)[43]. The termination of the Younger Dryas event in the area, as an example, must have occurred at latest at 11.55 ka under the assumption that the section EL08 (indicated by asterisk) truly indicates a rising lake level (see text for details).

and ISM domain[26]. Neither our shoreline nor the lake-sediment record in the Suguta Valley includes the time interval of the YD. However, we are able to use the onset of lacustrine sedimentation of the sequences that we have already investigated and compare those data with the results of our hydrological modelling about abrupt vs. gradual lake level changes, to estimate at least the date for the termination of this event. Using this approach, our results reveal that the age determination of the termination is more complex than expected: Periodic flooding at LN08 is precisely dated by charcoal at 11,200±20 years BP (Fig. 2.6, 2.8-2.10), and indicates an already existing lake of 235 m water depth. The age model (Fig. 2.9) of EL08 suggests a possible onset of the 195 m above basin floor located sequence at 11.4 ka, and already deep lacustrine sedimentation is documented at BG08 11,300±110 ka ago, located 180 m above the present basin floor. Assuming an abrupt onset of lake level rise from a desiccated basin, as it is suggested by various studies[23,26,56] we would expect a termination of the YD around 11.35 ka, when LN08 is used as reference sequence, and 11.6 ka for EL08 as reference site, according to the hydro-balance model (Fig. 2.13). Since almost a 200 m deep lake is indicated by the sedimentation pattern at BG08 and EL08 11.3 ka ago, the estimated termination using LN08 is not favoured when assuming an abrupt termination. Using EL08 as reference sequence, the mismatch of time difference between the two onset ages of lacustrine sedimentation at LN08 and EL08 when following the abrupt lake level curve suggests either a not well established age model for EL08 or a more complex mechanism during the return to full humid conditions. We tend to exclude the possibility of an incorrect age model, due to an excellent correlation of the two age models of EL08 and BG08 (Fig. 2.9), both located along the eastern valley margin. We rather propose an interruption of precipitation resulting in a slowdown of sedimentation after 11.3 ka. The slowdown might be attributed to a monsoon weakening resulting in precipitation decreases, probably produced by a pronounced sunspot minimum between 11.3-11 ka (Fig. 2.4), that interrupted the abrupt termination of the YD (see main text for possible mechanisms for monsoon weakening). Allowing an age error of 100 years in the age model of EL08 would set the termination of the YD in the Suguta Valley to 11.6±100 years, which correlates with the onset of the ice accumulation on the Kilimanjaro[22] and onset of southeasterly strong monsoon winds[56].

2.4.2.3 Internal lake-level fluctuations during the AHP

The internal lake level fluctuations are indicated by abrupt changes in C/N ratios, grain-size variations and the abundances of snail shells in the sediments sections and the record of palaeo-shorelines. Correlations with ISM and WAM-wide proxy records are illustrated in Figure 2.4. LN08 provides the best insights for lake variations between 11.2-10.7 ka due to its high resolution and location close to the highest shoreline. This site therefore records each variation in sedimentation pattern within the basin, which can directly be used for shoreline estimation. Lake level rise from the termination of the YD was interrupted at 11.05 ka and lowered by 35 m. After having reached maximum lake levels, another lowering occurred at around 10.9 ka of ca. 60 m and at 10.7 ka of ca. 75 m. The observed intervals of lake level lowering correlate with the time known as the preboreal oscillation (PBO) where fairly and steadily rising temperatures in the northern hemisphere were interrupted by distinct cold events[57], concurrent with changes in atmospheric $\Delta^{14}C$[58]. The cold events are also visible in tropical regions through sea-surface temperature drops, e.g., in the Cariaco basin 11.1 ka ago[59] or monsoon weakening in Asia dated at 10.9 and 11.2 ka[3,4,26]. The correlation of such abrupt cold event throughout the whole northern hemisphere suggests a global climate mechanism (Fig. 2.4).

The time interval between 10.7-10.25 ka is rather difficult to reconstruct, since neither shoreline data nor higher elevated sediment sequences are yet provided. The estimation about maximum shorelines within that time period is an estimation only provided by internal variations of sediment geochemistry, snail abundances in EL08 and BG08 and hydrological modelling. The reconstructed lake stands below the MHS but also shows abrupt ups and downs of the water level at around 10.5 and 10.3 ka. Both time intervals are well-known global climate events, as it was recognized as higher dust input to the Kilimanjaro ice record, monsoon weakening recorded in the Arabian Sea[3,11] and Asian terrestrial sites[4,26,60], but also in the northern Atlantic where enhanced iceberg discharges[61] occurred (Fig. 2.4). It has been suggested that the event in the North Atlantic was

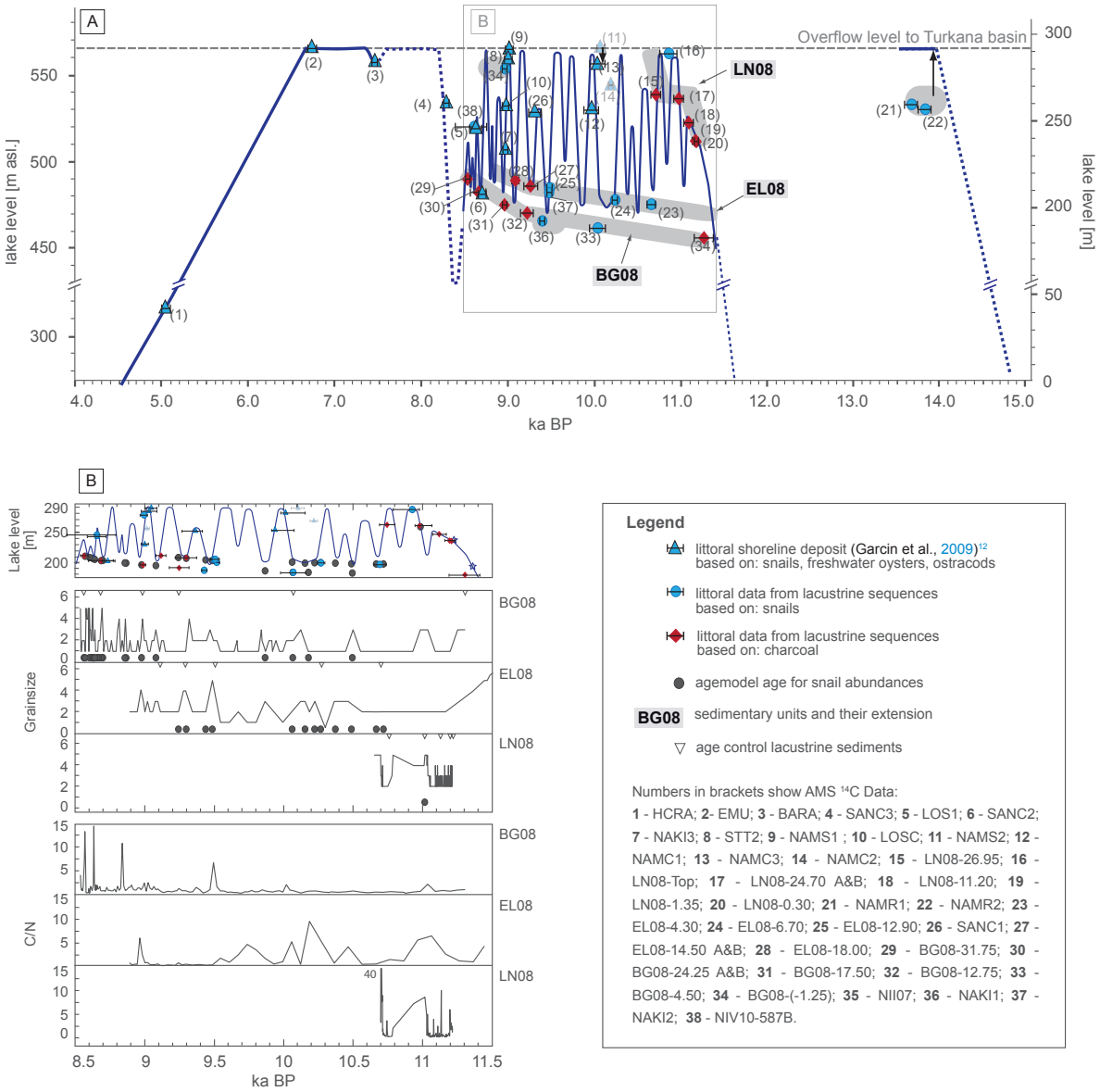

Figure 2.14 (A) Lake level record of palaeo-Lake Suguta during the African Humid Period (AHP) based on the (B) combination of shoreline measurements[12] and synchronous variations in sediment characteristics such as grain size variations, geochemistry and microfossil assemblages. Ages are displayed with 1-sigma error. Dotted lines in the lake level record showing estimations only based on hydromodel calculations and are not supported by proxy data.

triggered by a distinctly decrease in solar forcing as inferred from rising ^{10}Be values in Greenland ice cores[61]. According to the hydro-balance model, the time in between was not sufficient to fill the valley again until the MHS.

Between 10.25-9.95 ka, the lake level record is again supported by shoreline measurements[12] although only provided with large errors. However, the massive abundances of snails within the sediments and pronounced peaks in C/N ratios allow us to reconstruct lake-level variations during this time. We observe a comparatively long lake lowstand over 200 years, between 10.2-10.0 ka, which is also recorded in other monsoon influenced proxy sites in East Africa and Asia[3,22,60]. A pronounced sunspot minimum might be an explanation for this prolonged dry episode in East Africa. A short lake transgression is indicated by measured shorelines close to the MHS. Abrupt lake regression followed, however, that reached minimum elevations at around 9.9 ka, as indicated by snail shell abundances in BG08 and

grain-size increases in both sequences. The drought event in East Africa at around 9.9 ka coincides, within error bounds, with evidences for ISM weakening[26] and also North Atlantic cooling events[57,61].

A prolonged abrupt drying event occurred between 9.5-9.2 ka documented by basin wide snail shell distributions at 90 m below the MHS, and rapid increasing grain-sizes in BG08 and EL08, corroborated by a distinct C/N peak. The drought of 250 years duration was interrupted by a short lake transgression at around 9.4 ka as suggested by a high shoreline (SANC1) and decreasing grain-sizes. The entire time period correlates with enhanced drift ice events in the North Atlantic[61], but is restricted to a shorter time period in ISM records. The Kilimanjaro ice record[22] shows only enhanced dust input for the older part of the event between 9.6-9.4 ka, whereas for the younger part of this drought event humid conditions are indicated. Due to the return to sand deposition in BG08 and EL08 and major abundances of snail shells in EL08, we doubt a return to humid conditions earlier than 9.2 ka. An abrupt short-lived return towards another drought at 9.15 ka is evident in the sedimentary and palaeontological record in both studied sequences. The lake level dropped about 80 m within 70 years. This event is a climate event recognized also in other areas in the African[22] and ISM realm[3,26], but also observed, with smaller amplitudes, in Greenland ice cores, where it appears with an abrupt onset of a cooling and gradual return to warmer conditions explained through a freshwater influx to the North Atlantic[57].

Clear evidences for a major return to full humid conditions following this event are given by sediment contents as well as various shoreline measurements throughout the Suguta Valley. The MHS was reached as abruptly as the prior drought event occurred, however, it was only short-lived though pronounced humid period that terminated abruptly 9 ka ago. A 15 cm layer of intact snail shells in NII07 in the highest elevated lacustrine sequence, downward distribution of various shorelines, increasing grain-sizes in the studied sequences and snail shells propose an abrupt regression of 80 m. The event is less clear, but still visible within the errors in ISM records[3,26] and the Kilimanjaro dust record[22], indicating monsoon weakening and drought conditions, respectively. The return to more humid conditions at around 8.8 ka is only indicated by decreasing grain-sizes and missing snail shells in BG08, since sedimentation at EL08 is not documented any more and shoreline data are missing. Strong ISM activity was concluded from other studies in the domain[11,26,22] except in Oman[3], which might be related to dating uncertainties. The youngest set of data for a high-resolution reconstruction of lake level fluctuations in the Suguta Valley are provided by two independent sediment sequences (BG08, NIV10) and a shoreline (LOS1) between **8.75-8.5** ka, when abrupt fluctuating lake levels of 70-40 m below maximum shoreline were superimposed by a gradual drying trend. The return to full humid conditions was prevented according to the hydro-balance model of possible lake level changes between highly variable grain-sizes in BG08. The event is widely known from summer-biased study sites to show a gradual drying trend predating the 8.2 ka event[3,9-11].

Drought events, that we observed in the palaeo-Lake Suguta reconstruction, do correlate within small errors with ISM weakening events until far up to northern hemisphere events, where enhanced iceberg discharges occurred contemporaneous. Spectral analysis on $\delta^{18}O$ records from the ISM domain have demonstrated that solar forcing plays an important role in driving centennial to decadal precipitation changes in the area[4,10]. Cooling events in the North Atlantic were also attributed to solar irradiation changes[61]. The global occurrence of these events support the idea, that internal abrupt lake level fluctuations in the Suguta Valley are also attributed to variations in solar output, which becomes clear when comparing our data to the sunspot data set provided by Solanki et al. (2004)[28]. An explanation of how these events can cause abrupt precipitation changes in East Africa is given in the main text.

2.4.2.4 The 8.2 ka event in the Suguta Valley

The prior observed falling lake level as indicated by increasing grain-sizes towards non-lacustrine deposition in BG08 might have dropped even further down to a lake depth of only 140 m 8.45 ka ago, according to the hydro-model when an abrupt drying trend is assumed and less, if the trend was rather gradual. This restriction is caused by a shoreline (SANC3) dated at 8.3 ka in an elevation of a former lake depth of 260 m suggesting a major transgression. The pronounced drought at 8.4 ka is, although less extreme, visible from the North At-

lantic[61] over West Africa[13,23], East Africa[6,22] to the ISM domain[3,11,26,60]. Unfortunately, the 8.2 ka event itself is not documented by existing data in the Suguta Valley, which prevents us from providing a lake level estimation for this event.

2.4.2.5 Termination of the AHP in the Suguta Valley

The termination of the AHP occurred in the Suguta Valley after 6.8 ka, according to available data from shorelines. From hereon, the lake level dropped gradually by 260 m until about 5.0 ka as indicated by a series of palaeo-shorelines in the centre of the valley. Due to a large data gap between 6.8 and 5.1 ka, it cannot be ruled out, that the highstand might have lasted even longer. We emphasize, however, that the termination could have lasted at least until 5.2 ka, when an abrupt decline of palaeo-Lake Suguta is assumed or until 6.8-5.4 ka for a gradual lake level decline, according to our lake-balance modelling results. The main text provides a detailed discussion for possible mechanisms. Prolonged lake level highstands of Lake Turkana and the Ethiopian lakes and also Lake Bosumtwi from West Africa, support our hypothesis that the CAB, attracting moisture from the Atlantic Ocean, has been the major influence for high lake levels in East Africa, especially the East African Plateau. During the termination of the AHP when the ISM weakened, we propose a prolonged CAB influence to parts of the Ethiopian Plateau, whereas the East African Plateau was not reached by the CAB at that time anymore. This is very plausible, since the CAB is located in a NNE-SSW direction over Africa allowing the Ethiopian Plateau to be more affected by the CAB associated rainfalls than the East African Plateau.

2.4.3 ENSO influence in the Suguta Valley

Although the length of our record is probably too short to confidently unravel a possible early Holocene linkage between ENSO and drought events in tropical East Africa, it is worth noting that there is a generally opposite trend with weak or absent ENSO-like activity[7] during strong summer monsoons and slightly enhanced ENSO pattern during weakened monsoon/drought events in our record (Fig. 2.3). The strengthening of the WAM and ISM during maximum July insolation resulted in higher upwelling due to intensified easterly trade winds which in turn lowered the equatorial ocean temperatures and suppressed the IOD/ENSO dynamics by increasing the SST and pressure gradients across the Pacific[7,64,65]. Warm ENSO events in the ISM domain during the early to mid-Holocene seem therefore only the result of a monsoon weakening, which might be related to solar variations. Thus, we exclude warm ENSO events in East Africa during the early to mid-Holocene as the possible drivers for internal climate variability during the AHP and rather propose slightly enhanced ENSO active during droughts to have been only the result of monsoon weakening. This assumption is supported by the slight increase of ENSO around 6.8 ka when maximum northern July insolation is displaced by maximum equatorial September insolation due to precession changes. Whereas precessional forced decline in July insolation has weakened the ISM, associated with a southward decrease of the ITCZ and accompanied with the elimination of CAB influence to East Africa (see main text), the change to an equatorial insolation maximum in September sustained at least the intensity of the ITCZ during that month resulting in a circulation still strong enough to suppress IOD/ENSO anomalies.

2.4.4 Conclusions

Evidences summarized in this study are emerging that the entire Earth's climate is sensitive to small changes in solar output on sub-orbital time scales during the early to mid-Holocene. Abrupt precipitation changes are proposed to have been the main cause for rapid variations in the reconstructed lake record. The mechanism behind has caused changes in precipitation to at least modern values or even lower. This conclusion proposes an additional mechanism providing enhanced precipitation, which is not affecting the present day climatic pattern. A detailed discussion about the possibilities is given in the main text. It has explained, that topographic barriers play an important role in affecting large lakes in East Africa in the context of monsoon instability due to solar radiation fluctuations and associated displacements of circulation systems. According to the good correlation to other proxy records in East Africa and the ISM domain show that tectonic movement, which has caused an uplift of the western rift shoulder in the Suguta Valley, must have oc-

curred after the final lake retreat. The removal of the large water body probably has caused an isostatic rebound effect that could have induced fault activity. However, further work on the exact timing of this fault activation is necessary. The findings of this study contribute to our understanding of the influence and relationship between the West African and Indian monsoon systems, abrupt and gradual influencing mechanisms, and highlights the importance of the knowledge about the geographical, geological and climatologically situation of the study site used for palaeo-climate reconstruction.

2.5 Acknowledgements

This project was funded by the DFG Graduate School GRK1364 and two additional DFG grants to investigate the structural and environmental history of the Suguta Valley to M. Trauth and M. Strecker. A. Junginger received a DFG Graduate School GRK1364 doctoral fellowship to work on this project. We thank the Government of Kenya (Research Permits MOST 13/001/30C 59/10, 59/18 and 59/22), the Ministry of Water and Irrigation of Kenya and the University of Nairobi for research permits and support. We thank S. Roller, K. Wilson, A. Musiol, Y. Garcin, E. Odada, M. Strecker for inspiring discussions. We would also like to thank H. Douglas-Dufresne and P. Ilsley of Wild Frontiers Kenya, and B. Simpson and M. Watson of Tropic Air Kenya for logistical support during the helicopter expeditions to the Suguta Valley in 2007, 2008 and 2010.

Data are avaible in the Appendix 01-06 (see page 138 pp.).

2.6 References

1. deMenocal, P. et al. Abrupt onset and termination of the African Humid Period: rapid climate responses to gradual insolation forcing. *Quat. Sci. Rev.* 19, 347-361 (2000).

2. Morrill, C., Overpeck, J. T., Cole, J.E. A synthesis of abrupt changes in the Asian summer monsoon since the last deglaciation. *Holocene* 13,4, 465-476 (2003).

3. Fleitmann, D. et al. Holocene Forcing of the Indian Monsoon Recorded in a Stalagmite from Southern Oman. *Science* 300, 1737-1739 (2003).

4. Wang, Y.J et al. The Holocene Asian Monsoon: Links to Solar Changes and North Atlantic Climate. *Science* 308, 854-857 (2005).

5. Saji, N.H., Goswami, B.N., Vinayachandran, P.N. & Yamagata, T. A dipole mode in the Indian Ocean. *Nature* 401, 360-363 (1999).

6. Barker, P.A. et al. In: *Past Climate Variability through Europe and Africa* (eds Battarbee, R.W., Gasse, F., Stickley, C.E.) 117-138 (Kluwer Academic Publishers, 2004).

7. Moy, C.M., Seltzer, G.O., Rodbell, D.T. & Anderson, D.M. Variability of El Niño/Southern Oscillation activity at millennial timescales during the Holocene epoch. *Nature* 420, 162-165 (2002).

8. Stager, J.C., Mayewski, P.A. & Meeker, L.D. Cooling cycles, Heinrich event 1, and the desiccation of Lake Victoria. *Palaeogeogr. Palaeoclimatol. Palaeoecol.* 183, 169-178 (2002).

9. Weldeab, S., Lea, D.W., Schneider, R.R. & Andersen, N. Centennial scale climate instabilities in a wet early Holocene West African monsoon. *Geophys. Res. Lett.* 34, L24702, doi:10.1029/2007GL031898 (2007).

10. Neff, U. et al. Strong coherence between solar variability and the monsoon in oman between 9 and 6 kyr ago. *Nature* 411, 290-293 (2001).

11. Gupta, A.K., Das, M., & Anderson, D.M. Solar influence on the Indian summer monsoon during the Holocene. *Geophys. Res. Lett.* 32, L17703, doi:10.1029/2005GL022685 (2005).

12. Garcin, Y. et al. Late Pleistocene-Holocene rise and collapse of Lake Suguta, northern Kenya Rift. *Quat. Sci. Rev.* 28, 911-025 (2009).

13. Shanahan, T.M. et al. Paleoclimatic variations in West Africa from a record of late Pleistocene and Holocene lake level stands of Lake Bosumtwi, Ghana. *Palaeogeogr. Palaeoclimatol. Palaeoecol.* 242, 287-302 (2006).

14. Nicholson, S.E. A review of climate dynamics and climate variability in eastern Africa. In: *The Limnology, climatology and paleoclimatology of the East African lakes* (eds Johnson, T.C. & Odada, E.O.), 25-56, Gordon & Breach, Amsterdam (1996).

15. Ritchie, J.C. & Haynes, C.V. Holocene vegetation zonation in the eastern Sahara. *Nature* 330, 645-647 (1987).

16. Niedermeyer, E.M. et al. Orbital- and millennial-scale changes in the hydrologic cycle and vegetation in the western African Sahel: insights from individual plant wax δD and $\delta^{13}C$. *Quat. Sci. Rev.* 29, 2996-3005 (2010).

17. Hoelzmann, P., Kruse, H. & Rottinger, F. Precipitation estimates for the eastern Saharan palaeomonsoon based on a water balance model of the West Nubian Palaeolake Basin. *Global Planet. Change* 26, 105-120 (2000).

18. Marzin, C. & Braconnot, P. Variations of Indian and African monsoons induced by insolation changes at 6 and 9.5 kyr BP. *Clim. Dyn.* 33, 215-231 (2009).

19. Hailemichael, M., Aronson, J.L., Savin, S., Tevesz, M.J.S. & Carter, J.G. δ18O in mollusk shells from Pliocene Lake Hadar and modern Ethiopian lakes: implications for history of the Ethiopian monsoon. *Palaeogeogr. Palaeoclimatol. Palaeoecol.* 186, 81-99 (2002).

20. Patricola, C.M. & Cook, K.H. Dynamics of the West African Monsoon under Mid-Holocene Precessional Forcing: Regional Climate Model Simulations. *J. Clim.* 20, 694-716 (2007).

21. Overpeck, J., Anderson, D., Trumbore, S. & Prell, W. The southwest Indian Monsoon over the last 18000 years. *Clim. Dyn.* 12, 213-225 (1996).

22. Thompson, L.G. et al. Kilimanjaro Ice Core Records: Evidence of Holocene Climate Change in Tropical Africa. *Science* 298, 589-593 (2002).

23. Weldeab, S., Lea, D.W., Schneider, R.R. and Andersen, N. 155,000 Years of West African Monsoon and Ocean Thermal Evolution. *Science* 313, 1303-1307 (2007).

24. Richardson, J.L. & Dussinger, R.A. Paleolimnology of mid-elevation lakes in the Kenya Rift Valley. *Hydrobiologia* 143, 167-174 (1986).

25. Mulitza, S. et al. Sahel megadroughts triggered by glacial slowdowns of Atlantic meridional overturning. *Paleoceanography* 23, PA4206, doi:10.1029/2008PA001637 (2008).

26. Dykoski, C.A. et al. A high-resolution, absolute dated Holocene and deglacial Asian monsoon record from Dongge Cave, China, *Earth Planet. Sci. Lett.* 233, 71-86 (2005).

27. Berger, A. & and Loutre, M.-F. Insolation values for the climate of the last 10 million years. *Quat.Sci. Rev.* 10, 297-317 (1991).

28. Solanki, S.K., Usoskin, I.G., Kromer, B., Schüsseler, M. & Beer, J. Unusual activity of the Sun during recent decades compared to the previous 11,000 years. *Nature* 431, 1084-1087 (2004).

29. Johnson, T.C., Halfman, J.D. & Showers, W.J. Paleoclimate of the past 4000 years at Lake Turkana, Kenya, based on the isotopic composition of authigenic calcite. *Palaeogeogr. Palaeoclimatol. Palaeoecol.* 85, 189-198 (1991).

30. Brown, F.H. & Fuller, C.R. Stratigraphy and tephra of the Kibish Formation, southwestern Ethiopia. *J. Hum. Evol.* 55, 366-403 (2008).

31. Tamers, M.A., Validity of Radiocarbon Dates on Terrestrial Snail Shells. *American Antiquity* 35/1, 94-100 (1970).

32. Fritz, R. & Poplawski, S. 18O and 13C in the shells of freshwater molluscs and their environments. *Earth Planet. Sci. Lett.* 24, 91-98 (1974).

33. Olsson, I.U. The importance of the pretreatment of wood and charcoal samples. In: *Proc. 9th Conv. Los Angeles and La Jolla, 1976: Radiocarbon Dating* (eds. Berger, R. & H.E. Suess), 613-618 (1979).

34. Gizaw, B. The origin of bicarbonate and fluoride concentrations in waters of the Main Ethiopian Rift Valley, East African Rift system. *J. Afr. Earth Sci.* 22, 391-402 (1996).

35. Stuiver, M., & Reimer, P.J. Extended ^{14}C data base and revised 3.0 ^{14}C age calibration program. *Radiocarbon* 35, 215-230 (1993).

36. Reimer, P.J. et al., IntCal04 terrestrial radiocarbon age calibration, 0-26 cal kyr BP. *Radiocarbon* 46, 1029-1058 (2004).

37. Lu, S. Lithological factors affecting magnetic susceptibility of subtropical soils, Zheijan Province, China. *Catena* 40, 359-373 (2000).

38. Williamson, D. et al. Mineral-magnetitic proxies of erosion/oxidation cycles in tropical maar-lake sediments (Lake Tritrivakely, Madagascar): paleoenvironmental implications. *Earth Planet. Sci. Lett.* 155, 205-219 (1998).

39. Meyers, P.A. Applications of organic geochemistry to paleolimnological reconstructions: a summary of examples from the Laurentian Great Lakes. *Org. Geochem.* 34, 261-289 (2003).

40. Pointier, J.P., Delay, B., Toffart, J.L., Lefevre, M. & Romero-Alvarez, R. Life history traits of three morphs of Melanoides Tuberculata (Gastropoda: Thiaridae), an invading snail in the French West Indies. *J. Molluscan Studies* 58, 415-423 (1992).

41. Leng, M.J., Lamb, A.L., Lamb, H.F. & Telford, R.J. Palaeoclimatic implications of isotopic data from modern and early Holocene shells of the freshwater snail Melanoides tuberculata, from lakes in the Ethiopian Rift Valley. *J. Paleolimnol.* 21, 97-106 (1999).

42. Blodgett, T.A., Lenters, J.D. & Isacks, B.L. Constraints on the origin of paleolake expansion in the central Andes. Available online at http://www.earth-

interactions.org (1997).

43. Bookhagen, B., Haselton, K. & Trauth, M.H. Hydrological modeling of a Pleistocene landslide-dammed lake in the Santa Maria Basin, NW Argentina. *Palaeogeogr. Palaeoclimatol. Palaeoecol.* 169, 113-127 (2001).

44. Bergner, A.G.N., Trauth, M.H. & Bookhagen, B. Paleoprecipitation estimates for the Lake Naivasha Basin (Kenya) during the last 175 k.y. using a lake-balance model. *Global Planet. Change* 36, 117-136 (2003).

45. Dühnforth, M., Bergner, A.G.N. & Trauth, M.H. The hydrological budget of the Nakuru-Elmenteita basin, Central Kenya Rift, during the Early Holocene wet period. *J. Paleolimnol.* 36, 281-294 (2006).

46. New, M., Lister, D., Hulme, M. & Makin, I. A high-resolution data set of surface climate over global land areas. *Clim. Res.* 21, 1-25 (2002).

47. Griffith, J.F. Climates of Africa. *World survey of climatology* 10, Elsevier Publishing Company, Amsterdam, Netherlands (1972).

48. Hastenrath, S. & Kutzbach, J.E. Paleoclimatic estimates from water and energy budgets of East African Lakes. *Quaternary Research* 19, 141-153 (1983).

49. Bougeault, P. Evaporation models in hydrology. In: *Land surface evaporation – measurement and parameterizations* (eds. Schmugge, T.J. & André, J.C.), 93-120, Springer New York (1998).

50. Rowntree, P.R. Atmospheric parameterization schemes for evaporation over land: basin concepts, and climate modeling aspects. In: *Land surface evaporation – measurement and parameterization* (eds. Schmugge, T.J. & André, J.C.), 5-29, Springer New York (1991).

51. Schmugge, T.J. & André, J.C. In: *Land surface evaporation – measurement and parameterization* (eds. Schmugge, T.J. & André, J.C.), 424 pp., Springer New York (1991).

52. Dunkley, P.N., Smith, M., Allen, D.J. & Darling, W.G. The Geothermal Activity and Geology of the Northern Sector of the Kenya Rift Valley. *British Geological Survey Research Report* SC/93/1, 185pp., NERC, Nottingham (1993).

53. Kniess, U. Hydrologische Modellierung im Zentralen Kenya-Rift, *Diploma thesis at University of Potsdam* (2006).

55. Maley, J. Late Quaternary climatic changes in the African rain forest: the question of forest refuges and the major role of sea surface temperature variations. In: Paleoclimatology and Paleometeorology: modern and past patterns of global atmospheric transport (eds. Leinen, M. & Sarnthein, M.), NATO Adv. Sci. Inst., Ser. C, *Math. Phys. Sci.* 282, 585-616 (1989).

56. Talbot, M.R., Filippi, M.L., Jensen, M.B. & Tiercelin, J.-J. An abrupt change in the African Monsoon at the end of the Younger Dryas. *Geochem. Geophys. Geosyst.* 8, Q03005, DOI 10. 1029/2006GC001465 (2007).

57. Rasmussen, S.O., Vinther, B.M. , Clausen, H.B. & Andersen, K.K. Early Holocene climate oscillations recorded in three Greenland ice cores. *Quat. Sci. Rev.* 26, 1907-1914 (2007).

58. Björck, S., Rundgren, M., Ingolfsson, O. & Funder, S. The Preboreal oscillation around the Nordic Seas: terrestrial and lacustrine respones. *Journal of Quaternary Science* 12, 455-466 (1997).

59. Lea, D.W., Pak, D.K., Peterson, L.C. & Hughen, K.A. Synchroneity of Tropical and High-Latitude Atlantic Temperatures over the Last Glacial Termination, *Science* 301, 1361 (2003).

60. Hong, Y.T. et al. Correlation between Indian Ocean summer monsoon and North Atlantic climate during the Holocene. *Earth Planet. Sci. Lett.* 211, 371-380 (2003).

61. Bond, G. et al. Persistent Solar Influence on North Atlantic Climate During the Holocene. *Science* 294, 2130-2136 (2001).

62. Alley, R.B. & Ágústsdóttir, A.M. The 8k event: Cause and consequences of a major Holocene abrupt climate change. *Quat. Sci. Rev.* 24, 1123-1149 (2005).

63. Rohling, E. J. & Pälike, H. Centennialscale climate

cooling with a sudden cold event around 8,200 years ago. *Nature* 434, 975-979 (2005).

64. Clement, A.C., Seager, R. & Cane, M.A. Supression of El Niño during the mid-Holocene by changes in the Earth's orbit. *Paleoceanography* 15, 731-737 (2000).

65. Liu, Z., Kutzbach, J. & Wu, L. Modeling Climate Shift of El Niño Variability in the Holocene. *Geophys. Res. Lett.* 27, 2265-2268 (2000).

66. Gasse, F. & Fontes, J.-C. Palaeoenvironments and Palaeohydrology of a tropical closed lake (Lake Asal, Djibuti) since 10,000 yr B.P. *Palaeogeogr. Palaeoclimatol. Palaeoecol.* 69, 76-102 (1989).

67. Gasse, F. Evolution of lake Abhé (Ethiopia and TFAI) from 70,000 b.p. *Nature* 265, 42-45 (1977).

68. Gillespie, R., Street-Perrott, F.A. & Switsur, R. Postglacial arid episodes in Ethiopia have implications for climate prediction. *Nature* 306, 680-683 (1983).

69. Grove, A.T., Street, F.A. & Goudie, A.S. Former Lake Levels and Climatic Change in the Rift Valley of Southern Ethiopia. *The Geographical Journal* 141/2, 177-194 (1975).

70. Tiercelin, J.-J. & Vincens, A. Le Demi-Graben de Baringo-Bogoria, Rift Gregory, Kenya, 30,000 Ans d'Histoire Hydrologique et Sédimentaire. Bull. Centres de Rech. Expl. Prod. Elf-Aquitaine, Pau, France 11, 249–540 (1987).

71. Hillaire-Marcel, C. & Casanova, J. Isotopic hydrology and paleohydrology of the Magadi (Kenya)-Natron (Tanzania) basin during the Late Quaternary. *Palaeogeogr. Palaeoclimatol. Palaeoecol.* 58 , 155-181 (1987).

72. Casanova, J. & Hillaire-Marcel, C. Chronology and Paleohydrology of Late Quaternary High Lake Levels in the Manyara Basin (Tanzania) from Isotopic Data (^{18}O, ^{13}C, ^{14}C, Th/U) on Fossil Stromatolites. *Quaternary Research* 38, 205-226 (1992).

73. Camberlin et al., 1997, Rainfall anomalies in the source region of the Nile and their connection with the Indian summer monsoon, *J. Climate* 10, 1380-1392 (1997).

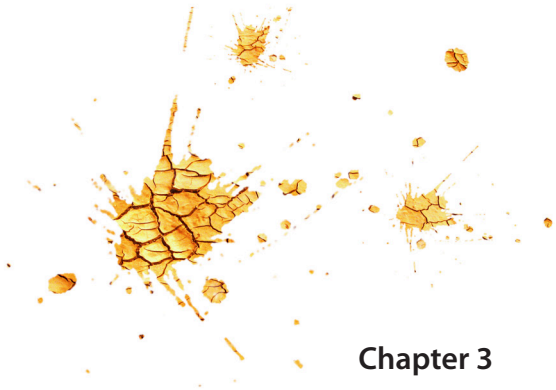

Chapter 3

Environmental variability in Lake Naivasha, Kenya, over the last two centuries

Stoof-Leichsenring, K.R., Junginger, A., Olaka, L.A., Tiedemann, R., Trauth, M.H.
in press: Journal of Paleolimnology (2011) doi:10.1007/s10933-011-9502-4

3.1 Environmental variability in Lake Naivasha, Kenya, over the last two centuries

Kathleen R. Stoof-Leichsenring[1*], Annett Junginger[2], Lydia A. Olaka[2], Ralph Tiedemann[1], Martin H. Trauth[2]

[1]Unit of Evolutionary Biology/Systematic Zoology, Institute of Biochemistry and Biology, University of Potsdam, Potsdam, Germany
[2]Institute of Earth and Environmental Sciences, University of Potsdam, Potsdam, Germany
*Corresponding author: Kathleen Stoof-Leichsenring, Unit of Evolutionary Biology/Systematic Zoology, Institute of Biochemistry and Biology, University of Potsdam, Karl-Liebknecht-Strasse 24-25, Haus 26, D-14476 Potsdam, Germany Tel: +49-331-977-5753, Fax: +49-331-977-5070, Email stoof@uni-potsdam.de

Kathleen R. Stoof-Leichsenring, Annett Junginger, and Lydia A. Olaka contributed equally to this work.

Abstract

Lake Naivasha, Kenya, is one of a number of freshwater lakes in the East African Rift System. Since the beginning of the 20th century, it has experienced greater anthropogenic influence as a result of increasingly intensive farming of coffee, tea, flowers, and other horticultural crops within its catchment. The water-level history of Lake Naivasha over the past 200 years was derived from a combination of instrumental records and sediment data. In this study, we analysed diatoms in a lake sediment core to infer past lacustrine conductivity and total phosphorus concentrations. We also measured total nitrogen and carbon concentrations in the sediments. Core chronology was established by ^{210}Pb dating and covered a ~186-year history of natural (climatic) and human-induced environmental changes. Three stratigraphic zones in the core were identified using diatom assemblages. There was a change from littoral/epiphytic diatoms such as *Gomphonema gracile* and *Cymbella muelleri*, which occurred during a prolonged dry period from ca. 1820 to 1896 AD, through a transition period, to the present planktonic *Aulacoseira* sp. that favors nutrient-rich waters. This marked change in the diatom assemblage was caused by climate change, and later a strong anthropogenic overprint on the lake system. Increases in sediment accumulation rates since 1928, from 0.01 g cm^{-2} y^{-1} to 0.08 g cm^{-2} y^{-1} correlate with an increase in diatom-inferred total phosphorus concentrations since the beginning of the 20th century. The increase in phosphorus accumulation suggests increasing eutrophication of freshwater Lake Naivasha. This study identified two major periods in the lake's history: 1) the period from 1820 to 1950 AD, during which the lake was affected mainly by natural climate variations, and 2) the period since 1950, during which the effects of anthropogenic activity overprinted those of natural climate variation.

3.1.1 Introduction

Lake sediments are frequently analysed to make paleoenvironmental inferences regarding changes in lake hydrology and surrounding ecosystems. These environmental changes can be caused by climatic fluctuations, by geomorphological and geological processes within the catchment area, and by human activities. The most recent climate records in lake-sediment archives are frequently overprinted by a local anthropogenic signal, confounding interpretation of environmental changes that were due to solely natural processes (Hausmann et al. 2002; Lotter and Birks 1997). Lake sediments may also fail to reflect past climate changes accurately in cases where non-climatic factors such as geomorphic and hydrologic setting influence the system (Fritz 2008). In the Naivasha basin, the last 100 years have been characterized by intense anthropogenic influence within the catchment, such as the damming of input rivers and the farming of coffee, tea and flowers around the lake (Verschuren 1996).

Diatoms in lake sediments are frequently used as bioindicators to infer ecological changes that have occurred within a lake and its surrounding catchment (Osborne 2000). This is possible because dia-

toms are remarkably sensitive to variations in water nutrient content, conductivity and pH. Past lakewater chemistry can be inferred from diatom valves in a sediment core, using transfer functions (Gasse et al. 1995). Such transfer functions have been developed from regional-scale studies in Africa (Gasse et al. 1995) and from combined, worldwide datasets (European Diatom Database Initiative, EDDI, http://craticula.ncl.ac.uk/Eddi/Lake

Naivasha was listed as a Ramsar site in 1995 (www.ramsar.org) and its one-million-year history has been investigated over various timescales. Studies of its most recent history indicate the increasing importance of human influences, in addition to natural factors, on ecosystem changes (Verschuren et al. 2000; Trauth et al. 2003, 2005). The human population in the town of Naivasha and the area around the lake has increased 50-fold over the past three decades, to ~120,000 (Edeghonghon Jimoh et al. 2007). Consequently the aquatic health of the lake has become increasingly important for the people who depend on it. It is particularly important to protect the lake against increasing eutrophication (Hubble and Harper 2001). Anthropogenic influence since the beginning of the 20th century is reported to have caused major changes in nutrient input, plankton composition and macrophyte abundance (Ballot et al. 2009; Hubble and Harper 2001). Published data on the floral shift, however, cover only the period between 1929 and 2005 AD, and because data collection was relatively patchy, the data do not provide a clear picture of the timing of species changes (Ballot 2009; Hubble and Harper 2001).

This study refines the temporal resolution of the environmental record of Lake Naivasha, using a continuous and well dated sediment record from the lake, covering about the last 200 years. The record reveals substantial changes in sedimentation rate and diatom assemblages, which were caused by human activities rather than by climate-driven processes.

3.1.2 Study site

At 1,889 m a.s.l., Lake Naivasha (0°55'S 36°20'E) is the highest closed-basin lake in the East African Rift System (Fig. 3.1). The modern lake covers an area of about 180 km^2 and has a water volume of ~0.85 km^3 (Bergner et al. 2003), a catchment area of 3,400 km^2 and an average depth in 1983 of 8 m (Verschuren 1999). Crescent Island Crater (CIC) is a partially-submerged crater in the eastern part of the lake that represents the area of greatest water depth, 16 m in 1983 (Verschuren 2001). At low water levels, the crater becomes increasingly isolated from the main lake, and as a result, becomes chemically distinct (Hubble and Harper 2001).

The regional climate of this equatorial lake basin

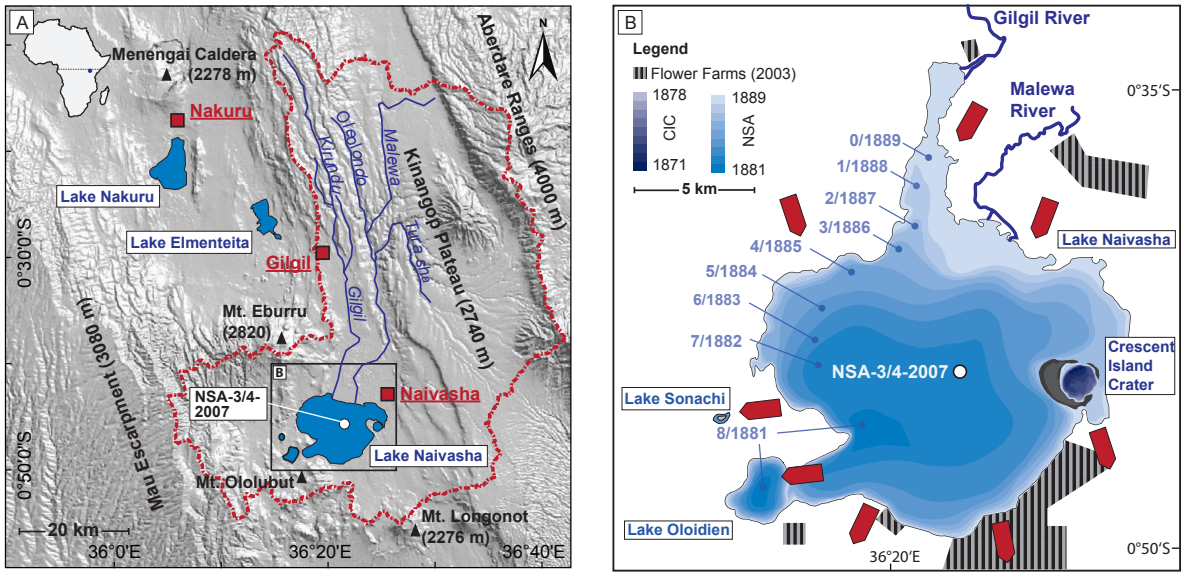

Figure 3.1 (A) Location map for Lake Naivasha within the highest basin of the Kenyan Rift System, together with the catchment area and sites discussed in the text. (B) Bathymetry of the Lake Naivasha main lake, and its satellite basins Crescent Island Crater and Lake Oloidien (1983), and Lake Sonachi (1990) (modified from Åse et al. 1986; Hickley et al. 2004; Verschuren 1999). Coring locality shown as white circle; arrows show the direction of groundwater flow, taken from Gaudet and Melack (1981).

is influenced by the seasonal migration of the Intertropical Convergence Zone (ITCZ), causing a strongly bimodal annual cycle, with rains in March/April and October/November (Nicholson 1996). The area receives additional rainfall from the "Congo air boundary," with westerly to south-westerly airflow during August and September, the so-called September rains (Nicholson 1996). Average rainfall in the vicinity of the lake is ~650 mm yr^{-1}, whereas the Aberdare Range in the eastern part of the catchment receives up to 2,400 mm yr^{-1}. Interannual variations in precipitation are linked to E-W adjustments in the zonal Walker circulation associated with the Indian Ocean Dipole and the El Niño/Southern Oscillation (Saji et al. 1999; Moy et al. 2002). There is considerable variation in rainfall, temperature and vegetation throughout the catchment area as a result of large differences in altitude.

Lake Naivasha is the second-largest freshwater lake in Kenya. It has a pH of ~8.1 (Åse 1987), which makes it unique in the semi-arid climate zone of the eastern arm of the Rift Valley, where other lakes are both alkaline and saline. Because potential evapotranspiration in the lake area is about 1,900 mm yr^{-1} (Clarke et al. 1990), the relatively low pH is attributed to high freshwater inflow from the Malewa and the Gilgil Rivers, which enter from the north. These two rivers drain the high-elevation Kinangop Plateau, and the Aberdare Range to the north and northeast, which receive high amounts of precipitation (Bergner et al. 2003). It is estimated that about 15% of the river input leaves the lake by underground seepage through porous volcanic material (Bergner et al. 2003). An understanding of this subsurface outflow process is fundamental to explaining the hydrochemical budget and solute export from the lake (Gaudet and Melack 1981; Ojiambo and Lyons 1996).

A major threat to Lake Naivasha is sediment pollution caused by human activities. The most important impacts are clearance of natural vegetation for agriculture, especially horticulture, and removal of the fringing papyrus swamps along the main inflow rivers, the Malewa and Gilgil, as these swamps buffer the lake from excess sediment input (Melack 1976; Harper et al. 1995). Consequences of sediment pollution are a reduction in water transparency and changes in the input and recycling of nutrients (Golterman et al. 1977). Additional factors that influence the health of the lake are the growing human population's activities in the upper catchment, which require increasing water abstraction from the lake and catchment (Jimho 2007). Since the 1920s, several exotic invasive species have been introduced into the lake, resulting in changes to the structure and dynamics of the food web. Despite these recent anthropogenic impacts, Lake Naivasha is still considered to be reasonably healthy (Hubble and Harper 2001).

3.1.3 Material and Methods

3.1.3.1 Core sampling

Parallel sediment cores (NSA-3 and NSA-4) were collected from the centre of Lake Naivasha (0°45'47.30"S, 36°21'58.31"E) in August 2007 with a KC Kajak sediment core sampler (KC-Denmark A/S) (Fig. 3.1). A transparent coring tube was used and the core was extruded in the field. The core lengths (37.8 cm for NSA-3 and 35.4 cm for NSA-4) were limited by our inability to penetrate deeper into the compacted sediment (Fig. 3.2).. Both cores were sampled at 2.1-cm intervals and samples were stored in the dark in Whirl-Pak® plastic bags. Once in the laboratory, samples were kept in the dark at 10°C. Samples from the NSA-4 core were used for ^{210}Pb dating, while the NSA-3 samples were analysed for sediment type, organic content, and diatoms.

3.1.3.2 Chronology (^{210}Pb)

Oven-dried subsamples from the Lake Naivasha NSA-4 sediment core were analysed for ^{210}Pb, ^{226}Ra and ^{137}Cs by direct gamma assay in the Liverpool University Environmental Radioactivity Laboratory using Ortec HPGe GWL series well-type, coaxial, low-background intrinsic germanium detectors (Appleby et al. 1986). ^{210}Pb was determined via its gamma emissions at 46.5 keV, and ^{226}Ra by the 295 keV and 352 keV γ-rays emitted by its daughter radionuclide ^{214}Pb following 3 weeks of storage in sealed containers to allow radioactive equilibration. ^{137}Cs was measured by its emissions at 662 keV. The absolute efficiencies of the detectors were determined using calibrated sources and sediment samples of known activity. Corrections were made for the effect of self-absorption of low energy γ-rays within the sample (Appleby et al. 1992).

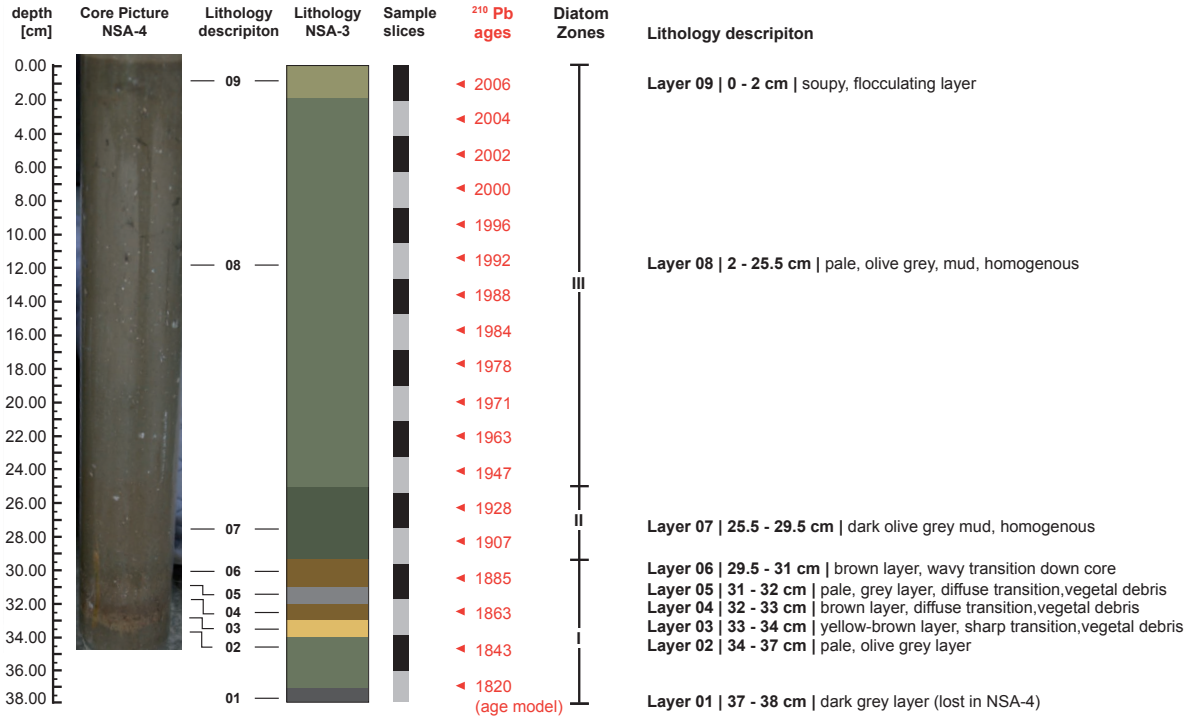

Figure 3.2 Lithology, chronology, sampling slices and diatom-based zonation of NSA-3/4. Sediment chronology in years AD, based on seventeen ^{210}Pb dates from NSA-4.

3.1.3.3 Sedimentology and Geochemistry

Total carbon (TC) and total nitrogen (TN) were analysed concurrently by IR spectroscopy and heat conductivity detection after burning weighed aliquots in an oxygen gas flow at 1,350°C, using a LECO CHN-2000 Elemental Analyzer. The TOC was determined after release of CO_2 in carbonates by reaction with hot 4% and 25% HCl, followed by analysis with the LECO CHN-2000 system. Total inorganic carbon (TIC) was obtained by subtracting TOC from TC. Mass accumulation rates (MARs) of sediment components were calculated from the bulk sediment accumulation rate (SAR) * %M/100, where %M is the percent mass of TIC, TOC or TN.

Prior to sedimentological analysis, mineral assemblages in samples from NSA-3 were determined by X-ray diffraction (XRD) analysis of powdered bulk samples, without further treatment, using a Siemens D5000 diffractometer. In addition, sediment samples NSA-3-1 to NSA-3-18 were examined with an optical microscope to semi-quantitatively cross-check the mineral content as well as the abundance of sponge spicules, macrophyte fossils, and other constituents.

3.1.3.4 Diatom counts and Transfer Functions

Between 0.25 and 0.35 g of sample material was processed for 90 minutes in 15-ml Falcon tubes containing 4 ml of 30% H_2O_2, which were placed in a water bath at 80°C. This was done to remove organic matter. After adding 10 µl of 2N HCl, sample tubes were filled with VE water and incubated overnight at 10°C. The supernatant was then discarded and samples were washed with VE water before being centrifuged at 3,000 rpm for 4 minutes. This washing step was repeated four times, after which 1:4 and 1:10 solutions were prepared and samples were settled on coverslips and dried overnight before being mounted on glass slides using Naphrax™. Diatom species identification was carried out using a Leica DM 4000B optical microscope at 1,000x magnification. A total of 300 to 500 valves were counted per slide. The diatom species were determined following Hustedt (1949), Gasse (1986) and Krammer and Lange-Bertalot (1986, 1988, 1991a, b). Diatom percentages were zoned using stratigraphically constrained cluster analyses with ZONE, an unpublished software tool provided by S. Juggins, University of Newcastle.

Major changes in the diatom assemblages over the last two centuries were determined by a detrended correspondence analysis (DCA) with CANOCO 4.5 software (ter Braak and Šmilauer 2002). The DCA also provided information about whether the species distribution was uniform or Gaussian with a single mode. The data were log-transformed in to stabilize the variance and rare species were down-weighted. A gradient length of 1.8 indicated a uniform species distribution. The main trends in diatom variations down-core were subsequently analysed using a principal component analysis (PCA) of the log-transformed species percentages.

Salinity, as represented by conductivity (log10 µS cm^{-1}), was reconstructed using the East African Salinity dataset included in the European Diatom Database (EDDI, http://craticula.ncl.ac.uk/Eddi/jsp/index.jsp). This dataset includes 579 diatom species identified from 187 samples which came from 98 sites between latitudes 19°N and 14°S and longitudes 27°N and 43°E. The sites range from Afro-alpine bogs at altitudes of up to 4,000 m to hypersaline lakes below sea level. The conductivity in these lakes ranges from 40 to 50,000 µS cm^{-1} and the pH from 5 to 10.9. In this study, results were back-transformed into µS cm^{-1} and classified according to the ecological habitats of the species: planktonic, planktonic/littoral, littoral and littoral/epiphytic diatoms. The total phosphorus (TP) was reconstructed using the EDDI combined TP dataset, including 347 samples from various European lakes. Finally, the results were back-transformed to total phosphorus values in µg l^{-1}.

Diatom-based inference models based on weighted averaging with inverse deshrinking (WAinv) were used for the reconstruction of conductivity and TP, as this gives an overall lower root mean-squared error (RMSE) of prediction (Birks at al. 1990). We used modern analog technique (MAT) analysis to test how well fossil diatom assemblages were represented in the dataset. This analysis evaluates the sample of the dataset for the closest analogues of floristic match by means of a similarity index. An index value above 100-150 indicates a poor floristic similarity to any of the samples from the underlying dataset, while values below this threshold indicate a high similarity. The MAT analysis indicates whether or not the analysed samples are similar to those of the underlying datasets, thus providing a measurement of the validity of the reconstructed environmental features.

3.1.4 Results

3.1.4.1 Chronology (^{210}Pb)

Total ^{210}Pb activity reached equilibrium with ^{226}Ra activity at a depth of about 33 cm (Tab. 3.1, Fig. 3.3a). Unsupported ^{210}Pb (Tab. 3.1, Fig. 3.3b) declined irregularly with depth. Concentrations in the top 15 cm were relatively constant, fluctuating around a mean value of 164 Bq kg^{-1}. Below 15 cm, there was a slow decline down to a depth of 22 cm, at which point there was a relatively abrupt change to a much steeper gradient. Concentrations below 30 cm were close to or below the detection limit. ^{137}Cs concentrations had a well defined peak between 20 and 25 cm depth, probably recording the 1963 fallout maximum from atmospheric testing of nuclear weapons (Tab. 3.1, Fig. 3.3c). Raw ^{210}Pb dates calculated using the CRS dating model (Appleby and Oldfield 1978) place 1963 at a depth of 20 cm, in relatively good agreement with the depth determined from the ^{137}Cs record (Tab. 3.1, Fig. 3.3d). The mean, post-1963 SAR calculated from the ^{137}Cs

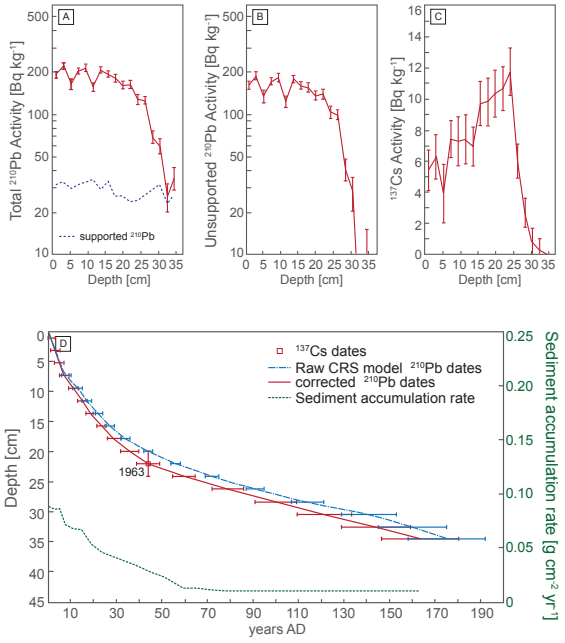

Figure 3.3 Radiometric chronology of Lake Naivasha sediment core NSA-4. Fallout radionuclides in the NSA-4 Lake Naivasha sediment core, showing (A) total and supported ^{210}Pb, (B) unsupported ^{210}Pb, (C) ^{137}Cs concentrations versus depth. (D) The raw CRS model ^{210}Pb dates and the 1963 depth determined from the ^{137}Cs record, together with the corrected ^{210}Pb dates and sedimentation rates calculated using the ^{137}Cs date as a reference point.

stratigraphic date is 0.055 g cm^{-2} y^{-1}, compared to the mean pre-1963 value calculated from the gradient of the ^{210}Pb profile of 0.010 g cm^{-2} y^{-1}. Corrected ^{210}Pb dates were calculated by applying the CRS model in a piecewise way using the ^{137}Cs date as a reference level (Appleby 2001). Results suggest that the relatively slow SAR persisted until the middle of the 20th century, but increased significantly thereafter (Tab. 3.2, Fig. 3.3). The mean SAR value during the past 10 years was 0.080 g cm^{-2} y^{-1}. Using the corrected ^{210}Pb chronology, the extrapolated age for the base of the NSA-3-18 core is 1820 AD, assuming a SAR of 0.01 g cm^{-2} y^{-1} at the maximum core depth.

3.1.4.2 Lithology and Geochemistry

Sediments of the core from the centre of Lake Naivasha consist of 37.8 cm of organic mud that shows layers of different colors in the lower part of the core (Fig. 3.2). Macroscopic observation is not supported by the XRD results. The large amount of organic matter in the sediment, including diatoms, overwhelms any mineralogical signal. Therefore, XRD is inapplicable for sediment investigations of the NSA-3 core. Diatom composition and geochemistry of the NSA-3 core, together with their paleo-environmental interpretations, are summarized in Figures 3.4, 3.6 and 3.7. TOC accumulation rates vary between 1.2 mg cm^{-2} y^{-1} and 6.2 mg cm^{-2} y^{-1}, with rates increasing towards the top of the core. The generally low TN accumulation rates show a similar trend, varying between 0.1 mg cm^{-2} y^{-1} and 0.8 mg cm^{-2} y^{-1}. TOC/TN ratios range between 4 and 9 and tend to increase slightly down-core. The accumulation of organic (TOC, TN) and inorganic (TIC) matter is almost constant throughout the period between 1843 and 1947 AD. After 1947, TOC, TC and TN accumulation rates increase regularly, all reaching a maximum in the uppermost sample, except for the TN rate, which decreases slightly in 2006. TIC accumulation rates fluctuate at the beginning of the 1970s, but show an overall increasing trend. Since MARs are a direct function of the bulk sedimentation accumulation rate, all MAR values increase significantly after 1947 AD (Tab. 3.2, Fig. 3.6). TOC/TN ratios vary between 8 and 9 in the period between 1843 and 1990 AD, but then show a decreasing trend until 2004, dropping to a value of 4 before again increasing slightly towards 2006. The quantity of fine-grained minerals is constant throughout the sediment core, whereas the numbers of macrophyte fossils and sponge spicules increase sharply down-core from sample NSA-3-15 to sample NSA-3-18.

Table 3.1
Fallout radionuclide concentrations in the Lake Naivasha core NSA-4-2007

Depth		^{210}Pb			^{137}Cs
		Total	Unsupported	Supported	
[cm]	[g cm^{-2}]	[Bq kg^{-1}]	[Bq kg^{-1}]	[Bq kg^{-1}]	[Bq kg^{-1}]
1.05	0.10	193.4 ± 10.8	161.9 ± 11.0	31.5 ± 2.1	5.4 ± 1.3
3.15	0.28	222.8 ± 11.9	189.9 ± 12.2	32.8 ± 2.5	6.3 ± 1.4
5.25	0.43	165.6 ± 14.2	135.8 ± 14.5	29.8 ± 3.0	3.9 ± 1.9
7.35	0.62	205.7 ± 9.8	173.9 ± 9.9	31.8 ± 1.7	7.4 ± 1.2
9.45	0.89	216.4 ± 12.9	183.7 ± 13.1	32.6 ± 2.2	7.3 ± 1.6
11.55	1.16	158.2 ± 11.2	123.9 ± 11.5	34.3 ± 2.7	7.4 ± 1.6
13.65	1.39	209.2 ± 10.4	180.2 ± 10.6	29.0 ± 2.0	7.0 ± 1.3
15.75	1.62	195.4 ± 9.7	162.3 ± 9.8	33.1 ± 1.7	9.7 ± 1.4
17.85	1.87	182.9 ± 12.0	156.6 ± 12.2	26.3 ± 2.3	9.8 ± 1.5
19.95	2.13	163.3 ± 9.6	137.2 ± 9.7	26.1 ± 1.8	10.4 ± 1.5
22.05	2.41	164.5 ± 10.9	140.6 ± 11.1	23.9 ± 2.1	10.7 ± 1.4
24.15	2.66	128.8 ± 10.7	104.6 ± 10.9	24.2 ± 2.2	11.8 ± 1.5
26.25	2.88	126.8 ± 7.7	99.9 ± 7.8	26.8 ± 1.5	6.0 ± 1.1
28.45	3.09	69.3 ± 7.1	40.6 ± 7.3	28.7 ± 1.5	2.7 ± 0.9
30.45	3.31	59.9 ± 7.4	27.9 ± 7.6	32.0 ± 1.6	0.9 ± 0.8
32.55	3.54	26.1 ± 6.0	3.2 ± 6.2	22.9 ± 1.3	0.3 ± 0.7
34.50	3.74	35.3 ± 6.6	8.4 ± 6.7	27.0 ± 1.3	0.0 ± 0.0

Table 3.2
^{210}Pb chronolgy of the Lake Naivasha core NSA-4-2007

Depth	Chronology				Sedimentation Rate		
[cm]	[g cm^{-2}]	AD	years	error	[g cm^{-2} y^{-1}]	[cm^{-2} y^{-1}]	± [%]
0.00	0.00	2007	0	± 0	-	-	-
1.05	0.10	2006	1	± 2	0.089	1.01	8.0
3.15	0.28	2004	3	± 2	0.086	1.09	7.8
5.25	0.43	2002	5	± 2	0.086	1.05	11.6
7.35	0.62	2000	7	± 2	0.073	0.67	7.5
9.45	0.89	1996	11	± 2	0.068	0.53	8.9
11.55	1.16	1992	15	± 2	0.066	0.56	11.0
13.65	1.39	1988	19	± 2	0.054	0.50	8.7
15.75	1.62	1984	23	± 2	0.046	0.41	9.5
17.85	1.87	1978	29	± 3	0.042	0.34	11.6
19.95	2.13	1971	36	± 4	0.036	0.31	12.5
22.05	2.41	1963	44	± 5	0.029	0.18	15.2
24.15	2.66	1947	60	± 5	0.013	0.12	13.6
26.25	2.88	1928	79	± 7	0.010	0.11	13.6
28.45	3.09	1907	100	± 9	0.010	0.10	13.6
30.45	3.31	1885	122	± 12	0.010	0.09	13.6
32.55	3.54	1863	144	± 15	0.010	0.10	13.6
34.50	3.74	1843	164	± 17	0.010	0.10	13.6

3.1.4.3 Diatom assemblages

Thirty-nine species were identified in the core, but only those whose abundances >0.5% were plotted in Figure 3.4. The species were grouped into four ecological types: planktonic, planktonic/littoral, littoral, and littoral/epiphytic, following Gasse (1986) and Gasse et al. (1995). Valve preservation was generally good throughout the core. Three diatom assemblage zones were identified in the core (Tab. 3.3, Tab. 3.4, Fig. 3.4).

Table 3.3
Stratigraphical zonation inferred by diatoms their dominant and subdominant diatom taxa.

Zone	Core depth [cm]	Age [year AD]	Dominant taxa	Subominant taxa
III	0 - 25.14	2006 - 1938	*Aulacoseira ambigua, Aulacoseira granulata*	*Synedra acus* sp.
II	25.14 - 29.45	1938 - 1896	*Aulacoseira granulata, Synedra acus* sp.	*Aulacoseira ambigua, Cymbella muelleri, Gomphonema gracile*
I	29.45 - 37.8	1896 - 1820	*Gomphonema gracile, Cymbella muelleri*	*Epithemia adnata, Aulacoseira granulata, Aulacoseira ambigua*

Zone I, between 38.7 and 29.5 cm, corresponds to the time interval between *ca.* 1820 and 1896 AD (samples NSA-3-18 to NSA-3-15). The diatom assemblage of this zone is dominated by the littoral/epiphytic and littoral diatoms *Gomphonema gracile* Ehrenberg (up to 26%), *Epithemia adnata* Kützing (up to 11%), *Cymbella muelleri* Hustedt (up to 22%), and *Navicula elkab* Müller (up to 18%). Abundances of planktonic species, such as *Aulacoseira ambigua* (Grunow) Simonsen and *A. granulata* (Ehrenberg) Simonsen, as well as the planktonic/littoral species *Synedra acus* Kützing, vary between 5% and 20%. In sample NSA-3-16 (33.6-31.5 cm, *ca.* 1863 AD), each of these planktonic species reaches a maximum abundance of only 5%, whereas *Cymbella muelleri* and *Navicula elkab* reach their maximum relative abundances within this zone, and reach similar abundances in samples NSA-3-18 to NSA-3-16. *Aulacoseira* sp. dominates in samples from NSA-3-16 to the top of the core. When *A. ambigua* is scarce, *A. granulata* is abundant, and vice versa.

Zone II ranges from 29.4 to 25.2 cm, corresponding to the time interval between *ca.* 1896 and 1938 AD (samples NSA-3-14 to NSA-3-13), and is transitional between Zones I and III. Within this zone, the planktonic/littoral *Synedra acus* is dominant, with a mean abundance of 23%. The planktonic species *A. ambigua* and *A. granulata* increase rapidly to peak abundances of 38% and 57%, respectively. The littoral and littoral/epiphytic species of flora decline and reach their minima around 1930 AD, shortly before the start of Zone III.

Zone III is the core interval between 25.1 and 0 cm, corresponding to the time interval between ca. 1938 and 2007 AD (samples NSA-3-12 to NSA-3-1). The diatom assemblage within this zone is characterized by *A. ambigua*, *A. granulata* and *Syndra acus*. The uppermost sample shows very high numbers of *Synedra acus*, however, with less frequent *A. ambigua* and *A. granulata*. The abundance of macrophytes and sponge spicules decreases within this zone, and they are almost absent between 1998 and 2004 AD (samples NSA-3-7 to NSA-3-2).

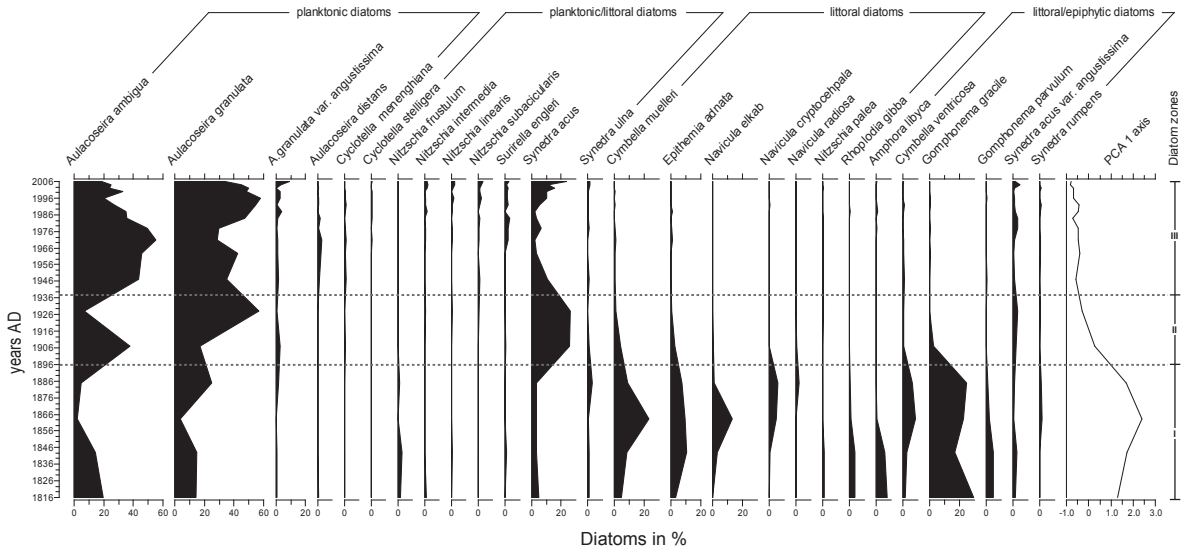

Figure 3.4 Summary of the diatom assemblages from Lake Naivasha core NSA-3, PC1 scores, and diatom-based zonation.

3.1.4.4 Statistical analysis and environmental reconstruction

The PCA of the data matrix of samples and the diatom percentages show that the first two principle components (PC) account for 72% of the total variance (PC1 63%, PC2, 9%). The PC1 scores are plotted in stratigraphic order, together with the distribution of diatom species (Fig. 3.4). Species and samples from the underlying dataset are plotted on the PC1 axis, with the inferred diatom zones marked in red ellipses (Fig. 3.5). The grouping of samples in this plot suggests that PC1 serves as an indicator for the ratio of planktonic diatom species (negative PC1 scores) to epiphytic/littoral diatom species (positive PC1 scores). Moving up-core, the PC1 scores change from -0.8 to 2.4 with the change from littoral/epiphytic to planktonic assemblages in transitional Zone II.

The modern analogue technique (MAT) analysis for the conductivity dataset indicates a good floristic match by comparing species composition of the analysed samples with those of the underlying samples in the dataset. All identified species are included in the East African salinity dataset. Because the East African conductivity dataset contains several samples from Lake Naivasha, it shows good agreement with the analysed samples. Samples NSA-3-18 to NSA-3-15 (ca. 1816 to 1885 AD), and in particular sample NSA-3-16 (ca. 1863 AD), perform relatively poorly because they show a high abundance of littoral and littoral/epiphytic species, which may not typically occur in any of the dataset samples. Sample NSA-3-16 has the highest similarity to a mud sample from Lake Kamuru in Uganda. Most of the analysed samples, however, correlate best with either a sediment sample from Lake Rugwero in Rwanda or a core-top sample from Lake Naivasha (Crescent Island Crater site). All three modern analogue samples are from freshwater lakes.

Results of the conductivity and TP reconstructions are shown in Figure 3.6. Reconstructions indicate the highest conductivity values in Zone I, about 731 µS cm^{-1} in sample NSA-3-16 - ca. 1863 AD, driven mainly by the occurrence of littoral species *Cymbella muelleri* and *Navicula elkab*. In particular, *N. elkab* favors highly saline (~13 mS cm^{-1}) and alkaline (~pH 9) waters (Gasse 1986). Apart from this sample, Zone I is characterized by an average reconstructed conductivity of 300 µS cm^{-1}. Conductivity values for

Table 3.4
Performance of the conductivity and TP models used for paleolimnological reconstructions.

Gradient	Method	r^2	RMSE	r_{jack}^2	RMSEP
Conductivity	WAinv	0.86	0.32	0.78	0.41
TP	WAinv	0.71	0.30	0.63	0.33

WAinv, weighted averaging with inverse deshrinking; RMSE, root mean squared error of prediction; RMSEP, jackknifed RMSE; r^2, jackknifed coefficient of determination.

Zones II and III are almost identical, generally varying between 150 and 185 µS cm^{-1}. The uppermost core sample (Zone III) shows a slightly higher conductivity value (215 The TP dataset includes only 34 of the 39 diatom species identified in our study. The MAT analyses for TP reconstructions were therefore of poorer quality than the conductivity reconstructions. Uppermost sample and samples NSA-3-18 to NSA-3-15 have the least similarity to the dataset samples, which relates to the fact that *Navicula elkab* and *Cymbella muelleri* are completely absent from the dataset. The diatom-inferred TP reconstruction yields lowest values in Zone I, including a minimum of 49 µg l^{-1} in sample NSA-3-16. Moderate TP values of ca. 80 µg l^{-1} are indicated for Zone II. After ~1938, the reconstructed TP values increase briefly to 155 µg l^{-1} and then decline to 100 µg l^{-1} at around 1970 AD. The reconstructed TP values subsequently increase to a maximum of 164 µg l^{-1} in 1996 (sample NSA-3-5) before once again decreasing slightly to 132 µg l^{-1} at present.

3.1.5 Discussion

The radiometric chronology of the Naivasha core is thought to be quite reliable for the time between 1907 and 2007 AD, showing a low, ±2-5 yr error range. The raw ^{210}Pb dates place 1963 at a depth of 20 cm, which is in relatively good agreement with the depth determined from ^{137}Cs.

The ^{137}Cs peak appears to preclude mixing as a cause of the irregular ^{210}Pb record. Before 1907 AD, errors on dates are greater, from ±9 years (sample NSA-3-14) to ±17 years (sample NSA-3-17). This section of the core also displays an apparent decrease in sedimentation rate, which must be interpreted with caution.

Sedimentation rates and geochemical data, together with the environmental reconstructions of conductivity and total phosphorus, conform with

the three diatom assemblage zones (Fig. 3.7). Zone I covers the time from 1820 to the end of the 19th century and was influenced mainly by natural climate variations, in particular by long periods of drought. Zone II represents a transition zone characterized by a shift from primarily climate-driven influences to a period when human increasingly altered the environment of Lake Naivasha. In Zone III, which covers the period from 1938 to 2007 AD, natural conditions in the lake are overprinted by anthropogenic influences, which are mainly reflected by high sedimentation rates and a rapid shift in the diatom assemblage.

3.1.5.1 Zone I (ca. 1820 to 1896 AD)

„Natural climatic variations – minor human activity"

Relatively low and constant bulk sediment accumulation rate (0.01 g cm^{-2} y^{-1}) and mass accumulation rates for TN (0.2 mg cm^{-2} y^{-1}) and TOC (2 mg cm^{-2} y^{-1}) indicate low sediment input from the catchment into Lake Naivasha during this period. The influence of human activity was minor because nomadic tribes only made sporadic use of the lake and its surroundings for water supply and food. The diatom-inferred TP values are relatively low, but increase slightly from 50 µg l^{-1} to 88 µg l^{-1} between 1863 and the end of Zone I. According to the classification scheme for warm-water tropical lakes, TP values serve as an indication of the shift from mesotrophic to eutrophic conditions (Salas and Martino 1991). A growing predominance of littoral and/or epiphytic diatom assemblages is indicative of rising conductivity values ranging between 290 µS cm^{-1} and 731 µS cm^{-1}, suggesting low water level in the lake, presumably caused by a drier climate. Low TN values and TOC/TN ratios ~9 reflect organic matter contributions from epiphytic and/or benthic diatoms and abundant aquatic macrophytes, both indicative of low water levels related to drier conditions (Meyers 2003). This interpretation is consistent with the large numbers of sponge spicules in the sediments, and the historically documented Laparanat-Mahlathule drought that caused low lake stands between 1760 and 1840 (Verschuren et al. 2000). Reconstructed lake levels for the Crescent Island Crater (CIC) indicate two major lowstands during this period (Verschuren et al. 2000), whereas East African rainfall anomalies reconstructed by Nicholson (2001) indicate a prolonged dry period with rare events of pronounced rainfall.

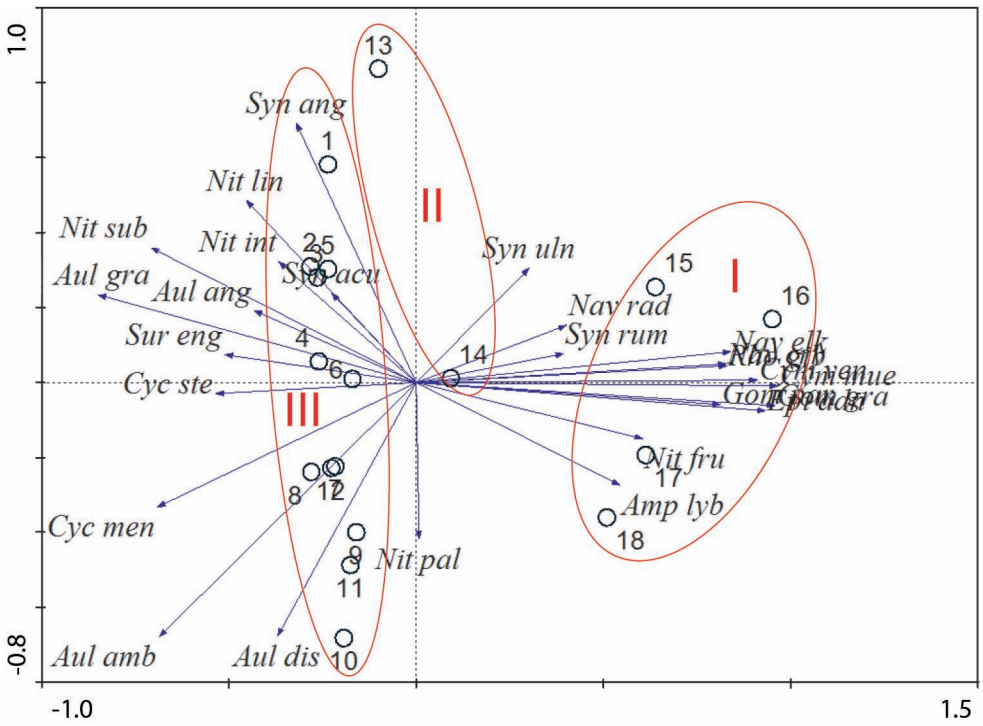

Figure 3.5 PCA biplot of species and sample data. Arrows represent species and circles represent samples. Ellipses indicate the diatom-inferred zones.

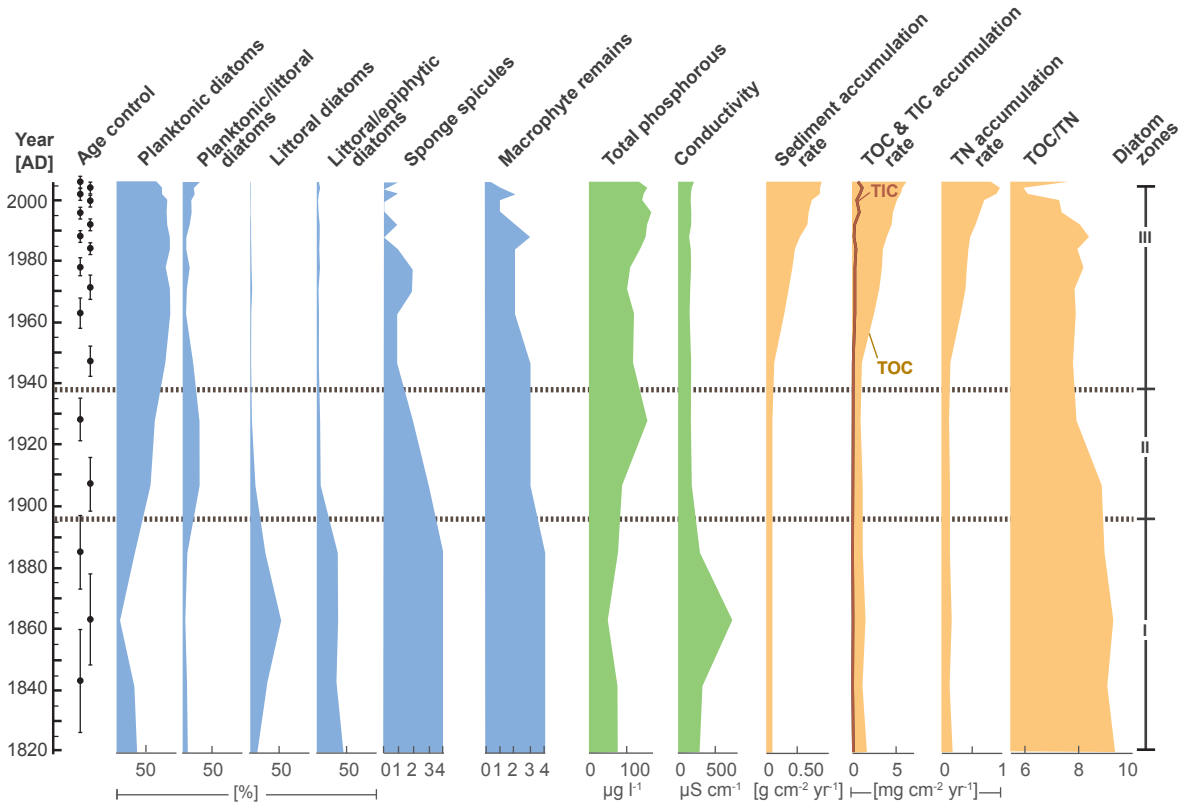

Figure 3.6 Down-core variations in diatom habitat preferences, diatom-based zonation, diatom-inferred conductivity and total phosphorous (TP) values, sediment accumulation rates (SAR) and mass accumulation rates for geochemical variables (TN-total nitrogen, TOC-total organic carbon, TIC- total inorganic carbon and the TOC/TN ratio) based on the age model. Age control is provided with error bars.

Zone I contains only one peak in inferred conductivity around 1863±15 AD, during the identified long dry period. This may have been a consequence of erosion and dissolution of salts formed during the long drought that occurred before 1840 AD, and perhaps lasted even longer, as suggested by the records of Verschuren (2000) and Nicholson (2001). Lake Naivasha is particularly sensitive to such declines in lake stage in that a small drop in lake level exposes a large area of lake bottom due to the shallow slope of the littoral area, particularly along the north shore. Declining lake level caused by a dry climate may have desiccated lake sediments where evaporites accumulated (LNROA 1993, Gaudet 1979). Thus, conductivity rises, rather than falls, with the onset of rains, as dissolved ions increase in the system with greater precipitation (Fig. 3.4). A rise in water level dissolved accumulated salts in the previously exposed sediments, which led to a brief increase in conductivity, with a peak of 731 µS cm^{-1} about 1863±15 AD (sample NSA-3-16). Thereafter, the Naivasha basin was persistently filled with water and the lake displayed lower conductivity. Considering the age error on sample NSA-3-16, it is not possible to identify exactly which precipitation event led to this early conductivity peak. It could have been the short wet period around 1850 AD (Verschuren 2000), alternatively 1860 or 1870 AD, years for which Nicholson (2001) inferred enhanced rainfall events.

Another explanation for the single conductivity peak is that lake level had decreased considerably after a long drought, which led to higher conductivity values in the Lake. Because sample NSA-3-16 represents ~20 years of lake history, and thus the average conductivity during that time, it is very difficult to infer the short-term environmental changes that occurred during that period, though there may have been high variability. It is difficult to compare our diatom record from the main basin of Lake Naivasha with lake level changes in the Crescent Island Crater. Although the basins are hydrologically connected from time to time, their bathymetries differ, and consequently, they may display differences in

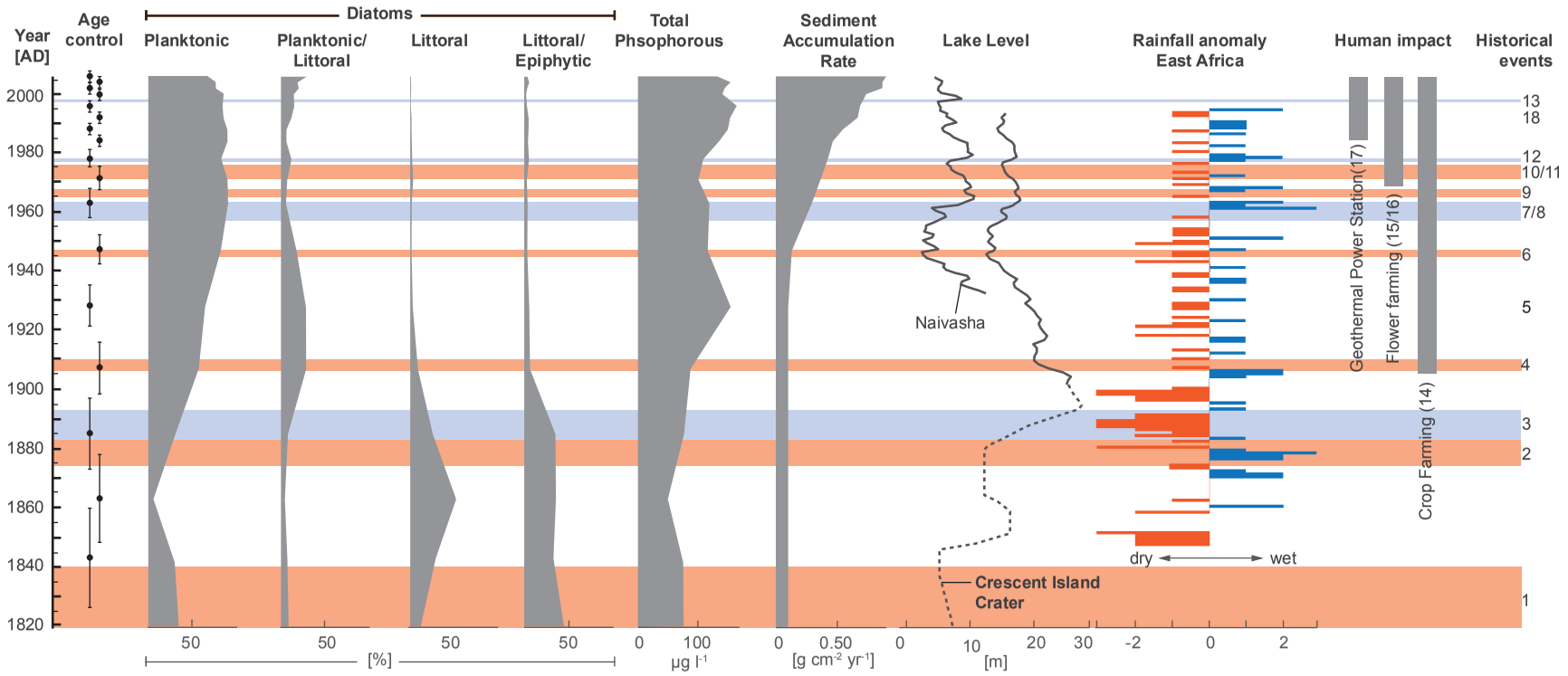

Explanation historical events & human impact

1 1760 - 1840 Laparanat drought (equatorial drought as part of the Little Ice Age); Lake Naivasha fell dry (a, b)
2 1870s - early 1880 nearly desiccation of Lake Naivasha and Lake Sonachi (c)
3 1883 - 1894 major transgression of Lake Naivasha following a decade of above-average rainfall (a)
4 1906 - 1910 low stand Lake Sonachi (d)
5 1928 Subukia Earthquake
6 1946 historical low stand Lake Naivasha (d)
7 1956 - 1958 wet period (e)
8 1961 - 1963 wet period (e, f, g)
9 1964 - 1967 drought
10 1972 - 1973 drought (d)
11 1975 - 1976 drought (d)
12 1977 - 1978 wet period (d)
13 1997 - 1998 El Nino - wet period
14 1904 - 1918 intensive coffee farming Aberdare Ranges
15 1969 begin flower farming
16 1982 intensive flower farming
17 1984 start Kengen thermal power station
18 ~1990 liberalization of fertilizers in Kenya (h)

Figure 3.7 Compilation of diatom assemblage variations, sediment accumulation rate (SAR), total phosphorus (TP) and historical records of environmental and land use data. Water levels for the main Lake Naivasha (NSA) are instrument-based while those for the Crescent Island Crater Lake (CIC) are a combination of instrumental (solid line) and sediment proxy (dashed line) (Åse et al. 1986; Verschuren et al. 2000). Rainfall anomaly for Eastern Africa (EA): data combined from rainfall proxy indicators for the 19th century and instrumental data for the 20th century, from Nicholson (2001). References to historical events: a - Nicholson 1995; b – Verschuren 2001; c – Sikes 1936; d – Verschuren 1999; e – Nicholson 1988; f - Vincent et al. 1979; g - Gaudet and Melack 1981; h – Ariga and Jayne 2006; blue bars indicate historical highstands of CIC/NSA or Lake Sonachi; red bars indicate historical lowstands of CIC, NSA or Lake Sonachi. Age control is provided with error bars.

sedimentation patterns and sensitivity to climate changes.

In general, high conductivity is indicated by the presence of two littoral species, *Cymbella muelleri* and *Navicula elkab*, and the littoral/epiphytic species *Gomphonema gracile*, which is very sensitive to pollution in modern lakes (Kelly et al. 2005). All three species favor water with moderate to high ionic strength, from 1,000 to 30,000 µS cm^{-1} (Gasse 1986). The conductivity values decrease up-core from ~1863 until the beginning of the 20th century, and remain constant at ~170 µS cm^{-1} thereafter. This change in water chemistry corresponds to a decrease in littoral and epiphytic diatom frequencies. After a generally dry period from 1820 to 1882 (Nicholson 2001) during which Lake Naivasha was nearly desiccated and its groundwater reservoirs emptied, a wetter period occurred from 1883 to 1894 (Nicholson 1995).

3.1.5.2 Zone II (ca. 1896 to 1938 AD)

„Transition zone - increased human activity"

From about 1883 to 1894 AD, Naivasha experienced a wetter period, indicated by a lake level highstand in the Crescent Island Crater (Verschuren et al. 2000), although sedimentation rates during that time were still low (0.01 g cm^{-2} y^{-1}). An increase in commercial farming of tea and coffee in the early 20th century had no discernible effect on sedimentation rate in the lake. Such large catchments are known to store sediments in sinks within the basins for many years before they transported to the lake. Nutrients, however, reach the lake much more quickly, as they are transported rapidly in dissolved form after rainfall events (Phillips 2003). This may explain the rapid increase in total phosphorus from around 1900 AD. Since the 1930s, the diatom-inferred TP values have exceeded 111 µg l^{-1}, indicating progressive eutrophication of the lake (Salas and Martino 1991). The arrival of the British colonists at the end of the 19th century and the intensive tea and coffee farming that followed coincide with nutrient enrichment of Lake Naivasha. Nutrient input favored planktonic species *A. ambigua* and *A. granulata*, both of which increased in abundance within this zone and maintain high abundance in Zone III. A slight decline in TOC/TN ratios towards values ~8 indicative of planktonic diatoms parallels the rising TP values (Meyers 2003). This implies a direct link to increased nutrient input in the lake from intensive coffee, tea and pyrethrum farming in the highland areas of the catchment.

Following this wet episode of the late 19th century, climate became drier beginning around 1910 AD, as indicated by a shift to a negative water balance (Nicholson 2001). Nevertheless, the large aquifers that filled during the wet period continued to provide groundwater to the lake, contributing to the low salinity in Lake Naivasha.

3.1.5.3 Zone III (ca. 1938 to 2007 AD)

„Human activity overprints natural climatic variation"

At the beginning of Zone III, the sediment accumulation rate increased to a maximum of 0.08 g m^{-2} y^{-1}. The most likely reason for this higher sediment accumulation rate was human activity within the catchment. Conversion of natural sediment traps such as papyrus swamps to horticulture and intensively farmed landscapes in the upper catchment fostered soil erosion and consequent sediment delivery to the lake. Anomalously high rainfall between 1962 and 1964 and a relatively wet period that continued through 1990 AD contributed to further degradation of the loose upper soil layers. The Ba/Ca ratios of marine corals off the East African coast (Fleitmann et al. 2007) support our interpretation of increasing erosion within Zone III since the year 1908±5 AD due to human activities in the Kenyan Highlands.

Eutrophication in Zone III was caused by an increased supply of phosphorus and nitrogen to the lake (Osborne 2000). The steady rise of *Aulacoseira* sp., which prefers nutrient-rich waters, coincides with a reduction in species that are more sensitive to pollution, such as *Gomphonema gracile*, and indicates the continuing eutrophication of Lake Naivasha. The diatom-inferred total phosphorus values show a positive trend since *ca.* 1963, increasing to 165 µg l^{-1} in 1996. This trend in TP is probably attributable to the increasing numbers of *Aulacoseira* within Zone III. *Aulacoseira* species occur commonly in eutrophic European and American lakes (Kilham et al. 1986; Karst et al. 1998; Anderson et al. 1990), and this genus is therefore regarded as an indicator of eutrophic conditions. Ballot et al. (2009) found TP values between 70 and 200 µg l^{-1} in Lake Naivasha from 2001 to 2005, and noted that the eutrophication of the lake was reflected by changes in the phy-

toplankton community, including a decrease in species richness. Modern Lake Naivasha is dominated by *Cyanocatena planktonica* (Cyanobacteria), *Pediastrum simplex* (Chlorophyceae) and *A. granulata*.

Along with rising SARs, TOC and TN accumulation rates rise between 1947 and 2007 AD. The TOC/TN ratios are fairly stable around 8 until 1990 AD. According to Meyers (2003), TOC/TN values between 4 and 8 reflect an abundance of nitrogen-rich proteinaceous organic matter source such as phytoplankton. Diatoms account for a large proportion of the algae in Lake Naivasha, and TOC/TN values around 9 drop even lower towards the top of the core. This may have been due to TN enrichment. An increase in TN could be attributed to the use of fertilizers in Kenya after 1990, when the fertilizer market was liberalized in the early 1990s (Ariga and Jayne 2006).
Total nitrogen and phosphorus are minor contributors to the conductivity of lake waters, as is silicate. These constituents, however, are important in biological cycles. They are often the drivers of productivity in continental waters and are incorporated into living organisms. Because of their contribution to the ionic strength of waters, is not surprising that diatom-inferred conductivity remained relatively constant (~170 µS cm^{-1}) during the eutrophication process.

The growing human population and intensive flower farming on the southern shore of the lake brought fertilizers into the lake and further promoted eutrophication. Despite inputs of sediments and nutrients, as well as dam construction and removal of water in the catchment areas, and water consumption by the Olkaria geothermal power station, Lake Naivasha remains a freshwater system. Even the documented lowstand of Lake Naivasha between 1944 and 1955 (~5 m lowering) did not increase the conductivity, according to the diatom flora. The hydrological balance of the lake is highly dependent on groundwater flow, which may explain the lack of a conductivity response to arid intervals (Telford and Lamb 1999; Ayenew et al. 2007). A recent study on Lake Beseka in the Ethiopian Rift Valley suggests a close relationship between tectonic activity and expansion of the lake due to enhanced groundwater discharge (Goerner et al. 2008). This model may also apply to Lake Naivasha, which is also situated within a highly tectonically active region.

3.1.6 Summary and Conclusions

In summary, this study has shown that over the last ~200 years, Lake Naivasha's water chemistry and biology have been influenced by natural climatic variations and anthropogenic activities. Lake Naivasha's water level responded to natural rainfall variations, as occurred in the period between 1820 and 1882 AD, when long dry periods led to low water levels and/or complete desiccation (Verschuren et al. 2000). The enduring Laparanat drought (1760-1840 AD) caused slightly saline conditions in the lake and favored the abundance of saline-tolerant diatoms such as *Navicula elkab* and *Cymbella muelleri*. In the generally wetter period from 1883 to 1894 AD, the lake received more freshwater from the catchment and groundwater reservoirs, which helped maintain the freshwater nature of the lake. These freshwater conditions favor diatoms such as *Synedra* sp. and *Aulacoseira* sp. that prefer waters with low conductivity. After 1900 AD, shorter wet and dry periods alternated and the lake level fluctuated in response to these variations. This is documented by instrumental lake level data since 1932 and by both proxy and instrumental rainfall data since 1850 (Nicholson 2001). The sediment accumulation rate increased from 1947 to 2007 AD, due to higher rates of soil erosion from cultivated areas within the lake catchment, rather than as a consequence of intensive rainfall. Higher erosion rates caused greater inputs of nutrients and pollutants to the lake. Nutrient-rich waters favored eutrophic diatoms such as *Aulacoseira* sp. and led to displacement of pollution-sensitive diatom species such as *Gomphonema gracile*.
Since the middle of the 20th century, intense anthropogenic activity around Lake Naivasha has led to cultural eutrophication, which has overprinted the influence of natural climate variation on the lake. Several previous studies have suggested that human activity, in particular agriculture, is the main reason for higher sediment fluxes into lakes (Mannion 1995; Bookman et al. 2010). In addition to inputs of soil and nutrients, transport of fertilizers, pesticides, and other pollutants resulting from intensive land use, has far-reaching implications for the future of Lake Naivasha and numerous other lakes (Plater 2006). This study demonstrated that Lake Naivasha is highly sensitive to changes in catchment activities. It will therefore be important to monitor conditions in the lake that are influenced by anthropogenic activities, to be able to manage

the lake wisely. The human population around the lake, as well as numerous other species, depend on the health of Lake Naivasha.

3.2 Acknowledgements

This project was carried out through the Graduate School's GRK 1364 research program on 'Shaping Earth's Surface in a Variable Environment', funded by the German Research Foundation (DFG). We are grateful to the Government of Kenya (Research Permits MOST13/001/30C 59/10, 59/18 and 59/22) and the University of Nairobi for the research permits and their support. We also thank Yannick Garcin and Laura Epp for the field support that they provided. We are grateful to Antje Musiol for the TC and TN measurements, and to Peter Appleby from the University of Liverpool for the ^{210}Pb dating. We would also like to thank Ulrike Herzschuh, Andreas Bergner and all of the graduate school members and participants for inspiring discussions. We also thank Ed Manning for professional proofreading of the manuscript.

Data are avaible in the Appendix 07-09 (see page 146 pp.).

3.3 References

Anderson NJ, Rippey B, Stevenson AC (1990) Change to a diatom assemblage in a eutrophic lake following point source nutrient re-direction: a paleolimnological approach. Freshwat Biol 23:205-217.

Appleby PG, Nolan PJ, Gifford DW, Godfrey MJ, Oldfield F, Anderson NJ, Battarbee RW (1986) ^{210}Pb dating by low background gamma counting. Hydrobiologia 141:21-27.

Appleby PG, Oldfield F (1978) The calculation of ^{210}Pb dates assuming a constant rate of supply of unsupported ^{210}Pb to the sediment. Catena 5:1-8.

Appleby PG, Richardson N, Nolan PJ (1992) Self-absorption corrections for well-type germanium detectors. Nucl Inst Methods B 71:228-233.

Appleby PG (2001) Chronostratigraphic techniques in recent sediments, in Tracking Environmental Change Using Lake Sediments. In: Last WM, Smol JP (eds) Volume 1: Basin Analysis, Coring, and Chronological Techniques. Kluwer Academic:171-203.

Ariga J, Jayne TS (2006) Can the market deliver? Lessons from Kenya's rising use of fertilizer following liberalization. Policy brief, Tegemeo Institute for Agricultural Development and Policy 7:1-4.

Åse LE (1987) A note on the water budget of lake Naivasha, Kenya. Geografiska Annaler 69A:3-4.

Ayenew T, Becht R, Lieshout van A, Gebreegziabher Y, Legesse D, Onyando J (2007) Hydrodynamics of topographically closed lakes in the Ethio-Kenyan Rift: The case of lakes Awassa and Naivasha. Journal of Spatial Hydrology 7:1.

Ballot A, Kotut K, Novelo E, Krienitz L (2009) Changes of phytoplankton communities in Lakes Naivasha and Oloidien, examples of degradation and salinization of lakes in the Kenyan Rift Valley. Hydrobiologia 632:359–363.

Bergner AGN, Trauth MH, Bookhagen B (2003) Paleoprecipitation estimates for the Lake Naivasha basin (Kenya) during the last 175 k.y. using a lake-balance model. Global Planetary Change 36:117-136.

Birks HJB, Line JM, Juggins S, Stevenson AC, and ter Braak CJF (1990) Diatoms and pH reconstruction. Philosophical Transactions of the Royal Society of London, B 327:263–278.

Bookman R, Driscoll CT, Effler SW, Engstrom DR (2010) Anthropogenic impacts recorded in recent sediments from Otisco Lake, New York, USA. J Paleolimnol 43:449–462.

Clarke MCG, Woodhall DG, Allen D, Darling G (1990) Geological, volcanological and hydrogeological controls on the occurrence of geothermal activity in the area surrounding Lake Naivasha, Kenya. Ministry of Energy 1-138.

Edeghonghon Jimoh H, Vogler C, Waters, JJJ (2007) Perceived and real sources of pollution in Lake Naivasha.
http://www.pdf-searcher.com/Perceived-and-real-sources-of-pollution-in-Lake-Naivasha.html, 01.12.2010.

EDDI, http://craticula.ncl.ac.uk/Eddi/jsp/, 12.09.2009

Fleitmann D, Dunbar RB, McCulloch M, Mudelsee M, Vuille M, McCanahan TR, Cole JE, Eggins S (2007) East African soil erosion recorded in a 300 year old coral colony from Kenya. Geophys Res Lett 34, L04401 doi:10.1029/2006GL028525.

Fritz SC (2008) Deciphering climatic history from lake sediments. J Paleolimnol 39:5-16.

Gasse F (1986) East African diatoms - Taxonomy, ecological distribution. Bibliotheca diatomologica 11. Cramer, Stuttgart, 20Gasse F, Juggins S, Ben Khelifa L (1995) Diatom-based transfer functions for inferring hydrochemical characteristics of African palaeolakes. Palaeogeogr, Palaeoclimatol, Palaeoecol 117:31–54.

Gaudet JJ, Melack JM (1981) Major ion chemistry in a tropical African lake basin. Freshw Biol 11:309-333.

Goerner A, Jolie E, Gloaguen R (2008) Non-climatic growth of the saline Lake Beseka, Main Ethiopian Rift. J Arid Environ 73, 3:287-295.

Golterman HL (1977) Sediments as a source of phosphate for algal growth. In: Golterman HL (ed), Interactions between sediments and fresh water. Proceedings of an International Symposium held at Amsterdam, 6-10 September 1976. The Hague, Dr W Junk Publishers, Wageningen, PUDOC pp 286–293.

Harper DM, Adams C, Mavuti K (1995) The aquatic plant communities of the Lake Naivasha wetland, Kenya: pattern, dynamics, and conservation. Wetlands Ecol Manag 3(2):111-123.

Hausmann S, Lotter AF, van Leeuven FN, Ohlendorf C, Lemcke G, Grönlund E, Sturm M (2002) Interactions of climate and land use documented in the varved sediments of Seebergsee in the Swiss Alps. Holocene 12:279–289.

Hubble DS and Harper DM (2001) What defines a healthy lake? Evidence from Lake Naivasha, Kenya, Aquat Ecosyst Health 4:243-250.

Hustedt F (1949) Süßwasserdiatomeen aus dem Albert-Nationalpark in Belgisch Kongo, In: Damas H (ed), Exploration du Parc National Albert (1935-1936). Hayez, Bruxelles.

Karst TL, Smol JP (1998) Tracking the cultural eutrophication history of Collins Lake (Southeastern Ontario, Canada) using paleolimnological techniques. Lake and Reservoir Manag 14:456-465.

Kelly MG, Bennion H, Cox EJ, Goldsmith B, Jamieson J, Juggins S, Mann DG , Telford JR (2005) Common freshwater diatoms of Britain and Ireland: an interactive key. Environment Agency, Bristol.

Kilham P, Kilham SS, Hecky RE (1986) Hypothesized resource relationships among African planktonic diatoms. Limnol Oceanogr 31: 1169:1181.

Krammer K, Lange-Bertalot H (1986–1991) Süβwasserflora von Mitteleuropa, vols. 2/1–2/4. Gustav Fischer Verlag, Stuttgart.

LNROA - Lake Naivasha Riparian Owners Association (1993) A three-phase environmental impact study of recent developments around Lake Naivasha. Phase I, An assessment of current information on the lake, relevant to a management plan, and recommendations for phase II of the study. LNROA, Naivasha, 109pp.

Lotter AF and Birks HJB (1997) The separation of the influence of nutrients and climate on the varve time-series of Baldeggersee, Switzerland. Aquat Sci 59:362–375.

Mannion AM (1995) Agriculture and environmental change: temporal and spatial dimensions. Wiley, Chichester.

Melack JM (1976) Limnology and Dynamics of Phytoplankton in Equatorial African Lakes. Ph.D Thesis, Duke University, USA.

Meyers PA (2003) Applications of organic geochemistry to paleolimnological reconstructions: a summary of examples from the Laurentian Great Lakes, Org Geochem 34:261. 289.

Moy, CM, Seltzer, GO, Rodbell, DT, and Anderson, DM, 2002, Variability of El Niño/Southern Oscillation activity at millennial timescales during the Holocene epoch: Nature, 420:162–165.

Nicholson SE, Kim J, Hoopingarner J (1988) Atlas of African rainfall and its interannual variability. Florida State University.

Nicholson SE (1995) Environmental change within the historical period. In: Goudie AS, Adams WM, Orme A (eds), The physical geography of Africa. Oxford Univ. Press, pp 60–75.

Nicholson SE (1996) A review of dynamics and climate variability in Eastern Africa. In: Johnson TC, Odada EO (eds), The Limnology, Climatology and Paleoclimatology of the East African Lakes. Gordon and Breach, Amsterdam, pp 25–56, 63–75.

Nicholson SE (2001) Climatic and environmental change in Africa during the last two centuries. Clim Res 17:123–144.

Ojiambo BS and Lyons WB (1996) Residence times and major ions in Lake Naivasha, Kenya, and their relationships to lake hydrology. In: Johnson TC, Odada EO (eds), The Limnology, Climatology and Paleoclimatology of the East African Lakes. Gordon and Breach, Amsterdam, pp 267–278.

Osborne PL (2000) Tropical Ecosystems and Ecological Concepts. University Press, Cambridge p 177–182.

Phillips J (2003) Alluvial storage and the long-term stability of sediment yields. Basin Res 15:153–163.

Plater AJ, Boyle JF, Meyers C, Turner SD, Stroud RW (2006) Climate and human impact on lowland lake sedimentation in Central Coastal California: the record from c. 650 AD to the present. Reg Environ Change 6:71–85.

www.ramsar.org, 29.11.2010

Salas HJ, Martino P (1991) A simplified phosphorus trophic state model for warm-water tropical lakes. Water Res 25:341-350.

Saji NH, Goswami BN, Vinayachandran PN, Yamagata T (1999) A dipole mode in the tropical Indian Ocean. Nature 401:360–363.

Sikes HL (1935) Notes on the hydrology of Lake Naivasha. Journal of East Africa and Uganda Natural History Society 13:74-89.

Telford RJ, Lamb HF (1999) Groundwater-mediated response to Holocene climatic change recorded by the diatom stratigraphy of an Ethiopian crater lake. Quat Res 52:63-75.

ter Braak CJF, Šmilauer P (2002) CANOCO references manual and user's guide to Canoco for Windows: software for Canonical Community Ordination version 4.5. Microcomputer Power, Ithica, NY.

Trauth MH, Deino AL, Bergner AGN, Strecker MR (2003) East African climate change and orbital forcing during the last 175 kyr BP. Earth Planet Sc Lett 206:297-313.

Trauth MH, Maslin MA, Deino A, Strecker MR (2005) Late Cenozoic moisture history of East Africa. Science 309:2051-2053.

Trauth MH, Maslin MA, Deino A, Junginger A, Lesoloyia M, Odada EO, Olago DO, Olaka LA, Strecker MR, Tiedemann R (2010) Human evolution in a variable environment: The amplifier lakes of Eastern Africa. Quaternary Sci Rev 29:2981-2988.

Vincent CE, Davies TD, Beresford AKC (1979) Recent changes in the level of Lake Naivasha, Kenya, as an indicator of equatorial Westerlies over East Africa. Clim Change 2:175-189.

Verschuren D (1996) recent and late Holocene paleolimnology of lakes Naivasha and Sonachi, Kenya. Ph.D Thesis, University of Minnesota, USA.

Verschuren D (1999) Influence of depth and mixing regime on sedimentation in a small, fluctuating tropical soda lake. Limnol Oceanogr 44:1103-1113.

Verschuren D, Laird KR, Cumming BF (2000) Rainfall and drought in equatorial east Africa during the past 1,100 years. Nature 403:410-414.

Verschuren D (2001) Reconstructing fluctuations of a shallow East African lake during the past 1800 yrs from sediment stratigraphy in a submerged crater basin, J Paleolimnol 25:297-311.

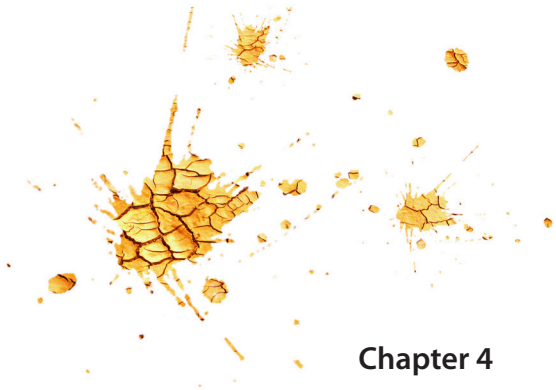

Chapter 4

Contributions to climate proxy sites in the East African Rift

Intraseasonal precipitation variability between 1996 - 2010

Lydia A. Olaka and Annett Junginger, Martin H. Trauth

in preparation for journal of *Climate Dynamics*

4.1 Contributions to climate proxy sites in the East African Rift - Intraseasonal precipitation variability between 1996 - 2010

Lydia A. Olaka[1,2] and Annett Junginger[1,2], Martin H. Trauth[1]

[1]Institute for Earth- and Environmental Sciences, University of Potsdam, Potsdam, Germany

[2]DFG Graduate school "Shaping the Earth's Surface in a Variable Environment", University of Potsdam

Lydia A. Olaka and Annett Junginger contributed equally to this work.

Abstract

Spatial and temporal heterogeneity of past climate transitions in East Africa interpreted from palaeoclimate proxy records obtained from basins within the East African Riftsystem (EARS) poses a challenge in distinguishing local from regional pattern. In order to improve our knowledge about past climate dynamics, an inter-basin comparison of high frequency precipitation variability offers the ability to distinguish the effects of local from regional dynamics. This study uses remotely sensed basin-averaged precipitation from FEWSNET for the period between 1996-2010. Our investigation focuses on the dynamics of intraseasonal rainfall distribution within the catchments of eleven lake basins of the EARS, namely Tana, Ziway, Awassa, Abaya, Turkana, Suguta, Baringo, Nakuru, Naivasha, Natron, and Manyara. The preliminary results revealed that rainfall in adjacent basins exhibits high complexities in the magnitudes of intraseasonal variability, biennial to triennial precipitation patterns and even are not necessarily correlated often showing opposite trends. The variability among the watersheds is driven by the complex interaction of catchment topography, shape, length and elevation, its relative location to the East African Rift System and predominant influence of the ITCZ and CAB, whose locations and intensities are dependent on the strength of low pressure cells over India, SST variations in the Atlantic, Pacific or Indian Ocean, QBO phases and the 11-year solar cycle. Among all seasons we observed, January-September beeing the season of highest and most complex rainfall variability, especially for the East African Plateau basins, most likely due to the irregular penetration of the CAB.

Note: This manuscript is an ongoing study. Therefore, results are very detailed listed making this manuscript extensive. The final manuscript ready for submission will be shortened and much more focussed.

4.1.1 Introduction

The East African Rift System (EARS) provides valuable accommodation space for lacustrine sediments containing valuable climate-proxies for investigating the Pleistocene-Holocene climate dynamics. However, differences in the timing of onset and termination of arid-humid transitions exist between different study sites often very closely located to each other (e.g., Verschuren et al., 2000; Russel and Johnson, 2007; Junginger and Trauth, subm.), which complicate the identification of pattern of palaeoclimatic change across the EARS. While these differences in the records could be attributed to dating uncertainties or sensitivities of applied proxies, the complexity in the topography plays a major role in modifying circulation patterns (Junginger and Trauth, subm.). In order to allow a well-grounded interpretation of climate variations obtained in paleoclimate records from the basins of the EARS, an understanding of mechanisms responsible for present day interannual to interdecadal climate variability is required.

East African rainfall is generally associated with the latitudinal migration of the Intertropical Convergence Zone (ITCZ) between ca. 10° north and south of the equator and associated seasonal eastward

shift of the Congo Air Boundary (CAB) over parts of East Africa (Nicholson, 1996; see details in chapter 2). At present day, significant precipitation anomalies are usually linked with sea-surface temperature (SST) anomalies in the Indian and Pacific Ocean associated with the Indian Ocean Dipole (IOD; Saji et al., 1999; Clark et al., 2003) and the El Niño Southern Oscillation (ENSO; Camberlin et al., 2001; Camberlin and Philippon, 2002) phenomenon. Additionally to these well-known phenomenons contribute the stratospheric quasibiennial oscillation (QBO; Indeje and Semazzi, 2000; Kane, 2009 and references therein), the Indian summer monsoon strength (ISM; Camberlin, 1997; Junginger and Trauth, subm.) and regular fluctuations in solar irradiation (Neff et al., 2001; Wang Y.I. et al., 2005; Kodera et al., 2007; Meehl et al., 2009) also to East African precipitation variations. Further, the existence of highly variable topography, vegetation and large inland lakes are also cited to cause significant spatial variability of rainfall distribution in East Africa (Nicholson, 1996; Indeje and Semazzi, 2000; Chan, 2008).
However, the direct contribution of these features to disperse precipitation pattern in East Africa has not been extensively investigated, yet, but would offer the potential to improve interpretations of climate proxies from these lake basins.

Generally, estimates of aerial precipitation for hydrological applications are made from point observations, that provide relatively accurate estimates at the geographically position of recording. In East Africa, where the rain gauge density is quite low, interpolation of these data in rain-fields over a wide area, where most rainfall has a convective origin with high spatial variability at the daily level exhibit a great deal of uncertainty (Meisner and Arkin, 1987; Dai, 2001). Recent technological advances in remote sensing techniques provide rainfall measurements at high spatial and temporal resolutions and offers possibilities to overcome the uncertainties of interpolation.

Here we use rainfall estimates from remotely sensed data to investigate the intraseasonal precipitation variability on the EARS basins, for the time period 1996-2010. We intend to provide insights into the complex interaction of local and regional climatic

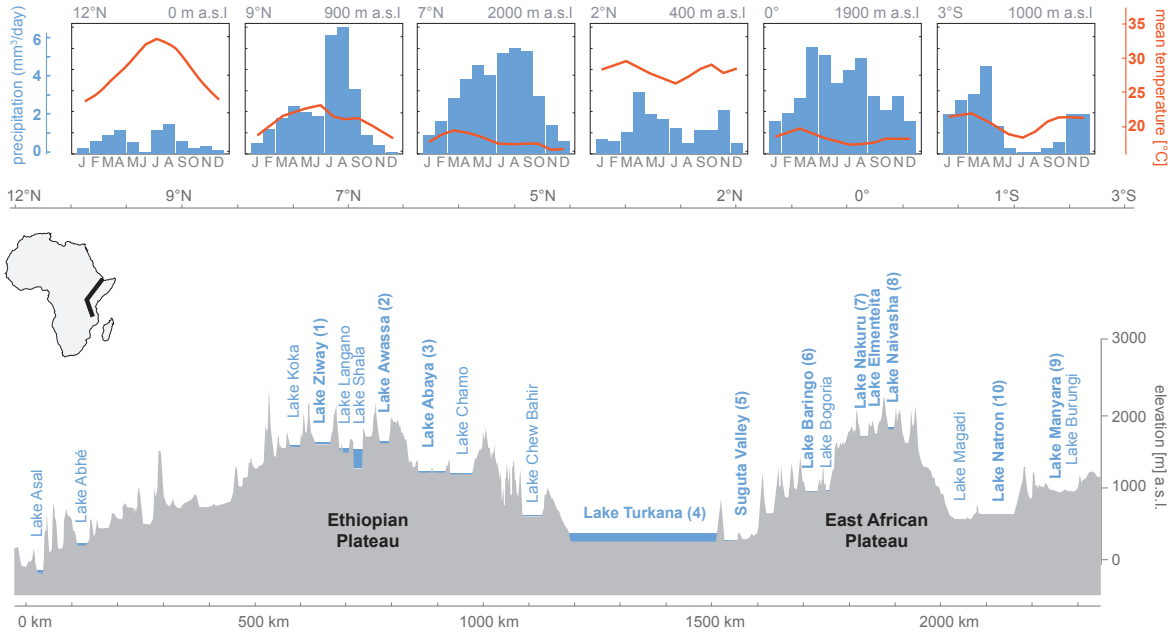

Figure 4.1 Cross-section of the eastern branch of the East African Rift System (EARS) showing the location of lake basins in relation to the geographical distribution of rainfall regimes across East Africa (insets). Present lake depths of most of the lakes are less than 8 m. Numbered (bold) lake basins (1-10) refer to studied sites in this study. Lake Tana (not displayed) is located not within the EARS, but also on the Ethiopian Plateau westwards at the same elevation as Lake Ziway.
Insets - the principal temperature-rainfall regimes along the transect are provided by http://iridl.ldeo.columbia.edu/maproom/ (March 2011) and refer to monthly mean data from 1961-1990.catchment of Nakuru. While dry warm air is migrating eastward where it absorbs moisture within the rift floor bypassing the Nakuru, Elmenteita and Naivasha lake bodies produces the even higher elevated eastern catchment boundaries of Naivasha rainfall.

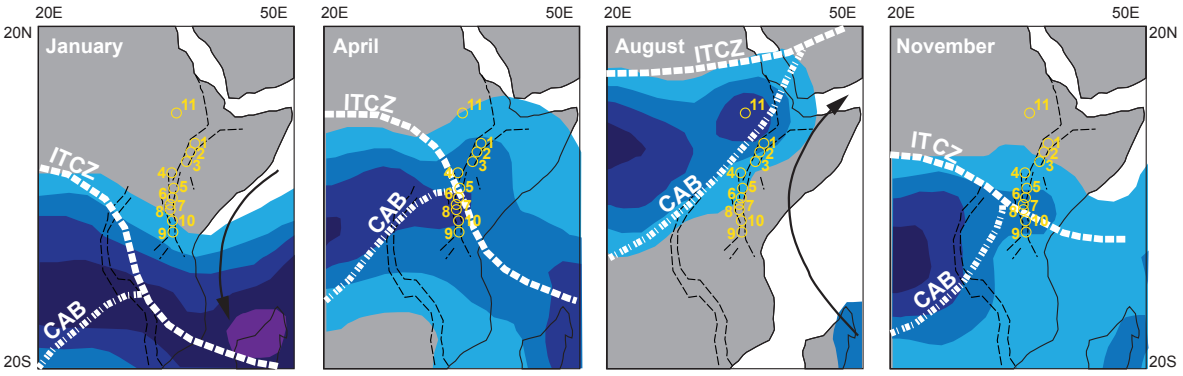

Figure 4.2 Synoptic climatology of tropical East Africa for four representative months discussed in this study. The blue shaded area (contours at 50 mm intervals) explains the seasonal migration of the Intertropical Convergence Zone (ITCZ) and associated rain belts across the studied region. The distribution is based on gauge data over land, and satellite estimates over sea. Dotted white lines show the mean position of the Congo Air Boundary (CAB) and ITCZ. Black dashed line outlines the East African Rift System and yellow numbered dots the studied lake basins. 1-Ziway, 2-Awassa, 3-Abaya, 4-Turkana, 5-Suguta, 6-Baringo, 7-Nakuru, 8-Naivasha, 9-Manyara, 10-Natron, 11-Tana. Rainfall distribution was provided by: http://iridl.ldeo.columbia.edu/maproom/.Regional/.Africa/.Climatologies/Precip_Loop.html (March 2011) and refer to monthly mean data from 1961-1990.

processes in catchments along the topographically complex Rift system. We also attempt to identify the governing atmospheric circulation patterns leading to intraseasonal rainfall distribution in East Africa.

The results of this study foster a better understanding of intraseasonal disparity among catchments and the resultant perturbation of regional climate signatures recorded by climate proxies. Such studies have potential to improve calibration of Regional climate models (RCM's) currently required for future predictions efforts for rainfall and hydrological systems in this area (Stute et al., 2001; Donders et al., 2008).

4.1.2 Setting

4.1.2.1 Climatic setting of East Africa

East Africa is one of the most meteorological complex part of Africa due to the interaction of highly variable topography, large inland water bodies and maritime influence with several convergence zones, resulting in climate patterns that change over short distances (Nicholson, 1996). The general climate is controlled by the annual latitudinal migration of the ITCZ around the equator, between 10° north and south latitudes, following the overhead position of the sun with a time lag of 4-6 weeks (Nicholson, 1996). This migration produces a bimodal precipitation cycle along the equator with the so-called 'long rains' in March-May (MAM) and 'short rains' in October-November (ON). Although both of the rainy seasons are related to the seasonal migration of the ITCZ, they are not the mirror image of each other. This might be related to the longer march of the ITCZ northwards from February to August, whereas the southern retreat occurs faster between August to November (Suzuki, 2011). The 'long rains' therefore show heavier rainfall than the 'short rains', but the 'short rains' experience a larger degree of interannual variability relative to climatology (Hastenrath et al., 1993), hence the long rainy season is the most important East African agricultural season along the equator (Camberlin and Philippon, 2002). In contrast, the limits of the ITCZ migration path receive maximum rainfalls within only one rainy season, from December-February (DJF) and July-September (JAS) south and north of the equator, respectively (Fig. 4.1, 4.2).

Additional precipitation on equatorial and northern East Africa occurs when the northern most position of the ITCZ in July/August allows the southwestern humid Congo air stream, with recycled eastern Atlantic moisture brought from the Congo basin through the West-African monsoon, to reach parts of East Africa (Fig. 4.2; Nicholson, 1996; Camberlin, 1997; Okoola, 1999). This unstable flow from the Atlantic converges with drier air from the Indian Ocean along a northeast-southwest-trending zone known

as the CAB. The CAB is considered to bring during times of a strong ISM wet spells in the JAS months to East Africa (Camberlin, 1997; Okoola, 1999). Camberlin (1997) showed that an anomalous deep low over western India enhances the east-west pressure gradient between Africa and India, which results in enhanced eastwards winds from the Congo basin that cause the shift of the CAB further eastwards. Thus, the CAB is considered to play a major role in interannual variability (Camberlin and Philippon, 2002).

Precipitation associated with the ITCZ has its origin in large-scale moist advection from the Indian Ocean (Levin et al., 2009). Precipitation anomalies are therefore supposed to be linked to Indian Ocean SSTs anomalies attributed to the IOD with intensified (reduced) rains during high (lowered) SSTs in the western Indian Ocean (Saji et al., 1999). The highest rainfall variability in the course of IOD events is reported to affect East Africa in October/ November (Saji et al., 1999). Under certain conditions ENSO and IOD occur simultaneous, but the exact relationship between these two events is not fully understood yet (Charles et al., 2003; Saji et al., 2006; Meyers et al., 2007; Abram et al., 2008 ; Cai et al., 2009).
Significant relationships between QBO and JAS rainfall is also reported and to some lower degree also ON rainfalls and tends to enhance major negative swings in the Southern Oscillation associated with ENSO events (Indeje and Semazzi, 2000).
Additional influencing mechanisms to rainfall variability in East Africa are related to solar variations and resultant feed back mechanisms: for example, Meehl et al. (2009) discovered that small-scale solar radiation changes can cause precipitation variability due to the interaction of stratospheric and tropospheric processes causing the broadening and intensification of Hadley and Walker circulations and associated increases in trade winds producing a greater equatorial ocean upwelling and associated feed back processes. Kodera et al. (2007) explained that during periods of low solar activity a South Indian Ocean (SOI) anticyclone develops that causes a shift in the location of the descending branch of the anomalous Walker circulation with an expected trend towards high rainfall variability in the rainy season during boreal fall in East Africa. Solar variations were also discovered to influence the strength of the Indian and Asian summer monsoons, indirectly responsible for enhanced (suppressed) JAS rainfalls in East Africa during higher (lower) solar activity (Camberlin, 1997; Neff et al., 2001; Wang Y.I., 2005; Junginger and Trauth, subm.).

The intense studies of these processes lead to the advantage that the present decadal forecast of upcoming drier or wetter years have reached well precisions, whereas the seasonal forecasting in East Africa is still coarse. In this study we would like to explore how seasonal precipitation variability under influence of these influencing factors is distributed along the EARS and how those affect selected catchments of lake basins with different topography and shape that are used for paleoclimate studies.

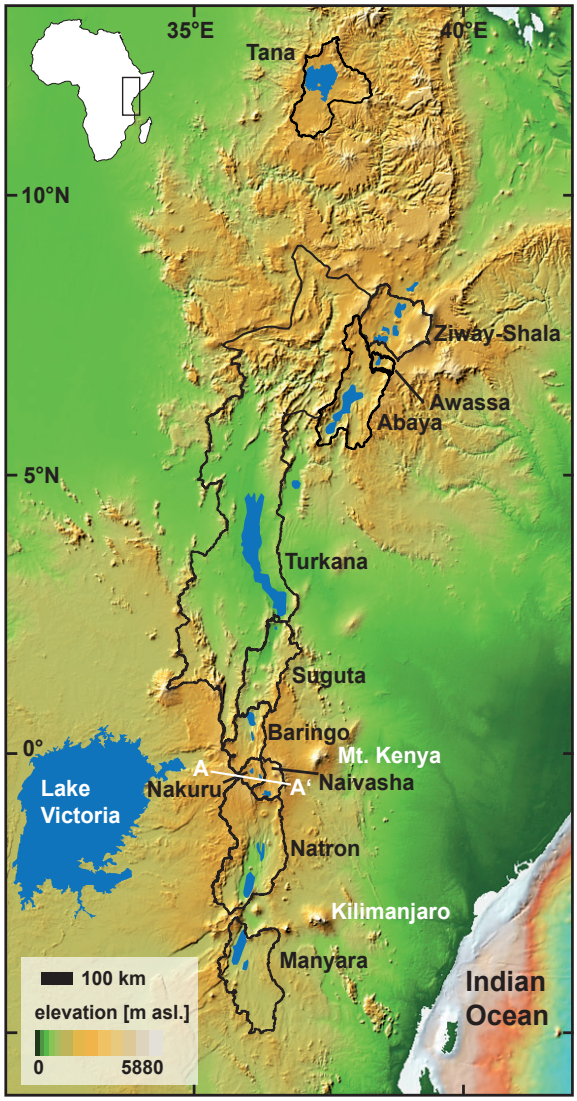

Figure 4.3 Catchments of the studied lake basins within the East African Rift System. Map created with GeoMapApp.

4.1.2.2 Topography

The EARS is a prominent feature in East Africa with high escarpments and numerous volcanic centres extending for several thousands of kilometres. The eastern arm of the rift aligns North-South with topography ranging from -155 m in the Danakil depression in northern Ethiopia to over 5000 m asl at Mt. Kilimanjaro or Mt. Kenya (Fig. 4.3). This rift expression has two main domed areas, which we refer to as plateaus in this study: the Ethiopian plateau (EP) and the East African plateau (EP), separated by the Turkana-Omo depression (Fig. 4.1). Along the rift there are numerous volcanic centres and high escarpments associated with it. The tectonic evolution in the rift has led to segmentation of the rift basins into various sizes. The highlands are thought to block the relatively moist unstable westerly flow of the Congo basin from reaching the coastal areas (Nicholson, 1996). Most great lakes in Eastern Africa are located within the rift valley bounded by roughly north-south striking faults. The basins are bordered on the two sides by high relief comprising almost continuous parallel mountain lines and scarps, sometimes called volcanic massifs. The catchments within the rifts are generally defined with boundaries in the escarpment and open lakes in the rift floor of various sizes (Fig. 4.3).

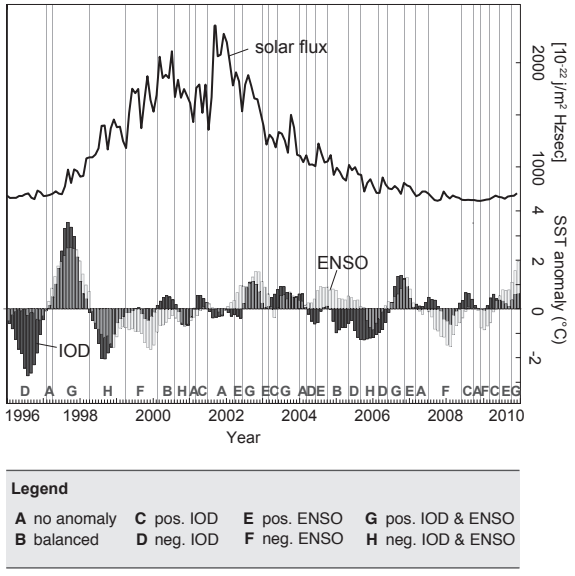

Figure 4.4 ENSO and IOD events during one 11-year solar cycle between 1996-2010. Letters refer to categorisation of ENSO and IOD events above 0.5 °C SST anomaly. Database: ENSO - monthly Nino.3.4 (http://www.cpc.ncep.noaa.gov/data/indices/nino34.mth.ascii.txt); IOD: monthly dipole mode index (DMI) from HadISST dataset (http://www.jamstec.go.jp/frsgc/research/d1/iod/). Solar flux: solar flux radio data set F10.7 (ftp://ftp.ngdc.noaa.gov/STP/SOLAR_DATA/SOLAR_RADIO/FLUX/Penticton_Adjusted/monthly/MONTHPLT.ADJ).

4.1.3 Materials and Methods

The data utilized in this study are rainfall estimates (RFE) acquired from the National Atmospheric and Oceanic Administration (NOAA) repository for the period 1996-2010 with a spatial grid resolution of 8 km. This high- resolution data in temporal and spatial domains provide good opportunity to study the rainfall characteristics especially in the humid tropics. The data before 2001- RFE 1.0 were used as algorithm that interpolated Meteosat and Global Telecommunication System GTS data and included warm cloud information for the decadal estimates. From 2001, RFE 2.0 is an improvement from RFE 1.0. The method uses cloud top temperature and station rainfall data that formed the basis of RFE 1.0. Meteosat 7 geostationary satellite infrared data is acquired in 30-minute intervals, and areas depicting cloud top temperatures of less than 235K are used to estimate convective rainfall. WMO Global Telecommunication System (GTS) data taken from ~1000 stations provide accurate rainfall totals, and are assumed to be the true rainfall near each station. Two new satellite rainfall estimation instruments are incorporated into RFE 2.0, namely, the Special Sensor Microwave/Imager (SSM/I) on board Defense Meteorological Satellite Program satellites, and the Advanced Microwave Sounding Unit (AMSU) on board NOAA satellites. All satellite data are first combined using a maximum likelihood estimation method, and then GTS station data is used to remove bias (FEWS NET). The data output used is the total decadal (10 day) data. For details on the method please refer to http://www.cpc.ncep.noaa.gov/products/fews/rfe.shtml.

The focus of our study lies on the detection of seasonal rainfall variations and its local impact to the East African Rift System (EARS). We selected eleven regions in East Africa for this study because the rainfall distribution in this area exhibits high seasonal variability (Fig. 4.1, 4.2). The eleven regions are catchment boundary extent of lakes along the two plateaus of the EARS with highly variable topography from N-S (Fig. 4.1, Fig. 4.3). The selected lake basins from the Ethiopian Plateau (EP) are: Tana; Zi-

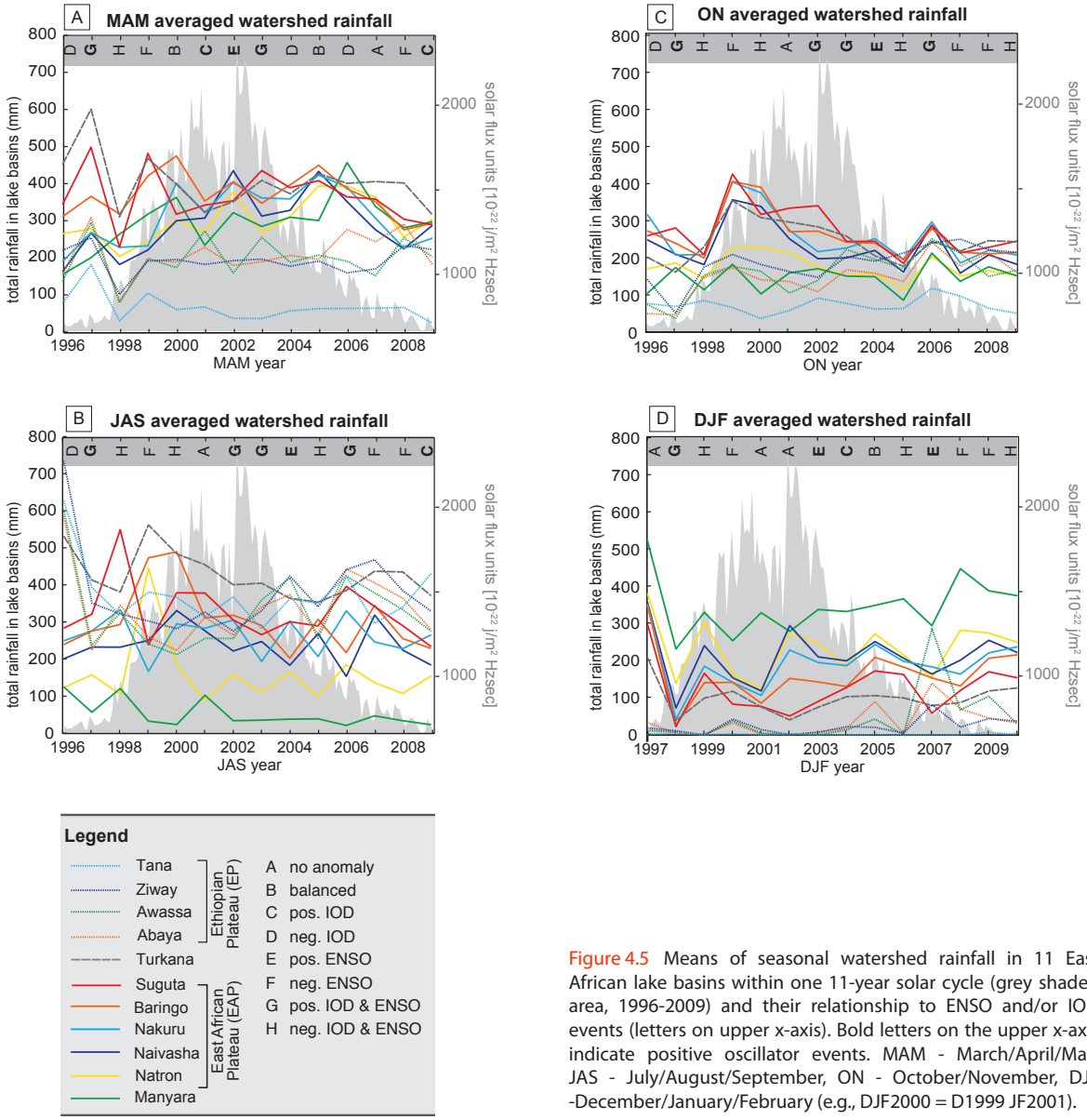

Figure 4.5 Means of seasonal watershed rainfall in 11 East African lake basins within one 11-year solar cycle (grey shaded area, 1996-2009) and their relationship to ENSO and/or IOD events (letters on upper x-axis). Bold letters on the upper x-axis indicate positive oscillator events. MAM - March/April/May, JAS - July/August/September, ON - October/November, DJF -December/January/February (e.g., DJF2000 = D1999 JF2001).

way including the lakes Ziway, Shalla, Langano, and Abiyata; Awassa; Abaya including the lakes Abaya and Chamo (Tab. 4.1). Lake basins from the East African Plateau (EAP) are Baringo including the lakes Baringo and Bogoria; Nakuru including the lakes Nakuru and Elmenteita; Naivasha; Natron including the lakes Natron and Magadi. Investigated basins on the foot of these two plateaus are the Manyara basin as the southernmost basin and Turkana as well as Suguta for examples of basins located in between the two plateau regions. To understand the seasonal variability we averaged the precipitation data for 4 seasons designated as December-January-February (DJF), March-April-May (MAM), July-August-September (JAS), and October-November (ON). DJF is considered as months showing the variability related with the maximum southward location of the ITCZ, MAM and ON the transitional times of the ITCZ over the equator, where ON is regarded to show highest variability during IOD/ENSO events, and JAS are considered to be the months of maximum northward position of the ITCZ and CAB's most eastern position causing high variable rainfall rather associated with ISM strength and largely independent from ENSO or IOD. We used the monthly Nino3.4 index for comparing ENSO events and the monthly dipole mode index (DMI) dataset from HadISST for summarizing IOD events. Solar flux data are based on the solar flux radio data set F10.7 (Fig. 4.4).

4.1.4 Results and Discussion

4.1.4.1 IOD/ENSO & the 11-year solar cycle 1996-2010

Figure 4.4 displays the various influencing mechanisms to East African Rainfall variability. For an easier identification of IOD and ENSO events in following figures, we categorized them by their parallel or single occurrence: We defined a 'no anomaly' stage (A), when SST variations in the Indian and/or Pacific Oceans ranged between -0.5 and 0.5°C; a 'balanced' mode (B) when opposite phases of IOD and ENSO co-occur; pure positive and negative IOD and ENSO (C-F) events, and times when both, IOD and ENSO, of the same phase occurred (G-H).

IOD and ENSO between 1996-2010 occurred in a complex pattern of combined and single events with no obvious relationship to each other. Different anomalies seem to develop within one year and show some indications of dependence to variations in the solar flux. Most of the events are suppressed during higher solar flux between 2000-2002 with the longest 'no-anomaly' event occurring from July 2001 to March 2002. The broad suppression of oscillator events during higher solar flux and build up of larger events outside indicates a kind of dependency. Meehl et al. (2009) has shown that during peaks in the 11-year solar cycle two interacting mechanisms, the top-down stratospheric response of ozone fluctuations to short-wave solar forcing and the bottom-up coupled ocean-atmosphere surface response, act together to enhance the climatological off-equatorial tropical precipitation maxima in the Pacific, lower the eastern equatorial Pacific SST and reduce low-latitude clouds to amplify the solar forcing at the surface. This mechanism leads to the intensification and broadening of the Hadley circulations resulting in a cold event–like response of supressed El Niño events (van Loon et al., 2004; van Loon and Meehl, 2008). Dynamical air-sea coupling produces then a transition to higher eastern equatorial SSTs a couple of years later when solar flux is diminished (Meehl et al., 2009).

4.1.4.2 Seasonal lake basin precipitation

This study aims to provide a detailed picture of the causes of present local precipitation variations within the EARS under consideration of the complex topography and the existing prevailing atmospheric conditions in order to help paleo-climate proxy studies to better understand discovered trends and fluctuations. For the following discussion, we grouped basins that are expected to show similar trends due to their geographically location (Fig. 4.3). The groups are: Tana; the central Ethiopian plateau (EP) basins Ziway, Awassa, Abaya; the central East African Plateau (EAP) lake basins Baringo, Nakuru, Naivasha; the basins Turkana and Suguta located between the two plateau regions and the southern most lake basins Natron and Manyara summarized in one group. The following discussion is supported by the Figures 4.5, 4.6, and 4.7. Information about sizes of lakes, catchment and geographical position are summarized in Table 4.1.

4.1.4.2.1 West-Ethiopian Plateau – Lake Tana

Catchment information Tana | Lake Tana is located at the northern most position (11°N) of the studied area outside the EARS in northwestern Ethiopia (Fig. 4.2, Fig. 4.3). The elevation of lake Tana on the EP is similar to the highest lakes in central Ethiopia at 1785 m asl and its catchment (16,500 km^2) has a similar size and circular shape to Ziway. Most of the rainfall receives the area in the southern catchment (Kebede et al., 2006).

MAM Tana | Tana received around 50 mm/MAM from 1996-2009 with exceptions in 1997 and 1999 (+150 and +50 mm/MAM, respectively) (Fig. 4.5A). According to Figure 4.2, the general low amounts of precipitation, is attributed to the peripherally location at the northern edges of the ITCZ.
In 1997 enhanced rainfall in the entire EARS occurred during a developing strong positive IOD/ENSO event of +1°C SST anomaly and must be related to a broadening of the rainfall center (Fig. 4.6). This broadening occurred from two sides, the Vic-

Figure 4.6 (see right page) N-S Topographic and precipitation swath profiles for the 4 different studied seasons in the East African Rift System. Grey shaded area explains topography. Green-blue-red lines show max-mean-min precipitation, respectively. EAP - East African Plateau; EP - Ethiopian Plateau. MAM, JAS, ON, and DJF explain studied seasons. Numbers refer to studied lake basins introduced in Fig. 4.1. The ITCZ is concentrated over the equator clearly indicated in ON and MAM, whereas in DJF it has reached the southern most position. The ITCZ in JAS has reached the northern most limits, however, the moisture bringing NE-SW trending CAB influences both plateau regions, which leads to irregular high rainfall in this season.

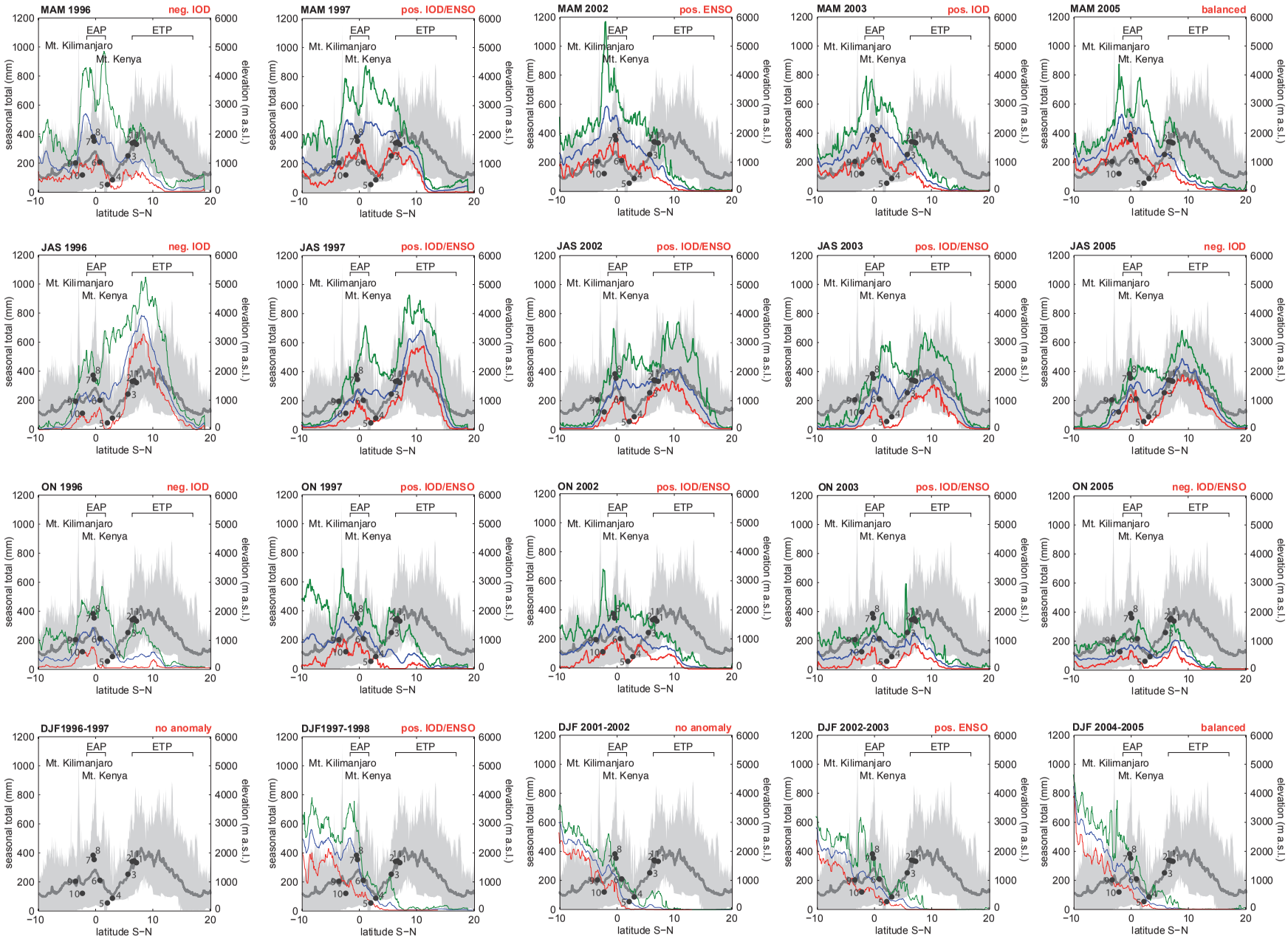
MAM 1996
neg. IOD
MAM 1997
pos. IOD/ENSO
MAM 2002
pos. ENSO
MAM 2003
pos. IOD
MAM 2005
balanced
JAS 1996
neg. IOD
JAS 1997
pos. IOD/ENSO
JAS 2002
pos. IOD/ENSO
JAS 2003
pos. IOD/ENSO
JAS 2005
neg. IOD
ON 1996
neg. IOD
ON 1997
pos. IOD/ENSO
ON 2002
pos. IOD/ENSO
ON 2003
pos. IOD/ENSO
ON 2005
neg. IOD/ENSO
DJF1996-1997
no anomaly
DJF1997-1998
pos. IOD/ENSO
DJF 2001-2002
no anomaly
DJF 2002-2003
pos. ENSO
DJF 2004-2005
balanced
EAP
ETP
Mt. Kilimanjaro
Mt. Kenya
seasonal total (mm)
elevation (m a.s.l.)
latitude S–N

Table 1
Lake basin information.

Lake Basin name	Lake basins included	Latitude [deg.]	Longitude [deg.]	Basin Floor [m asl.]	Basin Area [km²]
Tana	Tana	11°59'59N	37°17'53E	1785	16,500
Ziway	Ziway, Shala, Abiyata, Langano	07°58'48N	38°49'44E	1558	14,600
Awassa	Awassa	07°01'57N	38°25'50E	1680	1,455
Abaya	Abaya, Chamo	06°24'42N	37°52'38E	1268	33,060
Turkana	Turkana	03°39'53N	36°03'35E	375	130,860
Suguta	Suguta	02°13'41N	36°33'23E	275	12,800
Baringo	Baringo, Bogoria	00°38'03N	36°03'44E	997	6,200
Nakuru	Nakuru, Elmenteita	00°22'15S	36°05'23E	1770	2,390
Naivasha	Naivasha	00°46'29S	36°20'54E	1885	3,200
Natron	Natron, Magadi	02°19'50S	36°01'44E	600	184,000
Manyara	Manyara	03°37'25S	35°48'31E	960	23,207

toria basin and Mt. Kenya, which converged northwards into the depression of the two plateaus (Fig. 4.7A). Peak rainfall in 1999 correlate with anomalous high precipitation in Baringo, Turkana and Suguta, whereas other basins remain unaffected, proposes that moisture was received only from the West. The 1999 event occurred during the long lasting large La Niña (-1°C SST anomaly) event. Comparatively events in MAM 1998 and 2002 (Fig. 4.3) with both showing no impact to MAM rainfalls suggest that IOD/ENSO cannot account clearly for high precipitation outside the main rainy season in Tana, as well as the solar flux. Camberlin and Philippon (2002) reported also that impact of ENSO during MAM rainfalls in East Africa is only a rare phenomenon, due to the timing of phase shifts. Similar, no IOD season is considered to occur in March-May, because the general IOD season is regarded to be from July-November (Abram et al., 2008). Thus, the detection of mechanisms causing such a restricted distribution of moist air requires longer time series or isotopic studies.

JAS Tana | The climatological situation in JAS locates Tana in a triangle between the ITCZ to its north and the CAB slightly to its east. Rainfall should be therefore exclusively received from the southwest by the humid Congo airstream (Nicholson, 1996). JAS rainfall is highest and fluctuates between 300-400 mm/JAS with one exception of anomalous high rainfall (600 mm/JAS) in 1996 (Fig. 4.5B) during a negative IOD event (-2.9°C, Fig. 4.3). In 1996 a very intensified and broad rainfall cell covered almost whole East Africa west of the eastern EARS and north of 10°S. However, only the EP basins received high rainfalls. A similar, only slightly less intensive on developed in 1997 (pos. IOD/ENSO +3°C), but did not have such an affect as the 1996 event. Also minor fluctuations in rainfall during this season do not correlate with SST anomalies. This observation contrast general findings, that JAS precipitation in northeastern Africa or the western Rift Valley show a negative correlation with ENSO resulting in high droughts probabilities in El Niño years (e.g., Ininda et al., 1987; Camberlin, 1995; Camberlin et al., 2001). The regular rainfall fluctuations rather indicate a biennial precipitation pattern that might be related to one of the phases of the quasi-biennial circulation (QBO). Indeje and Semazzi (2000) showed significant relationships between QBO and seasonal rainfall occurring during boreal summer (June-August) that also tends to enhance major negative swings in the Southern Oscillation associated with ENSO and IOD events. This biennial pattern contrasts with

Figure 4.7 (see following pages) Overview of seasonal precipitation distribution for 1996-2010 in East Africa from data described in 4.1.3.
A) p. 105 March-April-May (MAM), B) p. 106 June-July-August (JAS), C) p. 107 October-November (ON); D) p. 108 December-January-February (DJF).

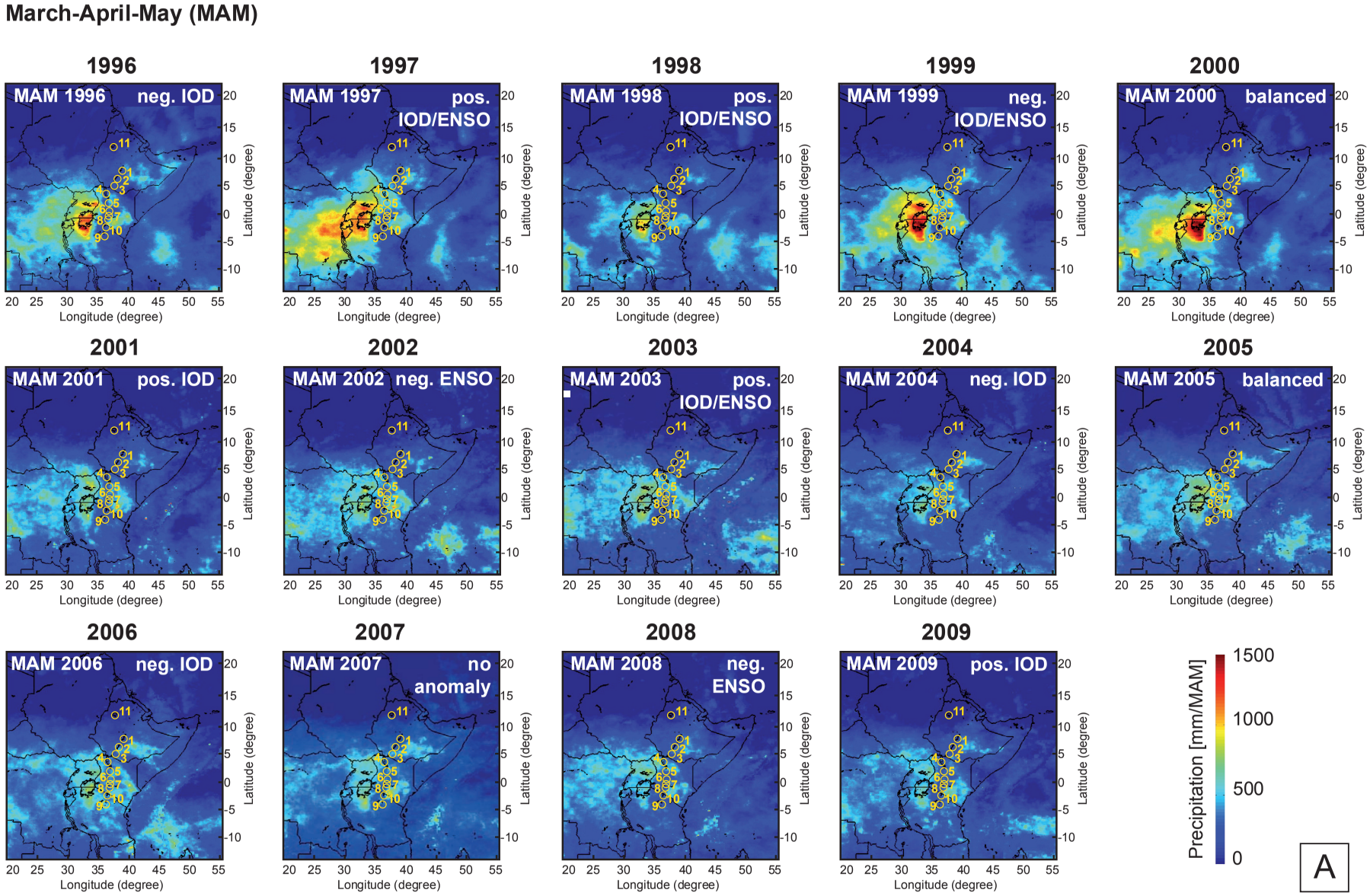
March-April-May (MAM)
1996
MAM 1996 neg. IOD
1997
MAM 1997 pos. IOD/ENSO
1998
MAM 1998 pos. IOD/ENSO
1999
MAM 1999 neg. IOD/ENSO
2000
MAM 2000 balanced
2001
MAM 2001 pos. IOD
2002
MAM 2002 neg. ENSO
2003
MAM 2003 pos. IOD/ENSO
2004
MAM 2004 neg. IOD
2005
MAM 2005 balanced
2006
MAM 2006 neg. IOD
2007
MAM 2007 no anomaly
2008
MAM 2008 neg. ENSO
2009
MAM 2009 pos. IOD
Longitude (degree)
Latitude (degree)
Precipitation [mm/MAM]
1500
1000
500
0
A

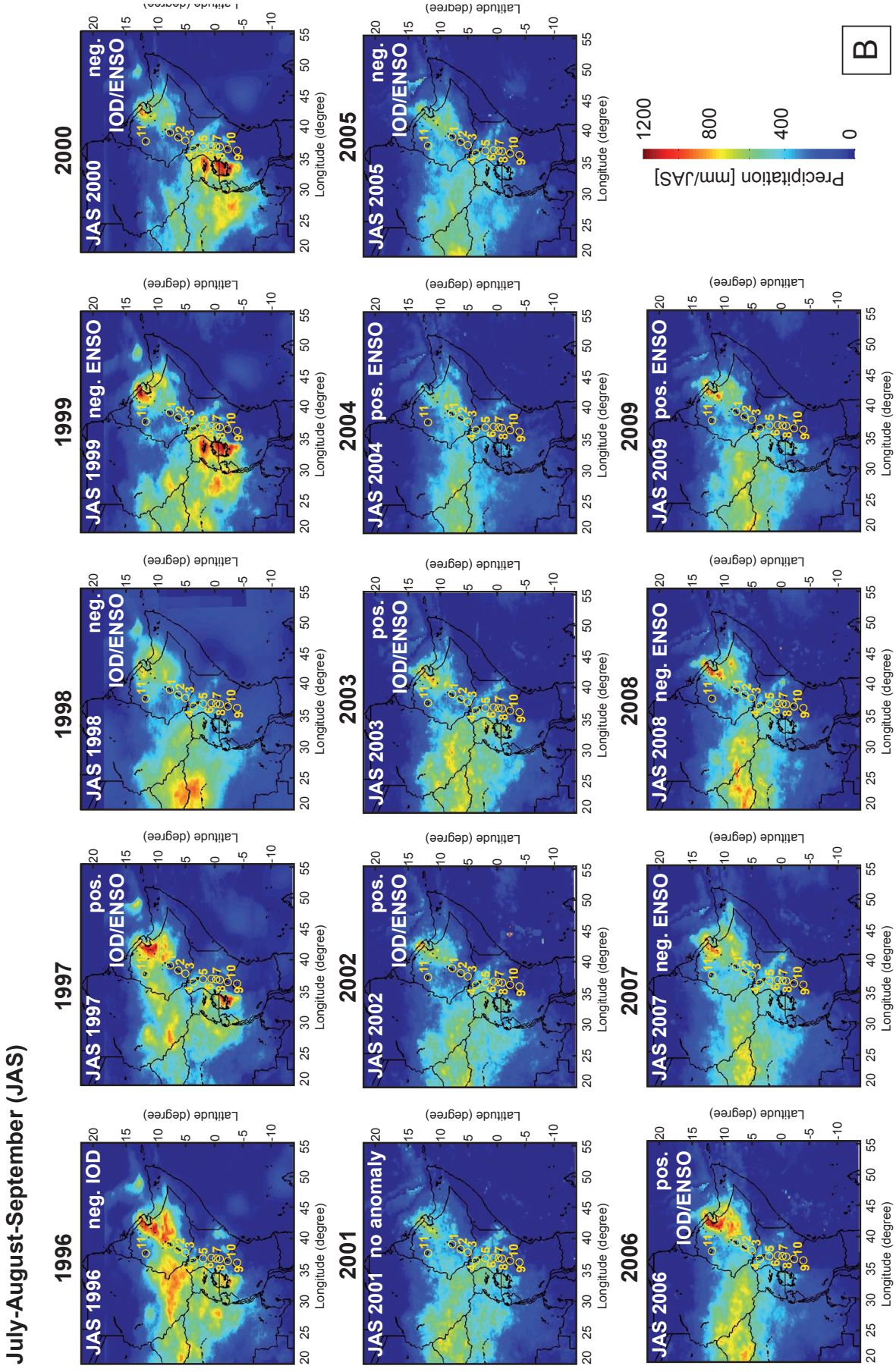
July-August-September (JAS)
1996
JAS 1996 neg. IOD
1997
JAS 1997 pos. IOD/ENSO
1998
JAS 1998 neg. IOD/ENSO
1999
JAS 1999 neg. ENSO
2000
JAS 2000 neg. IOD/ENSO
2001
JAS 2001 no anomaly
2002
JAS 2002 pos. IOD/ENSO
2003
JAS 2003 pos. IOD/ENSO
2004
JAS 2004 pos. ENSO
2005
JAS 2005 neg. IOD/ENSO
2006
JAS 2006 pos. IOD/ENSO
2007
JAS 2007 neg. ENSO
2008
JAS 2008 neg. ENSO
2009
JAS 2009 pos. ENSO
Latitude (degree)
Longitude (degree)
Precipitation [mm/JAS]
1200
800
400
0
B

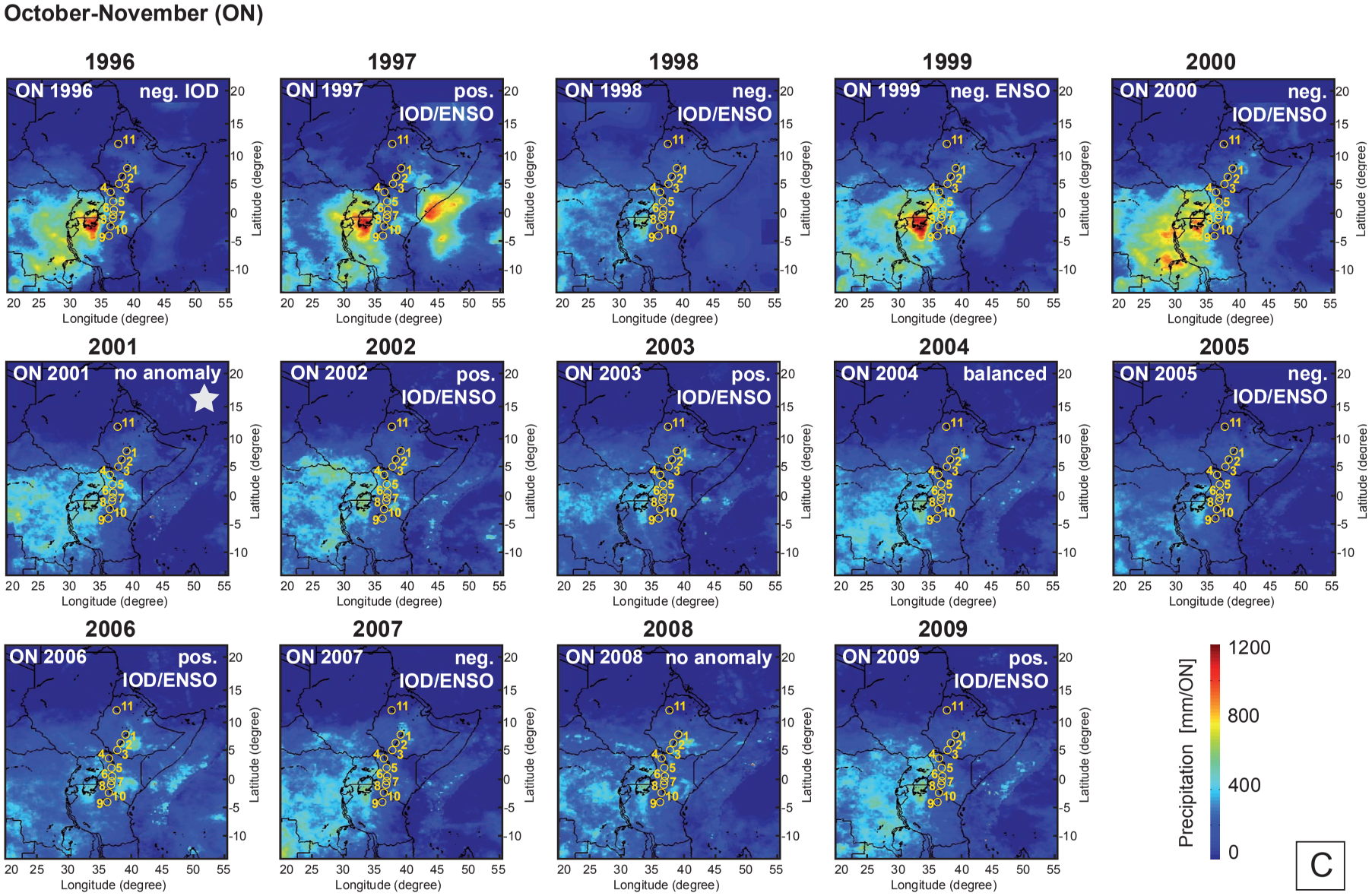
October-November (ON)
1996
ON 1996 neg. IOD
1997
ON 1997 pos. IOD/ENSO
1998
ON 1998 neg. IOD/ENSO
1999
ON 1999 neg. ENSO
2000
ON 2000 neg. IOD/ENSO
2001
ON 2001 no anomaly
2002
ON 2002 pos. IOD/ENSO
2003
ON 2003 pos. IOD/ENSO
2004
ON 2004 balanced
2005
ON 2005 neg. IOD/ENSO
2006
ON 2006 pos. IOD/ENSO
2007
ON 2007 neg. IOD/ENSO
2008
ON 2008 no anomaly
2009
ON 2009 pos. IOD/ENSO
Longitude (degree)
Latitude (degree)
Precipitation [mm/ON]
1200
800
400
0
C

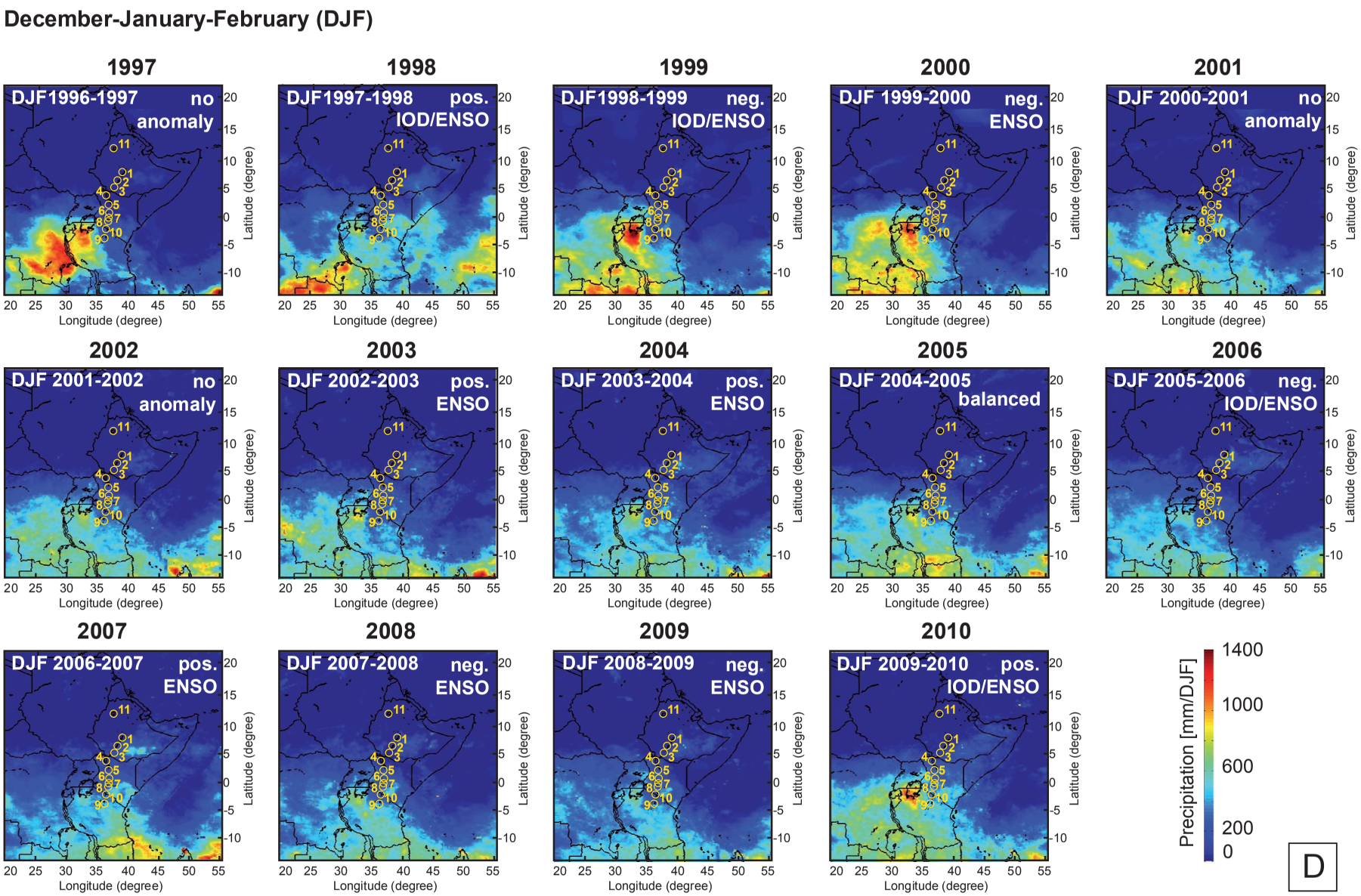
December-January-February (DJF)
1997
DJF1996-1997 no anomaly
1998
DJF1997-1998 pos. IOD/ENSO
1999
DJF1998-1999 neg. IOD/ENSO
2000
DJF 1999-2000 neg. ENSO
2001
DJF 2000-2001 no anomaly
2002
DJF 2001-2002 no anomaly
2003
DJF 2002-2003 pos. ENSO
2004
DJF 2003-2004 pos. ENSO
2005
DJF 2004-2005 balanced
2006
DJF 2005-2006 neg. IOD/ENSO
2007
DJF 2006-2007 pos. ENSO
2008
DJF 2007-2008 neg. ENSO
2009
DJF 2008-2009 neg. ENSO
2010
DJF 2009-2010 pos. IOD/ENSO
Longitude (degree)
Latitude (degree)
Precipitation [mm/DJF]
1400
1000
600
200
0
D

central EAP basins further east showing an opposite rainfall pattern with only temporal (1996-1998 and 2004-2006) correlations. We hypothesize that the opposite pattern requires two moisture sources whereas correlations account for one. In Figure 4.7B, two rainfall maxima exist, one northeast and one southwest of the catchment basin. It was reported that Tana receives most of its water in the southern catchment (Kebede et al., 2006) hence from the Congo Airstream, which we also see in comparison to the eastern located central EP basins and the rare correlations to each other. The EP basins in contrast, might receive large amounts of precipitation from a rainfall cell north of the central EP basins fueled by the Indian Ocean moisture. Diro et al. (2010a) reported the area of Tana basin especially in July-August to be largely correlated to warm SST anomalies in the Gulf of Guinea, producing excess rains over northern Ethiopia and deficits in southern Ethiopia. The atmospheric conditions behind are a weaker monsoon trough, a weaker westerly influx from the Atlantic, a weaker East African Low Level Jet (EALLJ) in the Indian Ocean and a weaker Tropical Easterly Jet (TEJ) mostly. During cold SST anomalies in the Gulf of Guinea all of them are strengthened producing less rainfall in northern Ethiopia and flooding in southern Ethiopia.
During times of in phase rainfall patterns over entire Ethiopia, one of those two cells must have broadened. This hypothesis could be supported by isotopic studies. In times of opposite patterns we agree with the observed opposite impact of SST variability in the Atlantic to the southern and northern parts of the EP. How QBO and SST variations in the Gulf of Guinea are related is one of the questions we are following.

ON Tana | Rainfall here is lowest with values around 50±20 mm/ON (Fig. 4.5C). The internal variations show no correlations to IOD or ENSO events, and also no correlation to the other studied basins. ON precipitation in Tana rather follow a triennial pattern. Such a triennial pattern was reported to affect rainfall in South Africa (Mason and Tyson, 1992; Kane, 2009). Further observations of African wide studies are needed to understand if such a pattern could also be observed only in parts of northeastern Africa, although not visible in other basins. The absence of such a clear pattern in other basins might only occur in basins that are not influenced by the ITCZ during this season (Fig. 4.2, Fig. 4.7C). However, longer time series are needed to support this hypothesis.

DJF Tana | Rainfall was not apparent in the entire study period (Fig. 4.5D). According the Figure 4.6 and 4.7D, north of 10° no rainfall centers developed.

Yearly precipitation Tana | Tana Basin yearly mean precipitation is the lowest in comparison to the other studied basins and controlled by JAS rainfalls clearly following trends and variations within this season, due to ON and MAM rainfalls only receiving low rainfall with less variability and DJF being dry (Fig. 4.10A). The biennial rainfall pattern is reflected in the yearly means over the entire study period.

4.1.4.2.2 Central-Ethiopian Plateau – Rift basins Abaya, Awassa, Ziway

Catchment information central EP rift basins | The investigated lake basins Ziway, Awassa and Abaya are close to each other in the central sector of the Ethiopian Rift in southern Ethiopia. The highest elevated basins are Ziway and Awassa (1558 and 1680 m asl, respectively; Fig. 4.1, Fig. 4.3). The catchments are of different sizes Abaya being the largest (33,060 km^2), followed by Ziway (14600 km^2) and then by Awassa's basin area that is the smallest (1455 km^2). The catchment shape of Ziway is broadly of circular shape extending over the western and eastern rift shoulder. The Awassa catchment shape is also rounded, although it only receives rainfall from the eastern rift shoulder (Fig. 4.3). Abaya's catchment is elongated and covers the Ethiopian highlands of ca. 2000 m asl down to ca. 1000 m asl from 7.5°N to 6°N (Fig. 4.1, Fig. 4.3).

MAM central EP rift basins | Precipitation of Ziway basin in MAM follows exactly the same trends from Tana basin, only showing higher amounts (Fig. 4.5A). Awassa follows a kind of biennial precipitation cycle and Abaya follows largely with suppressed amplitudes the trends of Awassa. Correlations to the EAP basins are not observed. Usual precipitation amounts in the three basins range around 200 mm/MAM. Exceptions occurred in 1997 and 1998, when rainfall was anomalous enhanced and lowered (±100 mm/MAM) during a developing coupled pos. IOD/ENSO and neg. IOD/ENSO, respectively. Except of Manyara received the entire EARS anomalous high rainfalls. In 2001 and 2003, only

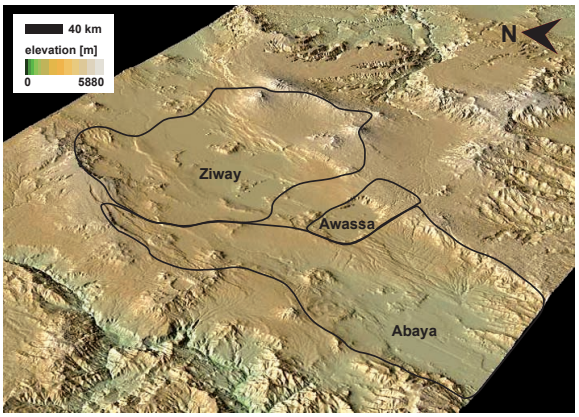

Figure 4.8 3D picture of central Ethiopian Plateau basins in order to explain topography of the east and western rift shoulders acting as barriers (created by GeoMapApp).

the small Awassa basin received enhanced rainfall of +100 mm/MAM during two small positive IOD events. In 2006 Abaya showed an opposite trend of higher rainfall in 2006 (La Niña) than Ziway and Awassa with slightly lowered rainfall. In 2008, during the end of a La Niña event, received Awassa, Ziway, Abaya (and Turkana) higher rainfalls whereas the basins further south remained unaffected. Despite some correlations of positive SST anomalies with enhanced rainfalls in the area, basin wide consistencies are missing, which might be attributed to the local affects of topography and hence distribution of rainfall. According to previous studies that showed only peripherally impact of IOD and ENSO (Camberlin and Philippon 2002; Abram et al., 2008), those rainfall fluctuations might be related to other mechanisms.

The ITCZ during this season is producing highest rainfalls over the EAP (Fig. 4.2, Fig. 4.5A). The exceptional high precipitation in 1997, that affected the entire East African rift basins was related to a broader rainfall maximum that was located over the entire studied area (Fig. 4.6). Figure 4.7A shows the rainfall maximum being located over lake Victoria and Mt. Kenya, which merged towards the north far into the EP.

Exceptional high rainfalls in the smallest Awassa basin in 2001 and 2003 was not caused by the mechanism used to explain the 1997 event since the rainfall maximum over the equator shows a clear positioning over the EAP during this time (Fig. 4.6). Since Awassa is small and only draining the eastern Ethiopian escarpment, a local rainfall maximum as it appears in many years over the eastern plateau (Fig. 4.7A) might have large impacts to the basin, possibly due to its highest elevation and constitution of its eastern catchment boundaries being slightly lower than the one from Ziway further north (Fig. 4.8). Due to the obvious biennial rainfall pattern, we hypothesize the QBO, which accounts for 36% of the MAM rains over eastern Africa (Indeje and Semazzi, 2000), brings moisture from this easterly located rainfall cell to the westerly located, comparatively small basin during one of its phases. Why the other basins are not showing such a distinct cycle might be attributed to their larger catchments capturing more influences from N-S directed anomalies affecting the ITCZ.

JAS central EP rift basins | Rainfall during this season is highest in all basins (250-400 mm/JAS) and trends are similar (Fig. 4.5B). Ziway is receiving highest amounts of rainfall and shows lowest variability, whereas Abaya and Awassa received similar lower amounts but higher variability, which is interesting since Awassa catchment is by far the smallest (Fig. 4.3, Tab. 4.1). Generally, central EP basin precipitation indicates a biennial pattern that is the opposite of Tana basin and shows amplification of positive phases in 1996 and 2004-2009, whereas lower amplitudes are observed in 1997-2003 during higher solar flux. Within the studied period higher (lower) precipitation, do not clearly follow expected negative (positive) phases of IOD/ENSO (Camberlin et al., 2001; Diro et al., 2010a).

The rare correlation to IOD/ENSO might explain the irregular influence of the humid southwestern Congo Airstream that is rather affected by SST variations in Atlantic (e.g., Nicholson, 1996; Fig. 4.2). Correlations to Tana basin, that is largely affected by the CAB, are therefore expected, which was the case in 1996, and 2003-2006. The position of the CAB is known to correlate to a pressure low along western India that pulls during below normal conditions the CAB further eastwards and enhances rainfall in the EARS (Camberlin, 1997). Thus, in phase rainfall with Tana occurs during times of anomalous low pressure over India accompanied with an eastward shift of the CAB. However, according to Figure 4.7B is such a clear shift of western rainfall cells not obvious. A second hypothesis is therefore attributed to the northern most rainfall maximum that is usually located over Tana basin (Fig. 4.2 August) and might be part of the CAB zone. The E-W as well as N-S shift and broadening might be responsible for in and out of phase correlations of those two areas. Outside

anomalous pressure lows along western India or influence of rainfall centres over northern Ethiopia can develop the well observed opposite JAS rainfall pattern between the northern and southern parts of Ethiopia (Diro et al., 2010a). The observed biennial pattern is most likely attributed to the QBO (Indeje and Semazzi, 2000), as explained in Tana, with offset of phases probably due to different moisture inflow. The reduction of amplitudes during higher solar flux must be related to the general reduction of IOD/ENSO as explained in 4.1 responsible for QBO rainfall amplitudes in East Africa. Why the general amount of rainfall is against reports (van Loon et al., 2004; van Loon and Meehl, 2008) not enhanced, remains to be explained.

ON central EP rift basins | Rainfall in the rift basins of the EP is homogeneous distributed (100-200 mm/ON) with very low variability (Fig. 4.5C). Awassa receives again the highest rainfalls, which might be related to humid air masses entering from the northeast and being caught due to its highest elevation. However, since variations are similar in all basins, we assume that the homogenous rainfall must be attributed to the peripherally influence of the ITCZ producing high rainfalls in the Turkana-Suguta depression whilst ascending towards the EAP (Fig. 4.2, 4.6). Anomalous drought (50 mm/ON) conditions occurred in 1997 during a large coupled positive IOD/ENSO when a the extreme rainfall cell over the Victoria basin extended southward around the EAP (Fig. 4.6, Fig. 4.7C; see chapter 4.1.4.2.5). Similar correlations of negative IOD/ENSO phases and enhanced rainfall in EP with opposite trends over the EAP are consistent with reports of previous studies (Camberlin et al., 2001; Diro et al., 2010a). The fact, that this pattern is now better developed than in JAS can be explained by the absent influence of E-W moisture associated with the CAB.
Interestingly, an opposite rainfall trend is also indicated for a multiannual period between 1998-2005 where a slight gradual increase in EP catchment means is observed whereas EAP basins experienced a gradual decrease in precipitation with achieving similar amounts dependent on the distance to the ITCZ by 2005. An explanation for the observation of a long-term opposite trend could not found in the literature therefore allowing just hypothesis to follow. Since the trend occurred during higher solar flux of the 11-year cycle we hypothesize that the reported La Niña state pattern (van Loon et al., 2004; van Loon and Meehl, 2008) might affect the EP basins similar to real ones that enhance (reduce) rainfalls over the EP(EAP. Additionally, a northward broadening of the Hadley cell as it was reported during higher solar flux (Meehl et al., 2009) could bring more rainfall to the EP basins. Although very thin, indications of a broader rain producing cloud coverage in Figure 4.7C (ON) is visible.
In contrast, in 2006 during also a positive IOD/ENSO all basins experienced higher rainfalls. This indicates that besides IOD or ENSO additionally influencing mechanism might still work to create for rainfall variability and its distribution.

DJF central EP rift basins | Rainfall in DJF is around zero between 1997-2004 with one excursion in 2000 towards 50 mm/DJF (Fig. 4.5D). Rainfall between 2005-2010 is highly variable (0-300 mm/ON). Peak rainfall in 2005, 2007-2009 does not follow a preferred direction of SST anomalies in the Pacific or Indian Ocean. Interestingly highest rainfall and variability experienced again Awassa basin that is the smallest basin in the studied area located between Ziway and Abaya (Fig. 4.3). Peak precipitation is possibly associated with the development and extension of a small precipitation cell in the highlands of the eastern Ethiopian Rift fueled by the Indian Ocean (Fig. 4.7D). How moisture-laden winds reaching the central EP basins must be dependend on wind strength and location. Often, Awassa basin profits the most, probably due to its highest elevation and direct path of the local rainfall center trough a narrow depression along its eastern catchment boundaries (Fig. 4.8). Finding the reasons for the creation of such a small rainfall cell is the key for understanding unexpected flooding during DJF.

Yearly precipitation central EP rift basins | JAS is the explained to be the main rainy season in central Ethiopia. According to Figure 4.10B-D is that the case only for Tana and Ziway, whereas in Abaya and Awassa ON and MAM are contributing with almost the same amounts to the yearly averages. DJF only slightly alters the signal in times of anomalous rainfall in the season, which is usually dry. Thus, any impact factors to ON, MAM and JAS largely affecting the yearly rainfall, which is important to know when wishing to understand proxy-records from one of the lakes.

4.1.4.2.3 Lakes in between two plateaus - Lake Suguta & Turkana

Catchment information Suguta & Turkana | Turkana and Suguta basins are located in the depression between the two plateau regions of the EAP and EP. Turkana catchment size (130,860 km^2) is about 10 times greater than Suguta. The catchment of Turkana has a long N-S extension draining both plateau regions while the watershed of Suguta, which is also elongated drains only the northern flanks of the EAP (Fig. 4.3). On the EAP side, the catchments are located next to each other. Lake Turkana is the largest lake in the studied regions with an area of about 73,000 km^2 with tendencies to produce their own climatology (Ferguson and Harbott, 1982; Nicholson, 1996; Johnson and Malala, 2009).

MAM Suguta and Turkana | Rainfalls in Turkana and Suguta exhibit during MAM similar values (300-600 mm/MAM) and same trends, which is surprising due to the much smaller size of Suguta basin, indicating Turkana to receive only moisture from the northern EAP similar to Suguta. From 1996-2000 both basins show high variability with high rainfalls in 1996 and 1999 (neg. IOD and La Niña, resp.) and pronounced drought in 1998 similar to the EP basins during the onset and termination of a large positive coupled IOD/ENSO event. From 2000-2005 stable rainfall conditions and less variable amounts similar to Tana, Ziway and Abaya basins from the EP are observed. The drying trend after 2005 as observed in the central EAP basins occurred also in Suguta, whereas Turkana received longer (until 2008) high precipitation similar to Abaya basin.
High amounts of rainfall in 1997 and 1999 must be related to a broadening of the rainfall centre from Victoria basin and/or Mt. Kenya northward merging between the two plateau regions (Fig. 4.7A). Although the basins of Nakuru and Naivasha show a peak in 1997, the amounts are still below normal, which might explain an even shifted centre of maximum rainfall northwards. The swath profile for 1997 (Fig. 4.6) indicates that a moisture low was centred over Naivasha and Nakuru whereas around the plateau region precipitation was high and extended northwards. Mt. Kenya might have played a role in leading moisture from the Indian Ocean to the different regions. This situation should be achieved through a mechanism that produces enhanced winds northwards towards the depression between the two plateau regions, possibly attributed to an anomalous northward position of the ITCZ in MAM probably related to an early onset of a strong ISM. Since no other rainfall anomalies within the studied time period to one of the oscillator events occurred, we exclude their impact, which is supported by earlier studies that have not observed an influence of ENSO/IOD during MAM to East Africa (Camberlin and Philippon, 2002; Abram et al., 2008).
Our explanation for similar rainfall amounts between 2001-2005 in both basins and EP basins pertains to the position of the ITCZ around the equator during this season, with no exceptional displacements (Fig. 4.6, Fig. 4.7A).
Prolonged humidity until 2008 in the Turkana correlating to EP basins does not correlate with IOD/ENSO. In Figure 4.7A is clearly visible that same moisture sources can be excluded to cause enhanced rainfalls in the basins. We thus assume rainfall in both areas to be attributed to two moisture sources: one moisture cell is located in the western catchment of Turkana, that does not reach Suguta and a second independent moisture cell overt he eastern EP that affects the central EP basin. Causes for this situation are not well understood yet, but we hypothesize that Lake Turkana's convection itself produces convection centres (Nicholson and Yin, 2004) that are transported by westward-directed winds probably towards the CAB to Turkana's western catchment. Same causes for westward winds are assumed for transporting moisture from the small rainfall cell over the eastern EP to its central basins. Isotope studies could help to support this theory.

JAS Suguta and Turkana | In this season, Turkana receives highest rainfall (400-550 mm/JAS, Fig. 4.5C), which is attributed to the elongated N-S trending catchment allowing more moisture to capture of the N-S directed CAB that has the highest influence in JAS rainfalls to equatorial East Africa and northwestern Ethiopia (e.g., Nicholson, 1996; Fig. 4.2). However, highest variability is observed in Suguta (200-580 mm/JAS). Both catchment means only correlate between 2000-2006. Opposite trends exist in 1998-2000, and 2007-2008. In 1998 floods in Suguta and droughts in Turkana occurred during a negative coupled IOD/ENSO event, whereas in 1999 droughts in Suguta and floods in Turkana appeared during a pure La Niña. Additionally, the 2000 floods in Suguta and droughts in Turkana during a balanced IOD/ENSO event show that there is no

large correlation of rainfalls to one of the oscillator events, which could assign the irregular influence of the CAB bringing recycled humidity from the Congo basin (e.g., Nicholson, 1996; Fig. 4.2).
Local precipitation during this season is governed to a lesser degree by moisture provided by the ITCZ since it is located far north and irregularly by the CAB, dependent on their intensity controlled by various factors and location north and east, respectively, dependent of the strength of a west-Indian low (Camberlin, 1997). Since one third of the Turkana catchment falls onto the zone of direct CAB influence over the western EP (Fig. 4.2) we would expect Turkana and Tana to show similar trends, which is the case except of 2007-2009. The observed biennial rainfall pattern in Tana is not observed in Turkana, which we attribute to an overprinting by lake basin internal processes related to convection and precipitation processes (Nicholson and Yin, 2004) over the Lake Turkana, which we also attribute to the less high variable rainfall in JAS here.
Correlations of trends in catchment means in Turkana and Suguta in 2001-2006 must be attributed to a shifted CAB further eastwards, although not bringing a large amount of water to the basin. Central EP rainfall trends correlate with trends of Suguta also between 2003-2006, which supports our hypothesis of an eastward shifted CAB. Different amounts of rainfall must be related to various interacting factors such as SST of the Atlantic, the pressure low over western India and hence intensity of the CAB reaching only partly or fully the studied regions. Precipitation of high amounts along the flanks of the EP and EAP might also control how much rainfall the areas finally receive.
JAS rainfalls in the Turkana but especially the Suguta basin are largely dependent on the influence of the CAB whose intensity and location is dependent on many interacting factors. Thus, an intensified CAB with higher moisture available being pulled eastwards due to a deeper pressure low over (western) India could provide this region by additional high amounts of rainfall as it was proposed for the early to mid Holocene (Junginger and Trauth, subm.)

ON Suguta and Turkana | During the 'short rains' season, Suguta receives higher rainfall than Turkana and is generally highest together with Baringo compared to the other basins from the EAP during the entire study period (Fig. 4.5C). This must be related to the ITCZ's southward migration being captured along the northern base of the EAP where it produces higher rainfalls while ascending (Fig. 4.6). Due to high elevations of the EAP is the centre of the ITCZ displaced over the Victoria basin (Fig. 4.7C). Turkana and Suguta follow the same trends, although less variability is seen in Turkana, which must be attributed to basin internal convection processes related to the large Lake Turkana as explained for other lakes by Nicholson and Yin (2004). Most of peak precipitation correlates with positive ENSO or IOD whereas negative events produced lowered rainfalls, consistent with previous publications about the highest influence of ENSO/IOD being regarded during the 'short rains' (e.g., Hastenrath et al., 1993; Nicholson, 1996; Camberlin et al., 2001; Clark et al., 2003). However, one exception occurred in 1999, where a large la Niña event produced anomalous high rainfalls. Catchment means and trends correlate also with the central EAP basins, which must explain the same influencing mechanisms. For an explanation we refer to the discussion section of central EAP basins in ON (see 4.1.4.2.4).

DJF Suguta and Turkana | Precipitation in Suguta and Turkana range between 80-200 mm/DJF with variabilities largely in phase only that the Suguta receives higher amplitudes with somewhat extreme interannual differences (Fig. 4.5D). Turkana on the other hand appears stable with small amplitudes of variability in the studied period. In comparison with basins from the central EAP south to Natron shows an increase of variability despite same general trends as observed in Turkana and Suguta. We attribute this development to the combination of the ITCZ being located at its southernmost position, distance from the rainfall centre, high topography and Lake Turkana's intrabasin precipitation.
Suguta and Turkana basins are showing the lowest amounts of rainfall of the compared basins because they are located far away from the direct influence of the ITCZ additionally shielded by the EAP. The distance from the ITCZ in addition to Lake Turkana's internal convection processes (Nicholson and Yin, 2004) leading to additional precipitation resulting in lower variability. However, the peripherally influence of the ITCZ must be still abundant due to the good correlations of the basins south of them. Correlations with rainfall trends of the southern basins must be attributed to a broadening of the ITCZ causing maximum rainfalls over the Victoria basin (see also 4.1.4.2.4).

Yearly precipitation Turkana & Suguta | The direct comparison of yearly catchment means in Figure 4.10E-F indicate higher rainfall fluctuations in the Turkana basin, whereas Suguta received during the entire study period similar amounts of rainfall with only low fluctuations and a continuous drying trend. Annual precipitation to Suguta is provided by JAS, ON, and MAM rainfall equally, however, with complex variations: JAS and MAM generally showing the opposite rainfall pattern, indicating a general pattern of either high rainfall in MAM or JAS but never both being high. ON shows not a clear pattern since rainfall followed from 1999-2002 MAM rainfalls and from 2003-2009 JAS, indicating some larger dependencies that requires further investigations. However, due to opposite trends in MAM and JAS in a balanced annual rainfall with low variability is ON the season that can cause variabilities of annual precipitation. In contrast, annual precipitation to Turkana is only controlled by the seasons JAS and MAM of minor impact by ON. DJF shows minor values of lowest variability, hence not contributing to rainfall variability to Turkana.

Interestingly, Turkana's basins means do not follow in none of the investigated seasons and also not in the yearly means one of the basins from the EP. This observation is important, since many studies presume Lake Turkana largely to reflect the climate from the Ethiopian basin, due to the only large and permanent Omo River that drains the western highlands of Ethiopia. We also discovered that precipitation over the EP is compared to the EAP low, even in the yearly means. In consideration that Turkana is the only large lake in the eastern branch of the EARS, besides basin intern evaporation and precipitation, water from the EAP must also contribute to the lake, probably not in large rivers, but probably in small runoffs or groundwater. This observation is important for understanding why Turkana can persist even longer droughts.

4.1.4.2.4 Central East African Plateau – Baringo, Nakuru, Naivasha

Catchment information central EAP rift basins | The basins are located on the East African plateau in close proximity but with significant differences in their catchments (Fig. 4.3). Baringo is the largest catchment (6,200 km^2) in contrast to Naivasha (3200 km^2) and Nakuru (2390 km^2). The catchments of Nakuru and Naivasha are located along the same latitude and receive water either from the western and eastern rift margins, respectively. In contrast, Baringo basin drains both sides of the rift and due to its N-S elongation the central EAP highlands ca. 2000 m down to 1000 m asl from 0.5°S to 1.5°N (Fig. 4.1, Fig. 4.3).

MAM central EAP | MAM rainfalls in the central EAP basins show same trends over the entire study period but the amplitudes of variability are quite different (Fig. 4.5A). Whereas Baringo received high rainfall (400-500 mm/MAM) before 2001, Nakuru and Naivasha experienced extended drier MAM seasons (200-300 mm/MAM). After 2001, rainfall amounts in all basins are similar (350-400 mm/MAM) with highest amplitudes in interannual variations observed in the Naivasha catchment, especially in 2002 and 2005. A general decline in rainfall to 250 mm/MAM occurred after 2005. We see no correlation of rainfall variability related to ENSO/IOD in MAM, which is consistent with previous studies (Camberlin et al., 2001; Camberlin and Philippon, 2002).
Higher rainfalls in the Baringo, and even higher in Turkana and Suguta between 1996-2001 in comparison to Nakuru and Naivasha must be attributed to a mechanism that caused higher MAM rainfalls further north in between the two plateaus. We relate this mechanism to a northward broadening of the rainfall maximum over Victoria basin and/or Mt. Kenya (Fig. 4.6, 4.7A) probably related to a anomalous northward location of the ITCZ that produced higher low level winds carrying moisture northwards, probably associated with an early onset of the ISM (see also 4.1.4.2.3). This rainfall maximum was even more restricted to the northern base of the EAP in 1999 since Nakuru and Naivasha remained low (Fig. 4.7A). The reasons for this distribution must be related to a combination of topography, enhanced low level winds towards the northeast and northwest, and a mechanism that produced a low over the depression between the two plateau regions. ITCZ monitoring would help to proof the hypothesis.
From 2001-2009 the lake basins of Nakuru and Naivasha that have a similar size and drain either the western or eastern part of the rift (Fig. 4.3), respectively, indicate high MAM rainfalls falling the western parts of the EAP most likely related to a rainfall maximum over Victoria basin (Fig. 4.7A). Baringo, whose catchment covers both sides of the rift, supports this hypothesis since rainfall amounts follow-

ing rather Nakuru values than Naivasha.

Highest amplitudes in the Naivasha (and Natron) basin such as in 2002 and 2005 might explain a protrusion of additional moisture from the east towards the eastern escarpments. According to Figure 4.7A a rainfall maximum occurs always in the East in the region around Mt. Kenya. We assume that high rainfall peaks in Naivasha might be attributed to transport or a intensification/broadening of this rainfall maximum. In a Figure 4.6 (2002) is nicely shown how rainfall was restricted to the EAP and caught between Mt. Kilimanjaro and Kenya. Controlling factors must be related to a strengthening of ITCZ convection causing enhanced low level winds transporting humid air masses around the volcano and probably even further east. This hypothesis could be proofed by isotopic studies.

JAS central EAP | During this season rainfall in all basins varies between 200-300 mm/JAS, except of 1999-2000 when Baringo received up to 500 mm/JAS similar to Turkana basin. Rainfall trends, however, are of large difference among the three basins not following a clear pattern related to IOD or ENSO. We rather see that Naivasha and Baringo basins are showing the same trend whereas Nakuru shows the exact opposite (Fig. 4.5B). Despite opposite precipitation variability we see a clear biennial precipitation between 2001-2008 (Fig. 4.5B). This out of phase pattern of Nakuru is however in phase with Natron (1996, 2000-2009), Tana basin (2000-2009), the Suguta basin over almost the entire study period (except 2002, 2009) and EP basins 2002-2006 indicating the influence of the same moisture source. This moisture source must be related to the CAB since ITCZ rainfall is excluded due to its northernmost position in JAS (Fig. 4.2). In fact was observed by earlier studies that August rainfalls in Nakuru basin are one of the highest (Vareshi, 1982). As shown in Tana basin that is under the fully influence of the CAB in JAS showing a clear biennial rainfall cycle, we hypothesize that between 2002-2006, when the biennial pattern was well developed in Nakuru, that the CAB influenced this region regularly, most likely associated with a strong pressure low over western India (Camberlin, 1997). The observed biennial pattern is most likely attributed to the QBO explained by Indeje and Semazzi (2000) that discovered in a N-S direction through the EARS a separation of phase changes in the QBO. These phase changes might be

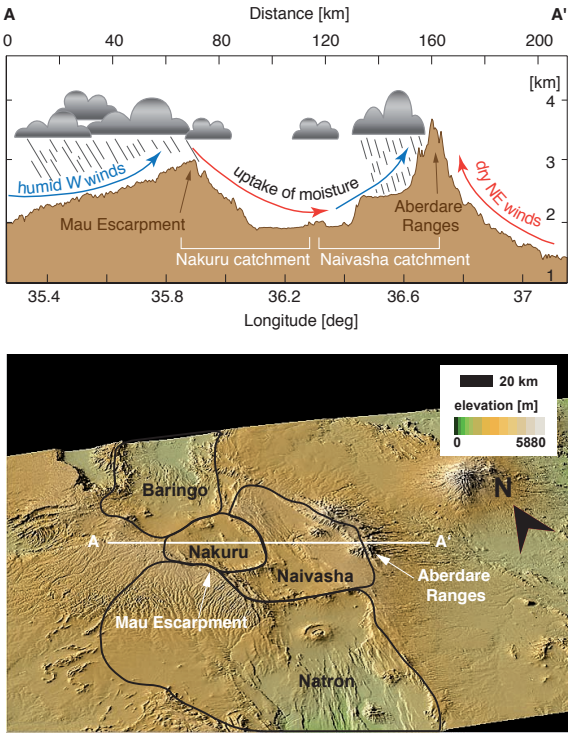

Figure 4.9 3D picture of central East African Plateau basins (A) and cross-section through the highest elevated basins Nakuru and Naivasha (B) (created by GeoMapApp). B) Naivasha basin received lower amounts in ON despite a larger catchment that could be related to topography related rain out of moisture coming from the Victoria basin to the western catchment of Nakuru. Dry warm air then is migrating eastward where it absorbs moisture within the rift floor bypassing the Nakuru, Elmenteita and Naivasha lake bodies. When reaching the eastern catchment boundaries of Naivasha, ascending airmasses poduce rainfall along the Abadare ranges, however less intense.

attributed to even different influences of moisture. According to Figure 4.7B a small, elongated rainfall cell extending in a small band from the southeast towards the northeast to Mt. Kenya could account for another moisture source even fuelled by another ocean (Indian Ocean) than the CAB (Atlantic Ocean). JAS rainfalls over the central EAP follow a complicated pattern that requires further investigations. Beside the QBO might contribute also the ISM strength and solar flux to rainfall variability. In order to understand the mechanisms behind this complexity, longer time series are needed additionally to isotopic studies that support or disprove the influence of hypothesized moisture sources.

ON central EAP | During this season, all EAP basins including Turkana and Suguta show same trends and similar amounts between 200-400 mm/ON (Fig. 4.5C). Exceptional high precipitation was meas-

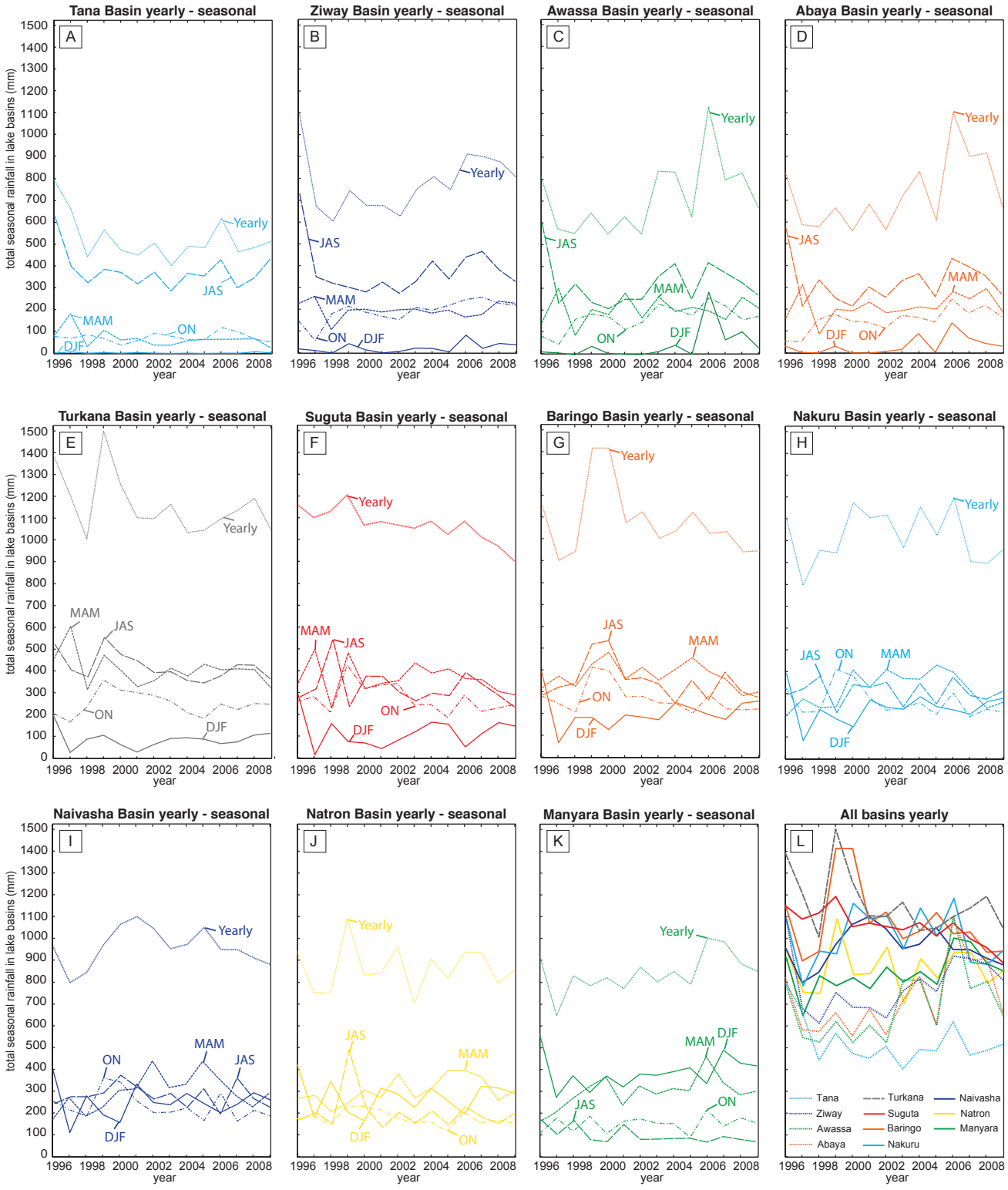

Figure 4.10 Yearly versus seasonal catchment precipitation means for 11 lake basins from the East African Rift System in order to discover most influencing season for yearly precipitation trends.

ured in 1999-2000, and 2006. Similar precipitation amounts in all catchments must be attributed to changes within the same moisture source, which is the ITCZ in this season. A good correlation of peak precipitation to positive ENSO/IOD seem to be the main cause of any alteration within the ITCZ. However, one exception occurred in 1999, where a large la Niña event produced anomalous high rainfalls.
Almost identical amounts received Nakuru, Baringo, and Suguta despite large differences in their catchment sizes, which we relate to a contribution of moisture provided from the Victoria basin. Naivasha basin generally received slightly lower amounts that could be related to topography related rain out of this moisture over the western catchment of Nakuru (Fig. 4.9). While dry warm air is migrating eastward where it absorbs moisture within the rift floor bypassing the Nakuru, Elmenteita and Naivasha lake bodies produces the even higher elevated eastern catchment boundaries of Naivasha rainfall that contributes to slightly lowered catchment means in Naivasha.
Only during the EARS wide event in 2006 reached Naivasha the amounts of the adjacent Nakuru basin, which might be attributed to either a higher moisture and stronger winds from the west allowing precipitation to reach also the Naivasha basin, or similar to MAM that an easterly moisture source entered the Naivasha area. According to Figure 4.7C the latter assumption might be responsible for the EARS wide enhanced precipitation. We see that whole eastern East Africa is affected by unusual high moisture. A NE-SW trending rainfall band over the Indian Ocean extends along the entire East African coast, a precipitation cell developed east of the central EP basins and a rainfall cell around Mt. Kenya. In contrast, almost no precipitation centre developed over the Victoria basin. The mechanisms behind such a development require some further investigations.
Although rainfall amounts in Naivasha are still below Nakuru, Suguta and Baringo in 1999-2000 the previous mechanism works as well. In both years developed an anomalous intensive rainfall maximum along the western EARS including the Victoria basin. However, in 1999 and additional rainfall maximum developed around Mt. Kenya and mechanisms lead to both the eastwards extension from the rainfall centre over lake Victoria and westward extension of the moist air masses over the Aberdare ranges (Fig. 4.7C). In contrast stands the 2000 event, where the Mt. Kenya precipitation maximum was smaller, which might not have reached the northeastern escarpment of Suguta anymore, due to a large reduction in rainfall here.
In comparison of all studied basins we see a clear separation of a gradual, steep decrease in rainfall over the EAP between 1998-2005 and an opposite trend with a slight gradual increase in the EP catchment means. Until this stage of the study we cannot give a well-grounded explanation but assume some relations to the enhanced solar flux. Enhanced solar flux within the 11-year cycle is proposed to produce a La Niña state pattern (van Loon et al., 2004; van Loon and Meehl, 2008), which reduces, similar to real La Niña or negative IOD events in ON rainfall whereas over the EP rainfall increases (Camberlin et al., 2001; see also 4.1.4.2.2).

DJF central EAP | In this season, we see that all the EAP basins are largely in phase. Naivasha basin receives highest rainfall followed by Nakuru and then Baringo. Precipitation ranges from 100-300 mm/DJF. A triennial precipitation pattern with high rainfall is followed by a 2 year-reduction of rainfall is observed most clearly recorded in the Naivasha and Nakuru basin. Enhanced amplitudes in rainfall within the triennial pattern do not clearly follow IOD or ENSO events indicating a larger influence of the triennial pattern than the IOD/ENSO. A triennial precipitation pattern was reported from a rainfall study in southern Africa (Kane, 2009). Reasons for those and amplifying mechanisms need some further readings and will be provided before paper submission.
The event of anomalous high homogeneous distributed rainfall from Manyara basin toward Turkana in DJF1997 is related to a restrict rainfall maximum far southwest of the Victoria basin closely located to Manyara (Fig. 4.7D) that must explain the clear position of the ITCZ as also seen in Figure 4.6. Rainfall was therefore most likely coming from the south-southwest, clearly indicated by rainfall amounts within the basins decreasing from south to north. Until this stage of the study we cannot explain reasons for out-of-phase high rainfall.

Yearly precipitation central EAP | The direct comparison of yearly catchment means in Figure 4.10G-I reveals a complicated picture of annual vs. seasonal precipitation in the three adjacent basins. Baringo's annual rainfall follows either Turkana or Naivasha and hence their variability (Fig. 4.10L). JAS and MAM are of the same importance in the amounts of

yearly catchment precipitation in Baringo followed by ON and DJF (Fig. 4.10G). Nakuru and Naivasha are a good example for topography related rainfall variations, since they both have similar catchment sizes and are located on top of the EAP next to each other, draining one of the escarpments of the EARS. Thus, yearly averages vary largely between the two basins, with Nakuru showing highest variability and Nakuru comparatively low. Hence influencing mechanism to the adjacent basins are largely different, which are discussed above. However, both annual catchments precipitation consists of an almost equal contribution of rainfalls of all seasons (Fig. 4.10H-I).

4.1.4.2.5 Southern East African Plateau Lakes - Natron and Manyara

Catchment information Natron and Manyara | The Natron (2°S, 600 m asl) and Manyara (3°S, 960 m asl) catchments are the southern most basins of the study area. They occupy areas of lowest elevation at the terminal end of the eastern arm of the EARS (Fig. 4.1, Fig. 4.3). Both catchments are elongated in their N-S direction, but Natron is the largest with 184,000 km^2 whereas Manyara only covers an area 23,207 km^2. An additionally feature most likely important for rainfall distribution is, that Natron's catchment originates in the northwestern escarpment of the EAP south of the Mau Escarpment (0.5°S) while Manyara's catchment boundaries is marked by the Mbulu Plateau and various volcanoes farther south (5°S) of the terminal lake.

MAM Natron and Manyara | Precipitation in the watersheds ranges between 300±100 mm (Fig. 4.5A). Although the two basins are adjacent to each other, significant variability in rainfall exists with respect to the two basins, which are partly in and out of phase with each other. IOD and ENSO events do not correlate with precipitation variability in the calculated catchment means in both basins. Natron follows over the entire study period rainfall variabilities of Naivasha and Nakuru attributed to the same moisture source (ITCZ), whereas Manyara shows temporal opposite trends. The reason for correlations of Natron basin with central EAP basins is attributed to its northern catchment covering both sides of the rift shoulders adjacent to Nakuru and Naivasha, hence being affected by the influencing mechanisms. Moist air masses entering the EARS from the southeast might bring precipitation only to the southern basins that could be an explanation for slightly differing amounts in Natron, such as in 2006. One major role might play Mt. Kilimanjaro as moisture barrier leading low and mid level moisture-laden winds around and therefore control flow directions from the south-eastern Indian Ocean to either Manyara or Natron basin. A study about snow accumulation on Mt. Kilimanjaro suggested a circulation pattern over Madagascar to be one of the most controlling factors (Chan et al., 2008). Precipitation from the Indian Ocean mostly falling in Manyara basin in contrast to rainfall largely provided by a rainfall maximum over Victoria basin affecting the central EAP basins including Natron could be observed also in isotopic studies.
However, additionally to the build up of circulation patterns over northern Madagascar, we assume, that since this season's rainfall is principally controlled by the location and strength of the ITCZ, variations in these parameters might drive in or out of phase relation between these two basins.

JAS Natron and Manyara | In this season the ITCZ has reached its northernmost position north of the EP whereas the CAB reaches central EAP basins temporal (Fig. 4.2). Thus, rainfall is low in the studied region with Manyara basin showing lowest values (20-50 mm/JAS) with three excursions towards 120 mm/JAS in 1996, 1998, and 2001 (Fig. 4.5B). Natron receives slightly more rainfall in a regular pattern between 100-200 mm/JAS, with one excursion in 1999 towards anomalous high rainfall (450 mm/JAS; La Niña), an event only also observed in Turkana and Baringo. Despite this observation we exclude IOD and ENSO to be responsible for this oscillation since we see no regular dependency. We related the regular biennial rainfall pattern in Natron that is in phase with Nakuru (1996-1997, 2001-2009) and Tana (1997-2009), and out of phase with Manyara. We relate the biennial rainfall pattern to the QBO that was reported to show significant relationships to seasonal rainfall in boreal June-August (Indeje and Semazzi, 2000).
A phase change of the biennial pattern occurred between 2000-2001, also seen in the basins of Turkana and Baringo, which could be attributed to a mechanism that has overprinted the signal, restricted to lower elevated basins.
Large differences between Manyara and Natron are here again attributed to the catchment locations.

Natron mean precipitation follows largely the trends from the central EAP basins since its catchment is draining the southern top of the EAP and is therefore largely affected by moisture and its variabilities entering this region (see 4.1.4.2.4 JAS discussion). In contrast, Manyara precipitation is largely controlled by precipitation falling in its higher elevated catchment further south, which is largely controlled by the Indian Ocean dynamics including a low over Madagascar and related wind flow (Chan et al., 2008). To confirm this argument some further investigations of Indian Ocean dynamics are needed.

ON Natron and Manyara | Rainfall over Natron and Manyara fluctuates between 150±50 mm/ON, which is similar to the central EP basins (Fig. 4.5C). In this season, like in MAM, we observe in phase trends of Natron catchment means and the central EAP basins, which is attributed to Natron's catchment draining the top of the EAP. Similar to MAM follows Manyara basin temporarily trends of Natron, but also shows independent rainfall fluctuations. A biennial circulation pattern in Manyara is indicated and explained to have some relation to ON rainfall, although less high than in JAS (Indeje and Semazzi, 2000). In general, we see correlation of positive IOD/ENSO events to higher precipitation in the studied region and vice versa for negative phases.
During this season, the ITCZ is located again over the equator and moves southwards with precipitation to be expected falling only in the catchments that are located in its vicinity, such as Natron. The reason, why Manyara, despite having its catchment located farther south, follows often Natron, must be related to the southeastward extension of the rainfall maximum over the Victoria basin (Fig. 4.7C).
The southeastward extension of a heavy precipitation cell in 1997 during the largest coupled IOD/ENSO event within the study period causing only enhanced rainfall in those two basins must have worked exactly as proposed. An equatorial rainfall maximum was centred over the Victoria basin and extended southeastwards around the EAP (Fig. 4.7C). According to the Figure 4.6 was the expected rainfall maximum over the equator and split to an additional centre south of the equator. In the swath-profile in Figure 4.6 lead this southward extension to the picture of a spitted version of the ITCZ. Since the EAP basins remained unaffected, these south-east-directed winds seem to be weaker than usual. Questions need to be answered, if during a coupled positive IOD/ENSO event (trade) winds are weaker.

DJF Natron and Manyara | During this season we observe highest precipitation values for Manyara basin relative to Natron and all other studied catchments (Fig. 4.5D), which confirms expectations, because of the ITCZ having reached its southernmost location. Similar to all other seasons follows Natron again rainfall variations from the EAP basins (see 4.1.4.2.4 DJF discussion), whereas Manyara often shows individual or opposite trends. Varying phases of the two adjacent catchments are those, that Natron basin shows like the central EAP basins a triennial rainfall pattern, whereas Manyara follows a biennial pattern, similar to ON season, although being the exact opposite phase to ON. Despite the opposite trends between ON and DJF in Manyara basin, the same alteration occurred between 2002-2003. Due to the out phase picture we assume different moisture sources or at least different paths reaching the two catchments. We see no IOD or ENSO influencing the observed rainfall variability.

Yearly precipitation Natron & Manyara | Annual precipitation in both basins is comparatively high, only slightly less than of the central EAP basins (Fig. 4.10L). Annual mean precipitation in Natron is similar highly fluctuating whereas Manyara basin appears stable with a biennial pattern of lower amplitude. Similar is the seasonal contribution to the yearly values, with Natron receiving similar amounts of rainfalls in all seasons similar to the central EAP basins, whereas MAM and DJF are the most influencing seasons for annual rainfall in Manyara basin. As explained above, receive those adjacent basins due to their catchment location from different moisture sources precipitation, which could be monitored by isotopic studies.

4.1.5 Preliminary summary and conclusions

The on-going investigation of climate dynamics along the EARS is an important study in order to distinguish regional from local processes to improve climate proxy interpretations and forecasting. By using rainfall estimates from remotely sensed data between January 1996 and February 2010 we have observed interesting dynamics that we think are behind high precipitation gradients in this topographically complex region. Although the analysed

period is too short to make conclusive statements, some preliminary inferences can be made. We discovered a rather complex picture of basin precipitation showing low and high amplitudes in intraseasonal variability, being in or out of phase with each other, exhibiting a biennial to triennial precipitation patterns and or being (not) affected by IOD and ENSO. These variabilities are reflected in considerable spatial variation in watershed precipitation from even adjacent basins along the EARS. In **MAM** correlate within the studied time period Tana, Ziway and Abaya; Turkana and Suguta; Naivasha, Natron, Nakuru, and Baringo and no relation to any basins showed Manyara and Awassa. In **JAS,** best correlation showed Nakuru and Suguta; Tana and Natron, Baringo; Naivasha and Turkana; Awassa, Abaya and Ziway, no similar trends are observed to Manyara basin. **ON** precipitation was most similar among the Awassa, Abaya and Ziway basins; Baringo, Nakuru, and Naivasha; Natron, Turkana and Suguta, with no correlation to Manyara and Tana. During **DJF** Baringo, Nakuru, Naivasha and Natron nicely followed the same trends on the East African Plateau, whereas on the Ethiopian Plateau the basins Awassa, Abaya and Ziway correlated. Suguta and Turkana show some correlations, although Turkana appears with rather smoothed values compared to Suguta.

Among all seasons we observed that JAS is the season of highest complex rainfall variability especially over the East African Plateau. Mechanisms behind are not understood yet, but might explain already this season to be one of the most sensitive to climate variability.
We also discovered that most of the basins received considerable amounts of rainfall outside the main rainy seasons or even similar values than during the main rainy season, hence enhancing the number of climate influencing mechanisms causing rainfall variability that are important to understand for interpreting climate-proxy data. Rainfall summarized in yearly catchment means shows that Awassa and Abaya are best correlating together with Ziway that only shows lower amplitudes in its fluctuations. Baringo and Naivasha correlate well. Surprisingly, Suguta and Manyara, both located along the base of the East African Plateau roughly correlate in their yearly trends the most, which is also the case for Nakuru and Natron. No similar trends, however exhibit Turkana, and Tana.
The variability among the watersheds is driven by a) the shape and length of the catchment and its relative location to the EARS, b) which side of the EARS (east or west) is the catchment draining in interaction with the c) prevailing wind directions and thus d) their position relative to the ITCZ and/or CAB and d) strength of the circulation systems itself. The internal variability of the influencing circulation systems is controlled by various factors, such as ISM, solar flux, IOD/ENSO, SST variations in the Atlantic and QBO. As Turkana shows the lowest variability, we assume internal lake basin processes related to the large inland water body.
Juxtaposed on the topography and inland lakes convection control the onset, timing and intensities of moisture-laden winds entering the studied basins. The Rift margins are playing an important role since they act as barriers that prevent moisture-laden winds to reach the studied basins under explained influencing factors responsible for ITCZ and CAB strength.

In order to better understand intraseasonal rainfall fluctuations we will include in our on-going work the in detail comparison and discussion of those climate influencing factors. In particular will this comprise the set up of correlation coefficients and will include latest published isotopic studies as support.

4.2 Supplementary information

4.2.1 - The coupling and dependency of IOD and ENSO – a literature overview

Since the discovery of the zonal IOD pattern (Saji et al., 1999, Webster et al., 1999) fundamental questions about its independence from ENSO, its natural modes of variability and its interaction with the Asian monsoon systems have been raised. It has been suggested, for example, that El Niño may generate IOD conditions by warming the western IOD region, and also reducing atmospheric convection and decreasing thermocline depth in the eastern IOD sector (e.g., Charles et al., 2003; Abram et al., 2008). Saji et al. (2006) reported, that although El Niño is a trigger of the IOD, other large-scale climate drivers also operate. This hypothesis is supported by the occurance of the rare combination of a positive IOD and La Niña event in 2007, providing unambiguous evidence for the Indian Oceans own capability to initiate and sustain a positive IOD event (Cai et al., 2009). A recent study on coral dipole mode index (DMI) revealed that only 56% coincide with El Niño, and 39% of IOD events occurred during a neutral ENSO explaining ENSO playing an important but not exclusive role in driving the IOD variability (Meyers et al., 2007; Abram et al., 2008).

Another study by Kodera et al. (2007) relate a coupling of ENSO and IOD to a development of a South Indian Ocean (SIO) anticyclone during periods of low solar activity whereas high solar activity prevents its development. The direct cause of the difference in the SIO anticyclone is explained as a shift in the location of the descending branch of the anomalous Walker circulation with an expected trend towards high rainfall variability in the rainy season during boreal fall in East Africa (Kodera, 2007). Ashok et al. (2004) studied the relative influence of ENSO and the IOD on the variability of the Indian summer rainfall and showed that the IOD, while significantly influencing the ISM rainfall, also significantly reduces the impact of ENSO on the Indian summer rainfall whenever these events with the same phase co-occur.

An additional circulation, the tropospheric biennial oscillation (TBO), has been reported to be an important mode of interannual variability in the Indo-Pacific, possibly interacting with both ENSO and IOD (Izumo, 2008). It involves a coupling with the seasonal evolution of Pacific SST interannual anomalies and is often, but not always, associated with El Niño (La Niña) conditions (Meehl and Arblaster, 2002a; Meehl et al., 2003). The transition and relationship of the TBO and strong or weak ISM is only roughly understood.

Another oscillation system is the stratospheric Quasi-biennial oscillation (QBO), which shows significant relationships to seasonal rainfall occurring during boreal summer (June-August) and tends to enhance major negative swings in the Southern Oscillation associated with ENSO events (Indeje and Semazzi, 2000). It has been suggested that the difference of QBO during June-August minus QBO in October-December to be a good indicator for the non-occurrence of drought over eastern Africa when it is positive and vice versa in a negative case (Indeje and Semazzi, 2000). Also, their correlation analysis results indicate that about 36% of the variability of the long-rains season over eastern Africa is associated with the QBO-Index. Comparison of the QBO-Index and the DMI indicates that the two climate variables may be significantly related. The season with the weakest relationship is December-February. It is however, noted that although the coherence between QBO-Index and rainfall during the long-rains is significantly high, there are some wet/dry years where strong and prolonged ENSO years have reduced the relationship between the long rains and lower equatorial zonal wind (Indeje and Semazzi, 2000).

4.2.2 - Additional information about solar influences to IOD and ENSO – a literature overview

Meehl et al. (2009) gave in detail the following overview: Two mechanisms have been explained as a possible amplifying mechanism: (1) the top-down response of ozone to the ultraviolet (UV) part of the solar spectrum that varies by a few percent. Peaks in solar forcing cause the enhanced UV radiation, which stimulates additional stratospheric ozone

production and UV absorption, thus warming that layer differentially with respect to latitude (Meehl et al., 2009). The changes in the stratosphere modify tropical tropospheric circulation and thus contribute to an enhancement and pole-ward expansion of the tropical precipitation maxima through a broadening of the Hadley cell (e.g., Kodera and Kuroda, 2002; Haigh et al., 2005; Meehl et al., 2009). (2) A second "bottom up" mechanism that can magnify the response to an initially small solar forcing involves air-sea coupling and interaction with incoming solar radiation at the surface in the relatively cloud-free areas of the subtropics. Thus, peaks in solar forcing produce greater energy input to the ocean surface in these areas, evaporating more moisture, and that moisture is carried by the trade winds to the convergence zones where more precipitation occurs. This intensified precipitation strengthens the Hadley and Walker circulations in the troposphere, with an associated increase in trade wind strength that produces greater equatorial ocean upwelling and lower equatorial SSTs in the eastern Pacific, a signal that was first discovered in observational data (van Loon et al., 2004). The enhanced subsidence produces fewer clouds in the equatorial eastern Pacific and the expanded subtropical regions that allow even more solar radiation to reach the surface to produce a positive feedback (Meehl et al., 2009). Dynamical air-sea coupling produces a transition to higher eastern equatorial SSTs a couple of years later (Meehl et al., 2009).

There is observational evidence for a strengthened Hadley circulation in peak solar forcing years associated with intensified tropical precipitation maxima, a stronger descending branch in the subtropics, and a stronger ascending branch in the lower latitudes (van Loon and Labitzke, 1994); a pole-ward expansion of the Hadley circulation in peak solar years, with stronger ascending motions at the edge of the rising branch, as well as a stronger Walker circulation with enhanced upward motions in the tropical western Pacific connected to stronger descending motions in the tropical eastern Pacific (Gleisner and Thejll, 2003) and enhanced summer season off-equatorial climatological monsoon precipitation over India (e.g., Kodera, 2004). This cold event–like response to peak solar forcing is different from cold events (also known as La Niña events) in the Southern Oscillation in that, among other things, zonal wind anomalies in the stratosphere are opposite in sign (van Loon and Meehl, 2008). Meehl et al. (2009) has shown that the two interacting mechanisms, the top-down stratospheric response of ozone fluctuations to short-wave solar forcing and the bottom-up coupled ocean-atmosphere surface response, act together to enhance the climatological off-equatorial tropical precipitation maxima in the Pacific, lower the eastern equatorial Pacific sea surface temperatures during peaks in the 11-year solar cycle and reduce low-latitude clouds to amplify the solar forcing at the surface.

4.3 Acknowledgements

This paper has received equal contribution form the first two authors. We thank the Graduate School GRK 1364, funded by the German Research Foundation (DFG), for giving the opportunity to bring together young scientists from different subjects. We thank also the DAAD for funds to L. Olaka and the DFG for funds to A. Junginger.

4.4 References

Abram, N.J., Gagan, M.K., Cole, J.E., Hantoro, W.S., and Mudelsee, M. Recent intensification of tropical climate variability in the Indian Ocean. *Nature Geoscience* 1, 849-853 (2008).

Ashok, K., Guan, Z., Saji, N.H., and Yamagata, T. Individual and combined influences of the ENS and Indian Ocean Dipole on the Indian summer monsoon. *J. Clim.* 17, 3141-3155 (2004).

Cai, W., Pan, A., Roemich, D., Cowan, T., and Guo, X. Argo profiles a rare occurrence of three consecutive positive Indian Ocean Dipole events, 2006-2008. *Gephys. Res. Lett.* 36, L08701, doi: 10.1029/2008GL037038 (2009).

Camberlin, P. & Philippon, N. The east African March-May rainy season : associated atmospheric dynamics and predictability over the 1968-97 period. *J. Clim.* 15, 1002-1019 (2002).

Camberlin, P., Janicot, S., and Poccard, I. Seasonality and atmospheric dynamics of the teleconnections between African rainfall and tropical sea-surface temperature: Atlantic vs. ENSO. *Int. J. Climatol.* 21, 973-1005 (2001).

Camberlin, P. Rainfall anomalies in the source region of the Nile and their connection with the Indian summer monsoon. *J. Clim.* 10, 1380-1392 (1997).

Camberlin, P. June-September rainfall in North-Eastern Africa and atmospheric signals over the tropics: a zonal perspective. *International Journal of Climatology* 15, 773-783 (1995).

Chan, R.Y., Vuille, M., Hardy, D.R., and Bradley, R.S. Intraseasonal precipitation variability on Kilimanjaro and the East African region and its relationship to large-scale circulation. *Theor. Appl. Climatol.* 93, 149-165 (2008).

Charles, C.D., Cobb, K., Moore, M.D., and Fairbanks, R.G. Monsoon-tropical ocean interaction in a network of coral records spanning the 20th century. *Marine Geology* 201, 207-222 (2003).

Clark, C.O., Webster, P.J., and Cole, J.E. Interdecadal Variability of the Relationship between the Indian Ocean Zonal Mode and East African Coastal Rainfall Anomalies. *Journal of Climate* 16, 548-554 (2003).

Dai, A. Global precipitation and thunderstorm frequencies. Part II: Diurnal variations. *J. Clim.* 14, 1112–1128 (2001).

Diro, G.T., Grimes, D.I.F., and Black, E. Teleconnections between Ethiopian summer rainfall and sea surface temperature: part I – observation and modeling. *Clim. Dyn.,* DOI 10.1007/s00382-010-0837-8 (2010a).

Donders, T.H., Wagner-Cremer, F., and Visscher, H. Integration of proxy data and model scenarios for the mid-Holocene onset of modern ENSO variability. *Quat. Sci. Rev.* 27, 571-579 (2008).

Ferguson, A. J. D. and Harbott, B. J. Geographical, physical and chemical aspects of Lake Turkana. In: *Lake Turkana: A Report on the Findings of the Lake Turkana Project 1972 - 1975* (ed. Hopson, A.J.), Volume 1. London, Overseas Development Administration, 1 – 108 (1982).

Gleisner, H. and Thejll, P. Patterns of tropospheric response to solar variability. *Geophys. Res. Lett*. 30, 1711, doi: 10.1029/2003GL017129 (2003).

Hastenrath, S., Nicklis, A., and Greischar, L. Atmospheric-hydrospheric mechanisms of climate anomalies in the western equatorial Indian Ocean. *J. Geophys. Res.* 98, 20219–20235 (1993).

Haigh, J.D., Blackburn, M. and Day, R. The response tropospheric circulation to perturbations in lower stratospheric temperature. *J. Clim.* 18, 3672–3691 (2005).

Hastenrath, S., Nicklis, A., and Greischar, L. Atmospheric-hydrospheric mechanisms of climate anomalies in the western equatorial Indian Ocean. *J. Geophys. Res.* 98, 20219–20235 (1993).

Indeje M., Semazzi, F. H. M. & Ogallo, L. J. ENSO signals in East African rainfall seasons. International *Journal of Climatology* 20, 19-46 (2000).

Ininda, J., Desalegne, B., and Befekadu, A. The char-

acteristics of rainfall in Ethiopia and its relationship to El Niño–Southern Oscillation. In: *Proceedings of the First Technical Conference on Meteorology Research in Eastern and Southern Africa*, Kenya Meteorology Department, Nairobi, 133–135 (1987).

Izumo, T. The Role of the Western Arabian Sea Upwelling in Indian Monsoon Rainfall Variability. *Journal of Climate* 21, 5603-5623 (2008).

Johnson, T.C. and Malala, J.O. Lake Turkana and Its Link to the Nile. In: *The Nile* (ed. Henri J.). Monographiae Biologicae 89, 287-304 (2009).

*Junginger, A. & Trauth, M.H. Solar Variations and Holocene East African Climate. *subm. to Nature*, (2011).

Kane, R.P. Periodicities, ENSO effects and trends of some South African rainfall series: an update. *S. Afr. J. Sci*. 105, 199-207 (2009).

Kebede, S., Travi, Y., Alemayehu, T., and Marc, V. Water balance of Lake Tana and its sensitivity to fluctuations in rainfall, Blue Nile basin, Ethiopia. *Journal of Hydrology* 316, 233-247 (2006).

Kodera, K., Coughlin, K., and Arakawa, O. Possible modulation of the connection between the Pacific and Indian Ocean variability by the solar cycle. *Geophys. Res. Lett.* 34, L03710, doi:10.1029/2006GL027827 (2007).

Kodera, K. Solar influence on the Indian Ocean Monsoon through dynamical processes. *Geophys. Res. Lett.* 31, L24209, doi:1029/2004GL020928 (2004).

Kodera, K. and Kuroda, Y. Dynamical response to the solar cycle. *J. Geophys. Res.* 107 (D24), 4749, doi:10.1029/2002JD002224 (2002).

Levin, N.E., Zipser, E.J., and Cerling, T.E. Isotopic composition of waters from Ethiopia and Kenya: Insights into moisture sources for eastern Africa. *J. Geophys. Res.* 114, D23306, doi:10.1029/2009JD012166 (2009).

Mason, S.J. and Tyson, P.D. The modulation of sea surface temperature and rainfall associations over southern Africa with solar activity and the quasi-biennial oscillations. *J. Geophys. Res.* 97, 5847–5856 (1992).

Meehl, G.A., Arblaster, J.M., Matthes, K., Sassi, F. and van Loon, H. Amplifying the pacific climate system response to a small 11-year solar cycle forcing, *Science* 325, 1114–1118 (2009).

Meehl, G. A., Arblaster, J. M., and Loschnigg, J. Coupled ocean–atmosphere dynamical processes in the tropical Indian and Pacific Oceans and the TBO. *J. Climate*, 16, 2138–2158 (2003).

Meehl, G. A. and Arblaster, J. M. The tropospheric biennial oscillation and Asian–Australian monsoon rainfall. *J. Climate* 15, 722–744 (2002a).

Meisner, B. and Arkin, P. Spatial and annual variations in the diurnal cycle of large-scale tropical convective cloudiness and precipitation. *Mon. Wea. Rev.* 115, 2009 –2032 (1987).

Meyers, G. A., McIntosh, P. C., Pigot, L., and Pook, M. J. The years of El Nino, La Nina, and interactions with the tropical Indian Ocean. *J. Clim.* 20, 2872– 2880 (2007).

Neff, U. et al. Strong coherence between solar variability and the monsoon in Oman between 9 and 6 kyr ago. *Nature* 411, 290-293 (2001).

Nicholson, S. and Yin, X. Mesoscale Patterns of Rainfall, Cloudiness and Evaporation over the Great Lakes of East Africa. In: *The East African Great Lakes: Limnology, Palaeolimnology and Biodiversity* (eds. Odada, E. and Olago, D.) 12, 93-119 (2004).

Nicholson, S.E. A review of climate dynamics and climate variability in eastern Africa. In: The *Limnology, climatology and paleoclimatology of the East African lakes* (eds. Johnson, T.C. & Odada, E.O.) Gordon & Breach, Amsterdam, 25-56 (1996).

Okoola, R. A diagnostic study of the Eastern African monsoon circulation during the northern hemisphere spring season. *Int. J. Climatol.* 19, 143–168 (1999).

Russel, J.M. and Johnson, T.C. Little Ice Age drought in equatorial Africa: Intertropical Convergence Zone migrations and El Niño-Southern Oscillation variability. *Geology* 35, 21-24 (2007).

Saji, N.H., Xie, S.-P., and Yamagata, T. Tropical Indian Ocean Variability in the IPCC Twentieth-Century Climate Simulations. *J. Climate* 19, 4397-4416 (2006).

Saji, N.H., Goswami, B.N., Vinayachandran, P.N. & Yamagata, T. A dipole mode in the Indian Ocean. *Nature* 401, 360-363 (1999).

Stute, M., Clement, A.C., and Lohmann, G. Global climate models: past, present, and future. *Proceedings of the National Academy of Sciences* 98 (19), 10,529–10,530 (2001).

Suzuki, T. Seasonal variation of the ITCZ and its characteristics over central Africa. Theor. Appl. Climatol. 103, 39-60 (2011).

van Loon, H., and Meehl, G.A. The response in the Pacific to the sun's decadal peaks and contrasts to cold events in the Southern Oscillation. J. Atmos. Sol. Terr. Phys. 70, 1046-1055 (2008).

van Loon, H., Meehl, G.A., and Arblaster, J.M. A decadal solar effect in the tropics in July–August. *J. Atmos. Sol. Terr. Phys*. 66, 1767–1778 (2004).

van Loon, H. and Labitzke, K. The 10–12 year atmospheric oscillation. *Meteorol. Z*. 3, 259–266 (1994).

Vareshi, E. The ecology of Lake Nakuru (Kenya). III Abiotic factors and primary production. *Ibid*. 55, 81 101 (1982).

Verschuren, D., Laird, K.R., and Cumming, B.F. Rainfall and drought in equatorial east Africa during the past 1,100 years. *Nature* 403, 410-414 (2000).

Wang, Y.J et al. The Holocene Asian Monsoon: Links to Solar Changes and North Atlantic Climate. *Science* 308, 854-857 (2005).

Webster, P. J., Moore, A. M., Loschnigg, J. P., and Leben, R. R. Coupled ocean–atmosphere dynamics in the Indian Ocean during 1997–98. *Nature* 401, 356–360 (1999).

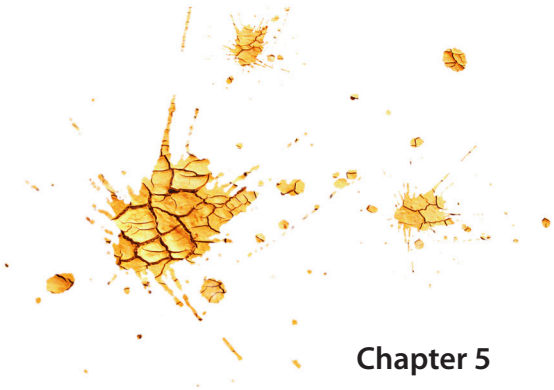

Chapter 5

Summary, Conclusions, Outlook

Annett Junginger

5.1 Summary and Conclusions

In order to understand pronounced humidity changes in the East African Rift System (EARS) leading to high, but fluctuating lakes during the African Humid Period (AHP; 15-5 ka, 1 ka = 1000 calibrated years BP) and to contribute new findings to current debates about Holocene climate variability in East Africa, this doctoral research project was performed on three different spatial and temporal scales for the past 15,000 years along the EARS using a multidisciplinary approach that integrates sedimentological studies, hydrologic modelling, bio- and atmospheric analysis.

Late Pleistocene/Early Holocene | The results of the main study is a precisely dated, reservoir corrected, indirect palaeo-precipitation from the Suguta Valley, northern Kenya, that largely improved our knowledge about the last AHP. For the indirect reconstruction of the palaeo-precipitation history of equatorial East Africa, I developed a model to predict the magnitude of lake level changes from a certain lake sediment compositions. For the lake level reconstructions, I used a combination of sedimentological investigations on various sampled lake sequences, a previously published set of shoreline deposits and a water-balance model, which allowed me to decipher abrupt vs. gradual precipitation changes. The development of such a multiproxy study will be a useful method that can be applied to other lake level reconstructions or predictions, especially in the amplifier lake basins from East Africa.

This record, spanning the time interval from 14.8 to 5 ka, explains the synchronous onset of large lakes in East Africa with the longitudinal shift of the CAB over the East African and Ethiopian Plateaus as the consequence of a precessional-forced enhanced summer insolation over the northern hemisphere and associated larger atmospheric pressure gradients between India and East Africa. Enhanced insolation lead to the deepening of the Tibetan low causing strong enough to pull Congo Air Boundary (CAB) northeastwards. Only 26% of addtional rainfall was necessary to fill the 300 m deep and 2,200 km^2 large palaeo-lake Suguta. Water level changes of up to 100 m within less than 100 years in the reconstructed lake-level record are the result of abrupt precipitation changes as suggested by the hydro-balance model. The mechanism behind has caused changes in precipitation to at least modern values or even lower. I attribute these abrupt changes to a combination of the weakening of the ISM system due to centennial-scales solar irradiation decreases accompanied with a higher Tibetan low and therefore weakend pressure gradient preventing the CAB from being pulled over the high elevated East African Plateau and a general decrease of the atmospheric moisture availability. The nearly perfectly correlation of the Suguta record with short-time decreases of solar irradiation on centennial times scales and the occurrence of drought spells in other monsoon records, and freshwater pulses to the North Atlantic explain that the entire Earth's climate is sensitive to small changes in solar output on sub-orbital time scales during the early to mid-Holocene. Instead, the termination of the AHP in East Africa, which is highly debated whether being gradual or abrupt, is explained by this study to have occurred nonlinear despite a gradual weakening of the ISM in the course of the earth's precession cycle due to a change towards an equatorial insolation maximum ca. 6.5 ka ago, which prolonged a strong West-African monsoon (WAM) and hence high CAB intensity. Whereas the weakening of the ISM system resulted in the final prevention of CAB related rainfalls to the eastern East African Plateau that was necessary to sustain large lakes. Prolonged strong WAM and hence CAB intensity continued high lake levels on the Ethiopian Plateau over more than 1000 years, because the NNE-SSW trending CAB still might have reached parts of the Ethiopian Plateau additionally to enhanced boreal ITCZ precipitation. The record of Lake Turkana supports this interpretation since the lake was highly influenced from both, the Ethiopian plateau climate due to the major river input from the Omo River, but also via overflowing lakes from the East African Plateau during the AHP. However, Lake Turkana stopped overflowing into the Nile River around that time, when Lake Suguta highstand terminated ca. 6.8 ka ago.

Despite the new insights into the character of the termination of the AHP from the Suguta Valley lake-level record, our results clearly indicate the need for high-resolution, well-dated records for this interesting episode of climate change in East Africa. At present, the available data and their interpretation of humid-arid transitions of being abrupt or gradual

in the tropics should be handled with care, since dating uncertainties and the use of different sensitive proxies play beside the size of the area they integrate, the geographical, geological and climatologically situation a major role. These influencing factors should be included into consideration while concluding about the relative importance of drivers of climate change in the tropics.

The conclusions of this study largely help to resolve current debates, such as about the gradual versus abrupt onset and termination of the AHP and the role of the poorly understood CAB in producing large but highly fluctuating lakes in the eastern branch of the EARS. The study identifies new linkages between different sectors within the African-Asian monsoon system and their exact influence on equatorial East Africa's climate, in particular relative to each other and detects important mechanisms for abrupt drought episodes on sub-Milankovitch time scales to an area that is believed to have been the 'cradle of human kind'. In order to contribute to current debates of the AHP's influence on human expansions, technological innovations and food production, our findings about the dry-wet-dry transition nicely explains the transition from fishing to herding in nearby people in the course of changing availability of water and aquatic food associated with rapid fluctuating large lakes.

The past 200 years | The collaborative study about environmental changes in the Naivasha basin on lake sediments covering the last ~200 years, has shown that Lake Naivasha's water chemistry and biology have been influenced by natural climatic variations and anthropogenic activities. Lake Naivasha responded to natural rainfall variations and associated lake level fluctuations before 1947 clearly indicated by diatom assemblages. From 1760 to 1840 AD, the enduring Laparanat drought has caused slightly saline conditions in the lake and favoured the abundance of saline-tolerant diatoms such as *Navicula elkab* and *Cymbella muelleri*. In the generally wetter period from 1883 to 1894 AD, the lake received more freshwater from the catchment and groundwater reservoirs, which helped maintain the freshwater nature of the lake. These freshwater conditions favoured diatoms such as *Synedra* sp. and *Aulacoseira* sp. that prefer waters with low conductivity. After 1900 AD, shorter wet and dry periods alternated and the lake level fluctuated in response to these variations. This is documented by instrumental lake level data since 1932 and by both proxy and instrumental rainfall data since 1850. From 1947 on to 2007 AD, the accumulation rates of the sediment, nitrogen and organic carbon increased pronounced that we concluded as the result of higher rates of soil erosion from cultivated areas within the lake catchment, rather than the consequence of intensive rainfall. These higher erosion rates caused greater inputs of nutrients and pollutants to the lake, which in turn favoured the growth of eutrophic diatoms such as *Aulacoseira* sp. and led to the displacement of pollution-sensitive diatom species such as *Gomphonema gracile*.

This study demonstrated that Lake Naivasha is highly sensitive to changes in catchment activities. Since the middle of the 20th century, intense anthropogenic activity around Lake Naivasha has led to cultural eutrophication, which has overprinted the influence of natural climate variation to the lake. Beside the problems of masking valuable climate indicators, the additionally input of soil and nutrients, fertilizers, pesticides, and other pollutants resulting from intensive land use, has far-reaching implications for the future of Lake Naivasha and the people and numerous other species living in and around the lake. In order to contribute to the current debates about anthropogenic induced climate change over the past 200 years, it became during the study on sediments from Lake Naivasha ones again clear, that there is a compelling need of lake records from remote areas not affected by human activities to receive a pristine signal of climate variability of the historical past.

Recent climate variability: 1996 -2010 | Remotely sensed data for the time period between 1996-2010 are the base of this collaborative study to better understand and evaluate spatial heterogeneities in proxy-records used for paleo-climate reconstruction in the EARS. Understanding regional high frequency variability will allow us to decipher climate-proxy generating processes and improve forecasting of hydrological resources. This study uses basin-averaged precipitation from satellite rainfall estimates data from FEWSNET available at dekadal (10 days) scale and 8 km resolution for the period between 1996-2010. Our investigation focused on the dynamics of intraseasonal rainfall distribution within catchments of eleven lake basins in the EARS, name-

ly Ziway, Awassa, Abaya, Turkana, Suguta, Baringo, Nakuru, Naivasha, Natron, Manyara and Tana. The seasons are grouped as MAM, JAS, ON and DJF. Preliminary conclusions of this on-going study are that rainfall in adjacent basins can exhibit low or high amplitudes in intraseasonal variability, can show a biennial to triennial precipitation pattern and often even showing opposite trends, such as Nakuru and Naivasha, Natron and Manyara, or Tana and the central Ethiopian Plateau lakes. The variability among the watersheds is driven by the complex interaction of topography, in particular the shape, length and elevation of the catchment and its relative location to the EARS and predominant influence of one of the main convergence zones ITCZ or CAB, whose location and intensities are dependent on low developments along the west coast of India, sea surface temperature variations in the Atlantic, Pacific or Indian Ocean, Quasibiennial Oscillation phases and the 11-year solar cycle. Among all seasons we observed that JAS is the season of highest complex rainfall variability, especially for the East African Plateau basins most likely due to the irregular penetration of the CAB.

A first appliance of these findings can be taken to the main study of this doctoral thesis about the Suguta Valley and the termination of mid-Holocene East African lake levels. This study using recent remotely sensed data has shown, that JAS is the most complex season suggesting that any changes of it can bring more rainfall to equatorial East Africa or even less. The good correlation of Suguta and Nakuru in JAS confirms the comparison of those in the early to mid-Holocene study to be acceptable. This study also explained that prolonged high lake levels in the mid-Holocene Ethiopian Plateau basins compared to East African Plateau lake levels could be related to enhanced boreal fall rains, which we showed also to affect those basins peripherally. In the mid-Holocene study, I suggested that an equatorial insolation maximum in boreal fall might have prolonged the AHP in northern East Africa. Since boreal fall rainfall always affects the East African Plateau basins we did not assume those to be able to sustain high lake levels. I hypothesize, that an additional rainy season such as JAS rainfalls might have been responsible for developing large lakes with maximum lake levels in equatorial East Africa. Thus, the absence of JAS rainfalls provided by the CAB to the East African Plateau basins as the result of a stronger ISM caused an earlier termination of the AHP than over Ethiopian Plateau.

5.2 Outlook

This doctoral thesis has identified the topographic effects of the lake catchments in East Africa, which is key to explain regional moisture redistribution and the subsequent East-West and North-South precipitation gradients. I hypothesized that the location and intensity of the two convergence zones CAB and ITCZ in East Africa determine the degree and duration of drier or wetter periods on different time scales. However, the hypotheses regarding the pattern's underlying causes are speculative and will only be well designated by transects of stable isotope analysis such as Strontium and Oxygen. The next step would therefore be to test these hypotheses with isotopic studies also on different time scales, such as the early to mid-Holocene's AHP, the past 1000 years, as this shows contrasting drier and wetter conditions in East African proxy-records, and present day measurements.
For the AHP period I would suggest to collect material from paleo-lake deposits useful for isotopic studies, such as snail shells, which are widely distributed in early to mid-Holocene lake sediments, or plant leaf waxes extracted from those sequences. Finding surface sediments from the past 1000 years might be rather difficult as lakes were not as high as in the AHP and also have not lasted long enough to allow the accumulation and consolidation of large sediment bodies, especially in inhabited areas. Uninhabited areas, as for example the Suguta Valley, or the permanent freshwater lakes Awassa, Tana, Naivasha, and Turkana hardly drying out might provide necessary sediments. As we presented in chapter 4 a good overview of the seasonal moisture sources and their distribution in each lake basin in East Africa, the collection and study of present day water samples from river discharges and direct precipitation from selected areas in each basin and their isotopic impact to the terminal lake would establish the base for this isotopic study.

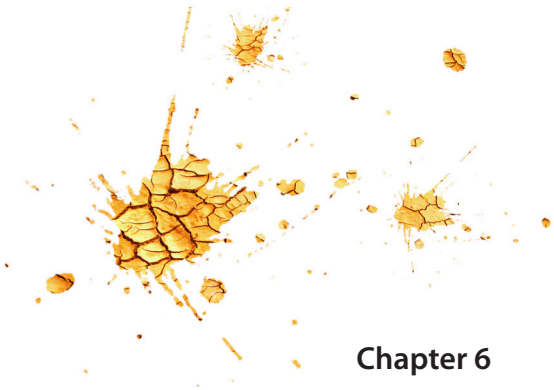

Chapter 6

Acknowledgements

Chapter 6 - Acknowledgements

I would like to take this chapter to express my thanks to all of the people that contributed to the successful completion of my PhD at the University of Potsdam.

First of all, I would like to thank my long-standing supervisor Prof. Martin Trauth for initiating this fantastic research project within the Graduate School GRK 1364 and supporting me since my diploma thesis. His broad knowledge and special way to look at data from an interdisciplinary point of view was most inspiring. I really appreciate his efficient work on numerous manuscripts, significantly improving whatever I wrote and always within an incredible short time. This efficiency was extremely helpful during the last months while my thesis was developing.
I'd like to express my thanks to Prof. Manfred Strecker from Potsdam University, Prof. Mark Maslin and Katy Wilson from University College London, Prof. Alan Deino from Berkeley, and Sybille Roller from TU Darmstadt for inspiring evening discussions on the campfire during the three expeditions to the Suguta Valley. Deep thankfulness goes in this context to Sybille and Katy, whom I've been working with successfully in the hot Suguta Valley in 2010, which was most efficient and a great pleasure.

I also would like to thank Antje Musiol, responsible for CNH measurements that were the base of the whole thesis. In this context, I also would like to thank Bernard Dieckmann, Ute Bastian, and Stephan Opitz from the Alfred Wegener Institute in Potsdam, to introduce me to the preparation techniques in grain size and clay mineral separation. At the GeoForschungsZentrum Potsdam I thank Norbert Nowaczyk for the introduction and measurement of magnetic susceptibility. In particular, I really thank Betti Richter, who was a great help during sample preparation and the most reliable student assistant I've ever met.

I thank kindly the German Research Foundation (DFG) for funding this project over the last four years and giving me the opportunity to finish my thesis within the set timeframe. Additionally, being part of a graduate school has the advantage of easily bringing PhD students from different research fields together, which has set up the base for two collaborative studies presented in this thesis. My special thanks go here to Kathleen Stoof-Leichsenring and Lydia A. Olaka, whom I really appreciated the work together, as we all learned a lot from each other's fields. In this respect I want to thank all PhD students of the GRK1364 for fruitful discussions, unprecedented team spirit, funny evenings in Potsdam's "Waschbar", and an unforgettable time during our two excursions to Kenya and the Indian Himalaya. Responsible for a large fraction of my happiness and balance are my close friends and colleges Silvi, Stephan, Alex, Jule and Andreas.

Finally, I would like to express my deep gratitude for the encouragement and infinite support in so many ways to my family. And last but not least my love and appreciation goes to Mik for his understanding and patience, and also for the fruitful discussions between a graphic designer and a scientist about graphic illustration. Thank you for layouting my thesis!

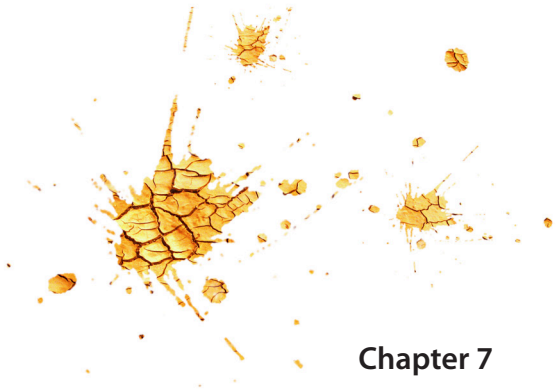

Chapter 7

Appendix

Appendix 01 - Climatology in The Suguta catchment area

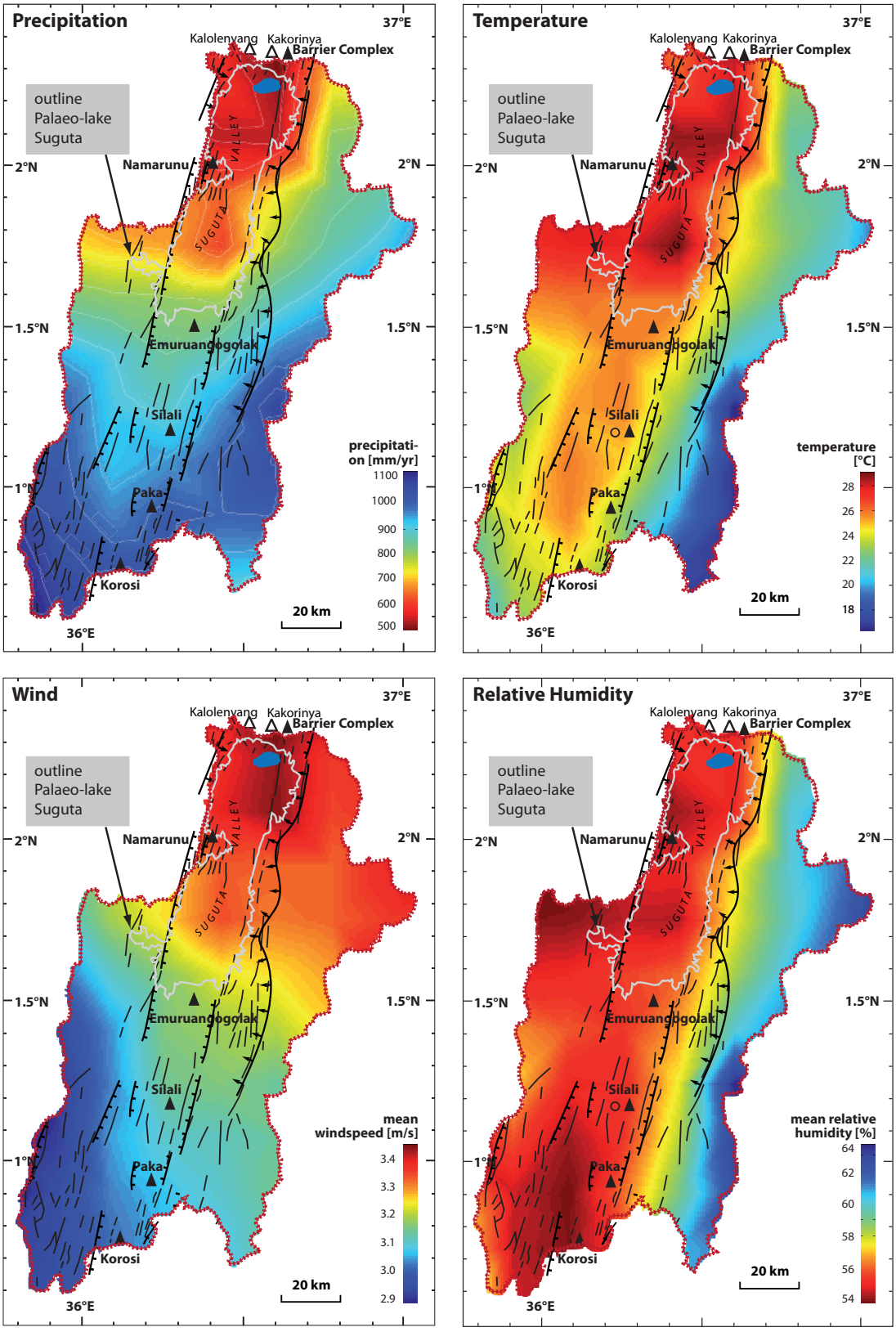

Appendix 1 Interpolated climate parameters for Suguta Valley catchment from gridded values provided by New et al. (2002).

Appendix 02 – Data for BG08

Sample location [m above base]	Age model ages [cal. BP]	Snails	Grain size	Magn. Susz.	TN [wt%]	TC [wt%]	TIC [wt%]	TOC [wt%]	TOC/TN	TC/TN
33.25	8546.00		5	0.00406	0.01	0.04	-0.10	0.14	11.24	3.52
33.00	8550.00		1	0.00190	0.66	0.87				1.32
32.75	8554.00		1	0.00184	0.88	0.64	-0.01	0.65	0.73	0.73
32.50	8558.00		2	0.00159	0.81	0.83				1.02
32.25	8562.00		2	0.00184	1.47	0.94				0.64
32.00	8566.00		2	0.00164	0.69	1.06				1.53
31.75	8570.00	x	2	0.00194	0.23	0.91	0.16	0.75	3.28	3.97
31.50	8574.00		2	0.00155	0.49	2.97	0.63	2.34	4.73	6.01
31.25	8578.00	x	1	0.00135	0.26	2.96	0.54	2.42	9.29	11.36
31.00	8582.00		1	0.00025	0.21	1.45	0.04	1.41	6.76	6.96
30.75	8586.00		5	0.00077	0.23	0.06				0.27
30.50	8590.00		4	0.00179	0.23	0.06				0.27
30.25	8594.00		4	0.00179	0.23	0.06				0.27
30.00	8598.00		4	0.00179	0.23	0.06				0.27
29.75	8602.00		5	0.00180	0.23	0.06	-0.10	0.16	0.68	0.27
29.50	8606.00	x	1	0.00045	2.58	2.62	0.34	2.28	0.89	1.02
29.25	8610.00		5	0.00254	0.66	0.12	-0.11	0.23	0.35	0.19
29.00	8614.00	x	3	0.00178	1.26	0.41				0.33
28.75	8618.00		3	0.00091	2.36	3.38	0.63	2.74	1.16	1.43
28.50	8622.00		2	0.00152	1.07	1.42				1.32
28.25	8626.00	x	2	0.00065	2.46	2.22	0.32	1.90	0.77	0.90
28.00	8630.00		4	0.00204	0.51	0.33				0.65
27.75	8634.00	x	5	0.00198	0.28	0.31				1.11
27.50	8638.00		2	0.00068	1.55	2.44	0.39	2.05	1.33	1.58
27.25	8642.00	x	2	0.00149	0.14	1.73	0.25	1.48	10.58	12.34
27.00	8646.00		2	0.00135	1.03	2.24	0.32	1.92	1.86	2.17
26.75	8650.00	x	3	0.00166	1.43	1.43	0.12	1.31	0.91	1.00
26.50	8654.00		1	0.00171	0.85	0.56				0.66
26.25	8658.00		1	0.00131	0.76	1.30	0.09	1.21	1.60	1.71
26.00	8662.00	x	1	0.00077	2.53	2.01	0.24	1.77	0.70	0.80
25.75	8666.00		1	0.00083	1.94	3.05	0.46	2.58	1.33	1.57
25.50	8670.00	x	1	0.00058	2.02	1.96				0.97
25.25	8674.00		2	0.00038	2.60	2.53	0.40	2.13	0.82	0.98
25.00	8678.00		2	0.00091	2.06	2.22				1.08
24.75	8682.00		2	0.00145	1.20	1.51				1.26
24.50	8686.00		2	0.00102	1.53	2.09	0.33	1.76	1.15	1.37
24.25	8690.00	x	3	0.00137	1.14	0.76				0.66
24.00	8701.11	x	5	0.00080	2.38	1.44				0.61
23.75	8712.22		1	0.00076	2.06	1.36	0.12	1.24	0.60	0.66
23.50	8723.33		2	0.00083	1.82	0.96				0.52
23.25	8734.44		2	0.00125	1.29	1.59	0.27	1.32	1.02	1.23
23.00	8745.56		1	0.00109	2.19	1.43	0.12	1.31	0.60	0.66
22.75	8756.67		1	0.00054	2.37	1.74	0.17	1.56	0.66	0.73
22.50	8767.78		2	0.00066	3.06	1.81				0.59
22.25	8778.89		1	0.00052	2.61	1.69	0.07	1.62	0.62	0.65
22.00	8790.00		1	0.00061	2.53	2.31	0.33	1.97	0.78	0.91
21.75	8801.11		1	0.00041	2.99	1.34	0.17	1.17	0.39	0.45
21.50	8812.22		3	0.00168	0.78	1.14	0.26	0.88	1.13	1.47
21.25	8823.33		4	0.00224	0.32	0.23	-0.11	0.34	1.05	0.72
21.00	8834.44		1	0.00123	1.30	1.41	0.12	1.29	0.99	1.08
20.75	8845.56		2	0.00183	0.21	1.93	0.30	1.62	7.79	9.26
20.50	8856.67		1	0.00056	2.44	3.53	0.60	2.94	1.20	1.45
20.25	8867.78	x	4	0.00202	1.24	0.83	0.14	0.69	0.56	0.67
20.00	8878.89	x	1	0.00074	2.33	1.97				0.85
19.75	8890.00		1	0.00035	3.15	3.78	0.62	3.16	1.01	1.20
19.50	8901.11		2	0.00131	1.31	1.62	0.26	1.36	1.04	1.24
19.25	8912.22		1	0.00063	1.79	2.98	0.50	2.47	1.38	1.66
19.00	8923.33		1	0.00051	2.27	2.10				0.92
18.75	8934.44		1	0.00066	1.94	1.44	0.19	1.25	0.64	0.74
18.50	8945.56		1	0.00086	2.12	1.59				0.75
18.25	8956.67		2	0.00152	1.30	1.49				1.14
18.00	8967.78		1	0.00072	1.73	1.99	0.22	1.77	1.02	1.15
17.75	8978.89		2	0.00046	2.24	1.93	0.23	1.70	0.76	0.86
17.50	8990.00	x	4	0.00180	0.49	0.55				1.13
17.25	9003.68		2	0.00068	1.04	2.09	0.37	1.71	1.65	2.01
17.00	9017.37		2	0.00182	1.24	0.70	0.11	0.58	0.47	0.56
16.75	9031.05		1	0.00057	0.75	1.60	0.36	1.24	1.65	2.13
16.50	9044.74		1	0.00080	2.18	2.34	0.53	1.81	0.83	1.07
16.25	9058.42		2	0.00121	1.76	1.49	0.14	1.34	0.76	0.84
16.00	9072.11		2	0.00182	0.90	1.26				1.40
15.75	9085.79	x	3	0.00156	1.49	1.18	0.26	0.93	0.62	0.80
15.50	9099.47		2	0.00054	2.35	2.22	0.34	1.88	0.80	0.95

Sample location [m above base]	Age model ages [cal. BP]	Snails	Grain size	Magn. Susz.	TN [wt%]	TC [wt%]	TIC [wt%]	TOC [wt%]	TOC/TN	TC/TN
15.25	9113.16		1	0.00108	1.63	1.08				0.66
15.00	9126.84		2	0.00069	2.57	1.06				0.41
14.75	9140.53		2	0.00103	2.56	0.82				0.32
14.50	9154.21		1	0.00089	2.96	1.14	0.13	1.01	0.34	0.38
14.25	9167.89		1	0.00145	2.02	1.04				0.51
14.00	9181.58		1	0.00112	2.27	1.16				0.51
13.75	9195.26		1	0.00100	2.37	1.07				0.45
13.50	9208.95		1	0.00085	2.78	1.30	0.22	1.07	0.39	0.47
13.25	9222.63		1	0.00110	2.24	1.35	0.17	1.18	0.53	0.60
13.00	9236.32		1	0.00102	2.14	1.33	0.23	1.10	0.51	0.62
12.75	9250.00		1	0.00147	1.32	1.38	0.16	1.22	0.92	1.04
12.50	9286.61		1	0.00117	1.97	1.29	0.31	0.98	0.49	0.65
12.25	9323.21		1	0.00137	2.04	1.27				0.62
12.00	9359.82		4	0.00230	1.01	0.38				0.37
11.75	9396.43		2	0.00140	2.63	1.13	0.75	0.38	0.14	0.43
11.50	9433.04		2	0.00138	1.61	2.03	0.43	1.60	0.99	1.26
11.25	9469.64		2	0.00165	1.81	1.50	0.31	1.19	0.65	0.83
11.00	9506.25		2	0.00119	2.63	0.63				0.24
10.75	9542.86		2	0.00185	1.94	0.85				0.44
10.50	9579.46		3	0.00331	0.47	0.40	0.14	0.25	0.54	0.84
10.25	9616.07		2	0.00169	0.33	1.87	0.45	1.42	4.34	5.73
10.00	9652.68		2	0.00215	0.84	1.13	0.28	0.85	1.02	1.35
9.75	9689.29		1	0.00142	2.03	1.23	0.17	1.06	0.52	0.61
9.50	9725.89		1	0.00120	2.10	1.29				0.61
9.25	9762.50		1	0.00101	2.67	0.94				0.35
9.00	9799.11		1	0.00119	2.38	0.96				0.40
8.75	9835.71		1	0.00122	2.52	0.77				0.31
8.55	9865.00		2	0.00123	2.60	0.81				0.31
8.50	9872.32		1	0.00093	2.71	0.73				0.27
8.25	9908.93		1	0.00047	2.91	0.57				0.20
8.00	9945.54		1	0.00102	2.61	1.10	0.14	0.96	0.37	0.42
7.75	9982.14		1	0.00180	2.23	1.01				0.45
7.50	10018.75		1	0.00174	2.00	1.35				0.68
7.25	10055.36		1	0.00111	2.83	1.16	0.20	0.97	0.34	0.41
7.00	10091.96		1	0.00095	2.23	1.08				0.49
6.80	10121.25		3	0.00233	0.90	0.64				0.71
6.75	10128.57		2	0.00189	1.40	1.09	0.19	0.90	0.64	0.78
6.50	10165.18	x	1	0.00181	1.74	1.04				0.60
6.25	10201.79		2	0.00168	2.57	1.22				0.48
6.05	10231.07		2	0.00197	2.02	0.83				0.41
6.00	10238.39		1	0.00149	2.11	0.84				0.40
5.75	10275.00		2	0.00248	1.38	0.78				0.56
5.50	10311.61		1	0.00139	2.36	1.46	0.26	1.20	0.51	0.62
5.25	10348.21		1	0.00131	2.17	0.81				0.37
5.00	10384.82		2	0.00211	0.54	0.95	0.18	0.77	1.43	1.76
4.75	10421.43		2	0.00231	1.39	1.04				0.75
4.50	10458.04	x	2	0.00192	1.47	0.92	0.17	0.75	0.51	0.63
4.25	10494.64		3	0.00303	1.13	0.25				0.22
4.00	10531.25		1	0.00151	1.60	0.87				0.55
3.75	10567.86		1	0.00230	1.44	0.84				0.58
3.50	10604.46		1	0.00115	2.22	0.82				0.37
3.30	10633.75		1	0.00213	2.44	0.73				0.30
3.25	10641.07		1	0.00181	2.04	0.89				0.44
3.00	10677.68		1	0.00145	2.46	0.88	0.17	0.71	0.29	0.36
2.75	10714.29		1	0.00148	2.19	0.97				0.44
2.50	10750.89		3	0.00235	1.29	0.76				0.59
2.25	10787.50		1	0.00130	1.97	0.73				0.37
2.00	10824.11		1	0.00122	2.67	0.69				0.26
1.75	10860.71		1	0.00139	2.18	0.80				0.37
1.50	10897.32		1	0.00108	2.96	1.07				0.36
1.25	10933.93		1	0.00140	1.84	0.85	0.20	0.65	0.35	0.46
1.00	10970.54		1	0.00131	1.64	0.64				0.39
0.80	10999.82		1	0.00120	1.69	0.58				0.34
0.75	11007.14		1	0.00121	1.56	0.27				0.17
0.50	11043.75		1	0.00170	1.39	0.53				0.38
0.25	11080.36		3	0.00215	1.31	0.65	0.08	0.57	0.43	0.50
0.00	11116.96		3	0.00177	0.82	1.50	0.71	0.79	0.96	1.83
-0.25	11153.57		1	0.00125	2.04	1.02	0.28	0.75	0.37	0.50
-0.50	11190.18		1	0.00110	2.06	1.39				0.67
-0.75	11226.79		1	0.00187	2.33	1.29				0.55
-1.00	11263.39		3	0.00197	1.52	1.14	0.42	0.72	0.47	0.75
-1.25	11300.00		1	0.00154	1.81	1.55	0.78	0.77	0.43	0.86

Appendix 03 – Data for EL08

Sample location [m above base]	Age model ages [cal. BP]	Snails	Grain size	Magn. Susz.	TN [wt%]	TC [wt%]	TIC [wt%]	TOC [wt%]	TOC/TN	TC/TN
24	8900		2	4.09E-03	0.69	0.87	0.23	0.64	0.93	1.27
23.5	8918.33		2	4.32E-03	1.38	0.61	-0.02	0.64	0.46	0.45
23	8936.67		2	5.24E-03	0.96	0.65	0.05	0.59	0.62	0.67
22.5	8955.00		2	4.76E-03	0.62	0.41	0.03	0.38	0.61	0.66
22	8973.33		4	7.01E-03	0.07	0.62	0.16	0.45	6.11	8.33
21.5	8991.67		3	6.17E-03	0.21	0.66	0.12	0.53	2.53	3.10
21	9010.00		2	4.50E-03	0.81	0.88	0.12	0.76	0.93	1.09
20.5	9028.33		3	6.08E-03	0.91	1.00	0.09	0.92	1.00	1.10
20	9046.67		2	4.11E-03	1.31	0.70	0.01	0.68	0.52	0.53
19.5	9065.00		2							
19	9083.33		3	5.45E-03	1.05	0.60	0.03	0.57	0.54	0.57
18.5	9101.67		3	4.68E-03	1.06	0.66	-0.06	0.72	0.68	0.63
18	9120.00		2	2.82E-03	2.25	0.90	0.17	0.73	0.32	0.40
17.5	9145.71		2	3.65E-03	2.91	1.18	0.26	0.92	0.32	0.41
17	9171.43		2	3.60E-03	2.01	1.36	0.44	0.92	0.46	0.68
16.5	9197.14		2	4.71E-03	1.87	1.12	0.30	0.83	0.44	0.60
16	9222.86		2	3.48E-03	2.33	0.91	0.11	0.80	0.34	0.39
15.5	9248.57	x	2	4.18E-03	0.91	1.04	0.20	0.84	0.93	1.15
15	9274.29		4	5.32E-03	1.72	1.04	0.21	0.83	0.48	0.61
14.5	9300.00	x	4	5.06E-03	1.18	0.82	0.08	0.74	0.63	0.69
14	9347.73		2	4.32E-03	1.69	0.99	0.22	0.77	0.45	0.58
13.5	9395.45		2	4.10E-03	1.83	1.37	0.32	1.05	0.57	0.75
13	9443.18	x	2	4.04E-03	2.04	1.05	0.22	0.83	0.41	0.51
12.5	9490.91	x	5	5.85E-03	0.83	0.42	0.02	0.40	0.48	0.50
12	9548.04		1	2.98E-03	0.98	2.35	0.50	1.85	1.88	2.39
11.5	9611.43		1	3.51E-03	1.04	1.17	0.10	1.07	1.03	1.13
11	9674.82		2	4.25E-03	0.36	1.02	0.10	0.92	2.60	2.87
10.5	9738.21		1	2.75E-03	0.49	2.85	0.51	2.34	4.80	5.85
10	9801.61		1	3.04E-03	0.56	2.54	0.50	2.04	3.63	4.52
9.5	9865.00		3	4.63E-03	0.60	1.20	0.10	1.10	1.85	2.01
9	9928.39		2	4.36E-03	1.41	1.18	0.26	0.92	0.66	0.84
8.5	9991.79		2	4.38E-03	0.55	0.86	0.23	0.63	1.15	1.57
8	10055.18	x	2	3.80E-03	0.20	1.16	0.10	1.07	5.35	5.83
7.5	10118.57		3	4.95E-03	1.25	0.76	0.02	0.74	0.59	0.61
7.25	10150.27	x	3							
7	10181.96		2	3.91E-03	0.13	1.94	0.67	1.27	9.64	14.70
6.7	10220.00	x	3							
6.5	10259.58		0.5	8.38E-04	0.11	0.68	0.07	0.61	5.73	6.45
6	10358.54	x	3	3.81E-03	0.61	0.47	-0.04	0.51	0.85	0.78
5.5	10457.50	x	3	4.04E-03	0.31	1.85	0.50	1.35	4.30	5.89
5	10556.46		2	3.17E-03	1.60	1.66	0.68	0.98	0.61	1.04
4.75	10605.94		2							
4.5	10655.42	x	2	2.52E-03	1.69	1.54	0.39	1.15	0.68	0.91
4.25	10704.90	x	2							
4	10754.38		2	4.57E-03	0.57	1.78	0.88	0.91	1.60	3.14
3.5	10853.33		2	3.67E-03	0.90	1.76	0.60	1.16	1.30	1.96
3	10952.29		2	4.24E-03	0.16	1.53	0.60	0.93	5.70	9.35
2.5	11051.25		2	4.88E-03	0.20	1.77	0.46	1.30	6.59	8.91
2	11150.21		2	4.05E-03	0.18	0.76	0.26	0.50	2.77	4.24
1.5	11249.17		3	6.01E-03	0.46	1.00	0.39	0.61	1.32	2.16
1	11348.13		4	6.46E-03	0.84	1.17	0.24	0.93	1.11	1.40
0.6	11427.29		5	7.66E-03	0.19	1.33	0.47	0.86	4.45	6.91
0.5	11447.08		5							
0.4	11466.88		5.5	7.66E-03						
0.1	11526.25		6	1.42E-02						
0	11546.04		7							

Appendix 04 – Data for LN08

Sample location [m above base]	Age model ages [cal. BP]	Snails	Grain size	Magn. Susz.	TN [wt%]	TC [wt%]	TIC [wt%]	TOC [wt%]	TOC/TN	TC/TN
39.95			5	5.38E-03	0.01	0.47	0.35	0.12	20.12	80.18
33.45	10698.20		5	3.31E-03	0.02	0.81	0.67	0.14	7.07	41.09
33.2	10700.00		3	4.98E-03	0.03	0.10				3.25
32.95	10701.80		3	4.65E-03	0.03	0.50				14.68
32.7	10703.60		3	5.26E-03	0.03	0.53	0.34	0.19	5.49	15.39
32.45	10705.40		2	3.38E-03	0.05	0.64	0.33	0.30	5.59	11.79
32.2	10707.20		2	4.02E-03	0.06	0.49				8.38
31.95	10709.00		3	5.78E-03	0.04	0.29				7.85
31.7	10710.80		2	4.67E-03	0.06	0.56	0.18	0.38	6.19	9.13
31.5	10712.24		4	5.79E-03	0.12	0.22				1.90
31.45	10712.60		2	5.15E-03	0.22	0.29				1.31
31.2	10714.40		2	5.48E-03	0.17	0.32	0.01	0.30	1.79	1.87
30.95	10716.20		2	4.58E-03	0.36	0.30				0.83
30.7	10718.00		2	4.18E-03	0.51	0.27				0.53
30.45	10719.80		2	4.28E-03	0.28	0.27				0.96
30.2	10721.60		2	4.75E-03	0.31	0.26				0.85
29.95	10723.40		2	3.87E-03	0.76	0.41				0.54
29.7	10725.20		2	4.38E-03	0.51	0.31				0.60
29.45	10727.00		2	4.55E-03	0.89	0.30				0.33
29.2	10728.80		2	4.14E-03	1.28	0.62				0.49
28.95	10730.60		2	4.03E-03	0.91	0.37				0.40
28.7	10732.40		2	3.54E-03	1.11	0.43				0.39
28.45	10734.20		2	3.78E-03	1.33	0.38				0.28
28.2	10736.00		2	2.98E-03	2.00	0.45				0.23
27.95	10737.80		2	4.48E-03	1.68	0.41				0.24
27.7	10739.60		2	3.61E-03	1.76	0.58	0.05	0.53	0.30	0.33
27.45	10741.40		2	4.67E-03	0.20	0.66				3.22
27.2	10743.20		2	5.44E-03	0.20	0.72	0.02	0.70	3.54	3.62
26.95	10745.00		2	4.88E-03	0.73	1.28				1.75
26.7	10747.50		2	5.42E-03	0.81	0.72	0.14	0.58	0.72	0.90
26.45	10750.00		2	4.91E-03	3.13	0.47				0.15
26.25	10779.71		3	5.44E-03	2.12	0.52				0.25
26.2	10787.14		5	5.35E-03	0.12	0.25	0.09	0.16	1.28	2.05
25.2	10935.71		4	6.08E-03	0.03	0.22	0.10	0.12	4.08	7.34
24.7	11010.00	x	4							
24.2	11016.15		5	5.52E-03	0.06	0.56	0.06	0.50	7.74	8.73
23.2	11028.46		5	5.97E-03	0.04	0.21				4.82
22.95	11031.54		4	5.58E-03	0.56	0.24	0.12	0.12	0.21	0.42
22.7	11034.62		5	3.15E-03	0.05	0.25	0.06	0.19	3.90	5.03
22.45	11037.69		3	6.66E-03	0.25	0.40				1.61
22.2	11040.77		3	5.14E-03	0.95	0.36				0.37
21.95	11043.85		3	6.66E-03	0.37	0.25				0.68
21.7	11046.92		3	4.91E-03	1.10	0.40				0.36
21.45	11050.00		2	5.83E-03	0.42	0.41	-0.03	0.44	1.06	1.00
21.2	11051.71		2	3.33E-03	4.08	0.34				0.08
20.95	11053.41		2	3.91E-03	2.53	0.45				0.18
20.75	11054.78		3	4.21E-03	1.79	0.71				0.40
20.7	11055.12		2	3.14E-03	6.09	0.29				0.05
20.45	11056.83		2	4.12E-03	2.28	0.59				0.26
20.2	11058.54		2	4.57E-03	1.40	0.49				0.35
19.95	11060.24		2	3.90E-03	2.83	0.42				0.15
19.7	11061.95		2	3.97E-03	2.55	0.51	0.04	0.47	0.19	0.20
19.45	11063.66		2	3.85E-03	1.56	0.45				0.29
19.2	11065.37		2	3.38E-03	3.44	0.41				0.12
18.95	11067.07		2	3.21E-03	1.45	0.66				0.45
18.7	11068.78		2	2.24E-03	4.50	0.43				0.10
18.45	11070.49		2	2.61E-03	2.02	0.60				0.30
18.2	11072.20		2	2.49E-03	1.75	0.59				0.34
17.95	11073.90		2	2.95E-03	1.88	0.82				0.43
17.7	11075.61		2	2.80E-03	2.22	0.55				0.25
17.45	11077.32		2	2.80E-03	2.01	0.55	0.03	0.51	0.26	0.27
17.2	11079.02		2	3.81E-03	0.20	0.80	0.09	0.71	3.51	3.96
16.95	11080.73		2	2.57E-03	2.43	0.60	0.04	0.56	0.23	0.25
16.7	11082.44		2	2.43E-03	3.28	0.45				0.14
16.45	11084.15		2	4.35E-03	1.63	0.48				0.30
16.2	11085.85		2	4.11E-03	3.77	0.94				0.25
15.95	11087.56		2	4.17E-03	3.14	0.96				0.31
15.7	11089.27		2	5.33E-03	0.83	0.47				0.57
15.5	11090.63		2	4.53E-03	1.33	0.66				0.50
15.45	11090.98		4	6.97E-03	1.33	0.67				0.50
15.2	11092.68		3	4.74E-03	0.94	0.51				0.54
14.95	11094.39		2	3.20E-03	1.54	0.75				0.49

Sample location [m above base]	Age model ages [cal. BP]	Snails	Grain size	Magn. Susz.	TN [wt%]	TC [wt%]	TIC [wt%]	TOC [wt%]	TOC/TN	TC/TN
14.7	11096.10		3	5.02E-03	0.34	0.31				0.92
14.5	11097.46		2	4.15E-03	0.77	0.60				0.79
14.45	11097.80		3	4.82E-03	0.97	0.26	0.01	0.25	0.25	0.26
14.2	11099.51		2	4.04E-03	2.54	0.46				0.18
13.95	11101.22		2	3.20E-03	3.18	0.68				0.21
13.7	11102.93		3	4.55E-03	2.39	0.36				0.15
13.45	11104.63		2	3.75E-03	2.04	0.61				0.30
13.2	11106.34		4	6.84E-03	0.72	0.19	0.05	0.14	0.19	0.27
12.95	11108.05		3	4.47E-03	0.19	0.46	0.12	0.34	1.83	2.46
12.7	11109.76		2	3.17E-03	2.57	0.55	0.03	0.53	0.20	0.21
12.45	11111.46		2	3.62E-03	1.55	0.80				0.52
12.2	11113.17		2	4.06E-03	3.11	0.57				0.18
11.95	11114.88		2	4.78E-03	1.62	0.46				0.29
11.7	11116.59		3	4.14E-03	2.20	0.79				0.36
11.5	11117.95		3	5.89E-03	1.35	0.20				0.15
11.45	11118.29		2	3.58E-03	1.32	0.50				0.38
11.2	11120.00		2	4.02E-03	1.12	0.99				0.88
10.95	11121.90		2	2.41E-03	4.22	0.53				0.13
10.7	11123.81		2	2.31E-03	3.68	0.64				0.17
10.45	11125.71		2	3.01E-03	2.39	0.80	0.07	0.73	0.31	0.34
10.2	11127.61		3	6.11E-03	1.04	0.29				0.27
9.95	11129.52		2	2.31E-03	1.86	0.90	0.03	0.87	0.47	0.48
9.7	11131.42		3	5.03E-03	0.18	0.82				4.50
9.45	11133.32		3	6.30E-03	0.04	0.39	0.12	0.28	7.20	10.20
9.2	11135.23		2	4.11E-03	0.80	0.59	0.06	0.52	0.65	0.73
8.95	11137.13		2	3.06E-03	2.87	0.63				0.22
8.7	11139.04		2	2.30E-03	3.16	0.65				0.21
8.5	11140.56		2	3.02E-03	1.75	0.93				0.53
8.45	11140.94		3	5.26E-03	1.82	0.57				0.32
8.2	11142.84		2	3.83E-03	1.83	0.84				0.46
7.95	11144.75		2	3.29E-03	1.20	0.81				0.68
7.7	11146.65		2	3.49E-03	2.05	0.87				0.42
7.45	11148.55		2	3.78E-03	1.26	0.58				0.46
7.2	11150.46		2	4.22E-03	1.56	0.55				0.35
6.95	11152.36		2	4.24E-03	1.50	0.44				0.29
6.7	11154.26		3	4.15E-03	0.74	0.17				0.24
6.45	11156.17		2	3.81E-03	1.85	0.46				0.25
6.25	11157.69		2	2.97E-03	1.77	0.38				0.21
6.2	11158.07		4	5.19E-03	0.87	0.26	0.12	0.15	0.17	0.30
5.95	11159.97		2	4.62E-03	1.89	0.40				0.21
5.7	11161.88		2	3.59E-03	1.58	0.56				0.36
5.45	11163.78		2	4.10E-03	1.85	0.27				0.14
5.2	11165.69		3	6.36E-03	0.73	0.34				0.47
4.95	11167.59		2	4.36E-03	1.22	0.88				0.72
4.7	11169.49		2	4.20E-03	0.99	0.59				0.60
4.5	11171.02		2	4.28E-03	1.29	0.82	0.08	0.74	0.58	0.63
4.45	11171.40		3	7.58E-03	0.77	0.08	-0.07	0.15	0.19	0.10
4.2	11173.30		2	5.05E-03	1.49	0.79				0.53
3.95	11175.20		3	6.72E-03	0.96	0.30				0.31
3.7	11177.11		2	4.45E-03	1.78	0.70				0.39
3.45	11179.01		2	4.82E-03	1.63	0.66				0.41
3.2	11180.91		2	4.69E-03	1.21	0.64				0.53
2.95	11182.82		2	3.57E-03	1.70	0.87				0.51
2.7	11184.72		4	5.82E-03	0.60	0.33				0.55
2.45	11186.62		2	4.16E-03	0.82	0.79				0.96
2.2	11188.53		3	5.37E-03	0.80	0.60				0.75
1.95	11190.43		2	3.47E-03	1.75	0.70				0.40
1.7	11192.34		2	4.33E-03	1.53	0.84				0.55
1.45	11194.24		2	3.86E-03	1.42	0.58	0.06	0.52	0.37	0.41
1.35	11195.00		2	3.95E-03	0.16	0.98	0.23	0.75	4.64	6.04
1.25	11196.43		3	3.87E-03	0.17	0.69				4.13
1.15	11197.86		2	3.09E-03	0.15	0.49				3.32
1.05	11199.29		4	4.73E-03	0.11	0.26				2.45
1	11200.00		2	3.50E-03	0.48	0.81	0.15	0.66	1.37	1.67
0.95	11200.71		4	5.54E-03	0.15	0.25				1.69
0.85	11202.14		2	4.86E-03	0.24	0.77	0.16	0.62	2.55	3.20
0.8	11202.86		3	6.13E-03	0.14	0.25				1.83
0.7	11204.29		3	5.42E-03	0.24	0.53				2.20
0.6	11205.71		3	5.34E-03	0.22	0.48	0.06	0.43	1.96	2.21
0.5	11207.14		2	3.54E-03	0.29	0.79				2.68
0.35	11209.29		4	5.88E-03	0.12	0.23				1.94
0.3	11210.00		2	5.45E-03	0.31	0.70				2.28
0.2	11211.43		2	4.75E-03	0.39	0.59				1.51
0.1	11212.86		2	4.02E-03	0.56	0.66				1.19
0	11214.29		2	4.08E-03	0.40	0.81	0.15	0.66	1.66	2.02

Appendix 05 - Palaeo-lake level curve for Suguta Valley

Palaeo-lake Suguta	
AHP	
(this thesis Fig 2.3)	
Year cal. BP	Lake level [m]
4011,00	0,00
6650,51	295,00
6991,45	295,00
7321,38	295,00
7354,38	293,34
7398,37	290,56
7442,36	287,24
7486,35	287,24
7519,35	291,12
7574,34	295,00
8168,23	295,00
8344,20	159,70
8366,19	158,04
8399,19	158,04
8531,16	241,21
8575,15	215,70
8586,15	230,12
8619,14	210,71
8641,14	254,52
8674,13	212,38
8740,12	293,34
8784,11	219,03
8817,11	250,08
8839,10	217,92
8872,10	265,06
8883,10	266,17
8905,09	263,39
8938,09	211,27
9004,07	294,45
9059,06	205,17
9081,06	204,06
9092,06	205,17
9147,05	293,89
9180,04	294,45
9246,03	214,04
9257,03	212,93
9290,02	214,04
9334,01	259,51
9367,01	259,51
9443,99	199,62
9542,97	293,89
9586,97	293,89
9652,95	230,68
9718,94	291,12
9751,93	291,67
9828,92	204,06
9861,91	203,51
9872,91	205,17
9949,90	292,23
9982,89	292,78
9993,89	291,12
10059,88	207,94
10081,87	205,17
10114,87	204,06
10169,86	204,61

continued right column...

Palaeo-lake Suguta	
AHP	
(this thesis Fig 2.3)	
Year cal. BP	Lake level [m]
10202,85	208,50
10279,84	291,67
10323,83	291,67
10378,82	210,16
10433,81	248,98
10499,80	199,62
10554,79	272,82
10587,78	272,82
10598,78	271,71
10675,76	212,93
10741,75	291,67
10774,75	292,23
10840,73	227,90
10906,72	290,56
10939,71	290,56
10961,71	290,01
11027,70	214,60
11071,69	255,08
11126,68	252,86
11181,67	246,20
11203,67	240,10
11258,66	233,45
11280,65	225,69
11313,65	217,37
11346,64	205,17
11368,64	193,52
11412,63	178,00
11621,59	0,00
12457,43	0,55
13216,29	294,45
13964,15	295,00
14800,00	0,55

Appendix 06 - Palaeo-lake levels Africa

Lake Bosumtwi	
(Shanahan et al.. 2006)	
Year cal. BP	Lake level [m]
0	6.91
350.79	6.91
1110.84	27.78
1987.82	28.38
2182.70	35.64
3020.71	36.54
3741.78	11.45
3839.22	8.42
4151.04	8.42
4696.71	80.09
7736.91	80.69
8399.51	36.54
8789.28	36.54
8945.19	115.77
10679.66	118.49
11595.62	45.92
12745.43	45.62
12842.87	63.76
13875.76	63.76
14304.51	28.08
14947.62	28.08
15590.74	-13.35
15863.58	-19.40

Lake Nakuru-Elmenteita	
(Richardson and Dussinger. 1986)	
Year cal. BP	Lake level [m]
17.32	4.60
2130.48	6.57
2442.26	8.54
2927.25	17.08
3256.35	24.96
3602.77	43.36
3706.70	53.87
3758.66	59.12
3879.91	59.12
4347.58	21.68
4468.82	17.08
4520.79	17.74
5421.48	176.06
6270.21	176.72
6859.12	149.78
7361.43	158.98
7863.74	149.78
8227.48	158.32
8400.69	179.34
8556.58	179.34
9024.25	93.28
9162.82	90.66
9249.42	93.28
9457.27	131.39
9595.84	166.20
9699.77	176.06
10998.85	180.00
11172.06	177.37
11968.82	44.01
12090.07	34.16
12228.64	32.19
12436.49	33.50
13042.73	176.72
13267.90	177.37
13545.03	177.37
13735.57	176.72
14722.86	7.88
14792.15	1.31

Lake Turkana	
(Brown & Fuller. 2008; Johnson et al.. 1991)	
Year cal. BP	Lake level [m]
135.43	0.00
154.78	25.92
328.90	64.32
464.33	2.88
677.15	32.64
831.92	14.40
1296.25	18.24
1818.62	59.52
2108.83	14.40
2399.03	24.00
3811.37	2.88
4159.61	94.08
4256.35	72.00
4449.82	67.20
4546.55	96.00
5088.27	96.96
5126.96	78.72
5397.82	96.96
5552.60	96.96
5610.64	79.68
5746.07	67.20
5881.50	96.96
6307.13	98.88
6616.69	98.88
6732.77	97.92
6984.28	120.00
7197.10	84.48
7622.73	45.12
7912.94	17.28
8261.18	63.36
8319.23	81.60
8996.37	119.04
9170.50	113.28
9344.62	78.72
9480.05	120.00
9673.52	99.84
9886.34	89.28
10118.50	88.32
10195.89	88.32
10273.28	96.00
10350.67	87.36
10466.75	85.44
10602.18	55.68
10602.18	104.64
10737.61	96.00
10931.08	89.28
11105.20	109.44
11414.75	46.08
11530.83	107.52
11704.96	92.16
11898.43	81.60
12652.96	74.88
12981.86	87.36
13136.64	90.24
13214.03	1.92

Lake Ziway-Shala	
(Gillespie et al.. 1983)	
Year cal. BP	Lake level [m]
20.57	3.70
1439.59	38.82
2323.91	38.82
2982.01	16.64
3187.66	13.87
4030.85	21.26
4421.59	25.88
5182.52	110
6580.98	109.08
6724.94	78.57
6951.16	109.08
7568.12	109.08
7958.87	1.85
8555.27	2.77
9748.07	110
10838.05	110
11393.32	4.62
12544.99	65.63
12688.95	68.40
12853.47	70.25
12894.60	0
15979.43	0.92

Appendix 07 - 200-year Sedimentology and diatom investigation for Lake Naivasha

Sedimentology of NSA-4-2007

sample number	Depth [cm]	age year AD	water content [%]	TOC [wt%]	TIC [wt%]	TC [wt%]	TN [wt%]	TOC/TN	TC/TN	TC [mg/cm-2/y-1]	TOC [mg/cm-2/y-1]	TIC [mg/cm-2/y-1]	TN [mg/cm-2/y-1]
1	1.05	2006	90.79	6.93	0.72	7.65	0.91	7.63	8.42	6.81	6.17	0.64	0.81
2	3.15	2004	93.42	6.64	1.32	7.96	1.12	5.94	7.12	6.84	5.71	1.13	0.96
3	5.25	2002	92.31	6.40	1.00	7.40	1.05	6.11	7.06	6.36	5.50	0.86	0.90
4	7.35	2000	90.66	6.97	0.68	7.65	0.96	7.27	7.98	5.58	5.09	0.50	0.70
5	9.45	1996	85.58	6.81	1.17	7.98	0.92	7.37	8.63	5.42	4.63	0.79	0.63
6	11.55	1992	90.54	6.80	0.40	7.20	0.85	8.04	8.51	4.75	4.49	0.26	0.56
7	13.65	1988	89.27	7.26	0.35	7.61	0.87	8.38	8.79	4.11	3.92	0.19	0.47
8	15.75	1984	90.10	7.58	0.90	8.48	0.95	7.95	8.89	3.90	3.49	0.41	0.44
9	17.85	1978	88.24	8.04	0.70	8.73	0.98	8.18	8.89	3.67	3.37	0.29	0.41
10	19.95	1971	88.14	8.52	0.81	9.33	1.09	7.84	8.59	3.36	3.07	0.29	0.39
11	22.05	1963	87.83	8.54	0.99	9.53	1.08	7.89	8.81	2.76	2.48	0.29	0.31
12	24.15	1947	89.58	8.41	0.74	9.15	1.08	7.78	8.47	1.19	1.09	0.10	0.14
13	26.25	1928	91.04	9.39	0.82	10.21	1.19	7.92	8.61	1.02	0.94	0.08	0.12
14	28.45	1907	90.57	11.77	0.59	12.36	1.33	8.86	9.30	1.24	1.18	0.06	0.13
15	30.45	1885	88.89	11.87	0.27	12.13	1.32	8.96	9.16	1.21	1.19	0.03	0.13
16	32.55	1863	90.72	15.04	0.71	15.75	1.62	9.28	9.72	1.57	1.50	0.07	0.16
17	34.65	1843	89.88	11.53	0.36	11.89	1.27	9.06	9.34	1.19	1.15	0.04	0.13
18	36.75	1816	89.92	16.64	1.11	17.75	1.78	9.35	9.97	1.77	1.66	0.11	0.18

Diatom assemblages and reconstructions for NSA-4-2007

sample number	Depth [cm]	age year AD	Zone	planktonic [%]	planktonic / littoral [%]	littoral [%]	littoral/ benthic [%]	CA 1 axis (PCA)	reconstr. Cond. [µS/cm]	reconstr. pH	TP µg/l
1.00	1.05	2006.00	I	67.47	28.94	0.40	2.79	-0.80	215.03	6.86	132.31
2.00	3.15	2004.00	I	76.91	18.70	0.38	4.77	-0.81	183.70	6.91	154.67
3.00	5.25	2002.00	I	77.53	20.04	0.56	2.43	-0.69	173.58	6.90	144.88
4.00	7.35	2000.00	I	86.10	14.41	0.34	1.19	-0.67	169.32	6.97	141.09
5.00	9.45	1996.00	I	84.27	14.90	0.17	2.15	-0.67	178.69	7.00	165.12
6.00	11.55	1992.00	I	86.07	11.64	0.98	4.10	-0.42	177.13	7.20	153.99
7.00	13.65	1988.00	I	89.81	6.02	0.93	4.01	-0.47	149.31	7.02	150.14
8.00	15.75	1984.00	I	90.18	5.94	1.29	3.36	-0.71	171.59	7.21	135.27
9.00	17.85	1978.00	I	83.36	11.71	1.70	4.58	-0.45	174.74	7.11	108.97
10.00	19.95	1971.00	I	90.24	6.90	2.86	2.02	-0.46	163.61	7.20	100.79
11.00	22.05	1963.00	I	91.39	5.48	1.17	2.94	-0.39	155.42	7.00	119.12
12.00	24.15	1947.00	I	82.57	17.62	0.99	2.57	-0.57	175.99	6.94	116.41
13.00	26.25	1928.00	II	64.86	28.31	2.41	4.82	-0.29	172.66	6.57	154.88
14.00	28.45	1907.00	II	57.99	28.55	8.62	5.75	0.28	184.88	6.99	87.50
15.00	30.45	1885.00	III	31.09	7.72	26.34	34.85	1.70	294.10	7.88	76.52
16.00	32.55	1863.00	III	6.29	4.20	54.08	35.43	2.41	731.14	8.72	49.35
17.00	34.65	1843.00	III	30.52	7.06	29.84	32.57	1.73	328.62	7.75	75.21
18.00	36.75	1816.00	III	34.91	8.54	11.95	44.59	1.29	289.93	7.40	75.74

Appendix 08 - Instrumental lake level data main lake Naivasha (S. Higgens)

Year AD	Lake level [m a.s.l.]	Lake level [m]
2008,50	1890,98	10,98
2008,42	1890,98	10,98
2008,33	1890,98	10,98
2008,25	1890,98	10,98
2008,17	1890,98	10,98
2008,08	1890,89	10,89
2008,00	1890,86	10,86
2007,92	1890,86	10,86
2007,83	1890,83	10,83
2007,75	1890,83	10,83
2007,67	1890,77	10,77
2007,58	1890,67	10,67
2007,50	1890,55	10,55
2007,42	1890,49	10,49
2007,33	1890,37	10,37
2007,25	1890,22	10,22
2007,17	1890,22	10,22
2007,08	1890,16	10,16
2007,00	1890,16	10,16
2006,92	1890,10	10,10
2006,83	1890,10	10,10
2006,75	1890,08	10,08
2006,67	1890,07	10,07
2006,58	1890,06	10,06
2006,50	1890,06	10,06
2006,42	1890,06	10,06
2006,33	1890,06	10,06
2006,25	1890,06	10,06
2006,17	1890,01	10,01
2006,08	1889,95	9,95
2006,00	1889,91	9,91
2005,92	1889,91	9,91
2005,83	1889,88	9,88
2005,75	1889,82	9,82
2005,67	1889,82	9,82
2005,58	1889,81	9,81
2005,50	1889,81	9,81
2005,42	1889,80	9,80
2005,33	1889,80	9,80
2005,25	1889,79	9,79
2005,17	1889,79	9,79
2005,08	1889,79	9,79
2005,00	1889,78	9,78
2004,92	1889,77	9,77
2004,83	1889,76	9,76
2004,75	1889,75	9,75
2004,67	1889,75	9,75
2004,58	1889,75	9,75
2004,50	1889,75	9,75
2004,42	1889,73	9,73
2004,33	1889,73	9,73
2004,25	1889,72	9,72
2004,17	1889,71	9,71
2004,08	1889,70	9,70
2004,00	1889,69	9,69
2003,92	1889,68	9,68
2003,83	1889,65	9,65
2003,75	1889,64	9,64
2003,67	1889,64	9,64

continued middle column...

Year AD	Lake level [m a.s.l.]	Lake level [m]
2003,58	1889,62	9,62
2003,50	1889,61	9,61
2003,42	1889,61	9,61
2003,33	1889,61	9,61
2003,25	1889,61	9,61
2003,17	1889,60	9,60
2003,08	1889,59	9,59
2003,00	1889,59	9,59
2002,92	1889,57	9,57
2002,83	1889,57	9,57
2002,75	1889,56	9,56
2002,67	1889,56	9,56
2002,58	1889,55	9,55
2002,50	1889,55	9,55
2002,42	1889,54	9,54
2002,33	1889,53	9,53
2002,25	1889,53	9,53
2002,17	1889,52	9,52
2002,08	1889,52	9,52
2002,00	1889,52	9,52
2001,92	1889,52	9,52
2001,83	1889,51	9,51
2001,75	1889,50	9,50
2001,67	1889,48	9,48
2001,58	1889,47	9,47
2001,50	1889,46	9,46
2001,42	1889,46	9,46
2001,33	1889,45	9,45
2001,25	1889,44	9,44
2001,17	1889,44	9,44
2001,08	1889,44	9,44
2001,00	1889,43	9,43
2000,92	1889,42	9,42
2000,83	1889,41	9,41
2000,75	1889,39	9,39
2000,67	1889,36	9,36
2000,58	1889,36	9,36
2000,50	1889,36	9,36
2000,42	1889,35	9,35
2000,33	1889,34	9,34
2000,25	1889,34	9,34
2000,17	1889,33	9,33
2000,08	1889,33	9,33
2000,00	1889,32	9,32
1999,92	1889,32	9,32
1999,83	1889,31	9,31
1999,75	1889,31	9,31
1999,67	1889,29	9,29
1999,58	1889,28	9,28
1999,50	1889,28	9,28
1999,42	1889,25	9,25
1999,33	1889,25	9,25
1999,25	1889,25	9,25
1999,17	1889,24	9,24
1999,08	1889,24	9,24
1999,00	1889,23	9,23
1998,92	1889,23	9,23
1998,83	1889,21	9,21
1998,75	1889,21	9,21

continued right column...

Year AD	Lake level [m a.s.l.]	Lake level [m]
1998,67	1889,21	9,21
1998,58	1889,20	9,20
1998,50	1889,20	9,20
1998,42	1889,20	9,20
1998,33	1889,20	9,20
1998,25	1889,19	9,19
1998,17	1889,19	9,19
1998,08	1889,18	9,18
1998,00	1889,16	9,16
1997,92	1889,15	9,15
1997,83	1889,15	9,15
1997,75	1889,15	9,15
1997,67	1889,15	9,15
1997,58	1889,14	9,14
1997,50	1889,14	9,14
1997,42	1889,13	9,13
1997,33	1889,13	9,13
1997,25	1889,12	9,12
1997,17	1889,12	9,12
1997,08	1889,12	9,12
1997,00	1889,11	9,11
1996,92	1889,11	9,11
1996,83	1889,09	9,09
1996,75	1889,09	9,09
1996,67	1889,09	9,09
1996,58	1889,08	9,08
1996,50	1889,08	9,08
1996,42	1889,07	9,07
1996,33	1889,07	9,07
1996,25	1889,06	9,06
1996,17	1889,04	9,04
1996,08	1889,04	9,04
1996,00	1889,04	9,04
1995,92	1889,04	9,04
1995,83	1889,04	9,04
1995,75	1889,03	9,03
1995,67	1889,03	9,03
1995,58	1889,01	9,01
1995,50	1889,01	9,01
1995,42	1889,01	9,01
1995,33	1889,00	9,00
1995,25	1889,00	9,00
1995,17	1888,99	8,99
1995,08	1888,99	8,99
1995,00	1888,98	8,98
1994,92	1888,98	8,98
1994,83	1888,98	8,98
1994,75	1888,98	8,98
1994,67	1888,97	8,97
1994,58	1888,97	8,97
1994,50	1888,96	8,96
1994,42	1888,96	8,96
1994,33	1888,96	8,96
1994,25	1888,95	8,95
1994,17	1888,95	8,95
1994,08	1888,94	8,94
1994,00	1888,94	8,94
1993,92	1888,94	8,94
1993,83	1888,93	8,93

continued next page...

Year AD	Lake level [m a.s.l.]	Lake level [m]
1993,75	1888,93	8,93
1993,67	1888,92	8,92
1993,58	1888,92	8,92
1993,50	1888,92	8,92
1993,42	1888,92	8,92
1993,33	1888,92	8,92
1993,25	1888,92	8,92
1993,17	1888,92	8,92
1993,08	1888,92	8,92
1993,00	1888,91	8,91
1992,92	1888,91	8,91
1992,83	1888,91	8,91
1992,75	1888,90	8,90
1992,67	1888,90	8,90
1992,58	1888,90	8,90
1992,50	1888,90	8,90
1992,42	1888,89	8,89
1992,33	1888,89	8,89
1992,25	1888,89	8,89
1992,17	1888,89	8,89
1992,08	1888,89	8,89
1992,00	1888,89	8,89
1991,92	1888,89	8,89
1991,83	1888,88	8,88
1991,75	1888,88	8,88
1991,67	1888,87	8,87
1991,58	1888,86	8,86
1991,50	1888,86	8,86
1991,42	1888,85	8,85
1991,33	1888,85	8,85
1991,25	1888,84	8,84
1991,17	1888,84	8,84
1991,08	1888,83	8,83
1991,00	1888,83	8,83
1990,92	1888,82	8,82
1990,83	1888,82	8,82
1990,75	1888,82	8,82
1990,67	1888,82	8,82
1990,58	1888,81	8,81
1990,50	1888,79	8,79
1990,42	1888,79	8,79
1990,33	1888,79	8,79
1990,25	1888,79	8,79
1990,17	1888,78	8,78
1990,08	1888,78	8,78
1990,00	1888,75	8,75
1989,92	1888,75	8,75
1989,83	1888,75	8,75
1989,75	1888,75	8,75
1989,67	1888,74	8,74
1989,58	1888,74	8,74
1989,50	1888,73	8,73
1989,42	1888,72	8,72
1989,33	1888,72	8,72
1989,25	1888,72	8,72
1989,17	1888,72	8,72
1989,08	1888,70	8,70
1989,00	1888,69	8,69
1988,92	1888,69	8,69
1988,83	1888,69	8,69
1988,75	1888,67	8,67
1988,67	1888,67	8,67
1988,58	1888,66	8,66
1988,50	1888,65	8,65

continued middle column...

Year AD	Lake level [m a.s.l.]	Lake level [m]
1988,42	1888,65	8,65
1988,33	1888,63	8,63
1988,25	1888,63	8,63
1988,17	1888,61	8,61
1988,08	1888,61	8,61
1988,00	1888,60	8,60
1987,92	1888,59	8,59
1987,83	1888,59	8,59
1987,75	1888,59	8,59
1987,67	1888,59	8,59
1987,58	1888,59	8,59
1987,50	1888,57	8,57
1987,42	1888,57	8,57
1987,33	1888,57	8,57
1987,25	1888,55	8,55
1987,17	1888,54	8,54
1987,08	1888,53	8,53
1987,00	1888,52	8,52
1986,92	1888,52	8,52
1986,83	1888,51	8,51
1986,75	1888,51	8,51
1986,67	1888,50	8,50
1986,58	1888,50	8,50
1986,50	1888,50	8,50
1986,42	1888,50	8,50
1986,33	1888,47	8,47
1986,25	1888,45	8,45
1986,17	1888,45	8,45
1986,08	1888,44	8,44
1986,00	1888,44	8,44
1985,92	1888,44	8,44
1985,83	1888,43	8,43
1985,75	1888,43	8,43
1985,67	1888,43	8,43
1985,58	1888,42	8,42
1985,50	1888,42	8,42
1985,42	1888,40	8,40
1985,33	1888,40	8,40
1985,25	1888,38	8,38
1985,17	1888,38	8,38
1985,08	1888,38	8,38
1985,00	1888,37	8,37
1984,92	1888,37	8,37
1984,83	1888,35	8,35
1984,75	1888,35	8,35
1984,67	1888,32	8,32
1984,58	1888,31	8,31
1984,50	1888,31	8,31
1984,42	1888,31	8,31
1984,33	1888,31	8,31
1984,25	1888,31	8,31
1984,17	1888,30	8,30
1984,08	1888,29	8,29
1984,00	1888,28	8,28
1983,92	1888,28	8,28
1983,83	1888,27	8,27
1983,75	1888,27	8,27
1983,67	1888,26	8,26
1983,58	1888,26	8,26
1983,50	1888,25	8,25
1983,42	1888,25	8,25
1983,33	1888,24	8,24
1983,25	1888,21	8,21
1983,17	1888,21	8,21

continued right column...

Year AD	Lake level [m a.s.l.]	Lake level [m]
1983,08	1888,19	8,19
1983,00	1888,19	8,19
1982,92	1888,18	8,18
1982,83	1888,18	8,18
1982,75	1888,17	8,17
1982,67	1888,17	8,17
1982,58	1888,16	8,16
1982,50	1888,15	8,15
1982,42	1888,15	8,15
1982,33	1888,15	8,15
1982,25	1888,15	8,15
1982,17	1888,14	8,14
1982,08	1888,14	8,14
1982,00	1888,10	8,10
1981,92	1888,09	8,09
1981,83	1888,06	8,06
1981,75	1888,05	8,05
1981,67	1888,04	8,04
1981,58	1888,03	8,03
1981,50	1888,03	8,03
1981,42	1888,02	8,02
1981,33	1888,02	8,02
1981,25	1888,02	8,02
1981,17	1888,01	8,01
1981,08	1887,96	7,96
1981,00	1887,95	7,95
1980,92	1887,95	7,95
1980,83	1887,94	7,94
1980,75	1887,93	7,93
1980,67	1887,92	7,92
1980,58	1887,91	7,91
1980,50	1887,91	7,91
1980,42	1887,90	7,90
1980,33	1887,89	7,89
1980,25	1887,89	7,89
1980,17	1887,88	7,88
1980,08	1887,88	7,88
1980,00	1887,87	7,87
1979,92	1887,86	7,86
1979,83	1887,85	7,85
1979,75	1887,85	7,85
1979,67	1887,85	7,85
1979,58	1887,85	7,85
1979,50	1887,83	7,83
1979,42	1887,83	7,83
1979,33	1887,82	7,82
1979,25	1887,82	7,82
1979,17	1887,81	7,81
1979,08	1887,81	7,81
1979,00	1887,81	7,81
1978,92	1887,81	7,81
1978,83	1887,80	7,80
1978,75	1887,80	7,80
1978,67	1887,80	7,80
1978,58	1887,79	7,79
1978,50	1887,78	7,78
1978,42	1887,78	7,78
1978,33	1887,77	7,77
1978,25	1887,76	7,76
1978,17	1887,73	7,73
1978,08	1887,72	7,72
1978,00	1887,72	7,72
1977,92	1887,72	7,72
1977,83	1887,72	7,72

continued next page...

Year AD	Lake level [m a.s.l.]	Lake level [m]
1977,75	1887,70	7,70
1977,67	1887,68	7,68
1977,58	1887,67	7,67
1977,50	1887,66	7,66
1977,42	1887,66	7,66
1977,33	1887,64	7,64
1977,25	1887,64	7,64
1977,17	1887,63	7,63
1977,08	1887,62	7,62
1977,00	1887,62	7,62
1976,92	1887,61	7,61
1976,83	1887,60	7,60
1976,75	1887,60	7,60
1976,67	1887,57	7,57
1976,58	1887,57	7,57
1976,50	1887,56	7,56
1976,42	1887,56	7,56
1976,33	1887,55	7,55
1976,25	1887,55	7,55
1976,17	1887,53	7,53
1976,08	1887,52	7,52
1976,00	1887,50	7,50
1975,92	1887,49	7,49
1975,83	1887,49	7,49
1975,75	1887,49	7,49
1975,67	1887,49	7,49
1975,58	1887,48	7,48
1975,50	1887,48	7,48
1975,42	1887,48	7,48
1975,33	1887,48	7,48
1975,25	1887,47	7,47
1975,17	1887,47	7,47
1975,08	1887,47	7,47
1975,00	1887,46	7,46
1974,92	1887,45	7,45
1974,83	1887,45	7,45
1974,75	1887,44	7,44
1974,67	1887,43	7,43
1974,58	1887,41	7,41
1974,50	1887,40	7,40
1974,42	1887,40	7,40
1974,33	1887,40	7,40
1974,25	1887,39	7,39
1974,17	1887,39	7,39
1974,08	1887,38	7,38
1974,00	1887,38	7,38
1973,92	1887,38	7,38
1973,83	1887,38	7,38
1973,75	1887,36	7,36
1973,67	1887,36	7,36
1973,58	1887,34	7,34
1973,50	1887,34	7,34
1973,42	1887,34	7,34
1973,33	1887,34	7,34
1973,25	1887,33	7,33
1973,17	1887,33	7,33
1973,08	1887,33	7,33
1973,00	1887,32	7,32
1972,92	1887,32	7,32
1972,83	1887,32	7,32
1972,75	1887,32	7,32
1972,67	1887,32	7,32
1972,58	1887,32	7,32
1972,50	1887,29	7,29

continued middle column...

Year AD	Lake level [m a.s.l.]	Lake level [m]
1972,42	1887,28	7,28
1972,33	1887,28	7,28
1972,25	1887,28	7,28
1972,17	1887,27	7,27
1972,08	1887,26	7,26
1972,00	1887,26	7,26
1971,92	1887,25	7,25
1971,83	1887,25	7,25
1971,75	1887,25	7,25
1971,67	1887,25	7,25
1971,58	1887,24	7,24
1971,50	1887,21	7,21
1971,42	1887,20	7,20
1971,33	1887,20	7,20
1971,25	1887,20	7,20
1971,17	1887,19	7,19
1971,08	1887,19	7,19
1971,00	1887,18	7,18
1970,92	1887,18	7,18
1970,83	1887,17	7,17
1970,75	1887,17	7,17
1970,67	1887,16	7,16
1970,58	1887,16	7,16
1970,50	1887,16	7,16
1970,42	1887,16	7,16
1970,33	1887,16	7,16
1970,25	1887,16	7,16
1970,17	1887,15	7,15
1970,08	1887,14	7,14
1970,00	1887,14	7,14
1969,92	1887,13	7,13
1969,83	1887,13	7,13
1969,75	1887,12	7,12
1969,67	1887,11	7,11
1969,58	1887,11	7,11
1969,50	1887,08	7,08
1969,42	1887,08	7,08
1969,33	1887,07	7,07
1969,25	1887,07	7,07
1969,17	1887,06	7,06
1969,08	1887,06	7,06
1969,00	1887,06	7,06
1968,92	1887,04	7,04
1968,83	1887,03	7,03
1968,75	1887,03	7,03
1968,67	1887,03	7,03
1968,58	1887,03	7,03
1968,50	1887,02	7,02
1968,42	1887,02	7,02
1968,33	1887,00	7,00
1968,25	1887,00	7,00
1968,17	1886,99	6,99
1968,08	1886,99	6,99
1968,00	1886,99	6,99
1967,92	1886,97	6,97
1967,83	1886,97	6,97
1967,75	1886,95	6,95
1967,67	1886,94	6,94
1967,58	1886,93	6,93
1967,50	1886,93	6,93
1967,42	1886,93	6,93
1967,33	1886,93	6,93
1967,25	1886,92	6,92
1967,17	1886,92	6,92

continued right column...

Year AD	Lake level [m a.s.l.]	Lake level [m]
1967,08	1886,92	6,92
1967,00	1886,92	6,92
1966,92	1886,91	6,91
1966,83	1886,90	6,90
1966,75	1886,89	6,89
1966,67	1886,89	6,89
1966,58	1886,88	6,88
1966,50	1886,88	6,88
1966,42	1886,87	6,87
1966,33	1886,87	6,87
1966,25	1886,87	6,87
1966,17	1886,87	6,87
1966,08	1886,86	6,86
1966,00	1886,85	6,85
1965,92	1886,84	6,84
1965,83	1886,84	6,84
1965,75	1886,84	6,84
1965,67	1886,83	6,83
1965,58	1886,82	6,82
1965,50	1886,82	6,82
1965,42	1886,82	6,82
1965,33	1886,82	6,82
1965,25	1886,82	6,82
1965,17	1886,81	6,81
1965,08	1886,80	6,80
1965,00	1886,80	6,80
1964,92	1886,79	6,79
1964,83	1886,79	6,79
1964,75	1886,79	6,79
1964,67	1886,78	6,78
1964,58	1886,77	6,77
1964,50	1886,77	6,77
1964,42	1886,77	6,77
1964,33	1886,76	6,76
1964,25	1886,76	6,76
1964,17	1886,76	6,76
1964,08	1886,75	6,75
1964,00	1886,75	6,75
1963,92	1886,75	6,75
1963,83	1886,75	6,75
1963,75	1886,74	6,74
1963,67	1886,73	6,73
1963,58	1886,73	6,73
1963,50	1886,73	6,73
1963,42	1886,73	6,73
1963,33	1886,73	6,73
1963,25	1886,72	6,72
1963,17	1886,72	6,72
1963,08	1886,71	6,71
1963,00	1886,71	6,71
1962,92	1886,70	6,70
1962,83	1886,70	6,70
1962,75	1886,70	6,70
1962,67	1886,69	6,69
1962,58	1886,69	6,69
1962,50	1886,68	6,68
1962,42	1886,66	6,66
1962,33	1886,66	6,66
1962,25	1886,66	6,66
1962,17	1886,66	6,66
1962,08	1886,66	6,66
1962,00	1886,66	6,66
1961,92	1886,65	6,65
1961,83	1886,65	6,65

continued next page...

Year AD	Lake level [m a.s.l.]	Lake level [m]
1961,75	1886,64	6,64
1961,67	1886,64	6,64
1961,58	1886,64	6,64
1961,50	1886,64	6,64
1961,42	1886,63	6,63
1961,33	1886,63	6,63
1961,25	1886,63	6,63
1961,17	1886,63	6,63
1961,08	1886,63	6,63
1961,00	1886,61	6,61
1960,92	1886,60	6,60
1960,83	1886,60	6,60
1960,75	1886,60	6,60
1960,67	1886,59	6,59
1960,58	1886,58	6,58
1960,50	1886,57	6,57
1960,42	1886,56	6,56
1960,33	1886,56	6,56
1960,25	1886,56	6,56
1960,17	1886,56	6,56
1960,08	1886,56	6,56
1960,00	1886,56	6,56
1959,92	1886,55	6,55
1959,83	1886,55	6,55
1959,75	1886,55	6,55
1959,67	1886,54	6,54
1959,58	1886,54	6,54
1959,50	1886,54	6,54
1959,42	1886,53	6,53
1959,33	1886,53	6,53
1959,25	1886,53	6,53
1959,17	1886,52	6,52
1959,08	1886,52	6,52
1959,00	1886,52	6,52
1958,92	1886,51	6,51
1958,83	1886,51	6,51
1958,75	1886,51	6,51
1958,67	1886,50	6,50
1958,58	1886,50	6,50
1958,50	1886,50	6,50
1958,42	1886,50	6,50
1958,33	1886,50	6,50
1958,25	1886,50	6,50
1958,17	1886,50	6,50
1958,08	1886,50	6,50
1958,00	1886,50	6,50
1957,92	1886,50	6,50
1957,83	1886,50	6,50
1957,75	1886,50	6,50
1957,67	1886,50	6,50
1957,58	1886,50	6,50
1957,50	1886,50	6,50
1957,42	1886,49	6,49
1957,33	1886,49	6,49
1957,25	1886,48	6,48
1957,17	1886,48	6,48
1957,08	1886,48	6,48
1957,00	1886,47	6,47
1956,92	1886,47	6,47
1956,83	1886,47	6,47
1956,75	1886,47	6,47
1956,67	1886,47	6,47
1956,58	1886,46	6,46
1956,50	1886,45	6,45

continued middle column...

Year AD	Lake level [m a.s.l.]	Lake level [m]
1956,42	1886,45	6,45
1956,33	1886,45	6,45
1956,25	1886,43	6,43
1956,17	1886,42	6,42
1956,08	1886,42	6,42
1956,00	1886,41	6,41
1955,92	1886,41	6,41
1955,83	1886,40	6,40
1955,75	1886,40	6,40
1955,67	1886,40	6,40
1955,58	1886,40	6,40
1955,50	1886,40	6,40
1955,42	1886,40	6,40
1955,33	1886,40	6,40
1955,25	1886,40	6,40
1955,17	1886,40	6,40
1955,08	1886,39	6,39
1955,00	1886,38	6,38
1954,92	1886,37	6,37
1954,83	1886,37	6,37
1954,75	1886,37	6,37
1954,67	1886,36	6,36
1954,58	1886,35	6,35
1954,50	1886,34	6,34
1954,42	1886,34	6,34
1954,33	1886,34	6,34
1954,25	1886,33	6,33
1954,17	1886,33	6,33
1954,08	1886,32	6,32
1954,00	1886,32	6,32
1953,92	1886,31	6,31
1953,83	1886,31	6,31
1953,75	1886,30	6,30
1953,67	1886,30	6,30
1953,58	1886,30	6,30
1953,50	1886,30	6,30
1953,42	1886,30	6,30
1953,33	1886,30	6,30
1953,25	1886,30	6,30
1953,17	1886,29	6,29
1953,08	1886,28	6,28
1953,00	1886,27	6,27
1952,92	1886,27	6,27
1952,83	1886,25	6,25
1952,75	1886,24	6,24
1952,67	1886,24	6,24
1952,58	1886,24	6,24
1952,50	1886,23	6,23
1952,42	1886,23	6,23
1952,33	1886,23	6,23
1952,25	1886,23	6,23
1952,17	1886,22	6,22
1952,08	1886,22	6,22
1952,00	1886,21	6,21
1951,92	1886,21	6,21
1951,83	1886,21	6,21
1951,75	1886,20	6,20
1951,67	1886,20	6,20
1951,58	1886,20	6,20
1951,50	1886,19	6,19
1951,42	1886,18	6,18
1951,33	1886,17	6,17
1951,25	1886,16	6,16
1951,17	1886,16	6,16

continued right column...

Year AD	Lake level [m a.s.l.]	Lake level [m]
1951,08	1886,16	6,16
1951,00	1886,15	6,15
1950,92	1886,15	6,15
1950,83	1886,15	6,15
1950,75	1886,15	6,15
1950,67	1886,15	6,15
1950,58	1886,15	6,15
1950,50	1886,13	6,13
1950,42	1886,13	6,13
1950,33	1886,13	6,13
1950,25	1886,13	6,13
1950,17	1886,12	6,12
1950,08	1886,12	6,12
1950,00	1886,12	6,12
1949,92	1886,11	6,11
1949,83	1886,11	6,11
1949,75	1886,10	6,10
1949,67	1886,10	6,10
1949,58	1886,10	6,10
1949,50	1886,09	6,09
1949,42	1886,09	6,09
1949,33	1886,09	6,09
1949,25	1886,09	6,09
1949,17	1886,09	6,09
1949,08	1886,09	6,09
1949,00	1886,09	6,09
1948,92	1886,08	6,08
1948,83	1886,08	6,08
1948,75	1886,07	6,07
1948,67	1886,07	6,07
1948,58	1886,06	6,06
1948,50	1886,05	6,05
1948,42	1886,05	6,05
1948,33	1886,04	6,04
1948,25	1886,03	6,03
1948,17	1886,03	6,03
1948,08	1886,02	6,02
1948,00	1886,02	6,02
1947,92	1886,02	6,02
1947,83	1886,01	6,01
1947,75	1886,01	6,01
1947,67	1886,01	6,01
1947,58	1886,00	6,00
1947,50	1886,00	6,00
1947,42	1885,99	5,99
1947,33	1885,99	5,99
1947,25	1885,99	5,99
1947,17	1885,98	5,98
1947,08	1885,98	5,98
1947,00	1885,97	5,97
1946,92	1885,97	5,97
1946,83	1885,96	5,96
1946,75	1885,95	5,95
1946,67	1885,95	5,95
1946,58	1885,95	5,95
1946,50	1885,95	5,95
1946,42	1885,94	5,94
1946,33	1885,94	5,94
1946,25	1885,94	5,94
1946,17	1885,93	5,93
1946,08	1885,92	5,92
1946,00	1885,92	5,92
1945,92	1885,92	5,92
1945,83	1885,92	5,92

continued next page...

Year AD	Lake level [m a.s.l.]	Lake level [m]
1945,75	1885,92	5,92
1945,67	1885,92	5,92
1945,58	1885,91	5,91
1945,50	1885,88	5,88
1945,42	1885,88	5,88
1945,33	1885,88	5,88
1945,25	1885,87	5,87
1945,17	1885,87	5,87
1945,08	1885,87	5,87
1945,00	1885,87	5,87
1944,92	1885,87	5,87
1944,83	1885,86	5,86
1944,75	1885,86	5,86
1944,67	1885,86	5,86
1944,58	1885,86	5,86
1944,50	1885,85	5,85
1944,42	1885,85	5,85
1944,33	1885,85	5,85
1944,25	1885,85	5,85
1944,17	1885,85	5,85
1944,08	1885,84	5,84
1944,00	1885,84	5,84
1943,92	1885,83	5,83
1943,83	1885,83	5,83
1943,75	1885,82	5,82
1943,67	1885,82	5,82
1943,58	1885,82	5,82
1943,50	1885,82	5,82
1943,42	1885,81	5,81
1943,33	1885,81	5,81
1943,25	1885,80	5,80
1943,17	1885,80	5,80
1943,08	1885,78	5,78
1943,00	1885,76	5,76
1942,92	1885,74	5,74
1942,83	1885,73	5,73
1942,75	1885,73	5,73
1942,67	1885,71	5,71
1942,58	1885,68	5,68
1942,50	1885,67	5,67
1942,42	1885,66	5,66
1942,33	1885,64	5,64
1942,25	1885,63	5,63
1942,17	1885,62	5,62
1942,08	1885,61	5,61
1942,00	1885,60	5,60
1941,92	1885,58	5,58
1941,83	1885,58	5,58
1941,75	1885,53	5,53
1941,67	1885,53	5,53
1941,58	1885,53	5,53
1941,50	1885,51	5,51
1941,42	1885,50	5,50
1941,33	1885,48	5,48
1941,25	1885,47	5,47
1941,17	1885,47	5,47
1941,08	1885,45	5,45
1941,00	1885,43	5,43
1940,92	1885,43	5,43
1940,83	1885,42	5,42
1940,75	1885,40	5,40
1940,67	1885,39	5,39
1940,58	1885,38	5,38
1940,50	1885,37	5,37

continued middle column...

Year AD	Lake level [m a.s.l.]	Lake level [m]
1940,42	1885,37	5,37
1940,33	1885,35	5,35
1940,25	1885,34	5,34
1940,17	1885,32	5,32
1940,08	1885,31	5,31
1940,00	1885,31	5,31
1939,92	1885,31	5,31
1939,83	1885,30	5,30
1939,75	1885,29	5,29
1939,67	1885,29	5,29
1939,58	1885,28	5,28
1939,50	1885,28	5,28
1939,42	1885,27	5,27
1939,33	1885,27	5,27
1939,25	1885,27	5,27
1939,17	1885,27	5,27
1939,08	1885,25	5,25
1939,00	1885,25	5,25
1938,92	1885,23	5,23
1938,83	1885,23	5,23
1938,75	1885,21	5,21
1938,67	1885,20	5,20
1938,58	1885,20	5,20
1938,50	1885,19	5,19
1938,42	1885,19	5,19
1938,33	1885,19	5,19
1938,25	1885,19	5,19
1938,17	1885,18	5,18
1938,08	1885,18	5,18
1938,00	1885,18	5,18
1937,92	1885,17	5,17
1937,83	1885,16	5,16
1937,75	1885,15	5,15
1937,67	1885,14	5,14
1937,58	1885,12	5,12
1937,50	1885,12	5,12
1937,42	1885,10	5,10
1937,33	1885,08	5,08
1937,25	1885,07	5,07
1937,17	1885,05	5,05
1937,08	1885,03	5,03
1937,00	1885,02	5,02
1936,92	1885,01	5,01
1936,83	1885,01	5,01
1936,75	1884,99	4,99
1936,67	1884,97	4,97
1936,58	1884,97	4,97
1936,50	1884,95	4,95
1936,42	1884,94	4,94
1936,33	1884,94	4,94
1936,25	1884,94	4,94
1936,17	1884,93	4,93
1936,08	1884,92	4,92
1936,00	1884,91	4,91
1935,92	1884,90	4,90
1935,83	1884,90	4,90
1935,75	1884,89	4,89
1935,67	1884,86	4,86
1935,58	1884,86	4,86
1935,50	1884,85	4,85
1935,42	1884,85	4,85
1935,33	1884,84	4,84
1935,25	1884,84	4,84
1935,17	1884,83	4,83

continued right column...

Year AD	Lake level [m a.s.l.]	Lake level [m]
1935,08	1884,82	4,82
1935,00	1884,82	4,82
1934,92	1884,81	4,81
1934,83	1884,79	4,79
1934,75	1884,79	4,79
1934,67	1884,78	4,78
1934,58	1884,77	4,77
1934,50	1884,75	4,75
1934,42	1884,74	4,74
1934,33	1884,74	4,74
1934,25	1884,72	4,72
1934,17	1884,72	4,72
1934,08	1884,70	4,70
1934,00	1884,70	4,70
1933,92	1884,69	4,69
1933,83	1884,69	4,69
1933,75	1884,68	4,68
1933,67	1884,64	4,64
1933,58	1884,63	4,63
1933,50	1884,62	4,62
1933,42	1884,62	4,62
1933,33	1884,62	4,62
1933,25	1884,61	4,61
1933,17	1884,61	4,61
1933,08	1884,59	4,59
1933,00	1884,58	4,58
1932,92	1884,57	4,57
1932,83	1884,56	4,56
1932,75	1884,50	4,50
1932,67	1884,50	4,50
1932,58	1884,46	4,46
1932,50	1884,44	4,44
1932,42	1884,43	4,43
1932,33	1884,42	4,42
1932,25	1884,39	4,39
1932,17	1884,26	4,26
1932,08	1884,25	4,25
1932,00	1884,25	4,25

Appendix 09 - Lake lake reconstruction of Crescent Island Crater (Åse et al., 1986; Verschuren et al., 2000)

Year AD	Lake level [m]
1993,6	15,5
1993	15,5
1992,6	15,23
1992,1	14,98
1991,7	15,04
1991,3	15,25
1990,9	15,38
1990,5	15,29
1990	15,21
1989,6	14,98
1989,2	14,73
1988,4	14,31
1987,2	14,55
1986,1	15,25
1984,9	15,77
1983,7	16,63
1982,6	16,96
1981,5	16,95
1980,6	17
1979,7	17,16
1978,8	17,33
1977,8	16,51
1976,9	15,18
1976	15,01
1975	15,29
1974,1	15,39
1973,2	15,65
1972,3	16
1971,3	16,71
1970,4	17,12
1969,5	17,36
1968,7	17,53
1968,1	17,59
1967,6	17,33
1967	17,01
1966,4	17,12
1965,8	17,31
1965,2	17,66
1964,7	17,83
1964,1	17,89
1963,5	17,5
1962,9	17,05
1962,3	16,71
1961,8	16,1
1961,2	15,11
1960,6	14,88
1960	14,99
1959,4	15,39
1958,9	15,71
1958,3	15,77
1957,7	15,56
1957,2	15,07
1956,6	14,58
1956,1	14,09
1955,6	13,61
1955	13,12
1954,5	12,94
1953,9	12,81
1953,4	12,92

continued middle column...

Year AD	Lake level [m]
1952,9	13,1
1952,3	13,48
1951,8	13,59
1951,2	13,31
1950,7	13,07
1950,1	12,86
1949,6	13,04
1949,1	13,36
1948,5	13,69
1948	14
1947,4	13,89
1946,9	13,66
1946,4	12,96
1945,8	12,58
1945,3	12,79
1944,3	13,11
1942,9	14,53
1941,6	14,91
1940,2	15,37
1938,8	16,26
1937,4	17,4
1936,1	16,84
1934,7	17,02
1933,3	17,98
1931,9	18,94
1930,6	19,47
1929,2	18,65
1927,8	19,43
1926,4	20,11
1925,1	20,48
1923,7	21,09
1922,3	20,75
1920,9	21,03
1919,6	21,5
1918,2	22,07
1916,8	21,63
1915,4	19,89
1914,1	20,46
1912,7	20,44
1911,3	20,09
1909,9	20,03
1908,6	20,72
1907,2	22,3
1905,8	24,62
1904,4	25,77
1903,1	25,32
1901,7	25,09
1900,3	25,44
1898,9	25,81
1897,6	26,18
1896,2	26,73
1894,8	27,17
1893,4	26,71
1892,1	24,79
1890,7	22,83
1889,3	20,84
1887,9	18,94
1886,6	17,71
1885,2	16,47

continued right column...

Year AD	Lake level [m]
1883,8	15,23
1882,4	13,94
1881,1	12,56
1879,7	12
1875,2	12
1873,2	12
1869,8	12
1867,8	12
1864,3	12
1862,3	14
1858,9	16
1856,9	16
1853,4	16
1851,4	16
1847,9	10,5
1845,9	5
1842,5	5
1840,5	5
1837	5
1835	5,33
1831,6	5,67
1829,6	6
1826,1	6,33
1824,1	6,67
1820,5	7
1818,5	8,82